NTNU – Trondheim
Norwegian University of
Science and Technology

# Literature review and evaluation of the UMR-PRU EoS for predicting solid formation in low temperature natural gas processing

Kristoffer Lavik Bjaanes

Master of Energy and Environmental Engineering
Submission date: April 2014
Supervisor: Even Solbraa, EPT
Co-supervisor: Eleni Panteli, Statoil

Norwegian University of Science and Technology
Department of Energy and Process Engineering

NTNU
Norwegian University
of Science and Technology

Department of Energy
and Process Engineering

EPT-M-2013-22

# MASTER THESIS

for

Stud. Kristoffer Bjaanes

Autumn 2013

***Literature review and evaluation of the UMR-PRU EoS for predicting solid formation in low temperature natural gas processing***

*Litteraturstudie og evaluering av UMR-PRU EoS for beregning av faststoffdannelse i naturgassprosessering ved lave temperaturer*

**Background and objective**

The motivation of the work is to increase the knowledge about thermodynamic modeling of freeze outs in natural gas systems and a deeper understanding of the phase behavior of natural gas mixtures, due to the problems experienced in cryogenic natural gas process-plants (NGL extraction/LNG processes). Critical components in natural gas mixtures introduce a risk of forming a solid coating and plugging the process equipment. Hence, it is relevant to examine methane rich binary mixtures containing components with high risk of freezing. Due to their high triple point temperatures, carbon dioxide, benzene and cyclohexane are regarded as the most critical components.

The preferred thermodynamic method for modeling the solid – fluid system is by describing the fluid phases with a traditionally equation of state in combination with an expression for the solid phase based on melting and triple point properties. This method is based on the assumption of a pure component solid phase, which does not always represent the precipitated substances in natural gas systems. However, it is the situation which represents the highest risk of crystallization at a given temperature.

The objective of this report is to review phase equilibrium of solid-fluid systems and to evaluate the performance of the UMR-PRU model. This model has been successfully used so far in predicting the dew points of natural gas systems. This work will focus on testing this model in solid-fluid equilibrium and compare it to other models.

**The following tasks are to be considered:**

1. Literatures review on available freezing point data for relevant for cryogenic natural gas processing (CO2, benzene, etc.)
2. Review of modelling methods used for solid-fluid equilibrium calculations.
3. Presentation of the UMR-PRU model and the solid model.
4. Evaluation of the UMR-PRU model on predicting the solid-fluid equilibrium.

-- " --

Within 14 days of receiving the written text on the master thesis, the candidate shall submit a research plan for his project to the department.

When the thesis is evaluated, emphasis is put on processing of the results, and that they are presented in tabular and/or graphic form in a clear manner, and that they are analyzed carefully.

The thesis should be formulated as a research report with summary both in English and Norwegian, conclusion, literature references, table of contents etc. During the preparation of the text, the candidate should make an effort to produce a well-structured and easily readable report. In order to ease the evaluation of the thesis, it is important that the cross-references are correct. In the making of the report, strong emphasis should be placed on both a thorough discussion of the results and an orderly presentation.

The candidate is requested to initiate and keep close contact with his/her academic supervisor(s) throughout the working period. The candidate must follow the rules and regulations of NTNU as well as passive directions given by the Department of Energy and Process Engineering.

Risk assessment of the candidate's work shall be carried out according to the department's procedures. The risk assessment must be documented and included as part of the final report. Events related to the candidate's work adversely affecting the health, safety or security, must be documented and included as part of the final report. If the documentation on risk assessment represents a large number of pages, the full version is to be submitted electronically to the supervisor and an excerpt is included in the report.

Pursuant to "Regulations concerning the supplementary provisions to the technology study program/Master of Science" at NTNU §20, the Department reserves the permission to utilize all the results and data for teaching and research purposes as well as in future publications.

The final report is to be submitted digitally in DAIM. An executive summary of the thesis including title, student's name, supervisor's name, year, department name, and NTNU's logo and name, shall be submitted to the department as a separate pdf file. Based on an agreement with the supervisor, the final report and other material and documents may be given to the supervisor in digital format.

☐ Work to be done in lab (Water power lab, Fluids engineering lab, Thermal engineering lab)
☐ Field work

Department of Energy and Process Engineering, 1 October 2013

Olav Bolland
Department Head

Even Solbraa
Academic Supervisor

Research Advisor: Eleni Panteli (Statoil)

## Preface

The thesis is written at the institute for Energy- and Process Technology at NTNU, in collaboration with Statoil. The process behind the finished result has been both exiting and educational, but also challenging.

My summer internship at Statoil Rotvoll in 2013, gave me the opportunity to write this thesis in collaboration with Statoil, which has been very valuable and rewarding. I would like to thank Eleni Panteli and Even Solbraa for taking the time to help me and make this thesis possible. I am very grateful for their feedback and motivation.

Finally, I would like to thank Mette for motivating and supporting me during this period.

Trondheim, 11.04.2014

Kristoffer Lavik Bjaanes

## Abstract

Small amounts of carbon dioxide and heavy hydrocarbons are usually present in natural gas mixtures. Due to the relatively high triple point temperatures of these components, they create potential risks of solid formation in cryogenic equipment, such as heat exchangers, pipes and valves. Accurate and reliable thermodynamic models for predicting the solid-liquid phase behavior are necessary for the design of cryogenic systems in order to avoid the freeze out conditions.

Traditionally equations of state have gained popularity due to the capability of representing both vapor and liquid phases. For describing the solid-liquid equilibrium, they are normally combined with an expression for the solid phase. This study presents a review of the existing modelling methods used for describing the solid-liquid equilibrium.

The main objective of this thesis is to evaluate the performance of the UMR-PRU model on predicting the solid-fluid phase equilibrium. The UMR-PRU model has previously been found to be an accurate model for dew point predictions in natural gas systems. In the report, the model has been compared to the Soave-Redlich-Kwong (SRK) equation of state and the simplified Perturbed-Chain Statistic Associating Fluid Theory (sPC-SAFT) equation of state. For describing the solid phase, a solid model based on sub-cooled liquid has been used.

In order to evaluate the thermodynamic methods, a substantial amount of experimental data has been collected. The experimental methods behind this work have been accounted for and the data has been evaluated in order to check the consistency. However, the experimental data for solid-liquid equilibrium are limited and this prevents to give the thermodynamic models a proper validation. New experimental data should be provided for these systems in the future.

The simulation results for the models UMR-PRU, SRK EoS and sPC-SAFT have been compared to the evaluated experimental data. The SRK equation of state fails in predicting the solid-liquid phase behavior without the binary interaction parameter. However, it shows good capability in correlating the experimental data with binary interaction parameter for all of the systems. In contrast to the SRK, the simplified PC-SAFT is very accurate predicting the solid-liquid phase behavior and proves to be less dependent of experimental data for correlation.

The UMR-PRU model gives reasonable predictions for $CO_2$-methane rich systems. However, at lower temperatures the deviations between experimental data and the UMR-PRU predictions start to increase. For the systems involving heavy hydrocarbons, the model fails predicting the freeze out temperatures when the temperature drops. The results indicate that the applicability of the UMR-PRU model should be extended in order to handle cryogenic conditions. New UNIFAC interaction parameters suited for lower temperatures are probably necessary.

## Sammendrag

Små mengder av karbon dioksid og tunge hydrokarboner finnes vanligvis i naturgass. På grunn av de relativt høye trippelpunktstemperaturene til disse komponentene, utgjør de potensielle farer for faststoff-dannelse i kryogeniske systemer, slik som i varmevekslere, rør og ventiler. For å kunne beskrive faseoppførselen til naturgassblandinger, hvor en faststoff-fase er inkludert, er det viktig med nøyaktige og pålitelige termodynamiske modeller.

Tilstandsligninger har tradisjonelt vært populære, på grunn av sine egenskaper til å beskrive faseoppførselen til væske- og gassblandinger. For å beskrive faststoff-fluid likevekts systemer, er de vanligvis kombinert med en ligning for å beskrive faststoff-fasen. I denne rapporten presenteres de ulike metodene som er benyttet for å beskrive faststoff-fluid likevekts systemer.

Hovedmålet med denne rapporten er å evaluere evnen UMR-PRU har til å beregne utfrysninger i naturgass. UMR-PRU modellen har tidligere vist å være en vellykket modell til å gjøre duggpunkts beregning i naturgass systemer. I denne rapporten har modellen blitt sammenlignet med modeller basert på tilstandslikningene Soave-Redlich-Kwong (SRK) og simplified Perturbed-Chain Statistic Associating Fluid Theory (sPC-SAFT). For å beskrive faststoff fasen, benyttes en faststoffs modell basert på underkjølt væske.

For å evaluere modellene har det blitt samlet inn eksperimentell data relevant for faststoff-fluid likevekts systemer for naturgass. Det er gjort rede for de eksperimentelle metodene bak arbeidet, og data har blitt evaluert for å se om de samsvarer. Rapporten avdekker at det er stor mangel på eksperimentell data for binære metanrike- tunge hydrokarbon blandinger. Mangel på data gjør det vanskelig å gi en god evaluering av de termodynamiske modellene.

Simuleringsresultatene for UMR-PRU, SRK EoS og sPC-SAFT har blitt sammenlignet med den tilgjengelig eksperimentelle dataen. Tilstandslikningen SRK har problemer med å beskrive faststoff-fluid systemer når det ikke benyttes en interaksjons parameter. Modellen viser allikevel å gi nøyaktige beregninger når interaksjonsparameteren er tilpasset etter eksperimentell data. I motsetning til SRK, gir sPC-SAFT rimelig gode beskrivelser av faststoff-fluid systemer, og er mindre avhengig av å korreleres etter eksperimentell data

UMR-PRU modellen viser gode beregninger for $CO_2$-metan rike blandinger. Allikevel, når temperaturen reduseres, blir avviket mellom modellens beregninger og den eksperimentelle dataen større. For metanrike-tunge hydrokarbon blandinger feiler UMR-PRU å gi gode beregninger når temperaturen reduseres. Resultatene gir en indikasjon på at UMR-PRU modellen bør utvides slik at den kan håndtere kryogeniske forhold. Nye UNIFAC parametere som er beregnet for lave temperaturer er trolig nødvendig.

# Contents

## List of figures

## List of tables

# 1. Introduction

According to BP [1], natural gas is projected to be the fastest growing fossil fuel (1.9% p.a.) over the next 20 years, with liquefied natural gas (LNG) trade increasing with 3.9 % per annum. Natural gas's share of global energy consumption was in 2012 23.9 %, with LNG accounting for 31.7% of the natural gas trade, BP [2].

Natural gas is liquefied to increase its energy density. At atmospheric pressure, the volume of the natural gas can be reduced to about 1/600 of the volume at standard gas condition. Thus, large quantities of natural gas can be transported in tanks by ship or truck, and for long distances LNG is preferred over pipeline transport.

The natural gas is liquefied at a temperature around -162$^{o}$C, and this requires energy intensive cooling processes. Thus, new solutions have been developed to optimize the thermodynamic processes involved in the liquefaction process. A challenge in the development of new designs, is to avoid precipitation of trace components in the feed gas. The main component in natural gas is methane (85-90%), but traces of $CO_2$, heavy hydrocarbons and water is also found in the feed gas. These components introduce a risk of precipitation of a solid phase during the cooling process, which can cause fouling and plugging on heat exchangers, pipes and valves.

The main impurity in natural gas is $CO_{2,}$ and due to its high triple point temperature, there is a high risk of solid formation. Other critical impurities are n-hexane, n-heptane, n-octane, cyclohexane and benzene. The understanding of the phase behavior of the components in methane and methane rich mixtures, is crucial in order to avoid potential freeze out conditions. By investigating the experimental work done for such systems, it is possible to get the required knowledge. However, as literature shows, there has been done limited work in evaluating the solid formation risk in low temperature processes.

The experimental data can be used to make accurate modelling tools to predict the solid formation in natural gas systems. Different thermodynamic models have been developed in order to give reliable predictions. Most of them are based on classical equations of state. However, there is discrepancy in the quality of these models.

In this work, all available experimental data found in the literature for solid-liquid equilibrium and solid-vapor equilibrium, are presented. The experimental data have been evaluated in order to check the consistency of such data. The experimental data have been used to evaluate the performance of three thermodynamic models: SRK and sPC-SAFT equations of state and the UMR-PRU model.

# 2. Solid-Liquid Phase Equilibrium

## 2.1 Introduction

The understanding of the phase behavior of solid-liquid equilibrium systems, is necessary in order to handle and discuss the experimental data and the modeling results. In this report, both binary and ternary systems have been investigated. Most of the experimental and modeling work has been done for binary systems, due to the simplicity of this system.

- Binary systems: Two components present in the solid-liquid equilibrium system, usually one solute and one solvent
- Ternary systems: Three components present in the solid-liquid equilibrium systems, usually one solute and two solvents.

The phases in equilibrium which is of interest in a solid-liquid equilibrium system can be divided into:

- Solid-Liquid equilibrium (SLE): One solid phase and one liquid phase
- Solid-Vapor equilibrium (SVE): One solid phase and one vapor phase
- Solid-Liquid-Vapor (SLVE): One solid phase, one liquid phase and one vapor phase present together in the equilibrium system

In an equilibrium system the variables of temperature, pressure, compositions etc. are easily changeable. This will have an effect on the phase transitions, critical points, etc. occurring in a phase equilibrium system. When there are multiple components in the systems, the phase behavior is more complex. A general rule has been proposed to describe how these variables affect each other. The Gibbs phase rule determines the number of degrees of freedom in a system and is given by [3]:

$$F = 2 + N - P \tag{3.1}$$

where F is the number of independent intensive properties called degrees of freedom, N is the number of components and P is the number of phases in thermodynamic equilibrium with each other. For binary systems N = 2, and thus P determines the degrees of freedom:

- For P = 2: This gives F = 2. That is, two properties must be specified to fix the intensive state of the system. This applies for the SLE or SLV systems.
- For P =3: This gives F = 3. That is, the intensive state is determined by a single intensive property value. This applies for the SLVE system.

## 2.2 Solid-liquid phase behavior of binary mixtures

The phase behavior of the different systems that are researched can be very different, due to the difference in thermodynamic properties such as triple point, critical point, etc. The molecular structure and difference in the properties between the solute and the solvent, will determine the phase behavior. There will be given a general classification of the solid-fluid equilibrium phase behavior, and then a more detailed description of the $CO_2$-methane and benzene-methane system is given. The study of the phase diagram of these systems will give the necessary understanding to evaluate the experimental data and the simulating results.

### 2.2.1 Classification of solid-fluid phase behavior of binary mixtures

Kohn and Luks [4] have classified the phase behavior of binary systems into four types. Three of these types are representative for the systems reported here.

#### 2.2.1.1 Type A phase behavior

The solid-liquid-vapor three-phase locus for the type A phase behavior, starts at the triple point of the solute and terminates at a quadruple point ($S_1$-$S_2$-L-V), near the triple point of the solvent. A quadruple point represents a point where four phases are in equilibrium. The SLV curve is represented with two branches terminating at each K-point. The two SLV branches can be seen in Figure 1, the first $S_1$-L-V branch is at low temperature and the second $S_2$-L-V is at a higher temperature. The K-points are where the liquid-vapor phase is in presence of a solid phase.

The $CO_2$-methane, benzene-methane, octane-methane and cyclohexane-methane are binary systems that belong to this type of phase behavior. All of these components have triple point temperatures that are higher than the critical temperature of methane. For systems like these, there will be a gap in the solubility curve occurring around the maximum point of the SLV curve.

Due to the difference in the properties of these systems (triple point temperatures etc.), the phase diagrams of these systems will vary. Figure 1 is a general illustration of this type of phase behavior. For the mentioned binary systems, the figure is more representative for the benzene-methane and the cyclohexane-methane systems, where the triple point temperatures are much higher than the critical temperature for methane.

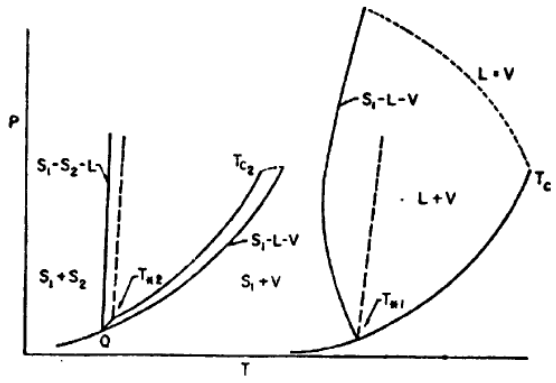


**Figure 1. Sketch of type A phase behavior**

### 2.2.1.2 Type B phase behavior

This is a system in which the solid-liquid-vapor locus runs from the triple point of the solvent to a quadruple point, occurring at the center of the SLV locus. At this point, immiscible liquids will form and combine with the vapor and solid phases. At the quadruple point there will be four phases; gas phase, two liquid phases and a solid phase. This gives a solubility curve that is non continuous, from low temperature to the triple point of the solute.

The heptane-methane system is an example of a type B phase behavior. For this system, the triple point temperature of heptane (182 K) is below the critical temperature of methane. The quadruple point will occur at a temperature below the critical temperature of pure methane (190.56 K) and at pressures considerably in excess of the critical for pure methane, Chang, et al. [5]. At this point the mixture will lose a $L_1$-phase and gain a $L_2$-phase, which is leaner in solute. Figure 2 illustrates this type of phase behavior. The three phase locus is separated into two branches. The low temperature branch (S-$L_1$-V) originates from the methane triple point, and ends up in the quadruple point (S-$L_1$-$L_2$-V) .The high temperature branch (S-$L_2$-V) starts at the quadruple point (S-$L_1$-$L_2$-V), and ends up in the solute triple point.

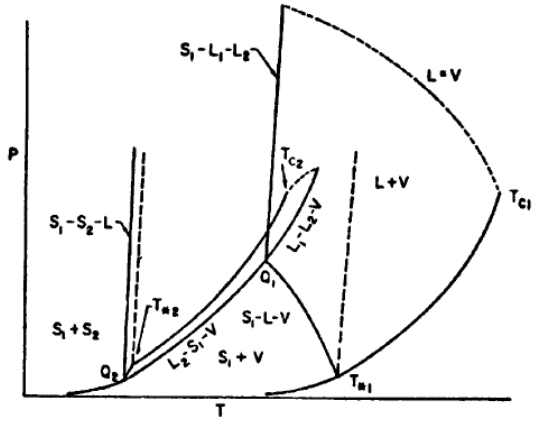


**Figure 2. Sketch of type B phase behavior**

### 2.2.1.3 Type C phase behavior

In this type of system there are no discontinues between the triple point of the solute, and the Q-point near the triple point of the solvent. Therefore, there will be no gap in the solubility curve for this system. The system can contain liquid-liquid immiscibility as shown in Figure 3.

The hexane-methane system is an example that belongs to this type of phase behavior. For systems like these, the triple point temperature of the solute is lower than the critical temperature of methane.

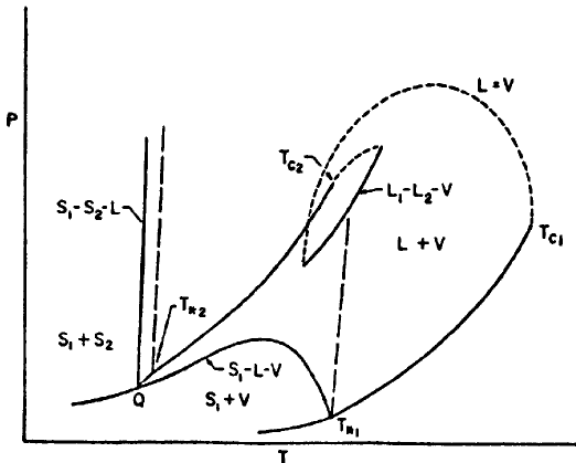


**Figure 3. Sketch of type C phase behavior**

## 2.2.2 Phase behavior of the $CO_2$-methane binary system

$CO_2$ has a triple point temperature of 216.58 K which is higher than the methane critical temperature (190.56 K). The methane-CO2 system belongs to the type A phase behavior, and there will be a gap in the solubility curve for this system.

The phase behavior of the methane-$CO_2$ binary system is illustrated in the pressure-temperature diagram in Figure 4. In this figure, the overall composition of the system is fixed. Gibbs phase rule gives two degrees of freedom for the two-phase region, and one for the three phase region. Thus, the SLVE system is represented by the line BDF (SLV three-phase loci) and is fixed when only one property is fixed. The lines FG and FH are also three-phase lines, but they are at temperatures below the triple point of methane, and are therefore irrelevant. An overall change in the composition will not change the SLV line, due to the degrees of freedom.

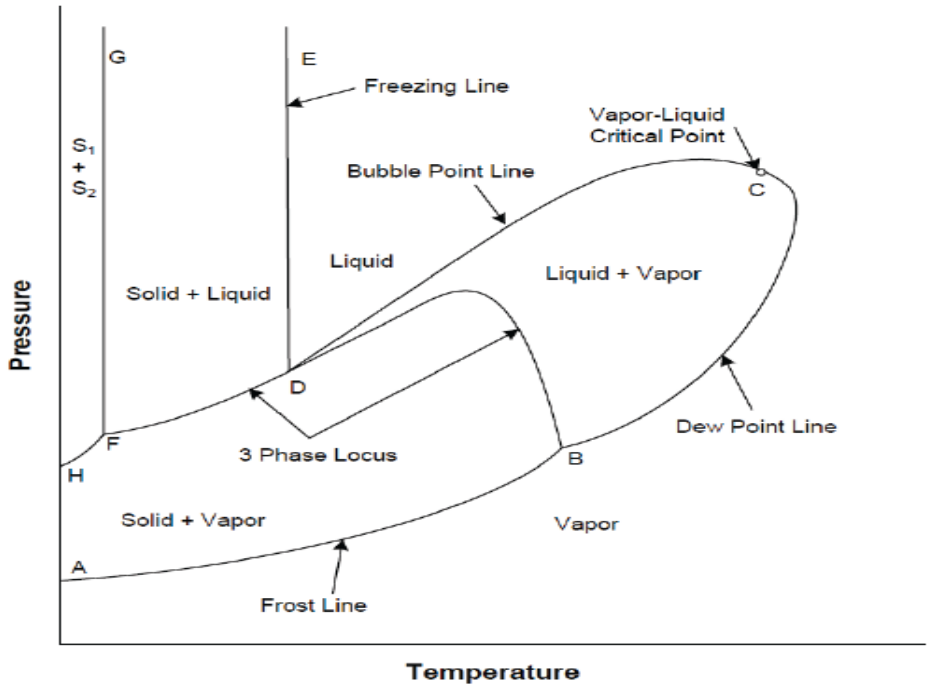


**Figure 4. Qualitative Pressure-Temperature Diagram of the Methane – Carbon Dioxide Binary [6]**

Line BD is the boundary between the liquid-vapor region and the solid-vapor region. When the temperature is lowered, the liquid-vapor region becomes unstable and $CO_2$ crystalizes. With further cooling, the solid $CO_2$ in the vapor phase will be dissolved by a liquid phase rich in methane.

Line DE, the freezing line, is the boundary between the liquid phase and the solid-liquid phase. When $CO_2$ exceeds the solubility limit in the liquid phase, solid $CO_2$ will precipitate in the mixture. Point B in the figure is the triple point for pure $CO_2$ and point F is the triple point for pure methane. The freezing line DE will vary between these points, following the SLV loci, when the overall composition is changed.

Line AB, the frost line, is the boundary curve between vapor and solid-vapor region. When $CO_2$ exceeds the solubility limit in the gas phase, solid $CO_2$ will form in the gas phase. The frost line, freezing line, dew point line and the bubble point line will be affected by a change in the overall composition.

### 2.2.3 Phase behavior of the benzene–methane binary system

Benzene has a triple point temperature of 278.83 K, which is much higher than the critical temperature of methane. In such systems, the critical locus is interrupted by the three-phase curve, with a high- and low-temperature branch. The branches are terminating in singular end points (K-points) having critical identity of the liquid and vapor phases, Kuebler and McKinley [7]. This is illustrated in the pT-diagram of the system in Figure 5. The low temperature branch originates in the triple point temperature of methane, and ends in the first critical end point of the

three-phase curve (K –points). The high temperature branch starts in the second critical end point, and ends in the triple point temperature of the solute.

The description of the phase behavior presented, is taken from the work of de Hemptinne [8]. In Figure 5 the dew-point line (1) is separating the liquid-vapor region, the freezing line (2) is separating the solid-liquid region, and the frost line (3) is separating the vapor-solid region. The dotted line (6) is the high- and low-temperature branches of the three-phase curve, with the two critical locus points (K-points) illustrated (5). For the light hydrocarbon, methane, the dew point line (4) is shown below.

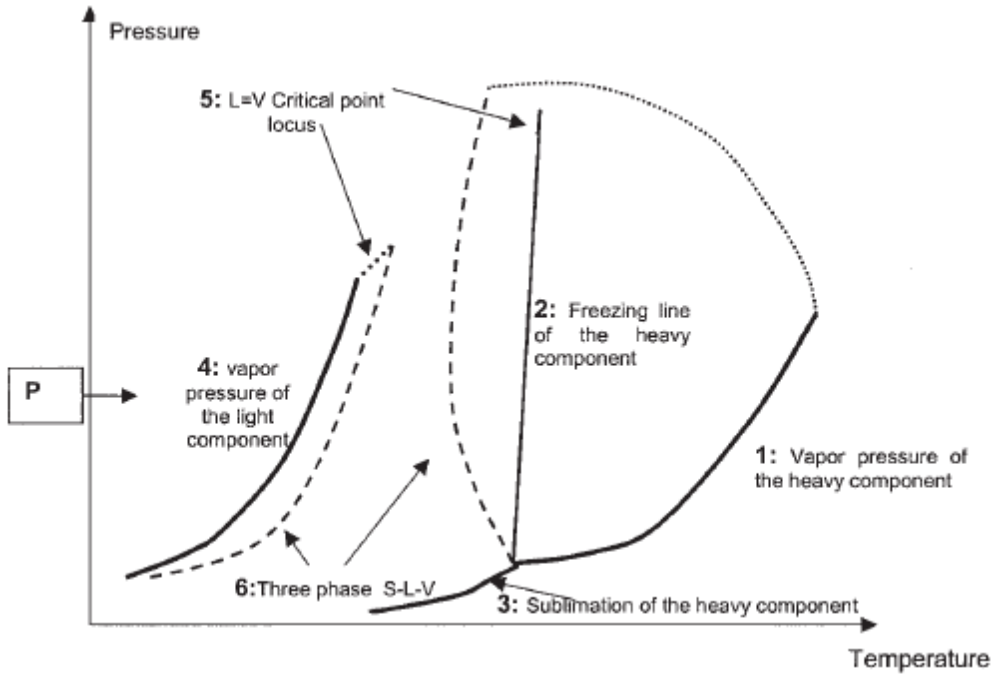


**Figure 5. Sketch of the benzene-methane phase diagram [8]**

The description of the phase transitions can be understood easier in a temperature-composition diagram. Figure 6 illustrates the benzene - methane phase transitions at constant pressure, which is taken between the triple point pressures and critical pressures. At high temperatures the mixture is always in the vapor phase (1). Cooling a mixture rich in benzene will result in a vapor-liquid phase (2), where the liquid phase is richer in benzene than the vapor phase.

When the mixture is rich in benzene, cooling the mixture will result in a vapor-liquid phase (2). The liquid phase will be richer than the vapor phase in benzene. If the mixture is very rich in benzene, there will be a transition between the vapor-liquid phase and a liquid phase (3). Further cooling will then give solid benzene formation, after passing the high temperature solid-liquid line (4). This represents the highest risk of benzene formation.

With moderate benzene concentrations, further cooling from (2) will give the solid-vapor region (6), after passing the high temperature three-phase branch (5). At this temperature the liquid becomes unstable and starts to crystallize, until all the liquid disappears. At low benzene concentrations, the benzene will crystalize directly from the vapor phase (1). Since natural gas contains several components, the three phases may coexist in this region.

At very low temperatures the low temperature three-phase line will occur. There will be a transition from the vapor-solid, which results in solid benzene formation. For mixtures rich in methane, there will be two phase-transitions. The first one is the low temperature three-phase line, where the mixture enters a vapor-liquid region (7). Here the methane concentration is so high that the solid benzene dissolves in the liquid. The second is a dew-point line, from (1) to (7). When the mixture in the vapor-liquid is further cooled, there will be a bubble-point transition to a liquid phase (9). Even further cooling will result in solid benzene formation, after passing the low temperature solid-liquid line (10).

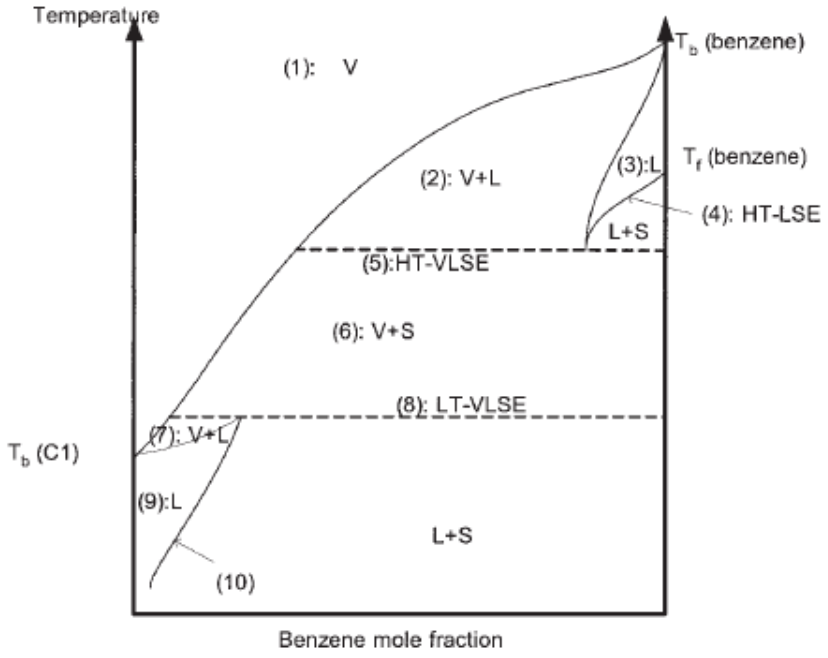


**Figure 6. Sketch of the benzene-methane phase diagram at fixed pressure [8]**

# 3. Thermodynamic Models for Solid-Fluid Calculations

## 3.1 Thermodynamic framework

The thermodynamic modelling of the solubility of a solid in a liquid solvent (i.e., solid-liquid equilibria), or at the triple point of a mixture (i.e., solid-liquid-vapor equilibria), is based on the fugacity balance. The fundamental theory governing thermodynamic equilibrium can be found in appendix A. For a solid-liquid equilibrium between a fluid phase (component 1 and 2) and a pure solid phase (component 2), the fugacity balance applies:

$$f_2^{1,liquid}(T,p) = f_2^{2,solid}(T,p) \tag{3.1}$$

where subscript 1 is the solvent in liquid phase, subscript 2 is the solute in solid phase, and $f^{liquid}$ and $f^{solid}$ are the fugacity of liquid and pure solid.

Two thermodynamic approaches are typically used for solid-fluid calculation: the activity coefficient model and the equation of state model. The models are combined with general mathematical terms for calculating the fugacity of the solid phase; solid model 1 and solid model 2 (see 3.4).

## 3.2 Review of thermodynamic models used for solid-fluid calculations

The activity coefficient approach has been used by Myers and Prausnitz [9], for calculating the solubility of $CO_2$ in liquid solvents at low temperatures. The model was related to pertinent intermolecular forces by a generalization of a Scatchard`s equation. To calculate the fugacity of the solid phase, the model based on sub-cooled liquid was applied.

Eggeman and Chafin [10] used the activity coefficient approach together with the solid model 2 (eq. 3.30), for $CO_2$ freeze out determination in vapor and liquid methane. To calculate the activity coefficient the Non-Random Two Liquid (NRTL) equation was applied. The activity approach can also be estimated from the group-contributing method UNIFAC, Gmehling, et al. [11].

Equations of states have gained popularity due to the capability of representing both vapor and liquid phases. Equations of state can typically be used over a wide range of temperatures and pressures, and they can be applied to mixtures of diverse components, ranging from light gases to heavy liquids. EoS can be used to calculate vapor-liquid, liquid-liquid, and supercritical fluid-phase equilibria without any conceptual difficulties. Wei and Sadus [12].

In the same article by Eggeman and Chafin [10] they also combined the Peng-Robinson EoS together with the solid model 1. They reported good results for both models when compared to experimental data. The authors were surprised over the ability of PR EoS to give accurately predictions, although some numerical problems were detected.

ZareNezhad [5] studied the prediction of $CO_2$ freeze out in cryogenic natural gas plants. He applied the Peng-Robinson equation of state to calculate the liquid fugacity and the solid model based on sublimation pressure to calculate the solid fugacity. ZareNezhad [5] also developed a semi-empirical quadratic temperature-dependent binary interaction parameter to express the interaction in the $CO_2$-$CH_4$ mixture. Their proposed thermodynamic model were able to give reliable predictions of the $CO_2$-$CH_4$ system.

In the paper by Carter and Luks [13] they suggested a more general approach to describe the solid-liquid equilibrium, which is less dependent on experimental data for correlation. The authors used the cubic Soave-Redlich-Kwong equation of state (SRK EoS) for describing the liquid phase, and the solid model 2 for representing the solid phase. They reported predicting results compared to the experimental data for the binary methane - $CO_2$ system. However, they noticed that the predictions were sensitive to the choice of binary interaction parameter.

In the work by Zhang, et al. [14], the SRK EoS is employed together with the solid model 1(eq. 3.29) for frost point predictions in the $CO_2$-methane system. He has also conducted experimental data for the $CO_2$-methane system at low temperatures. Agreements between the model predictions and the experimental data are reported. The same model was used in the paper by Zhang and Solbraa [15] , for the solubility of $CO_2$ and heavy hydrocarbons in gas mixture at low temperature . The modelling results correspond well with the experimental data.

In the report by Shen, et al. [16], the PR and SRK equations of state and solid model 1 are adopted to calculate the $CO_2$ solubility in $CH_4$ + $N_2$ and $CH_4$ + $C_2H_6$ mixtures. Results obtained from the models, are consistent with the experimental data. The authors have also derived two quadratic temperature-dependent $k_{CH_4-C0_2}$ correlations. De Guido, et al. [17] have developed two methods based on the SRK and PR EoS together with the solid model 2. The methods are used for prediction of SLV equilibrium of $CO_2$ mixture with n-alkanes or H2S. The models show good reliability when compared to experimental data.

Most of the thermodynamic models for solid-liquid calculations have been adapted and tested for the methane-$CO_2$ systems. $CO_2$ is the main impurity in natural gas, and most of the solid-liquid investigations are therefore on these types of systems. However, some work has also been done for systems containing methane and heavy hydrocarbons.

In the paper de Hemptinne [8] he investigates the risk of benzene crystallization in the LIQUEFIN gas liquefaction process. He has developed a model that uses the Peng-Robinson EoS with the Huron-Vidal mixing rule. Due to lack of experimental data for this system at low temperatures, the author was not able to give a comprehensive validation of the model. However, the author was able to match some conditions using the experimental data of Rijkers, et al. [18]. Rijkers experimental data is for rather high benzene concentration. The model predicted reasonable results compared to his experimental data.

Recent work done on systems containing methane and heavier hydrocarbons, is the work by Zhang and Solbraa [19]. Thermodynamic models based on SRK EoS and sPC-SAFT combined with solid model 2 (eq. 3.29), are used for calculating the solubility of heavier hydrocarbons in liquid methane. The van der Waals classic mixing rule is coefficient used with a single binary interaction. With optimized interaction parameters, the models are able to give good predictions compared to experimental data. The sPC-SAFT model is also able to give reasonable results with the interaction parameter set to zero.

## 3.3 Thermodynamic models for the fluid and gas phases

In this report, three models have been used to describe the fluid and gas phases: SRK EoS, sPC-SAFT EoS and the UMR-PRU model. The SRK EoS is widely used in the industry due to its simplicity and reasonable accuracy. The sPC-SAFT is more complicated in the structure than the SRK EoS, but has proven to be a successful model describing equilibrium systems, [19-21]. The UMR-PRU has so far been an accurate and efficient thermodynamic tool predicting dew points of natural gas systems, [22-24].

### 3.3.1 The soave Redlich Kwong equation of state

The SRK EoS of state is an improvement of the Redlich Known EoS. Soave [25] suggested a replacement of the term $a/T^{1.5}$ in the RK EoS with a more general temperature dependent term $a(T)$. This resulted in a significant improvement of the Redlich-Kwong equation, [12]:

$$Z = \frac{V}{V-b} - \frac{a(T)}{RT(V+b)} \tag{3.2}$$

$$\mathrm{a(T)} = 0.4274\left(\frac{\mathrm{R^2T^{c2}}}{\mathrm{p^c}}\right)\left\{1+\mathrm{m}\left[1-\left(\frac{\mathrm{T}}{\mathrm{T^c}}\right)^{0.5}\right]\right\}^2 \tag{3.3}$$

$$m = 0.480 + 1.57\omega - 0.176\omega^2 \tag{3.4}$$

$$b = 0.08664\frac{RT^c}{p^c} \tag{3.5}$$

where ω is the acentric factor. The accuracy of the SRK equation has been tested and proven by Soave to give satisficing results. Compared to the Redlich-Kwong equation, Soaves modification gave matched the experimental data, and it was able to give accurate prediction of the phase behavior of mixtures.

### 3.3.2 The Simplified PC-SAFT equation of state

The simplified Perturbed-Chain Statistics Associating Fluid Theory (sPC-SAFT) proposed by von Solms, et al. [26], is a modification of the PC-SAFT model and the SAFT model. Theory behind the SAFT model can be read in following articles,Chapman, et al. [27], [28].

The PC-SAFT equation of state is given by Gross and Sadowski [29]:

$$Z = Z^{id} + Z^{hc} + Z^{disp} \tag{3.6}$$

where $Z = pv/RT$ is the compressibility factor, $Z^{id} = 1$ is the ideal gas contribution, $Z^{disp}$ is the perturbation contribution, and $Z^{hc}$ is the hard-chain contribution given by:

$$Z^{hc} = \bar{m}Z^{hs} - \sum_i x_i(m_i - 1)\rho \frac{\partial \ln g_{ii}^{hs}}{\partial \rho} \tag{3.7}$$

$$\bar{m} = \sum_i x_i m_i \tag{3.8}$$

where $x_i$ is the mole fraction of chains of component $i$, $m_i$ is the number of segments in a chain of component $i$, $\rho$ is the total number of density in a of molecules, $g_{ii}^{hs}$ is the radial pair distrubiton function for segments of component $i$ in the hard sphere system, and the superscript $hs$ indicates quantities of the hard-sphere system.

The terms $Z^{hs}$ and $g_{ii}^{hs}$ , given in equation 3.7, have been simplified in the sPC-SAFT model. These modifications make the computational implementing in software tools easier, and it also reduces the computation times. The model has been documented to perform as well as the PC-SAFT model. More detailed theory behind the sPC-SAFT can be found in von Solms, et al. [26].

### 3.3.3 The UMR-PRU model

The theory behind the UMR-PRU EoS is based on the report by Louli, et al. [22]. The UMR-PRU model belongs to the class of EoS/$G^E$ models. It combines the PR EoS with an original UNIFAC EoS/$G^E$ model that employs temperature dependent group-interaction parameters through the Universal Mixing Rule (UMR) proposed by Voutsas, et al. [30].

The Peng-Robinson cubic EoS is given by:

$$P = \frac{RT}{v-b} = \frac{\alpha}{v(v+b)+b(v-b)} \tag{3.9}$$

With:

$$\alpha = a \cdot \alpha_c \tag{3.10}$$

$$\alpha_c = 0.45724 \cdot \frac{(RT_c)^2}{P_c} \tag{3.11}$$

$$a = \left[1 + m\left(1 - \sqrt{T_r}\right)\right]^2 \tag{3.12}$$

$$b = 0.07780 \frac{RT_c}{P_c} \tag{3.13}$$

where P is the pressure, R is the gas constant, T is the temperature, $v$ is the molar volume, $T_c$ the critical temperature, $P_c$ the critical pressure and $\alpha$ and $b$ are the attractive and co-volume EoS parameters.

The Universal Mixing Rule (UMR) proposed by Voutsas, et al. [30] is given by:

$$\frac{\alpha}{bRT} = \frac{1}{A}\frac{G_{AC}^{E,SG} + G_{AC}^{E,res}}{RT} + \sum_i x_i \frac{\alpha_i}{b_i RT} \tag{3.14}$$

$$b = \sum_i \sum_j x_i x_j b_{ij}, \quad b_{ij} = \left(\frac{b_i^{1/2} + b_j^{1/2}}{2}\right)^2 \tag{3.15}$$

where the parameter A depends on the EoS used (A = -0.53 for PR EoS), $G_{AC}^{E,SG}$ and $G_{AC}^{E,res}$ are the Staverman-Guggenheim term of the combinatorial part and the residual part of the excess Gibbs energy ($G^E$), respectively, obtained from the UNIFAC activity coefficient model:

$$\frac{G_{AC}^{E,SG}}{RT} = 5\sum_i x_i q_i \ln\frac{\theta_i}{\varphi_i}, \qquad \frac{G_{AC}^{E,res}}{RT} = \sum_i x_i v_k^i \left(\ln\Gamma_k - \ln\Gamma_k^i\right) \tag{3.16}$$

$$\theta_i = \frac{X_i r_i}{\sum_j X_j r_j}, \quad \varphi_i = \frac{X_i q_i}{\sum_j X_j q_j} \tag{3.17}$$

where $v_k^i$ is the number of groups of type k in molecule $i$ , $\Gamma_k$ is the group residual activity coefficient, and $\Gamma_k^i$ is the residual activity coefficient of group k in molecule $i$ , Fredenslund, et al. [31]. The residual contribution to the logarithm of the activity of group k is given:

$$\ln\Gamma_k = Q_k\left[1 - \ln\left(\sum_m \theta_m \Psi_{mk}\right) - \sum_m \frac{\theta_m \Psi_{mk}}{\sum_n \theta_m \Psi_{nm}}\right] \tag{3.18}$$

where the surface area fraction of group m in the mixture is defined as:

$$\theta_m = \frac{Q_m X_m}{\sum_n Q_n X_n} \tag{3.19}$$

And $X_m$ is the mole fraction of the group m in the mixture:

$$X_m = \frac{\sum_j v_m^{(j)} X_j}{\sum_j \sum_n v_n^{(j)} X_j} \tag{3.20}$$

The term $\Psi$ in the residual contribution is a function of group interaction parameters (IPs). Different types of IPs can be utilized. In the original UNIFAC-type model proposed by Hansen et al. (1992), linear T-dependent IP`s are utilized. But in in standard UNIFAC tables there are no parameters for pairs containing gases. They are instead calculated by considering them as separate groups, like in all EoS/$G^E$ models.

Louli, et al. [24] have evaluated new UNIFAC group interaction parameters containing gas. The IP`s were determined by fitting isothermal VLE experimental data. The IP`s were determined by fitting isothermal VLE experimental data using an objective function. The UNIFAC $\Psi$ function used in their study was:

$$\Psi = \exp\left[-\frac{A_{nm} + B_{nm}\cdot(T - 298.15) + C_{nm}\cdot(T - 298.15)^2}{T}\right] \tag{3.21}$$

### 3.3.4 The van der Waals mixing rule

Mixing rules are necessary when equations of state for pure fluids are used to calculate various thermodynamic properties of fluid mixtures. By applying mixing rules and combing rules, the same EoS used for pure fluids can be used for mixtures. The mixing rules relate the properties of the pure components to the properties of the mixture, Wei and Sadus [12].

The van der Waals one-fluid mixing rule is the most common mixing rule, and is expressed as:

$$a = \sum_i \sum_j x_i x_j a_{ij} \tag{3.22}$$

$$b = \sum_i \sum_j x_i x_j b_{ij} \tag{3.23}$$

where $a_{ii}$ and $b_{ii}$ are the constant of the equation for pure component, and $a_{ij}$ and $b_{ij}$ ($i \neq$ j) are the cross parameters determined by an appropriate combining $i$ rule, often given by:

$$a_{ij} = \sqrt{aiaj}(1 - k_{ij}) \tag{3.24}$$

$$b_{ij} = \frac{1}{2}(b_i + b_j) \tag{3.25}$$

where $k_{ij}$ is the binary interaction parameter.

The binary interaction coefficient is an empirical parameter to adjust the deviation between the actual state and the ideal state. In this work, the $k_{ij}$ has been correlated by fitting it to the experimental data. It can also be convenient to use temperature dependent $k_{ij}$ correlations. This has been done in the work by ZareNezhad [32] and Shen, et al. [16], where they suggested the following $k_{ij}$ equations for PR EoS and SRK EoS, respectively:

$$k_{ij} = -36.134\frac{1}{T^2} + 5.4835\frac{1}{T} + 0.09980 \tag{3.26}$$

$$k_{ij} = 107.48\frac{1}{T^2} + 5.649\frac{1}{T} + 0.0956 \tag{3.27}$$

## 3.4 Thermodynamic models for the solid phase

For the calculation of the fugacity of the solid phase, two different approaches are presented.

### 3.4.1 Solid model 1: Fugacity based on sublimation pressure

A general relation to calculate fugacity is given by, Prausnitz, et al. [33]

$$RT \ln \varphi_i = RT \ln \frac{f_i}{y_i P} = \int_0^P \left( \bar{v}_i - \frac{RT}{P} \right) dP \tag{3.28}$$

where $\bar{v}_i = (\partial V / \partial n_i)_{T,P,n_i}$ is the partial molar volume of component $i$ , $\varphi_i$ is the fugacity coefficient $i$, $f_i$ is the fugacity of $i$ and $y_i$ is the molar fraction of $i$.

Equation 3.28 can be used to calculate fugacity for vapor, fluid and solid phases. The equation may be used to derive the following expression for calculating fugacity of the solid phase:

$$f_i^{solid} = P_i^{sub} \varphi_i^{sub} exp \left[ V_i^{solid} \left( \frac{P - P_i^{sub}}{RT} \right) \right] \tag{3.29}$$

where $P_i^{sub}$ is the sublimation pressure of $i$, $\varphi_i^{sub}$is the fugacity coefficient of $i$ at sublimation pressure, and $V_i^{solid}$ is the molar volume of solid $i$.

For this equation, it is assumed that the solid only forms at temperatures below the triple point temperature of component $i$.

### 3.4.2 Solid model 2: Fugacity based on sub-cooled liquid

This model is an expression for the two states of Gibbs energy difference (the fugacity ratio): the pure substance in the solid state and pure substance in an assumed liquid state. Both states are under the same conditions of temperature and pressure.

The equation is directly derived from the thermodynamic principles, by calculating partial molar Gibbs energy change between the solid and liquid phases, Pedersen, et al. [34]:

$$f_i^{\circ s}(P) = f_i^{\circ l}(P) \exp\left( -\frac{\Delta H_i^f}{RT} \left[ 1 - \frac{T}{T_i^f} \right] - \frac{\Delta C_{Pi}}{RT} \left( T_i^f - T \right) + \frac{\Delta C_{Pi}}{R} \ln \frac{T_i^f}{T} + \frac{\Delta V_i (P - P_{atm})}{RT} \right) \tag{3.30}$$

The term $f_i^{\circ solid}(P)$ is the reference fugacity of component $i$ in solid state at pressure P and $f_i^{\circ liquid}(P)$ is the reference fugacity of component $i$ in liquid state at pressure P. *Pressure P and temperature T is calculated from the fluid phase model.* $\Delta H_i^f$ is the heat of fusion at the triple point, $\Delta C_{Pi}$ equals the difference between the solid- and liquid heat capacities for component $i$

and $\Delta V_i$ is the difference between solid- and liquid phase molar volumes of component $i$. $T_i^f$ is the melting temperature of component $i$ and $P_{atm}$ is atmospheric pressure.

In wax/asphaltene precipitation, it is common to neglect the last term of equation 3.30, which is known as the poynting correction factor, [35] This term is often very small, because the molar volume difference for liquid-solid transition is very small. Unless the pressure is very high, this term can be neglected.

# 4. Evaluation of Experimental Data

The experimental data have been conducted by several scientists with different experimental methods. It is therefore important to compare the data to check the consistency of the experimental data. For each systems investigated the experimental method behind the data will be accounted for. The description of the different methods can be found in Appendix B.

## 4.1 Solid-liquid data on $CO_2$-methane rich mixtures

$CO_2$ is the main impurity in natural gas, and most of the solid-liquid investigations are therefore on these types of systems.

### 4.1.1 Solid-liquid and solid-liquid-vapor data for binary $CO_2$-methane system

Table 1 includes the available experimental data published in the literature for solid $CO_2$ formation in liquid methane.

**Table 1. Experimental data for solid $CO_2$ formation in liquid methane**

| Solvent | Temperature [K] | | Mole [%] | | Pressure [bar] | | Type | Exp. Method | Ref. |
|---|---|---|---|---|---|---|---|---|---|
| | Min | Max | Min | Max | Min | Max | | | |
| $CH_4$ | 90.92 | 215.37 | 0 | 100 | 9.51 | 48.51 | SL/SLV | AnT | Katz [36] |
| $CH_4$ | 111.5 | 128 | 0.03 | 0.15 | - | - | SL | - | Boyle [37] |
| $CH_4$ | 166.48 | 177.59 | 1.9 | 5.2 | - | - | SLV | AnT | Sterner [38] |
| $CH_4$ | 110.7 | 194.6 | 0.03 | 12.6 | - | - | SLV | AnT | Cheung [13] |
| $CH_4$ | 129.65 | 201.26 | 0.16 | 20.5 | 3.62 | 48.18 | SLV | SynVis | Davis [14] |
| $CH_4$ | 110 | 218.3 | 0.03 | 100 | - | - | SL | - | Streich [39] |
| $CH_4$ | 111.6 | 193.3 | 0.02 | 12.8 | - | - | SL | - | Voss [40] |
| $CH_4$ | 158.15 | 201.29 | 1 | 20 | 28.93 | 47.52 | SL/SLV | AnPT | Pikaar [41] |
| $CH_4$ | 129.6 | 214.3 | 0.16 | 90 | 3.57 | 20.79 | | Correlation | Kurata[41] |
| $CH_4$ | 112 | 169.9 | 0.00213 | 2.896 | 0.93 | 23.15 | | AnPT | Shen[16] |

#### 4.1.1.1 Experimental work behind the data

The publications behind the data obtained by Boyle [37], Streich [39] and Voss [40] were not available, and are therefore not evaluated. The experimental data are directly obtained from the DECHEMA data series. Three authors have used analytical isothermal methods (AnT) to get their data, but with three different techniques to achieve equilibrium in the cell. Donnelly and Katz [36] used a technique by rocking the cell, Cheung and Zander [13] by stirring the mixture, and Sterner [38] by recirculating the vapor phase. Pikaar [42] used the analytical isobaric-isothermal method (AnPT), to obtain the solid liquid equilibrium data, and he measured the fluid composition with an infra-red analyzer. Shen, et al. [16] applied the AnPT method and chromatography was used to measure the sampling. Davis, et al. [14] used a synthetic visual

method (SynVis), or cryoscopic method to obtain the SL data. The work from Kurata [41] is a correlation of some data points from Davis and Katz.

#### 4.1.1.2 Correction and validation of experimental data

Figure 7 present all the available experimental data for solid $CO_2$ formation in liquid rich methane mixture. The Y axis is in logarithmic scale and represents solid $CO_2$ mole percent in the liquid rich methane mixture. Figure 7 shows that the data from Streich [39] have a higher solubility in the area 130 K – 180 K. The data are inconsistent compared to the other data, and are therefore excluded. At 190 K the data points from Donnelly and Katz [36] differs from the other data at this point. These data points are also excluded. The few data points from Sterner [5] are scattered compared to Voss [40] and Davis, et al. [43], and these are removed. In temperature range 110 K- 130 K the data from Voss [40] and Shen, et al. [16] are more consistent compared to the others. In Figure 8 the experimental data for the three phase SLV locus are presented for the $CO_2$-methane system. As can be seen from the figure, the data correspond well, except for the inconsistent data from Donnelly and Katz [36] at 195K - 200K. These data points are removed. The data from Kurata [41] is a correlation of the data from Davis and Katz

The data from Shen, et al. [16], Davis, et al. [43] and Kurata [41] will be compared to the simulation results for the solid-liquid $CO_2$-methane system.

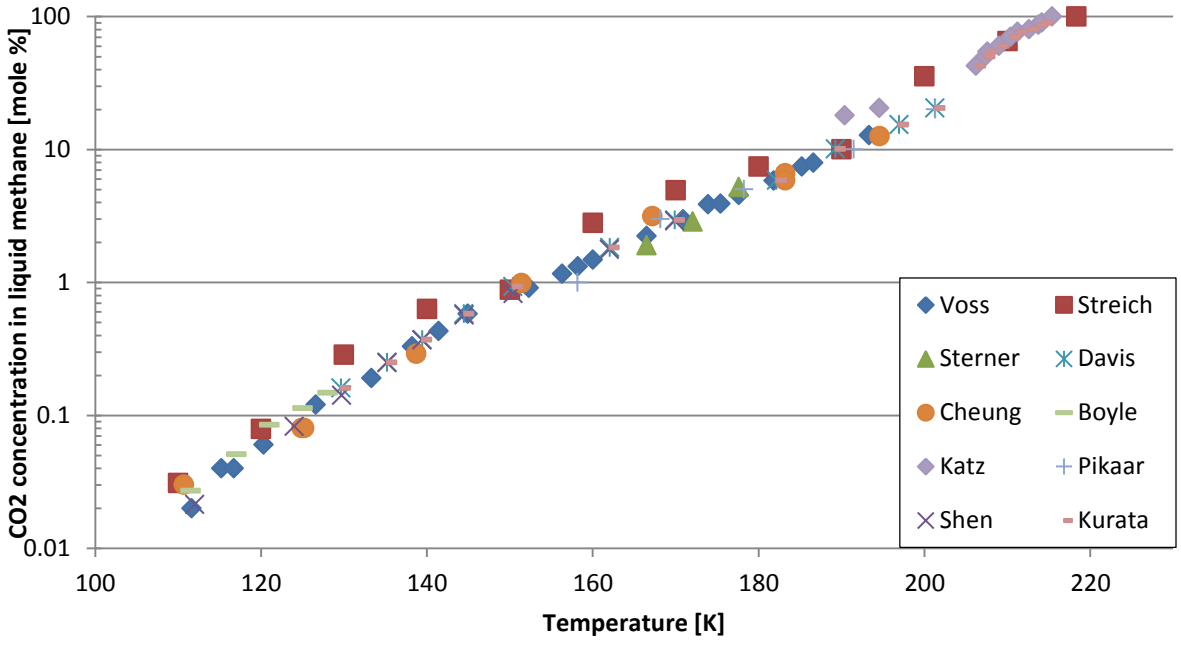


**Figure 7. Experimental SL and SLV data for the binary CO2-methane system**

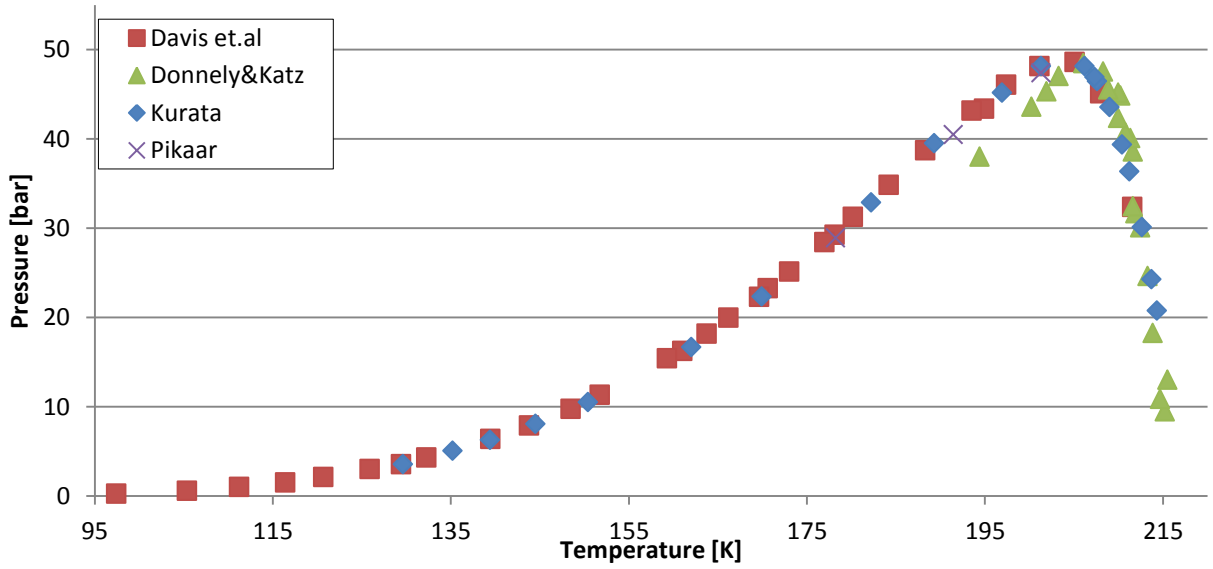


**Figure 8. Experimental SLV data for the binary $CO_2$-methane system**

### 4.1.2 Solid vapor data for $CO_2$-methane rich systems

Table 2 present the available experimental solid-vapor data for $CO_2$-methane rich systems.

**Table 2. Experimental data for solid CO2 formation in vapor methane**

| Solvent | Temperature [K] | | Mole [%] | | Pressure [bar] | | Type | Exp. Method | Ref. |
|---|---|---|---|---|---|---|---|---|---|
| | Min | Max | Min | Max | Min | Max | | | |
| $CH_4$ | 97.5 | 211.7 | 0.12 | 11.73 | - | - | SLV | AnT | Davis[43] |
| $CH_4$ | 113.15 | 210.15 | 1 | 20 | - | - | SV | SynNon | Pikaar [17] |
| CH4 + N2 | 137.5 | 198.1 | 0.12 | 10.67 | - | - | SV | SynVis | Agrawl[44] |
| $CH_4$ | 191.1 | 210.3 | 10.8 | 54.2 | - | - | SV | SynNon | Zhang[46] |
| CH4 + C2H6/N2 | 168.6 | 187.7 | 1 | 2.93 | - | - | SV | SynVis | Le[45] |

#### 4.1.2.1 Experimental work behind the data

The experimental data involving solid $CO_2$ formation in vapor methane rich mixtures are mostly frost point data. However, the data from Davis, et al. [43] are $CO_2$ formation taken along the SLV loci.

All authors have used non-sampling methods to obtain the solubility data, except Davis, et al. [43], who used a sampling method (AnT) and analyzed the samples with mass spectrometer. Agrawal and Laverman [44] and Le and Trebble [45] both used visual observation methods to obtain the data. Pikaar [17] used a synthetic non-visual method by investigating the p-T diagram. The experimental work by Zhang [46] was carried out in 2011 , and is probably one the most valuable sources of freeze point data for the $CO_2$-methane system. Zhang [46] used a synthetic non-visual method, where he recorded pressures and temperatures during the cooling and the

heating of the mixture. The intersecting point of the cooling line and heating line was taken as the frost points of the mixture, Zhang [46].

The experimental frost point data are taken at different $CO_2$ concentrations, which make it more difficult to verify the data. All of the experimental data will therefore be compared to the simulation results.

## 4.2 Solid-liquid data for HHC-methane rich mixtures

The traces of heavier hydrocarbons in natural gas can precipitate at low temperatures if it exceeds its solubility in the mixture. The experimental data represented here is for the components hexane, heptane, benzene, octane and cyclohexane in methane rich mixtures.

### 4.2.1 Solid-liquid and solid-liquid-vapor data for the binary hexane-methane system

Table 3 includes the available experimental data published in the literature for the binary hexane - methane system.

**Table 3. Experimental SL and SLV data for the binary hexane-methane system**

| Solvent | Temp. [K] | | Mole fraction | | Pressure [bar] | | Type | Exp. Method | Ref. |
|---|---|---|---|---|---|---|---|---|---|
| | Min | Max | Min | Max | Min | Max | | | |
| $CH_4$ | 90.03 | 178.71 | 0 | 1 | - | - | - | SynVis | Beck [47] |
| $CH_4$ | 162.88 | 177.80 | 0.195 | 1 | <0.0026 | 65.5 | SL/SLV | SynVis | Shim [50] |
| $CH_4$ | 161.3 | 176.2 | 0.062 | 0.915 | - | - | SLV | SynNon | Dickin.[48] |
| $CH_4$ | 138 | 164 | 4.22E-03 | 0.034 | 5.80 | 17.01 | SLV | SynVis | Luks[49] |
| $CH_4$ | 93.8 | 163.7 | 3.49E-05 | 0.15 | 68.99 | 130.27 | SL | AnPT | Kueble[50] |
| $CH_4$ | 103.4 | 150 | 1.37E-04 | 1.14E-05 | - | - | SL | AnPT | Neuma[51] |

#### *4.2.1.1 Experimental work behind the data*

Most of the solubility data have been obtained at the solid-liquid-vapor (SLV) equilibrium state. However, Kuebler and McKinley [50] and Neumann and Mann [51] obtained the data at the solid-liquid equilibrium state. Shim and Kohn [52] and Luks, et al. [49] and Beck, obtained from [47], used synthetic visual methods to obtain their data. Dickinson, et al. [48] used a non-visual method by investigating the cooling curve. Neumann and Mann [51] used an analytical method where he prepared the solution by mechanical stirring. Kuebler and McKinley [50] used a single-pass method, where the solvent flows through the solute and dissolves the solute.

The solubility is sensitive to extremely large changes in pressure, but for solid-liquid transition the change in volume is very small, which makes the pressure effect small. Shim and Kohn [22] studied the effect of the pressure change for the solid-liquid phase behavior. They reported that

the freezing points are increased to higher temperatures when the pressure is increased. This means that the solubility of hexane in liquid methane is decreased when the pressure is increased.

#### *4.2.1.2 Correction and validation of experimental data*

Figure 9 represents the available experimental data for the binary hexane-methane system. The Y axis is solid hexane mole percent in liquid methane, presented in a logarithmic scale. The X axis represents the temperature range. From Figure 9 it can be observed that some of the data obtained from Beck are in inconsistent with the rest of the data. The data from Beck are therefore excluded when comparing the experimental data with the modelling results. The rest of the data are consistent, but scattered points from 160 K to 165 K can be noticed. This temperature area is close to the maximum pressure along the three-phase line, where the two separate SLV lines converge together. In the article by Shim and Kohn [22] they commented this, and noticed that the composition is extremely sensitive to temperature in this region. This may be the reason for the uneven solubility values in this area.

Experimental data Shim and Kohn [22], Kuebler and McKinley [50] and Luks, et al. [49] will be compared against the simulation results for the binary hexane-methane system.

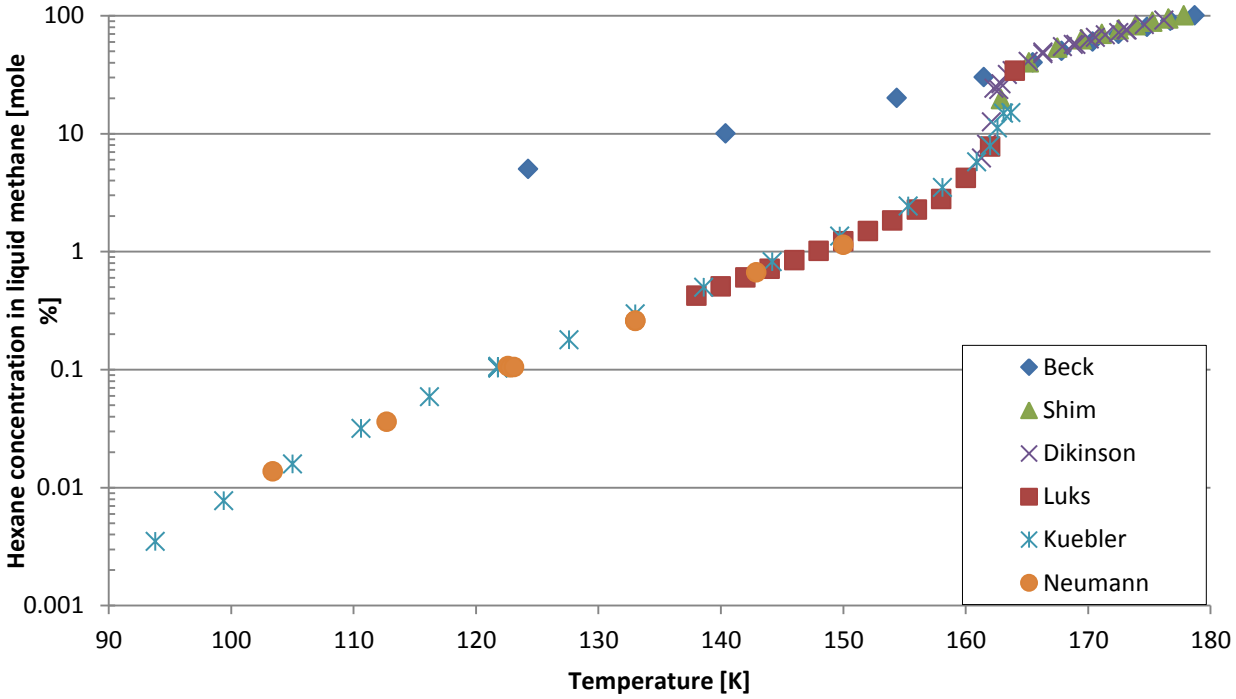


**Figure 9. Experimental SL and SLV data of the binary hexane-methane system**

## 4.2.2 Solid-liquid and solid-liquid-vapor data for heptane-methane rich mixtures

Table 4 contains available experimental data for heptane-methane rich mixtures.

**Table 4. Experimental SL and SLV data for heptane-methane rich mixtures**

| Solvent | Temperature [K] | | Mole fraction | | Pressure [bar] | | Type | Exp. Method | Ref. |
|---|---|---|---|---|---|---|---|---|---|
| | Min | Max | Min | Max | Min | Max | | | |
| $CH_4$ | 131 | 181 | 7.72E-04 | 0.903 | 3.7 | 21.87 | SLV | SynVis | Tiffin[53] |
| $CH_4$ | 94.2 | 166.5 | 9.10E-06 | 0.0237 | 5.61 | 95.8 | SL | AnPT | Kuebler[7] |
| $CH_4$ | 103.2 | 150 | 4.50E-03 | 0.32 | - | - | SL | ANPT | Neuma[51] |
| $CH_4$ + $C_2H_6$ | 146.1 | 170 | 6.06E-03 | 0.4183 | 7.75 | 18.1 | SLV | SynVis | Tiffin[53] |

### *4.2.2.1 Experimental work behind the data*

Two different experimental methods have been used to obtain these data. Tiffin, et al. [53] used a cryoscopic method (syntetic visual method) to obtain solubility data along the SLV curve. Kuebler and McKinley [7] and Neumann and Mann [21] obtained SL data with analytical methods, as described earlier, 4.3.1.1.

### *4.2.2.2 Correction and validation of experimental data*

In Figure 10 the experimental data are plotted to check the consistency from the different authors. The Y axis is in logarithmic scale and represents heptane mole percent in liquid methane. The figure shows that the data are matched reasonably well for the low temperature range in mind. However, it can be noticed that the SL data obtained by Kuebler and McKinley [7] gives a higher solubility compared to the data obtained by Tiffin, et al. [53] and Neumann and Mann [51]. This can probably be explained by their method of over pressuring their system (up to 95.8 bar), giving SL data for compressed liquid methane. The consequence of the high pressure and the compressed liquid methane are therefore lower freezing points. Also shown in Figure 10 is the quadruple point, occuring at 169.35 K. At this point there is a "jump" in the benzene concentration, to a leaner concentration, see section 2.2.1.2 Type B phase behavior.

The experimental data from Kuebler and McKinley [7] and Tiffin, et al. [53] will be compared to the simulation results for the hexane-methane system.

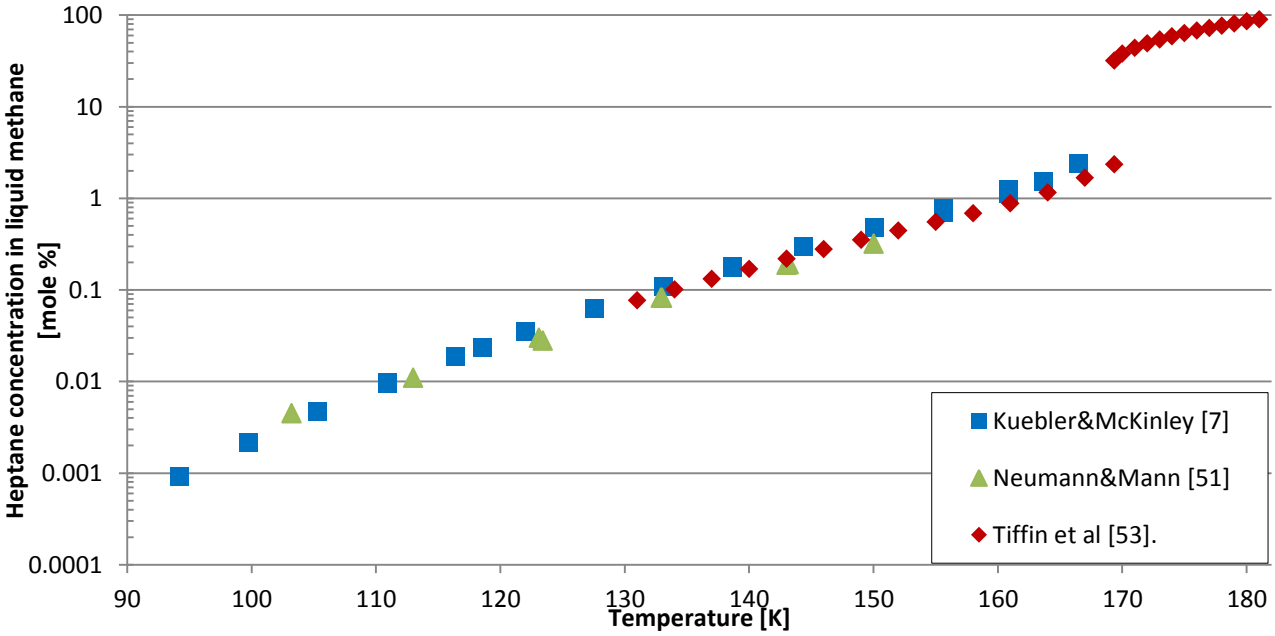


**Figure 10. Experimental SL and SLV data of the binary heptane-methane system**

In the published article by Tiffin, et al. [53] they also present experimental data for a ternary SLV system containing methane-ethane-n-heptane, with a methane/ethane solvent mixture ratio 8:1. This system is presented in Figure 11, where it is compared to the binary SLV system of methane-n-heptane. Figure 11 shows that the addition of ethane, increases the solubility of heptane in the liquid methane-heptane-ethane mixture. This is because the molecular structure of heptane is more similar to ethane compared to methane.

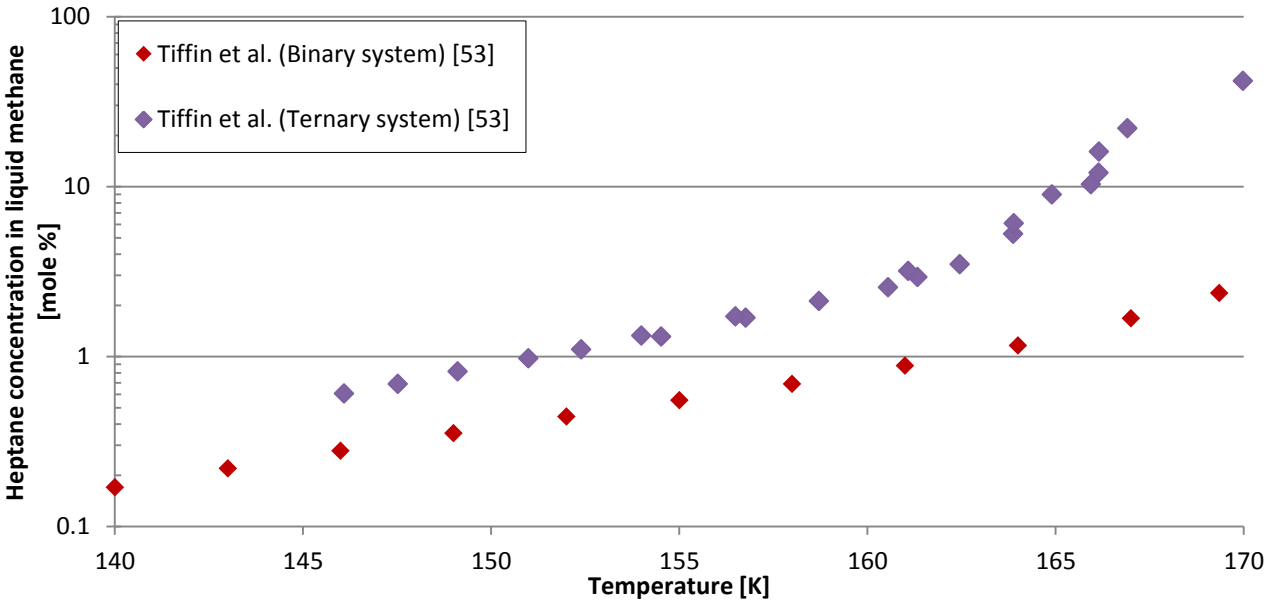


**Figure 11: Experimental SLV data of the methane-heptane and methane-heptane-ethane mixture**

### 4.2.3 Solid-liquid and solid-liquid-vapor data for the binary benzene-methane system

Table 1 contains the available experimental data for the binary benzene - methane system.

**Table 5. Experimental SL and SLV data for the binary benzene-methane system**

| Solvent | Temperature [K] | | Mole [%] | | Pressure [bar] | | Type | Exp. Method | Ref. |
|---|---|---|---|---|---|---|---|---|---|
| | Min | Max | Min | Max | Min | Max | | | |
| $CH_4$ | 99.4 | 199.8 | 3.90E-05 | 1.40E-01 | 54.1 | 136.8 | SL | AnPT | Kuebler [7] |
| $CH_4$ | 165 | 277.7 | 1.10E-02 | 9.82E+01 | 10 | 170 | SLV | SynVis | Luks[49] |
| $CH_4$ | 103.8 | 185.4 | 6.00E-04 | 4.83E-02 | - | - | SL | AnPT | Neum[51] |
| $CH_4$ | 148.05 | 177.95 | 3.09E-03 | 2.60E-02 | - | - | - | - | Teller[54] |
| $CH_4$ | 264.95 | 278.45 | 8.04 | 100 | 0.05 | 539.81 | SL/SV | SynVis | Rijkers[18] |

#### *4.2.3.1 Experimental work behind the data*

The three phase locus of the benzene-methane system was studied by Luks et al [49]. He obtained the data with a visual observation (SynVis) method. Figure 13 shows two SLV branches, one at low temperature and one at high temperature, which also can be recognized in Figure 5, section 2.2.3. This behavior occurs since benzene has a much higher triple-point temperature (278.7) than the critical temperature of methane (190.56 K). This also gives a critical point for the high temperature branch at a very high pressure level. The first critical locus point, referred to as K-point, is found at 190.5 K. The second K-point was not located by Luks et al [49], but the point was found by Rijkers, et al. [18] at 539.81 bar.

The experimental work by Teller and Knapp [54] is unpublished, and it is therefore not evaluated. The work by Rijkers, et al. [18] was the only source found concerning solid formation of heavy hydrocarbons in vapor methane. They used a synthetic visual observation method to determine the solid formation in both the vapor phase and the liquid phase. The work by Kuebler and McKinley [7] and Neumann and Mann [51] are the same as explained in 4.3.1.1.

#### *4.2.3.2 Correction and validation of experimental data*

Figure 12 presents all the available experimental SL and SLV data for the benzene-methane system at low temperatures. The Y axis is in logarithmic scale and represents benzene mole percent in liquid methane. The agreement is reasonably good between the data from Neumann and Mann [51] and Kuebler and McKinley [7]. However, at low temperatures the deviation starts increasing, and it also seems that the data from Neumann and Mann [51] are more linear than the data from Kuebler. Their work is based on the same experimental method, and they both have SL data at high pressures. The data from Teller and Knapp [54] follows the data from Kuebler and McKinley [7], but with lower solubility. The solubility data from Luks et al [49] are taken along the SLV loci. Figure 12 shows that the solubility data from Luks et al [49] are flattening out as the first K-point is approached. For the last data point the solubility has decreased, while the temperature have increased, Compared to the rest of the data there are large deviations at this

point. The reason for this behavior is explained in the work by Kohn and Luks [55]. The K-point (190.5 K) is very close to the critical point of pure methane (190.564 K). Thus the liquid phase begins to expand rapidly as the K-point is neared, accompanied by a drop in the solute solubility in that phase. This also makes the solubility very pressure sensitive in this area. Kohn and Luks [55] explains further that other authors take their data at higher pressure levels, which will be over this critical area.

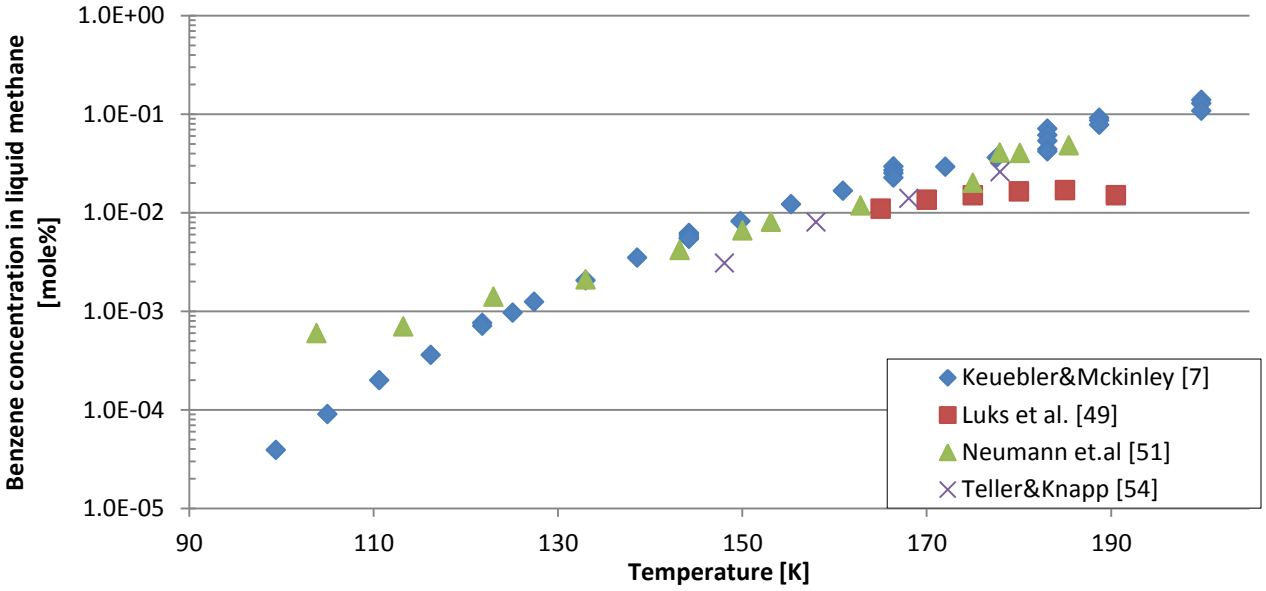


**Figure 12. Experimental SL and SLV data for the binary benzene-methane system**

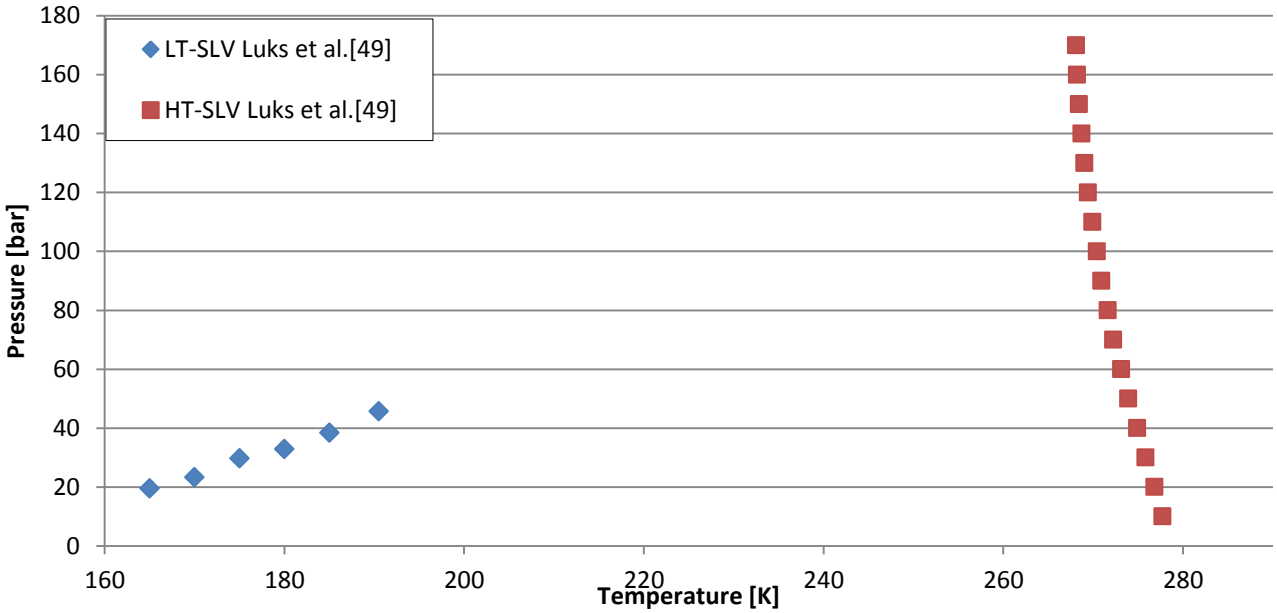


**Figure 13. Experimental data of the three-phase locus of the binary benzene-methane system**

### 4.2.4 Solid-liquid and solid-liquid-vapor data for octane-methane rich systems

Table 6 contains the available experimental SL and SLV data for octane - methane rich systems.

**Table 6. Experimental SL and SLV data for octane- methane rich systems**

| Solvent | Temperature [K] | | Mole [%] | | Pressure [bar] | | Type | Exp. Meth. | Ref. |
|---|---|---|---|---|---|---|---|---|---|
| | Min | Max | Min | Max | Min | Max | | | |
| $CH_4$ | 90.93 | 216.32 | 0 | 100 | - | - | SL | - | Brewer [47] |
| $CH_4$ | 156 | 191.15 | 0.0214 | 0.0592 | 13.4 | 45.9 | SLV | SynVis | Kohn et al. [57] |
| *$CH_4$ | 155 | 192.2 | 0.021 | 0.085 | 13.8 | 48.7 | SLV | SynVis | Kohn [4] |
| $CH_4$ | 165 | 191.15 | 0.0068 | 0.038 | 45.9 | 19 | SLV | SynVis | Kohn [4] |
| $CH_4$ | 109.9 | 150.13 | 0.00043 | 0.00307 | - | - | - | - | Teller[55] |
| *$CH_4$ | 165.55 | 216.5 | 44 | 100 | 20 | 46.07 | SLV | SynVis | Bradish[56] |
| $CH_4$ + $C_2H_6$ | 162.37 | 192.42 | 0.838 | 0.787 | 15.13 | 39.67 | SLV | SynVis | Tiffin [59] |
| $CH_4$ + $C_2H_6$ | 159.28 | 192.79 | 0.086 | 1.261 | 13.62 | 39.50 | SLV | SynVis | Kohn[4] |

*Pure methane (99 mole %)

#### *4.2.4.1 Experimental work behind the data*

The data from Brewer and Kurata [47] originates from the work by Papahronis. The work behind the data from Teller [55] was unfortunately not available, and thus not evaluated. The rest of the experimental data were obtained using cryoscopic techniques, see appendix B.2.1. The methane used in the different studies has mainly been "ultra pure" grade (99.97 mol%). However, in the work by Kohn and Luks [4] and Kohn and Bradish [56] pure grade methane (99 mole %) was also studied. The effect of purity on the systems is discussed later.

#### *4.2.4.2 Correction and validation of experimental data*

In Figure 14 and Figure 15 all the available experimental data for the low temperature binary octane methane system are shown. The Y axis is in Figure 14 in logarithmic scale and represents octane mole percent in liquid methane. Figure 15 shows the Pressure-Temperature diagram of the SLV three-phase loci. The only data available for very low octane concentrations are those from Teller. The figure shows that these data points are uneven and scattered. It's therefore difficult to give any validation for these points. They will however still be compared to the simulation results, since they roughly indicates where the freeze out will occur.

The agreements between the data from Kohn, et al. [57] and Kohn and Luks [4] are good , both with "ultra pure" methane. There are some deviations near the K-point, where the data from Kohn and Luks [4] gives higher solubility. It is clear from the figure that the solubility increases when a lower grade of methane is used. This probably means that more octane has disolved due to the precence of impurities Figure 14 shows that the octane concentration increases with

increasing temperatures but drops off as the K-point is approached. The reason for this behavior is that the K-point is close to the critical point of pure methane. Thus the liquid phase begins to expand rapidly as the K-point is neared, accompanied by a drop in the solute solubility in that phase. Kohn and Luks [58].

The experimental data for the octane-methane system are very limited. There are few data sets, and most of it is gathered from the same authors. The collected data will be compared do the simulation results for the octane-methane system. However, more experimental are required in order to validate the thermodynamic models thorughly.

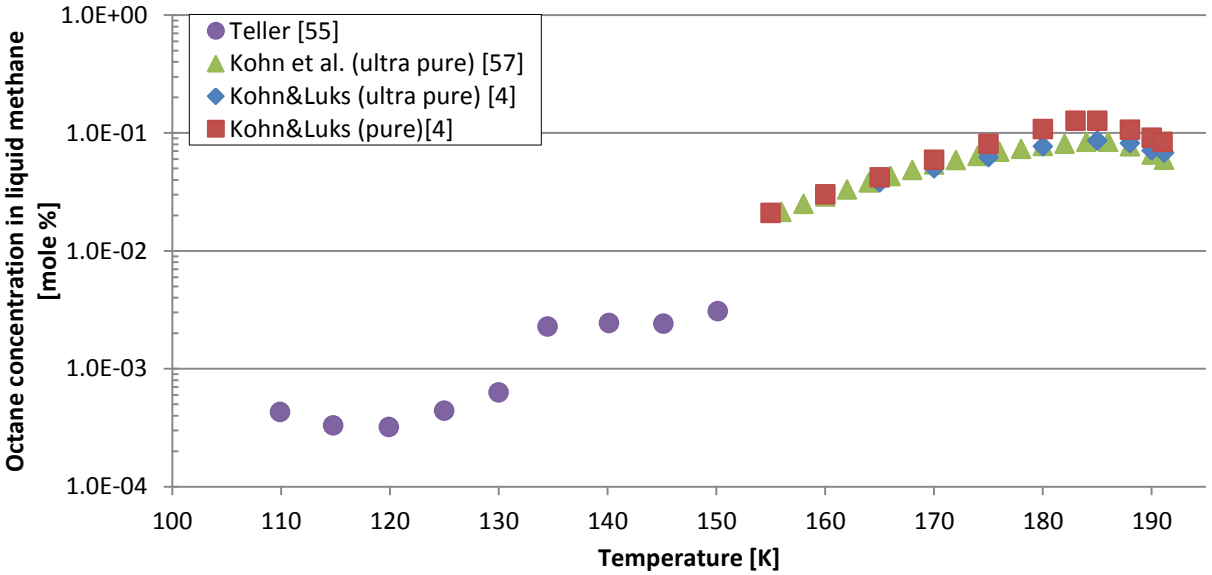


**Figure 14. Experimental SL and SLV data for the binary octane-methane system**

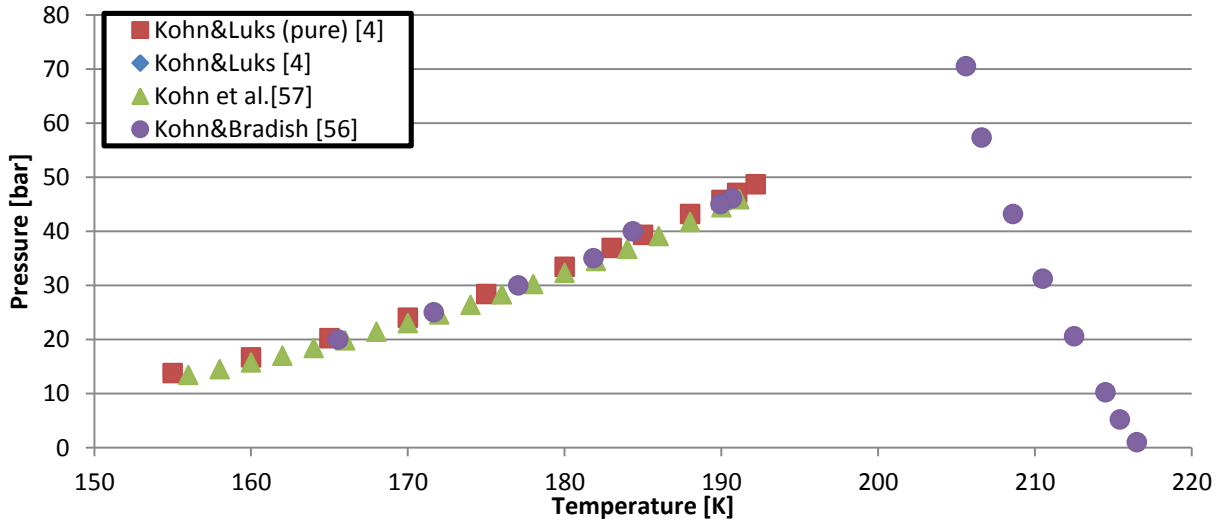


**Figure 15 Experimental data of the three-phase locus of the binary octane-methane system**

### 4.2.5 Solid-liquid-vapor data for cyclohexane-methane rich systems

Table 7 contains the available experimental SLV data for cyclohexane-methane rich systems.

**Table 7. Experimental SLV data for cyclohexane-methane rich systems**

| Solvent | Temperature [K] | | Mole [%] | | Pressure [bar] | | Type | Exp. Method | Ref. |
|---|---|---|---|---|---|---|---|---|---|
| | Min | Max | Min | Max | Min | Max | | | |
| $CH_4$ | 154 | 279.83 | 0.31 | 100 | 54.1 | 136.8 | SLV | SynVis | Kohn [57] |
| CH4 + C2H6 | 136.3 | 177.85 | 0.538 | 6.19 | 23.16 | 3.75 | SLV | SynVis | Tiffin[59] |

Experimental data for cyclohexane-methane rich systems are very limited. The only data obtained for the binary cyclohexane – methane system is the work by Kohn, et al. [57]. Tiffin, et al. [59] has done experimental work on a methane-ethane-cyclohexane system, but for rater high ethane concentrations, 20-30 %. To evaluate the thermodynamic models properly, new experimental data are required.

There are some interesting remarks worth mentioning for this system. Figure 16 shows the same phenomenon as discovered in the benzene-methane system and octane-methane system. The solubility starts to decrease as the K-point is approached. The same explanation applies here, see 4.2.4.2. However, an interesting observation is that cyclohexane is more soluble in methane compared to octane and benzene. This is illustrated in Figure 16. All of the three components belong to the A type system, see 2.2.1.1. However, as it can be seen in Figure 17, the locus of the high temperature branch bends towards the low temperature branch. This phase behavior is similar to the phase behavior of hexane-methane and heptane methane system. Proceeding below 200 K, the locus starts rising sharply to high pressure, which is similar behavior as benzene and octane.

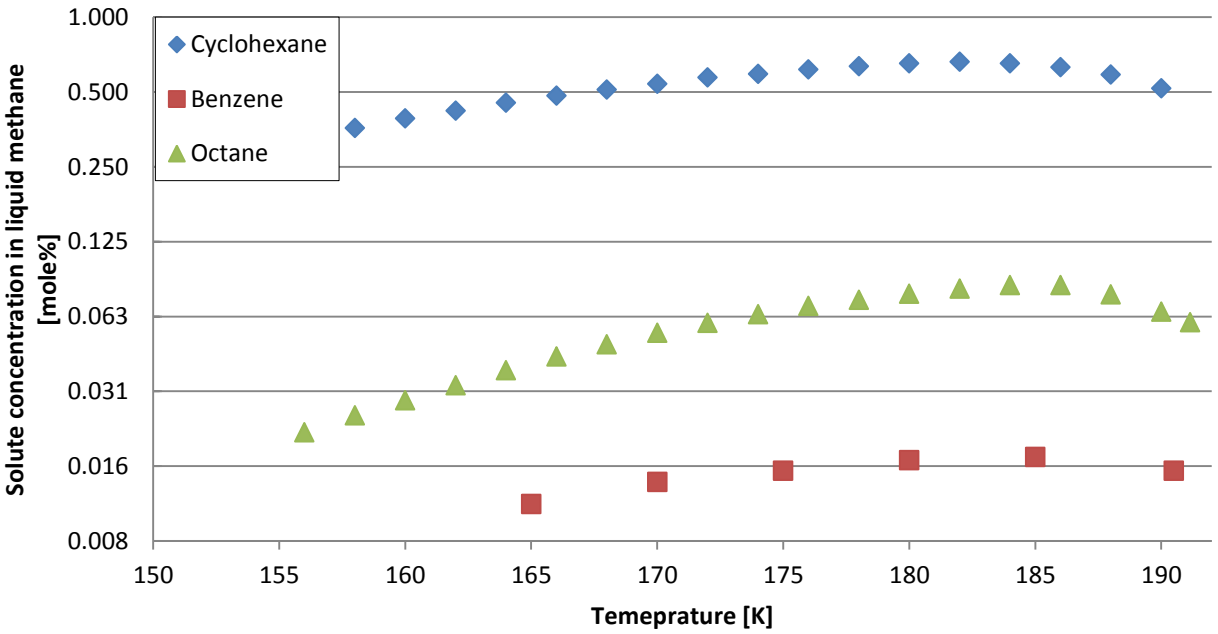


**Figure 16. Experimental SLV data for the binary cyclohexane-methane system compared to the benzene-methane system and octane-methane system**

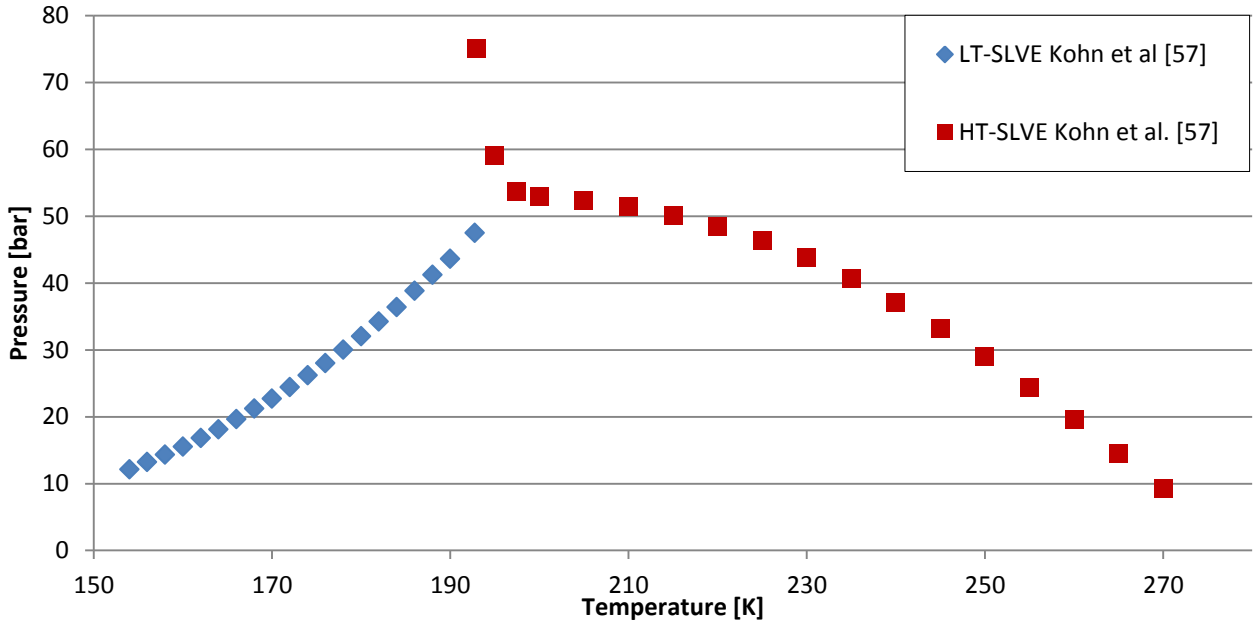


**Figure 17. Experimental data of the three-phase locus of the binary cyclohexane-methane system**

# 5. Modelling Results

## 5.1 Introduction

This chapter gives the modeling results by using the thermodynamic models UMR-PRU, SRK EoS and sPC-SAFT EoS. The model for calculating the fugacity in the solid phase is the solid model 2 based on sub-cooled liquid, given in equation 3.30. Table 8 shows the parameters that have been used in SRK EoS, sPC-SAFT EoS and the solid model 2.

For the solid model 2 (eq.3.30), the difference in heat capacity is set like the heat capacity of water. The effect of this is small, since the two terms with $\Delta C_{Pi}$ approximately cancel each other out. The last term of the equation has been neglected. This is a reasonable assumption, since the difference in molar volume between the solid phase and liquid phase are hardly noticeable.

**Table 8. Parameters used in the SRK EoS and sPC-SAFT EoS and the solid model 2.**

| SRK EoS [Appendix D] | | | sPC-SAFT EoS [29] | | | | Solid model 2, eq. 3.29 [App. D] | | | |
|---|---|---|---|---|---|---|---|---|---|---|
| Pc [bar] | Tc [K] | ω [-] | M [g/mol] | m [-] | U [Å] | /k [K] | $T_i$ [K] | ΔH [J/mol] | $\Delta C_p$ [J/molK] | ΔV [$m^3$/mol] |
| 45.99 | 190.56 | 0.01 | 16.04 | 1.00 | 3.70 | 150.0 | 90.69 | 941.4 | 37.12 | 0 |
| 73.83 | 304.21 | 0.22 | 44.10 | 1.31 | 3.25 | 92.2 | 216.58 | 9019 | 37.12 | 0 |
| 30.25 | 507.60 | 0.30 | 86.17 | 3.06 | 3.79 | 236.8 | 177.83 | 13080 | 37.12 | 0 |
| 27.40 | 540.20 | 0.35 | 100.20 | 3.48 | 3.80 | 238.4 | 182.57 | 14050 | 37.12 | 0 |
| 48.95 | 562.05 | 0.21 | 78.14 | 2.47 | 3.64 | 287.4 | 278.68 | 9866 | 37.12 | 0 |
| 24.90 | 568.70 | 0.40 | 114.23 | 3.81 | 3.83 | 242.8 | 216.38 | 20740 | 37.12 | 0 |
| 40.80 | 553.80 | 0.21 | 84.16 | 2.53 | 3.85 | 278.1 | 279.69 | 2740 | 37.12 | 0 |

The simulation tool used for the modelling is the Non-Equilibrium Simulator (NeqSim). The NeqSim program is developed by Even Solbraa at the Norwegian University of Science and Technology. NeqSim is based on rigorous thermodynamic and fluid mechanic models.

### 5.1.1 Comparison of experimental data and simulation results

The simulation results from the different systems will be compared to the experimental data evaluated in chapter 4. The method used for comparison between the predictions and experimental data is average absolute deviation AAD, giving in equation 5.1 and 5.2. For comparison of solid-liquid data, equation 5.1 will give the AAD in freezing point temperatures [K]. For comparison of solid-liquid-vapor data, both eq. 5.1 and eq. 51 can be used. Equation 5.1 will give then give AAD between predictions and experimental data relative to temperature (temperatures along the SLV loci), and equation 5.2 will give the AAD% relative to pressure (pressures along the SLV loci).

$$AAD = \frac{1}{n}\sum_{i=1}^{n}\left|\left(T_i^{calc} - T_i^{exp}\right)\right| \tag{5.1}$$

$$AAD\% = 100\frac{1}{n}\sum_{i=1}^{n}\left|\frac{P_i^{calc} - P_i^{exp}}{P_i^{exp}}\right| \tag{5.2}$$

## 5.2 Simulation results for $CO_2$-methane rich mixtures

The section includes the freeze out predictions of solid $CO_2$ in vapor and liquid methane rich mixtures. It was attempted to do simulations with the sPC-SAFT EoS. However, due to a lot of simulation problems occurring in NeqSim, this was not possible. This section therefore only includes simulation results done with UMR-PRU and SRK EoS.

### 5.2.1 SL and SLV data for the binary $CO_2$-methane system

#### 5.2.1.1 Predictions by UMR-PRU and SRK EoS without interaction parameter

Figure 18 and Figure 19 shows the predictive behavior of UMR-PRU and SRK for the binary $CO_2$-methane system. To check the predictive strength of SRK, the binary interaction parameter is set to zero. As seen from the first figure, SRK is not able to give any freeze out predictions compared to the experimental data. The UMR-PRU model is however able to give reasonable results, with AAD 1.85 K compared to the data from Kurata [41]. However, this is for a temperature range from 130 K - 214 K. At a lower temperature range the deviations starts to increase. Compared to the data from Shen, et al. [16] the AAD is 4.4 K at temperature range 112 K – 148.3 K.

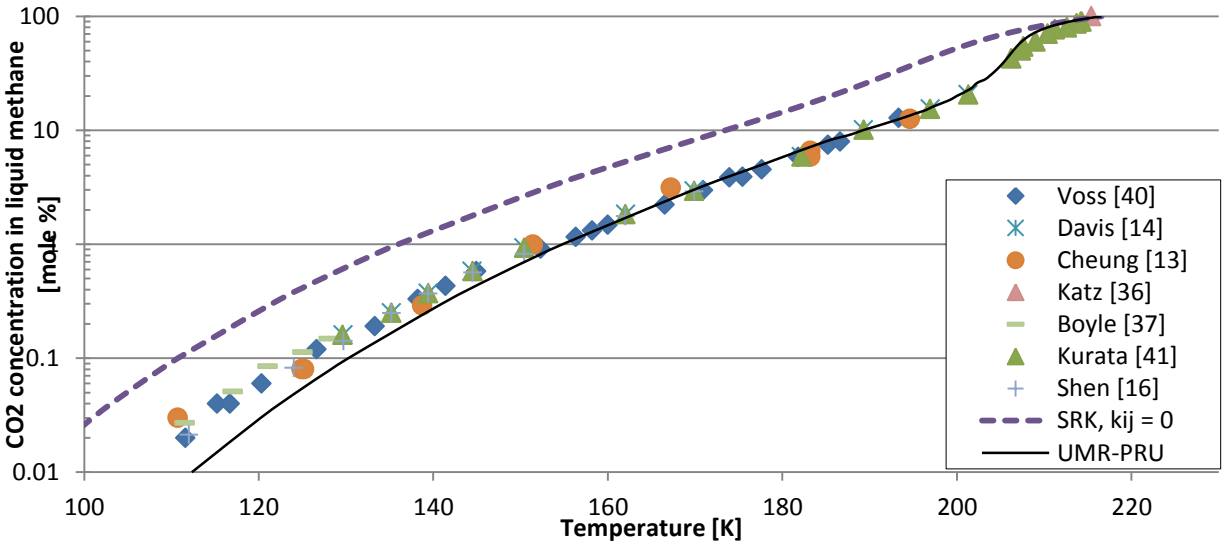


**Figure 18. Freezing point predictions by UMR-PRU and SRK EoS without $k_{ij}$ for the binary $CO_2$-methane system**

Figure 19 shows the simulated behavior of the SLV three-phase loci, where the pressures along the SLV loci have been predicted. SRK is unable to predict the pressures along the SLV three-phase loci. UMR-PRU however, gives accurate predictions where the AAD for pressures is 2.9%, compared to Kurata [41] .

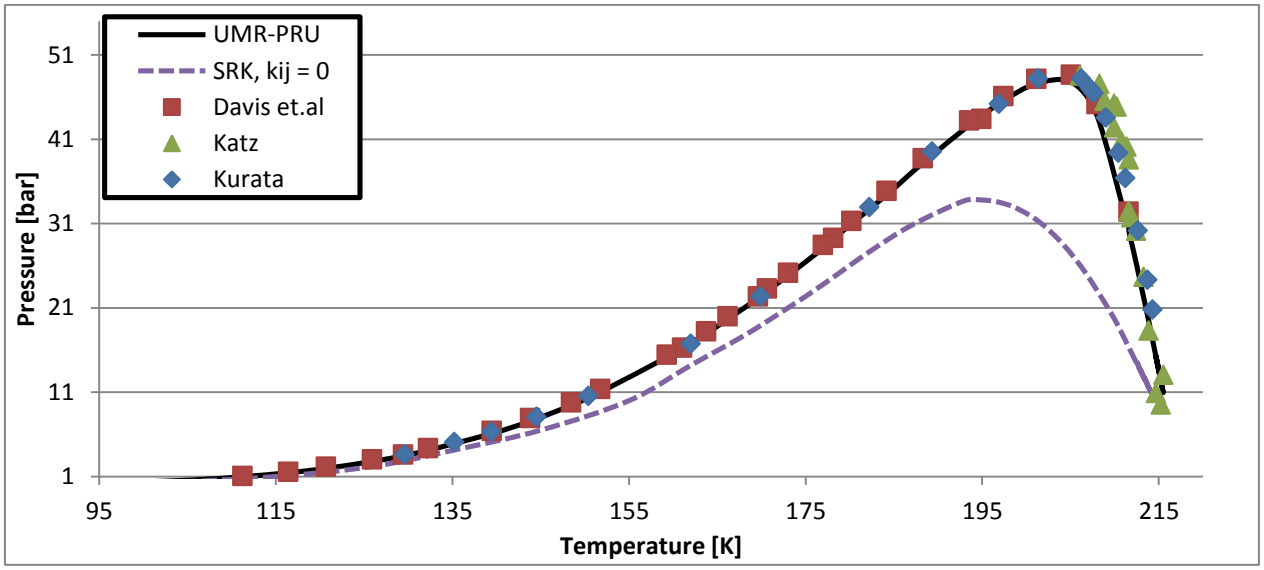


**Figure 19. Predictions of the three-phase SLV loci by UMR-PRU and SRK EoS for the binary $CO_2$-methane system**

### 5.2.1.2 Prediction by SRK EoS with interaction parameter

The binary interaction parameter was found in the NeqSim library, which is set to $k_{ij} = 0.0973$. Figure 20 and Figure 21 shows the predictions with the interaction parameter. SRK is now able to give reliable predictions for the whole temperature range. The AAD is 1.17 K compared to the data from Kurata [41], and AAD = 0.86 K compared to the data from Shen, et al. [16].

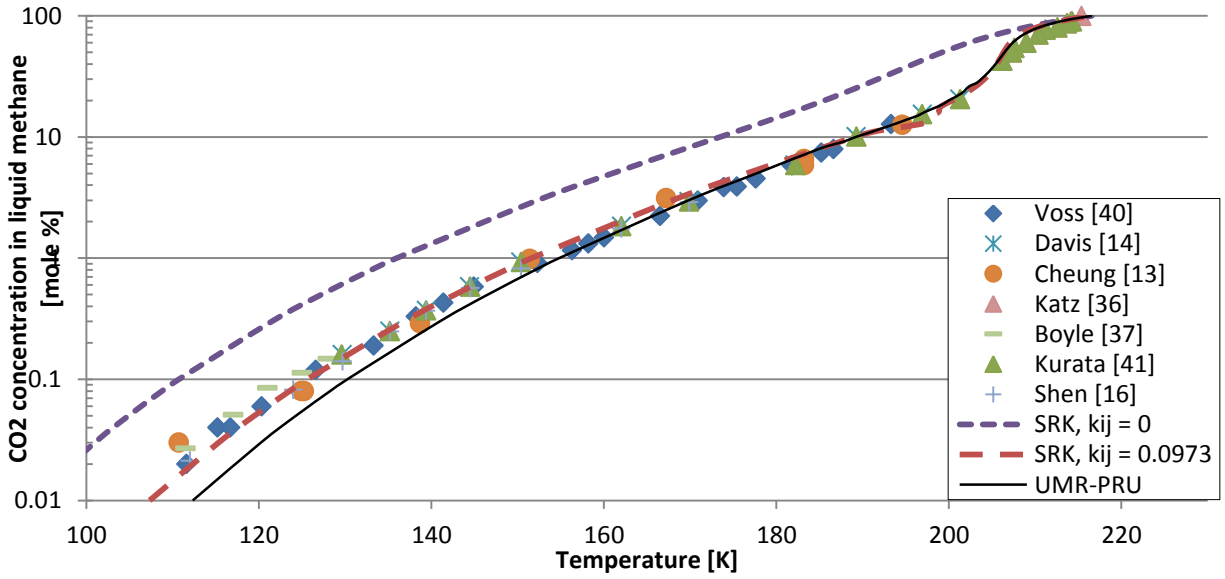

**Figure 20. Freezing point predictions with interaction parameter for the binary $CO_2$-methane system**

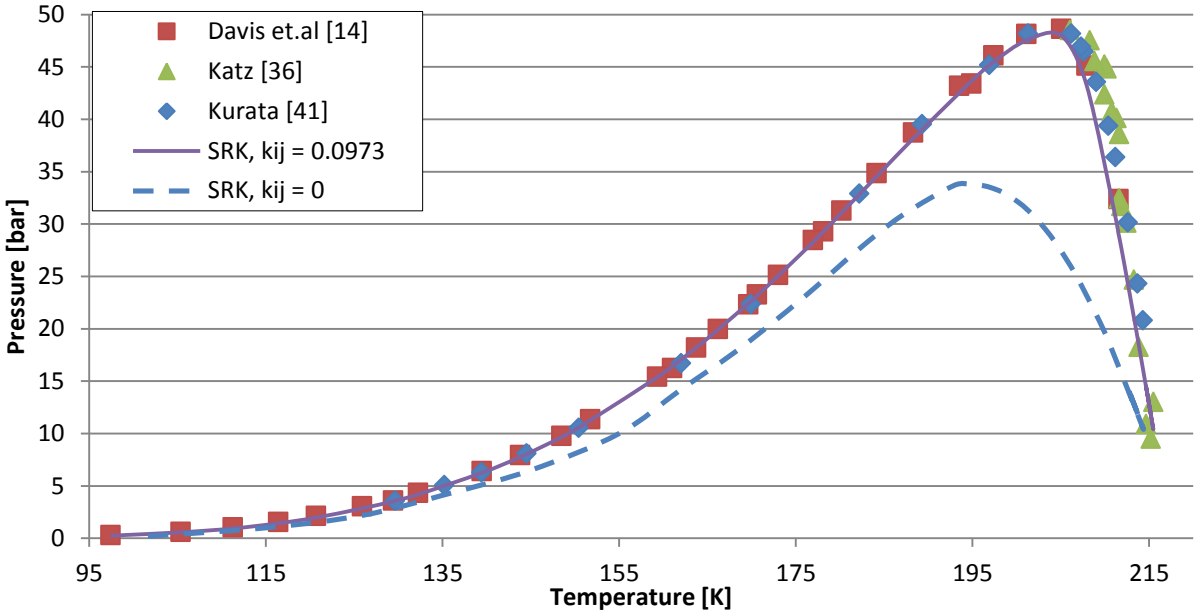


**Figure 21. Prediction of the three-phase SLV loci with interaction parameter for the $CO_2$-methane system**

### 5.2.1.3 Comparison of UMR-PRU and optimal SRK model

Figure 22 shows the freezing lines of $CO_2$ at different concentrations and pressures predicted by SRK EoS and UMR-PRU. It is clear from the figure that the pressure has a very small effect on the solubility of $CO_2$ in liquid methane. This is because the solid-liquid transition represents a very small change in volume. However, it can be noticed that this effect starts increasing when the maximum SLV loci is approached. This might be explained by the fact that the critical point of methane (46 bar, 190.58 K) is approached. The liquid methane vapor line may have an effect on the density in this area, and thus the solubility will be sensitive to the pressure.

Previously in Figure 20, it was shown that the SRK EoS with interaction parameter is able to give good predictions of the freezing temperatures at low temperatures. The UMR-PRU however started to predict poorer at lower temperatures. Figure 22 illustrates this in a temperature-pressure diagram. The deviation between SRK EoS and UMR-PRU starts to increase the temperature is decreasing. Here, SRK EoS represents a good correlation of the experimental data. It comes clear that the UMR-PRU model has problems predicting the freeze out at lower temperatures. This problem will be reflected in the discussion part.

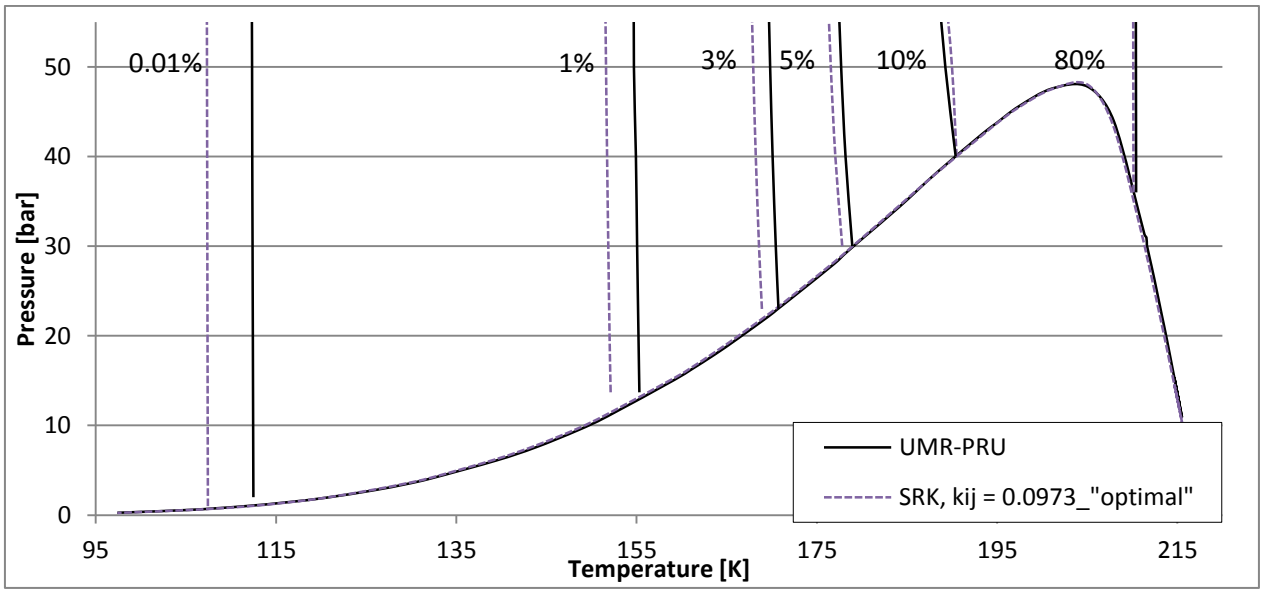


**Figure 22. Freezing point predictions by UMR-PRU and SRK at different concentration and pressure levels**

### 5.2.1 SL and SLV data for the binary $CO_2$-methane system

The simulations with SRK EoS for the solid-vapor system are done with same binary interaction parameters as applied for the solid-liquid predictions.

#### 5.2.1.1 Frost point predictions by SRK EoS and UMR-PRU for the $CO_2$-methane system

Figure 23 shows the frost point predictions by UMR-PRU and SRK EoS compared to experimental data. The simulation is done for the $CO_2$ concentrations indicated in the figure. The simulation result seems to be a good correlation of the experimental data. However, the UMR-PRU model has problems predicting the frost points when the $CO_2$ concentration is lowered.

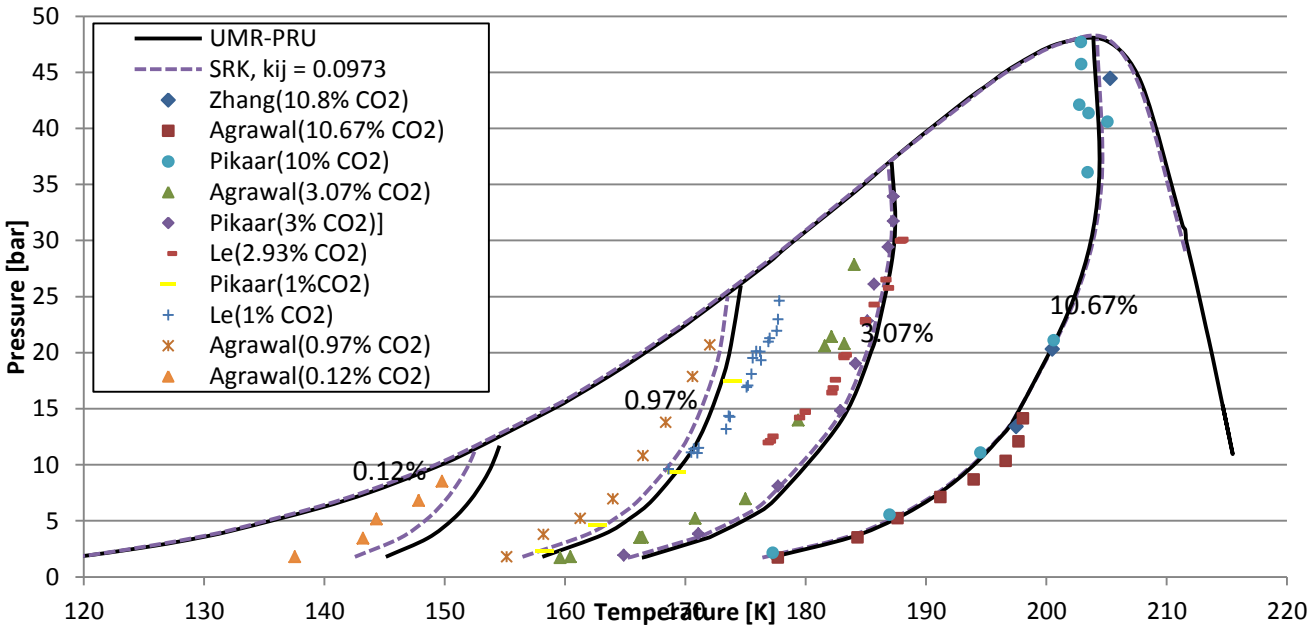


**Figure 23. Frost point predictions by UMR-PRU and SRK EoS compared to experimental data from: Zhang [46], Agrawal [44], Pikaar [41] and Le [45]**

Figure 24 shows the p-T diagram for the frost point predictions compared to the work by Zhang [46]. Both UMR-PRU and SRK EoS are able to give reasonable results. SRK gives an average absolute deviation of 0.698 K and UMR-PRU gives AAD 0.697 K.

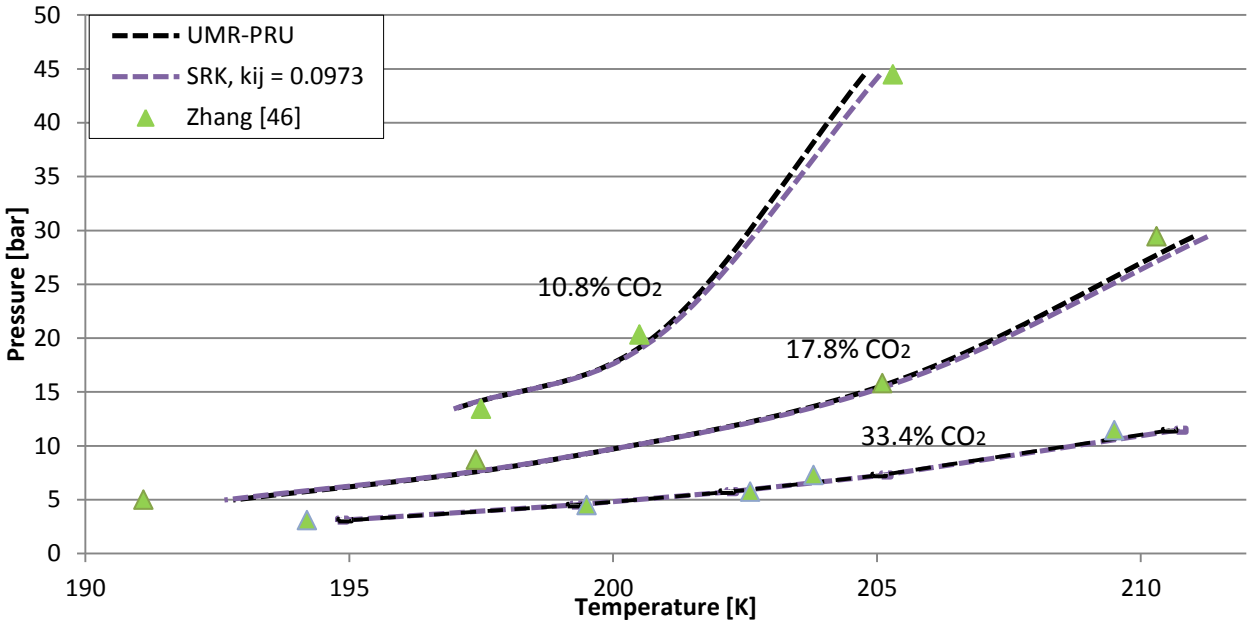


**Figure 24. Frost point predictions by UMR-PRU and SRK EoS compared to experimental data from Zhang [46]**

### 5.2.2 Predictions of solid $CO_2$ formation in vapor methane along the three-phase loci

Figure 25 shows the simulation results for $CO_2$ freezing points along the SLV loci in a vapor rich methane mixture, by SRK and UMR-PRU. The results are compared to the data from Davis, et al. [43] and 1 point from Agrawal and Laverman [44]. Both models are able to give good simulation results compared to the experimental data. However, for the mixture containing 0.12 mole % $CO_2$, the deviations are severe compared to Davis, et al. [43], with AAD 10 K for SRK and 11 K for UMR. To check the reliability of this point, data from Agrawal and Laverman [44] have been used for comparison. They did several frost points measurements with 0.12 mole % $CO_2$ mixtures. One of the points is close to the SLV curve, and has a pressure of 8.55 bar, which is close to the one from Davis (6.85 bar). They measured the freezing temperature to be 149.76 K at this point, which only deviates 1 K from SRK and 3 K for UMR-PRU.

To verify these simulation results, it is necessary to have more experimental SV data for the $CO_2$-methane system.

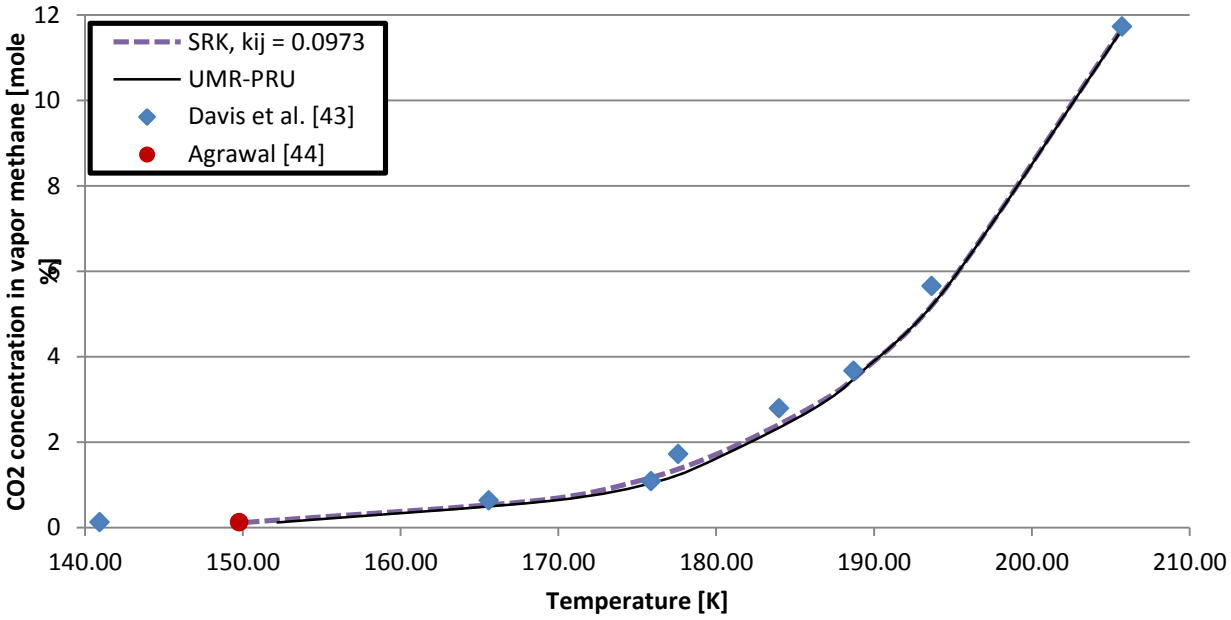


**Figure 25. Predictions of $CO_2$ freeze out along the SLV loci by SRK EoS and UMR-PRU for the $CO_2$-methane system**

### 5.2.3 SL, SV and SLV data for $CO_2$- natural gas mixtures

In natural feed gas components such as nitrogen and ethane are normally present. In the following sections, simulations have been done to see how these components affect the freeze out of $CO_2$.

#### 5.2.3.1 Carbon dioxide solid behavior in $CO_2$ – $N_2$ – $CH_4$ system

Figure 26 shows how nitrogen affects a system containing 1.94 % $CO_2$.The figure shows that; first, the addition of nitrogen causes $CO_2$ to freeze out earlier. This can probably be explained by that nitrogen, compared to methane, has a molecular structure and properties (triple point 63 K) that are different of $CO_2$. Thus, $CO_2$ will be less soluble in a mixture containing nitrogen. Second, the solid-liquid-vapor three phase temperatures have been lowered, giving a larger solid-vapor region. The reason for this is probably due to the low boiling point of nitrogen (77 K), which will try to make the mixture more gaseous. Third, there are no obvious effects on the frost point line, which can be explained by that the gas mixture behaves as an ideal gas at low pressures.

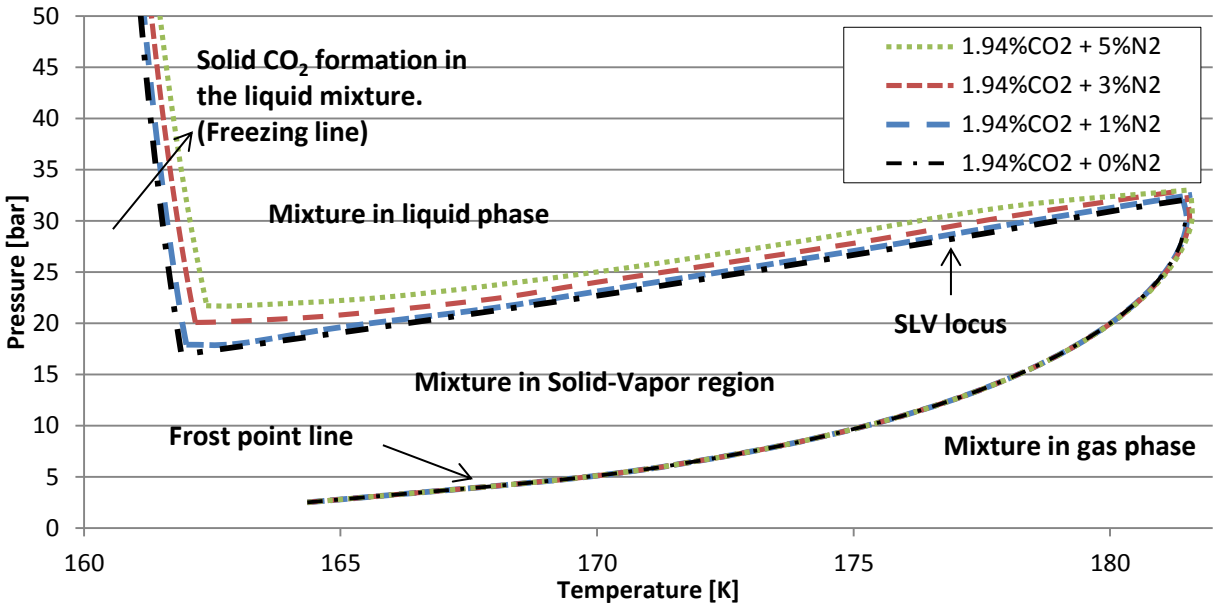


**Figure 26. Predicted $CO_2$ phase behavior by UMR-PRU and SRK EoS in various $CO_2$-$CH_4$-$N_2$ mixtures**

#### *Freeze out predictions of $CO_2$ in liquid nitrogen and methane*

Figure 27 shows the CO2 freeze out predictions in a mixture containing 98 % mole methane and 2 % nitrogen. The interaction parameters for SRK are taken from the work by Shen, et al. [16], with $k_{CH_4-CO_2} = 0.0956$ and $k_{CH_4-N_2} = 0.0312$. SRK is able to give accurate predictions results compared to Shen, et al. [12], with AAD 0.91 K. The UMR-PRU model gives very good prediction results at high CO2 concentrations. However, at lower concentrations the devations are increased,giving a total average deviation of 3.44 K.

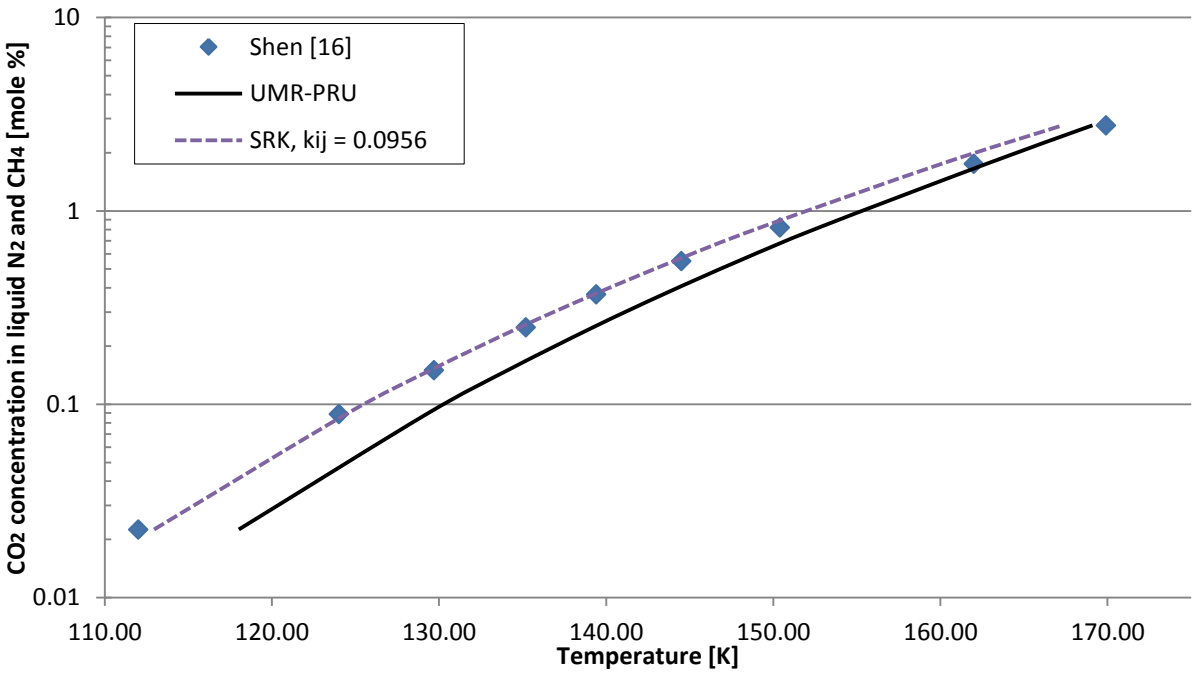


**Figure 27. Freeze out predictions by UMR-PRU and SRK EoS for $CO_2$-$CH_4$-$N_2$ mixture compared to data from Shen[16]**

There are some interesting results for this system. First, the addition of nitrogen in the methane + $CO_2$ mixture increases the solubility of $CO_2$ at temperatures below 126.8 K. At temperatures above 126.8 K, the solubility of $CO_2$ decreases in the mixture. Secondly, the solubility effect of adding nitrogen is decreased when the nitrogen concentration is increased. Figure 28 illustrates both remarks.

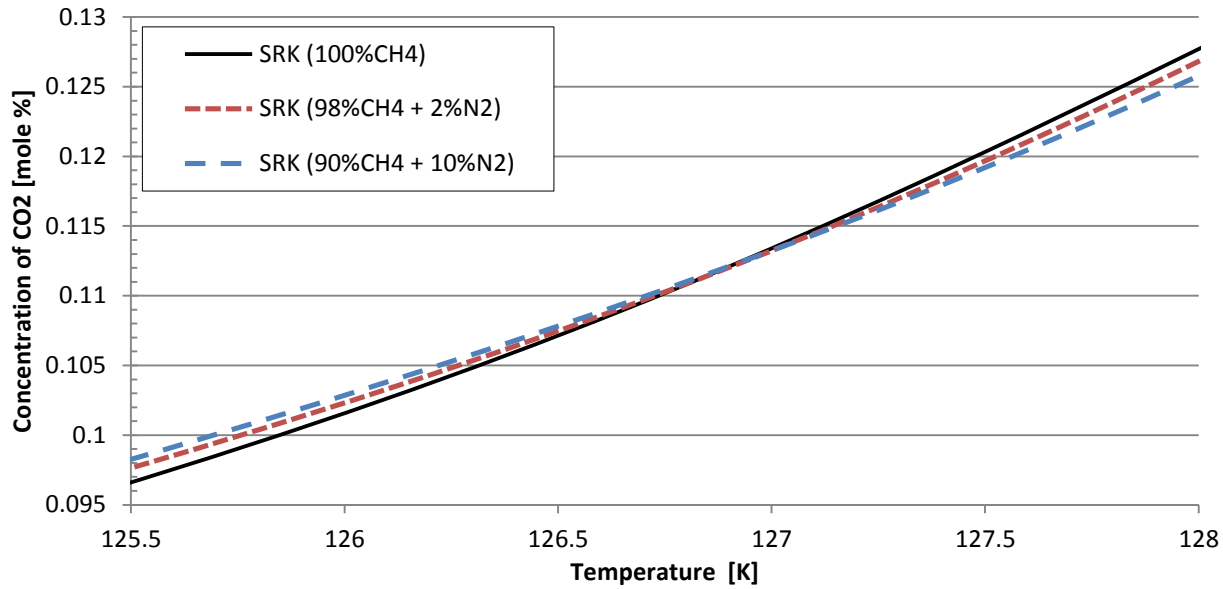


**Figure 28. Freeze out predictions by SRK EoS with various $CO_2$-$CH_4$-$N_2$ mixtures**

### *Frost point predictions of the $CO_2 - N_2 - CH_4$ system*

In Figure 29 and Figure 30 the prediction of the frost points for this system have been compared to experimental data from Agrawal and Laverman [44] and Le and Trebble [45]. Compared with Agrawal's data the AAD is 1.7 K for SRK and 3.64 K for UMR-PRU. Compared with the data from Le the AAD is 1.8 K for SRK and 2 K for UMR-PRU. The data from Le shows higher frost point temperatures with increased $N_2$ concentration, but the simulation results however, shows no obvious effect. Because of the lack of experimental data regarding this system, it is difficult to make any conclusion on the reliability of these experimental data, and thereby the simulation results.

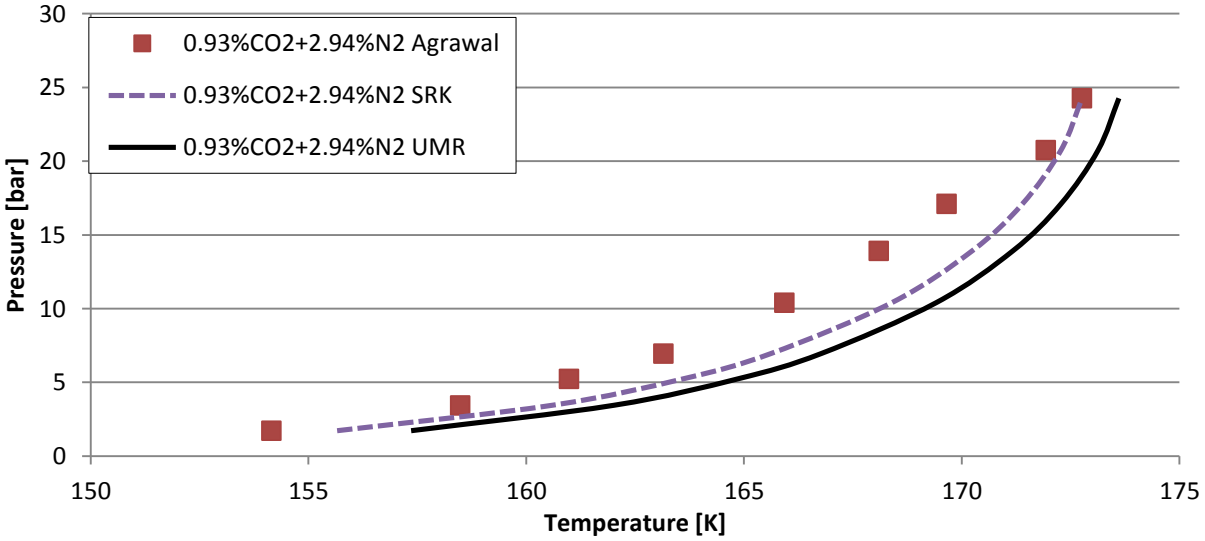


**Figure 29. Frost point predictions by UMR-PRU and SRK EoS for the $CO_2$-$CH_4$-$N_2$ system compared with experimental data from Agrawal [44]**

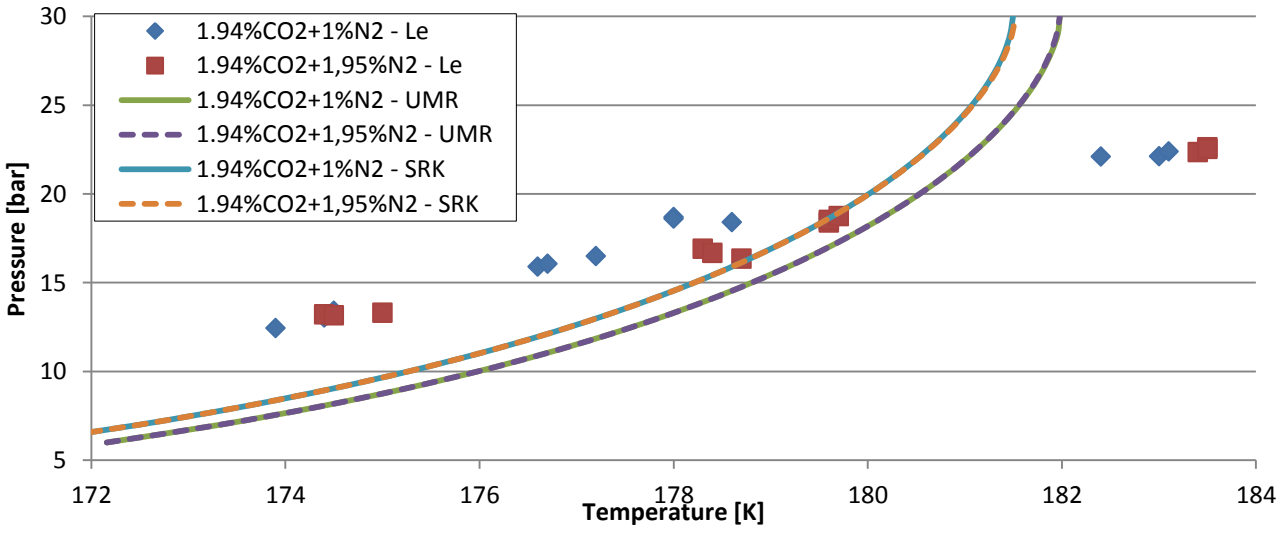


**Figure 30. Frost point predictions by UMR-PRU and SRK EoS for the $CO_2$-$CH_4$-$N_2$ system compared with experimental data from Le [45]**

### 5.2.3.2 Carbon dioxide solid behavior in $CO_2$ – $C_2H_6$ – $CH_4$ system

Figure 31 shows the simulation of how ethane affects a system containing 1.94 % $CO_2$. In contrast to nitrogen the addition of ethane decreases the freezing temperatures of $CO_2$. This is probably because the molecular structure of ethane is more similar to $CO_2$, and thus the solubility of $CO_2$ increases. The temperatures of the SLV locus have been increased, giving less area for solid formation in the solid-vapor region. This is probably due to the high boiling point of ethane (184 K), which tends to make the mixture less gaseous. Again, there are no obvious effects on the frost point lines adding ethane, probably due to ideal gas behavior. The bending of the lines which can be noticed is due to the decreased solid-vapor area, which makes the SLV loci to bend earlier.

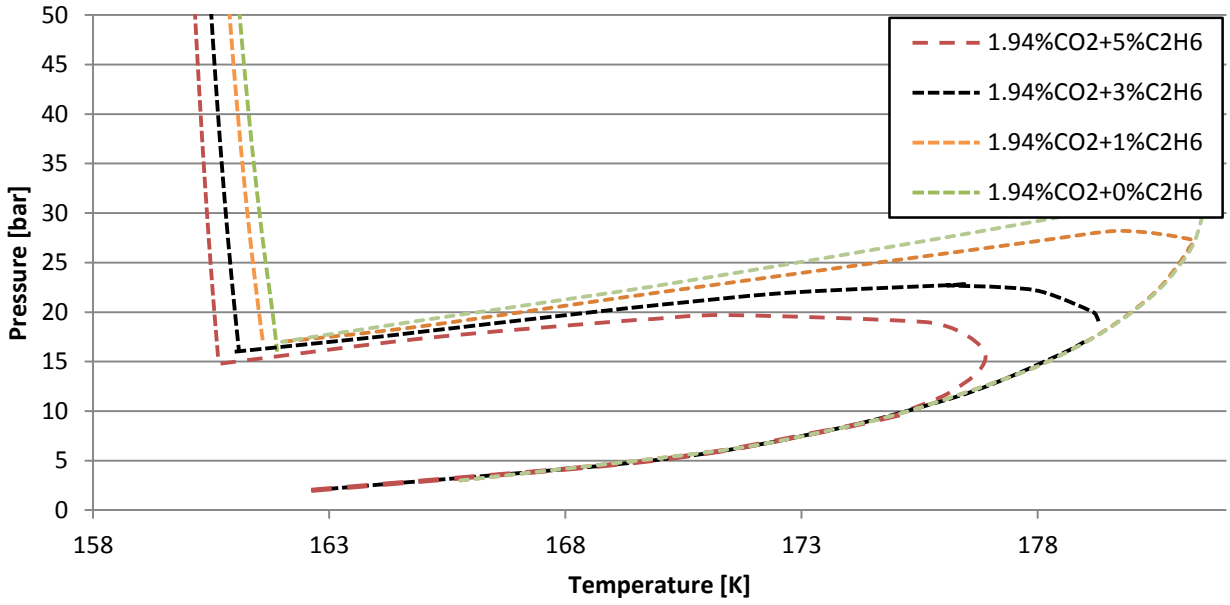


**Figure 31. Predicted $CO_2$ phase behavior by UMR-PRU and SRK EoS in various $CO_2$-$CH_4$-$C_2H_6$ mixtures**

### *Freeze out predictions of $CO_2$ in liquid nitrogen and methane*

Figure 32 shows the $CO_2$ freeze out predictions in a mixture containing 98 % mole methane and 2 % ethane. SRK is able to give accurate predictions results compared to Shen, et al. [12], with AAD 0.66 K. The AAD for UMR-PRU is 3.25 K. It was also done simulations for solvents containg 95% methane + 5% ethane, and 90% methane + 10% ethane. Compared to the experimental data, the AAD for SRK is increased and the AAD for UMR-PRU is decreased, when the ethane concent is increased.

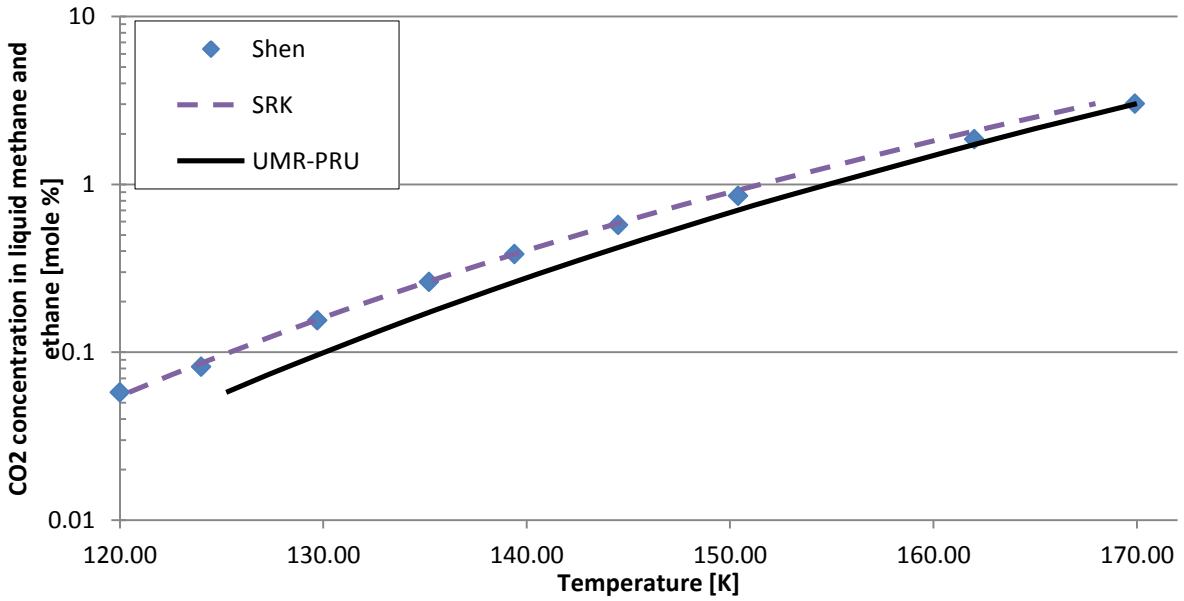


**Figure 32 Freeze out predictions for the $CO_2$-$CH_4$-$C_2H_6$ mixture by UMR-PRU and SRK compared with experimental data from Shen [12]**

### *Frost point predictions of the $CO_2$ – $C_2H_6$ – $CH_4$ system*

The simulation results of the $CO_2$ frost points for this system have been compared to the data from Le and Trebble [45]. For two systems containing 1.95 % $CO_2$ + 0.997 % $N_2$, and 1.96 % $CO_2$ and 1.99 % $N_2$ the AAD for SRK is 1.92 K and 2.185 K for UMR-PRU. The data from Le shows higher frost point temperatures, while the simulation shows no clear effect. Again, more accurate experimental data are required to give accurate conclusions of these results.

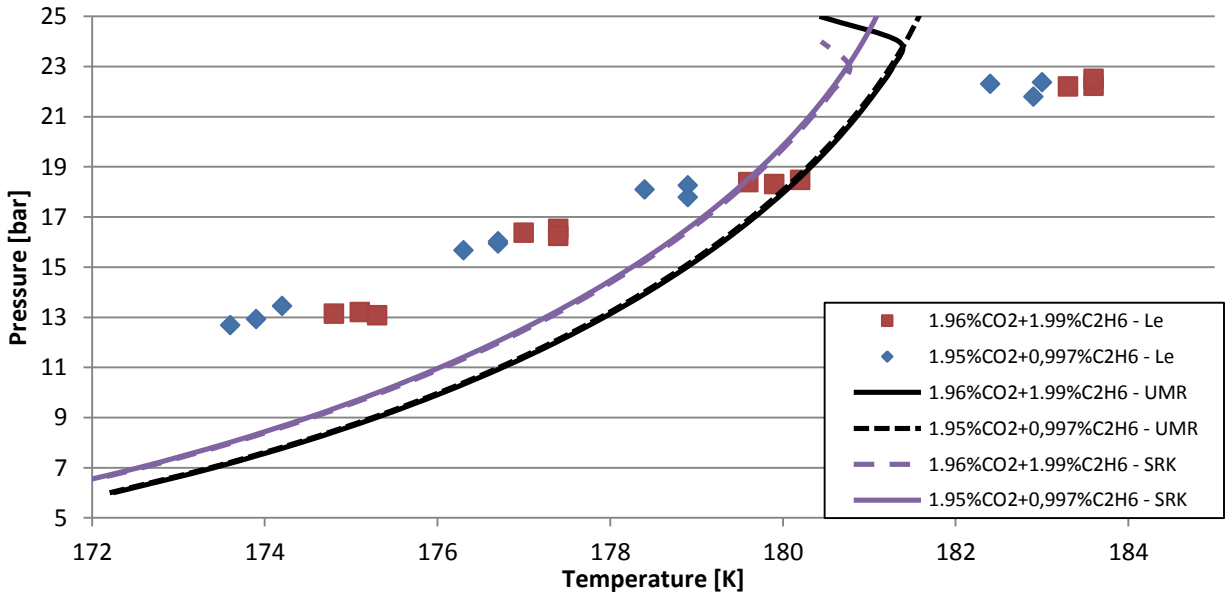


**Figure 33. Frost point predictions for the $CO_2$-$CH_4$-$C_2H_6$ by UMR-PRU and SRK compared with experimental data from Le[45]**

## 5.3 Simulation results for HHC-methane rich systems

For the simulation for the HHC-methane rich systems, all of the three models have been applied. However, a lot of simulation problems occurred with the sPC-SAFT EoS.

### 5.3.1 SL and SLV data for the binary hexane-methane system

#### 5.3.1.1 Prediction by UMR-PRU, SRK and sPC-SAFT without interaction parameter

To check the predictive strength of the different models, the binary interaction parameter is set to zero. Figure 34 shows the simulated behavior of the SLV three-phase loci for the three models. For this system the pressures along the SLV loci have been predicted and compared to experimental data. SRK EoS and UMR-PRU are not able to predict the pressures and compared to the experimental data by Shim and Kohn [52] and Luks, et al. [49] the AAD is 15.99 % for SRK and 19.35 % for UMR-PRU. The sPC-SAFT EoS is however able give a reasonable prediction of the pressures, with an AAD of 5.24 %.

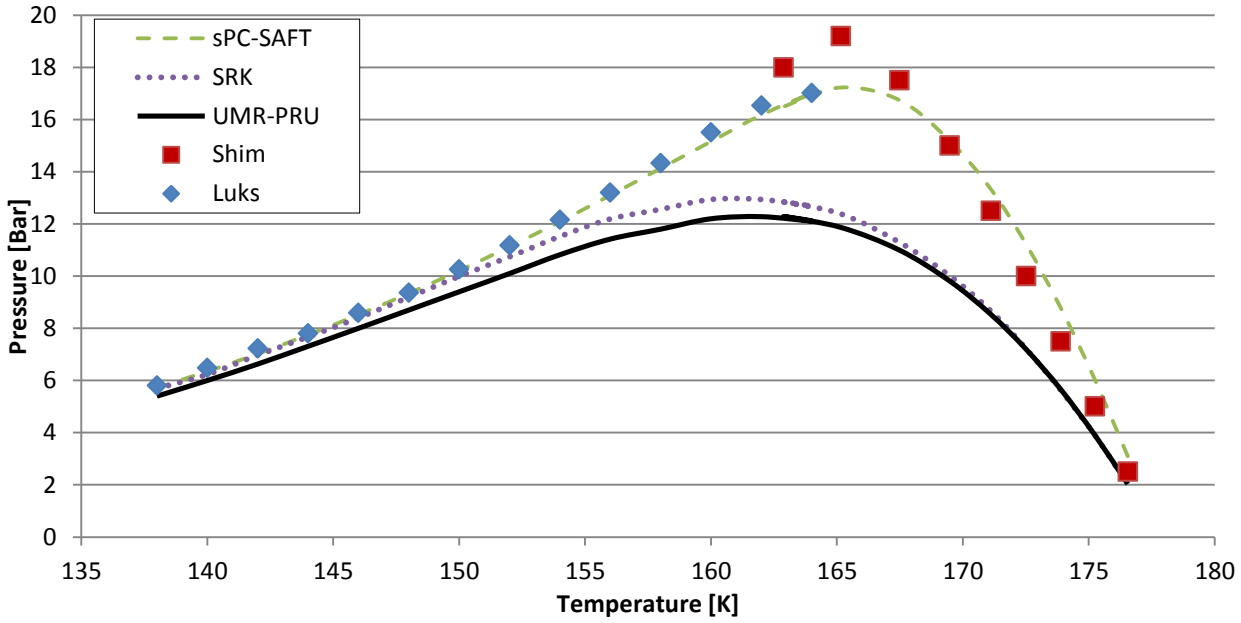


**Figure 34. Prediction of pressures along the SLV loci**

In Figure 35 the freeze out predictions along the SLV loci are shown. With high concentrations of hexane, all of the models are able to give reasonable predictions. However, when the concentration and temperature drops, SRK and UMR-PRU are not able to predict the freeze out. For the model based on UMR-PRU, the simulation fails completely when the hexane concentration goes below 10 mole %. The sPC-SAFT models is however able to give good predictions with AAD 1.78 K.

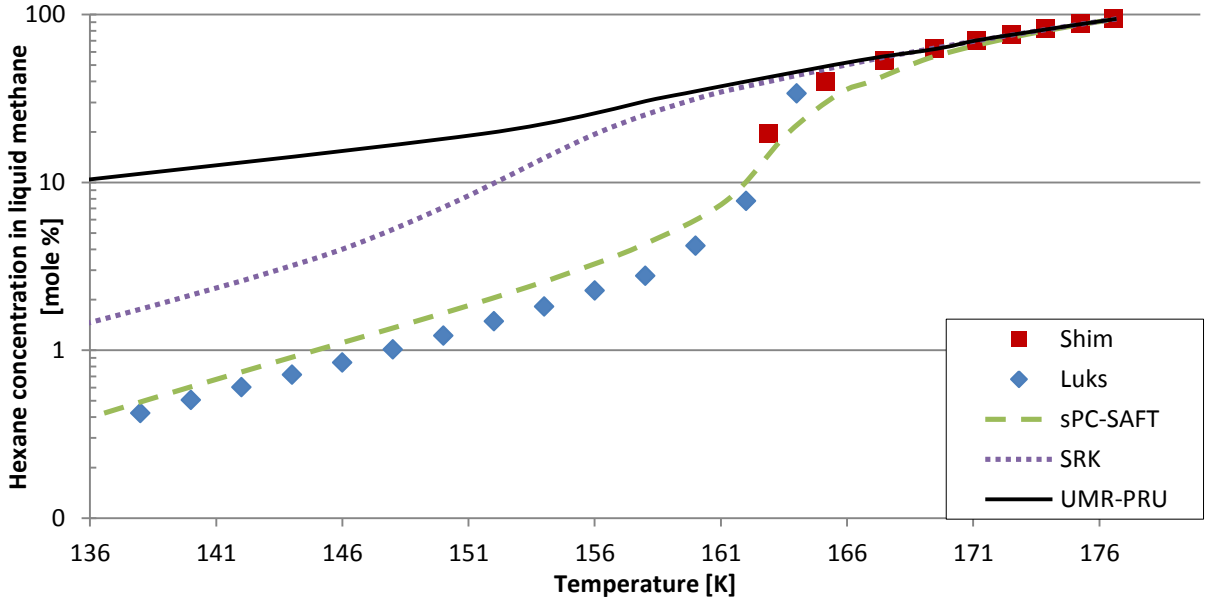


**Figure 35. Freeze out predictions of solid hexane in liquid methane along the SLV loci**

### 5.3.1.2 Predictions by SRK EoS and sPC-SAFT EoS with binary interaction parameters

Experimental data from Kuebler and McKinley [7] and Shim and Kohn [52] are used to find the optimal interaction parameter for SRK and sPC-SAFT. The optimal interaction parameter is found by minimizing the AAD between the freezing points compared to the experimental data.

#### *Prediction by SRK EoS with binary interaction parameter*

Table 9 shows the deviations for the freezing point predictions with different interaction parameters for the SRK EoS.

**Table 9.Freezing point predictions by SRK with different interaction parameters**

| SRK | kij = 0 | kij = 0.025 | kij = 0.03 | kij = 0.0325 | kij = 0.035 | kij = 0.05 |
|---|---|---|---|---|---|---|
| AAD [K] | 9.82 | 2.11 | 1.47 | **1.42** | 1.55 | 5.651 |

The optimal value will probably have an $k_{ij}$ in the area between 0.03 – 0.04. As indicated in Table 9 the best interaction parameter found for this system is $k_{ij} = 0.0325$, which minimizes the AAD to 1.42 K.

Figure 36 shows the freeze out predictions with the optimal interaction parameter for SRK EoS. The model is now able to give better results when compared to the experimental data. However, the figure shows that SRK gives lower solubility and higher freeze out compared to the experimental data when the temperature drops below 130 K. In the temperature area 160 K – 165 K the solubility changes rapidly, and SRK is not able to give good predictions. Figure 36 also shows the freeze out predictions at different pressure levels, and it can be seen that the increasing pressure only has an impact in the area 140 K -162, where increasing pressure increases the

solubility of solid hexane. This is opposite of what Shim and Kohn [52] reported in their article, see 4.3.1.1.

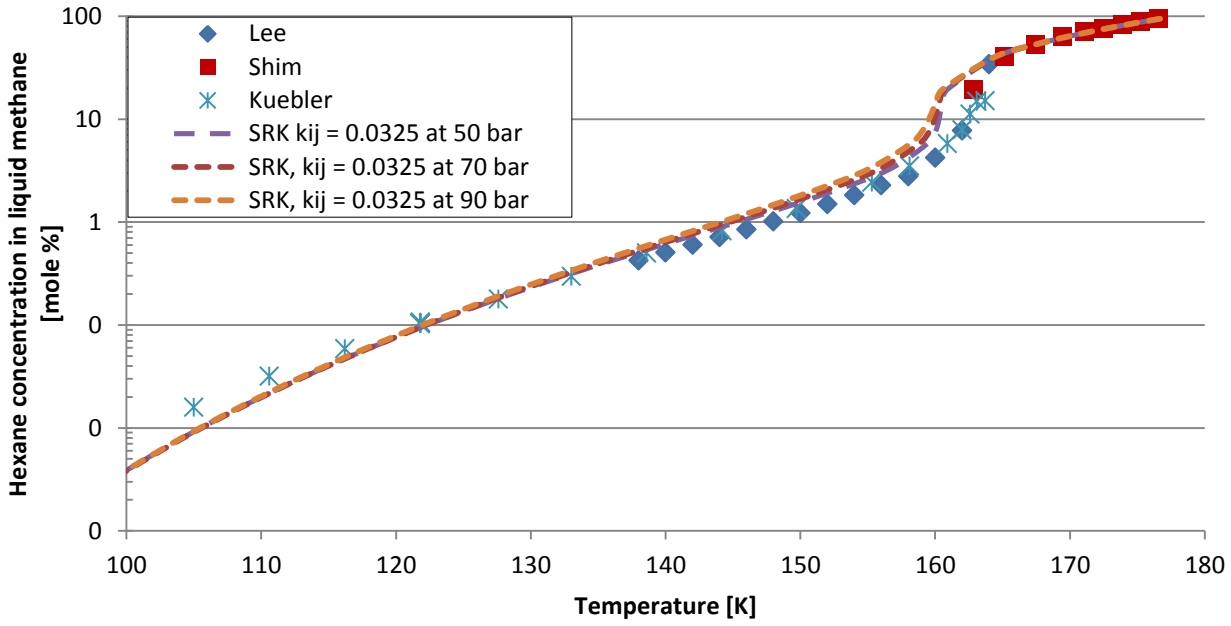


**Figure 36. Freeze out predictions of solid hexane in liquid methane at different pressures by SRK EoS**

In Figure 37 the PT-diagram of the SLV loci predicted by SRK with optimal interaction parameter is shown. The AAD for the pressures has been reduced to 2.79 %.

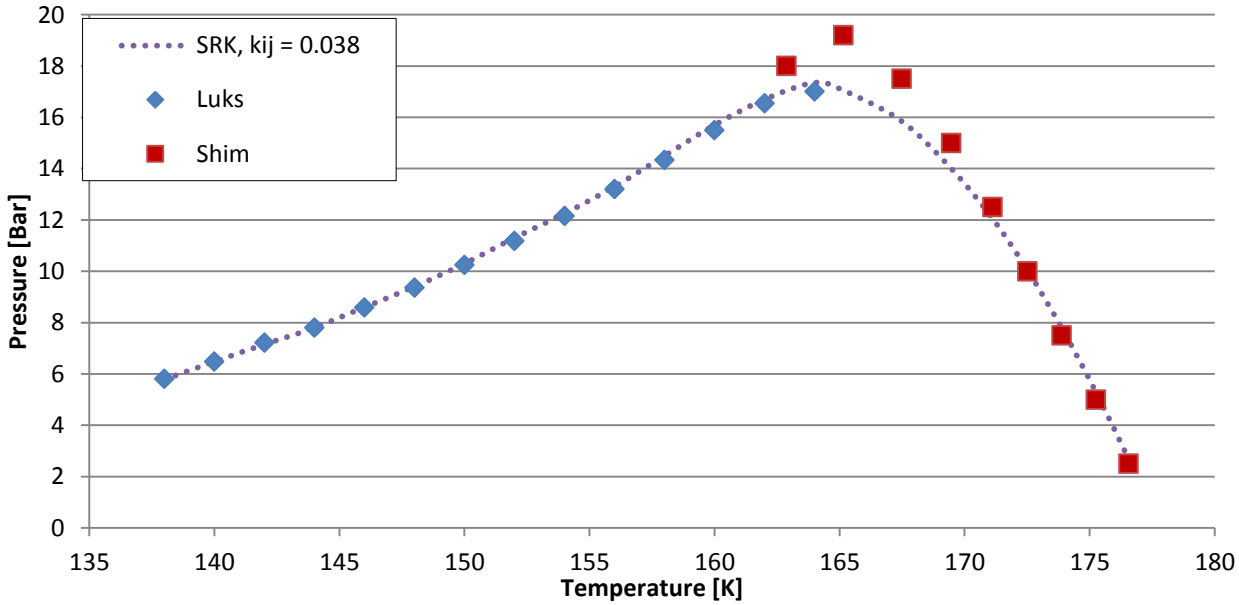


**Figure 37. Prediction of pressure along SLV loci by SRK EoS with optimal interaction parameter**

### *Prediction by sPC-SAFT EoS with binary interaction parameter*

Table 10 shows the deviations for the freezing point predictions by sPC-SAFT with different interaction parameters. There were a lot of problems during the simulations with sPC-SAFT, and especially the choice of pressure was crucial for the simulation to work. The freezes out predictions were done at pressures along the SLV loci, when simulations at higher pressure failed with sPC-SAFT

**Table 10. Freezing point predictions by sPC-SAFT with different interaction parameters**

| SRK | **kij = 0** | **kij = 0.005** | **kij = 0.01** |
|---|---|---|---|
| AAD [K] | **2.232** | **2.787** | 4.65 |

Figure 38 presents the sPC-SAFT simulations with different interaction parameters. The figure shows that increasing the interaction parameter gives lower solubility and thus earlier hexane freeze out. It's difficult to determine the optimal interaction parameter in this case. The figure suggest that the optimal $k_{ij}$ probably is between 0 – 0.005.

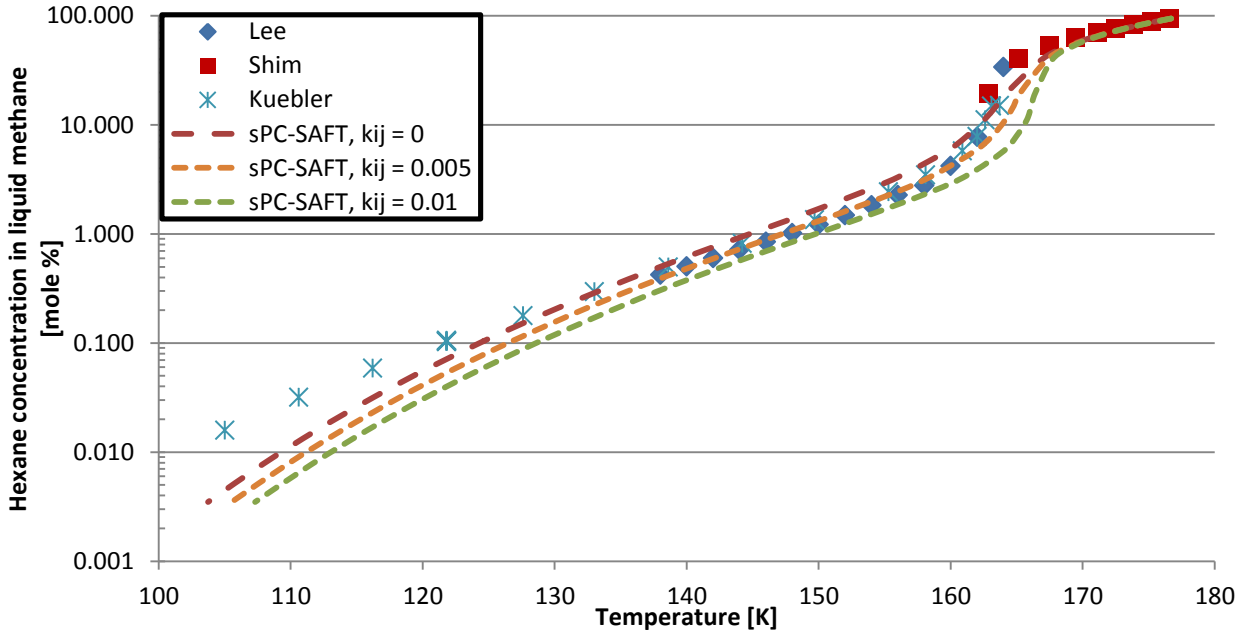


**Figure 38. Prediction of hexane solubility in liquid methane with different interaction parameters along the SLV loci**

### 5.3.2 SL and SLV data for the binary heptane-methane system

#### 5.3.2.1 Prediction by UMR-PRU, SRK and sPC-SAFT without interaction parameter

To check the predictive strength of the different models, the binary interaction parameter is set to $k_{ij} = 0$. Figure 39 and Figure 40 illustrates the predictive behavior of UMR-PRU EoS, SRK EoS and sPC-SAFT EoS for the methane-heptane system. Figure 39 shows the prediction of the SLV three-phase loci. Compared to the experimental data from Tiffin, et al. [53] neither SRK nor UMR-PRU are able to predict the pressures along the SLV three-phase loci. For SRK EoS the AAD for pressures is 20.17 % and for UMR-PRU its 19.18 %. The model based on sPC-SAFT predicts good results, giving AAD 4.97%.

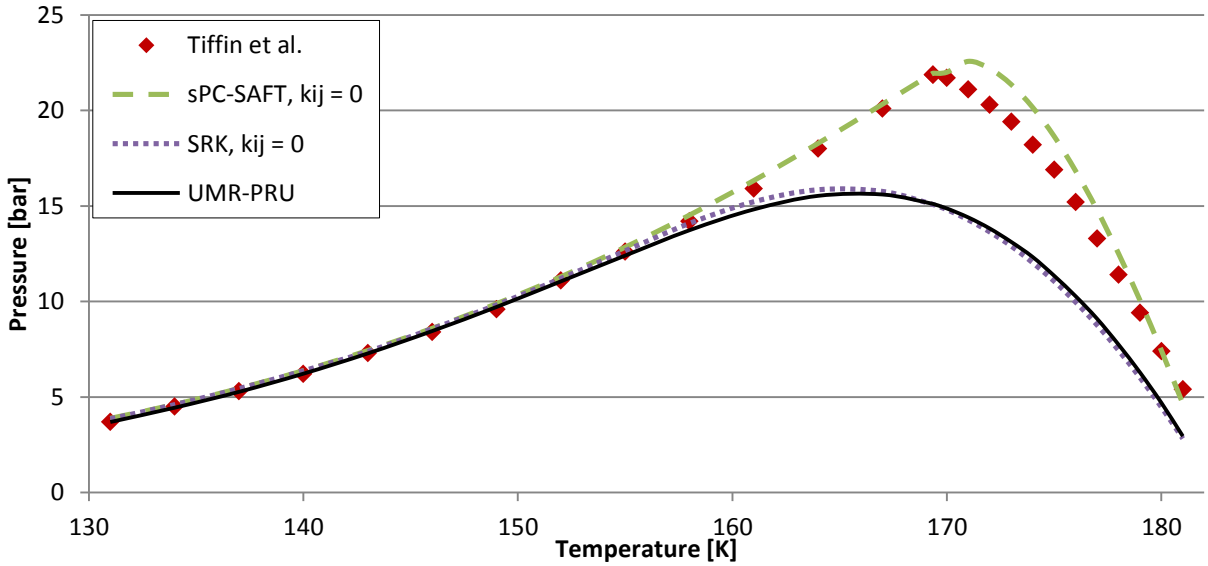


**Figure 39.Predictions of the SLV three phase equilibrium curve by UMR-PRU, SRK and sPC-SAFT**

Figure 40 shows the freezing point predictions of hexane along the SLV loci. SRK and UMR-PRU are only able to predict the freezing point temperatures for high concentration of heptane. At lower concentrations the UMR-PRU simulation fails, while SRK predicts freezing point temperatures that are too low. The model based on sPC-SAFT is however able to give reasonable results, with AAD 3.12 K. Larger deviations are noticed at lower temperatures.

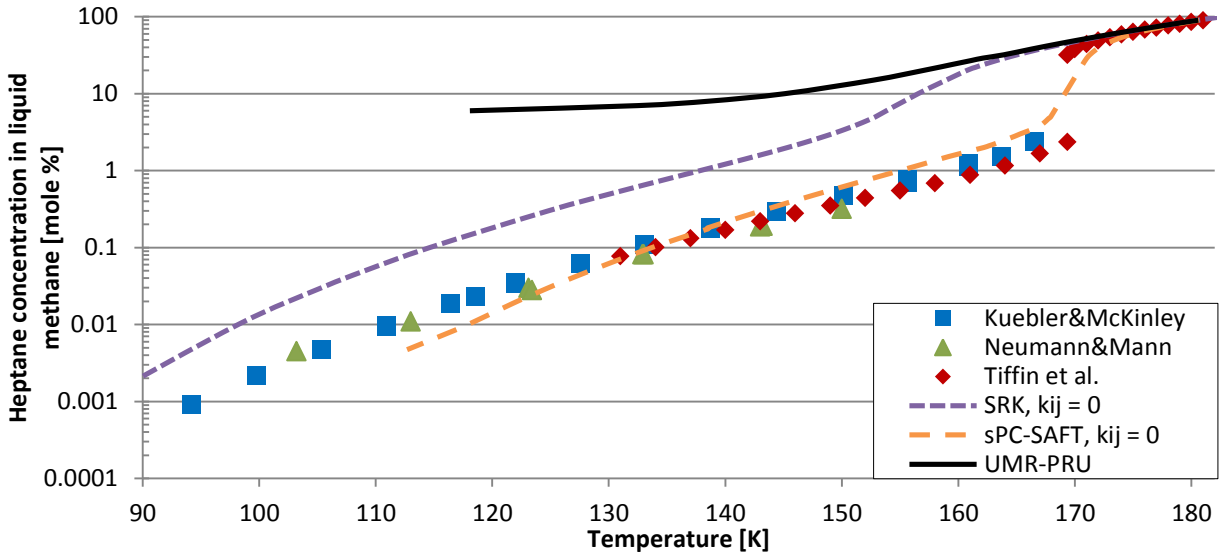


**Figure 40. Freeze out predictions by UMR-PRU, SRK and sPC-SAFT for the heptane-methane system compared to experimental data**

### *5.3.2.2 Prediction by SRK EoS and sPC-SAFT EoS with binary interaction parameter*

To find the optimal binary interaction parameter for SRK EoS and sPC-SAFT EoS, data points from Kuebler and McKinley [7] and Tiffin, et al. [53] have been used.

### *Prediction by SRK EoS with binary interaction parameter*

Table 11 shows the deviations for the freezing point predictions with different interaction parameters for SRK EoS. As indicated in Table 11, the best interaction parameter found is $k_{ij} = 0.038$, which minimizes the AAD to 1.76 K.

**Table 11. Freezing point predictions with different interaction parameters**

| SRK EoS | **kij = 0** | **kij = 0.03** | **kij = 0.035** | **kij = 0.036** | **kij = 0.037** | **kij = 0.038** |
|---|---|---|---|---|---|---|
| AAD [K] | 16.70 | 2.87 | 1.89 | 1.80 | **1.76** | 1.83 |

Figure 41 shows the prediction of the freezing point temperatures of heptane in liquid methane with the optimal interaction parameter. The simulations are performed at 40 bar and 50 bar. The simulation results gives reasonable results compared to the experimental data. There are however larger deviations at lower temperatures. SRK is now able to predict a quadruple point which occurs at 167.5 K, deviating 1.85 K from the quadruple point by Tiffin, et al. [53]. It can also be seen that the increasing pressure depresses the solubility of solid heptane in liquid methane, and that the quadruple point decreases towards a lower temperature.

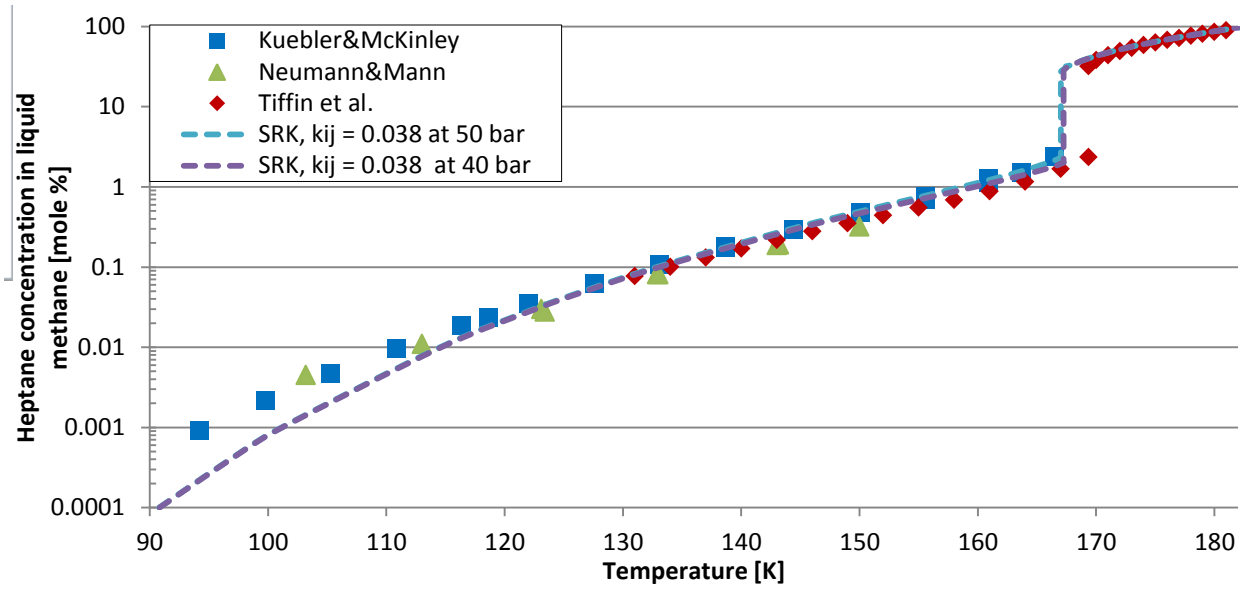


**Figure 41. Freeze out prediction by SRK EoS for the heptane-methane system optimal binary interaction parameter**

Figure 42 shows the pressure-temperature diagram of the SLV three-phase loci predicted by SRK EoS with optimal interaction parameter. The AAD% for the pressure has been reduced to 0.881. Larger deviations are noticed close to the maximum pressure point along the SLV loci.

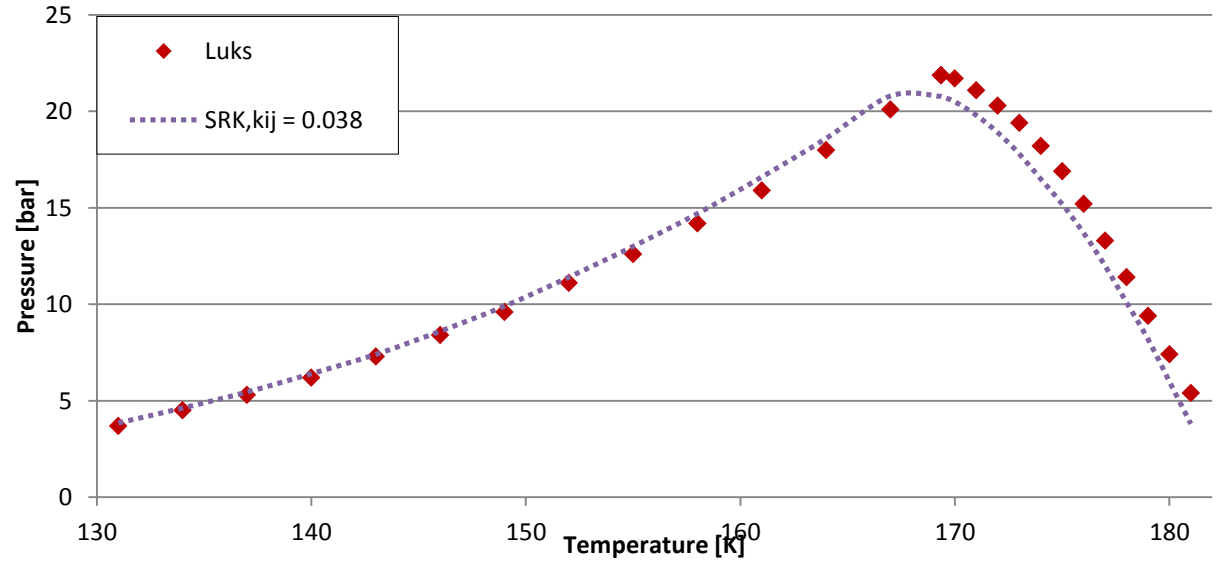


**Figure 42. Prediction by SRK EoS of the SLV three phase equilibrium curve with optimal interaction parameter**

***Prediction by sPC-SAFT with binary interaction parameter***

There were a lot of errors during the simulations with sPC-SAFT. The pressure had to be adjusted for almost every point to get the simulation to work.

Changing the interaction parameter for sPC-SAFT did not improve the predictions. Figure 43 shows that the deviations are increased with higher interaction parameter for the lowest temperature range. The optimized interaction parameter is probably between 0 – 0.005.

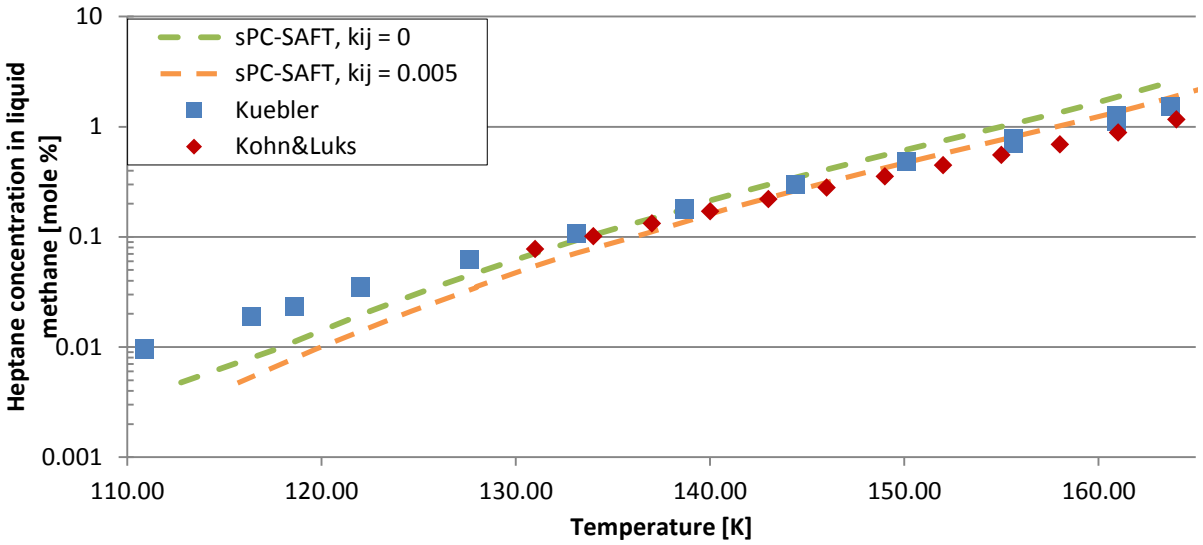


**Figure 43. Freeze out predictions by sPC-SAFT for the heptane-methane system with different interaction parameters**

### 5.3.3 SL and SLV data for the binary benzene-methane system

#### 5.3.3.1 Prediction by UMR-PRU, SRK and sPC-SAFT without interaction parameters

Figure 44 shows the freeze out predictions of solid benzene in liquid methane for low benzene concentrations. SRK and sPS-SAFT predicts freeze out temperatures that are much lower than the experimental data from Kuebler and McKinley [7]. The AAD is 17.1 K for SRK and 8.7 K for sPC-SAFT. The UMR-PRU model however, predicts freeze out temperatures that are higher than the experimental data, giving AAD of 6.9 K. For this system UMR-PRU doesn't fail during the simulations, and gives much better results compared to the system with heptane and hexane.

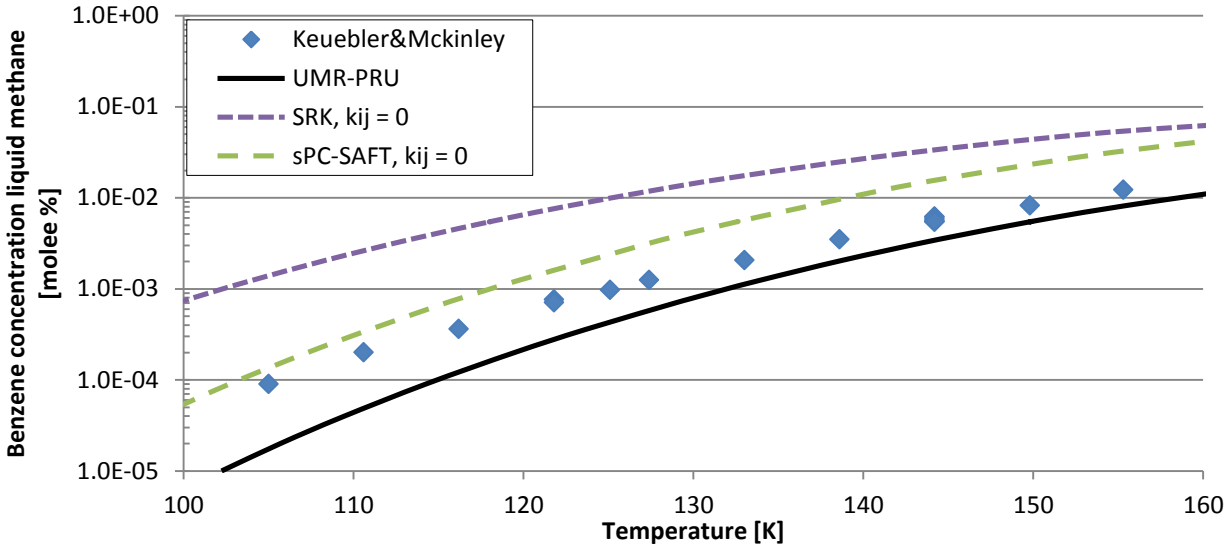


**Figure 44. Freeze out predictions of solid benzene in liquid methane**

Figure 45 shows the prediction of the low and high temperature three-phase branches for the binary benzene-methane system. All of the models are able to predict the behavior of the low temperature branch. For the high temperature branch UMR-PRU predicts the best result. The average deviation for the models are; 5.2 K for UMR-PRU, 7.14 K for SRK and 6.1 K for sPC-SAFT.

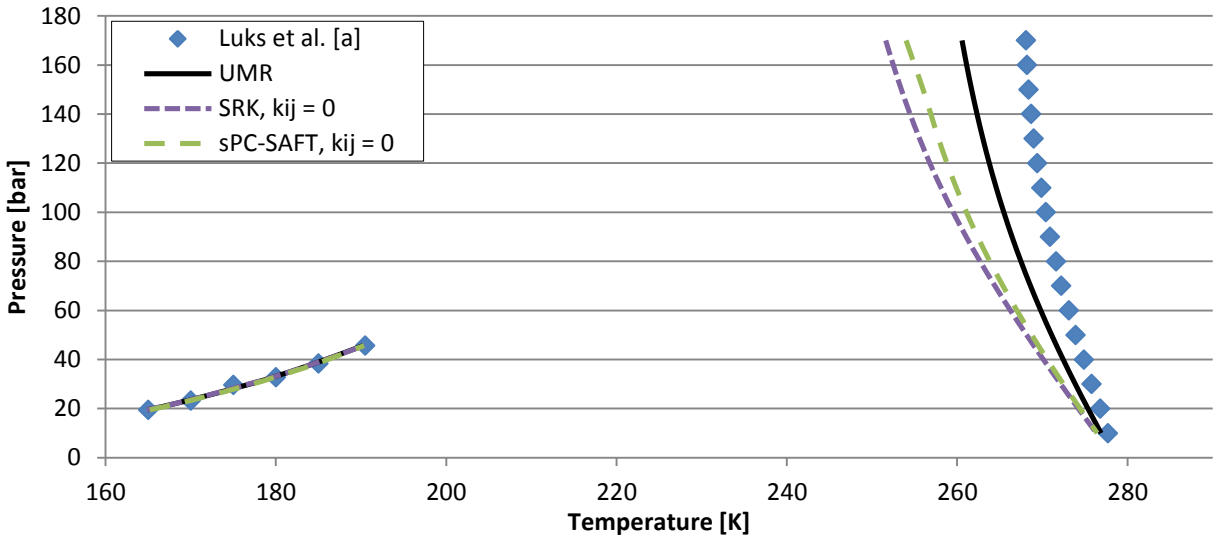


**Figure 45. Predictions of the methane-benzene SLV three phase loci**

### 5.3.3.2 Prediction by SRK EoS and sPC-SAFT with binary interaction parameter

The optimal interaction parameter was found by minimizing the AAD compared with the experimental data from Kuebler and McKinley [7]

#### *Prediction by SRK EoS with binary interaction parameter*

Table 12 shows the absolute average deviations with different binary interaction parameters for SRK EoS. The most promising interaction parameter found is $k_{ij} = 0.06$ , which reduces AAD to 0.78 K.

**Table 12. Freezing point predictions by SRK with different interaction parameters for the methane-benzene system**

| SRK | **kij = 0** | **kij = 0.05** | **kij = 0.058** | **kij = 0.06** | **kij = 0.062** | **kij = 0.05** |
|---|---|---|---|---|---|---|
| ADD [K] | 23.940 | 3.736 | 1.05 | **0.78** | 0.89 | 5.651 |

Figure 46 shows the freeze out predictions of solid benzene in liquid methane with optimized interaction parameter. The simulation result agrees well with the experimental data from Kuebler and McKinley [26]. From the figure it can be seen that the increasing pressure doesn't effect the freeze out temperatures.However, at higher temperature, around 145 K, a small increase in solubility is noticeable, and thus the freeze out temperatures have been lowered.

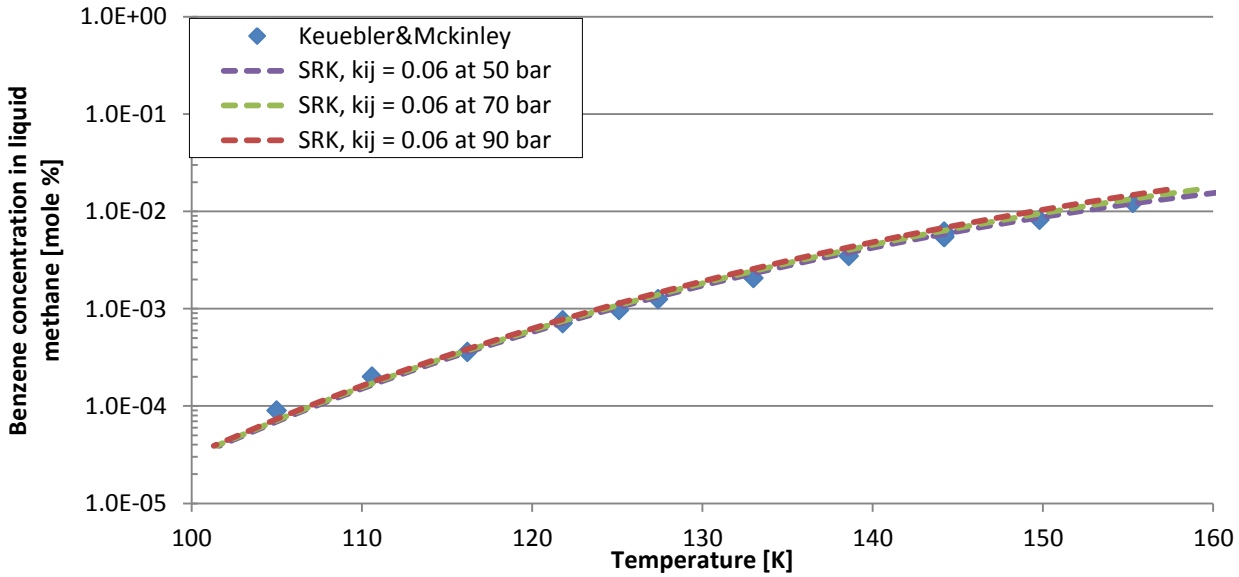


**Figure 46. Freeze out predictions by SRK with optimal interaction parameter**

### *Prediction by sPC-SAFT EoS with binary interaction parameter*

Table 13 shows the deviations for the freezing point predictions with different binary interaction parameters for sPC-SAFT EoS. The table indicates $k_{ij} = 0.025$ to be the best value. However, as seen in Figure 47, with this parameter the deviations are increase at low temperatures. The "optimized" interaction parameter is therefore chosen to be $k_{ij} = 0.02$

**Table 13. Freezing point predictions by sPC-SAFT with different interaction parameters for the methane-benzene system**

| sPC-SAFT | **kij = 0** | **kij = 0.02** | **kij = 0.025** | **kij = 0.03** |
|---|---|---|---|---|
| ADD [K] | 8.94 | 2.62 | 2.27 | 3.16 |

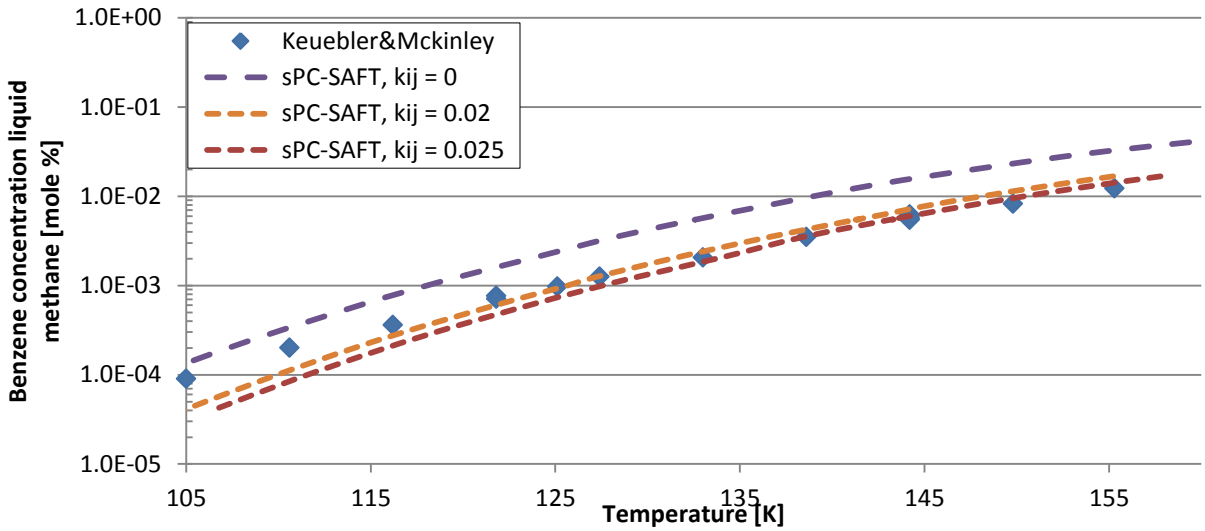


**Figure 47. Freeze out predictions by sPC-SAFT with different interaction parameter**

Figure 48 shows the p-T diagram for the SLV three phase loci predicted by SRK and sPC-SAFT with optimized interaction parameters. The AAD for sPC-SAFT has been reduced to 1 K and 3.3 K for SRK.

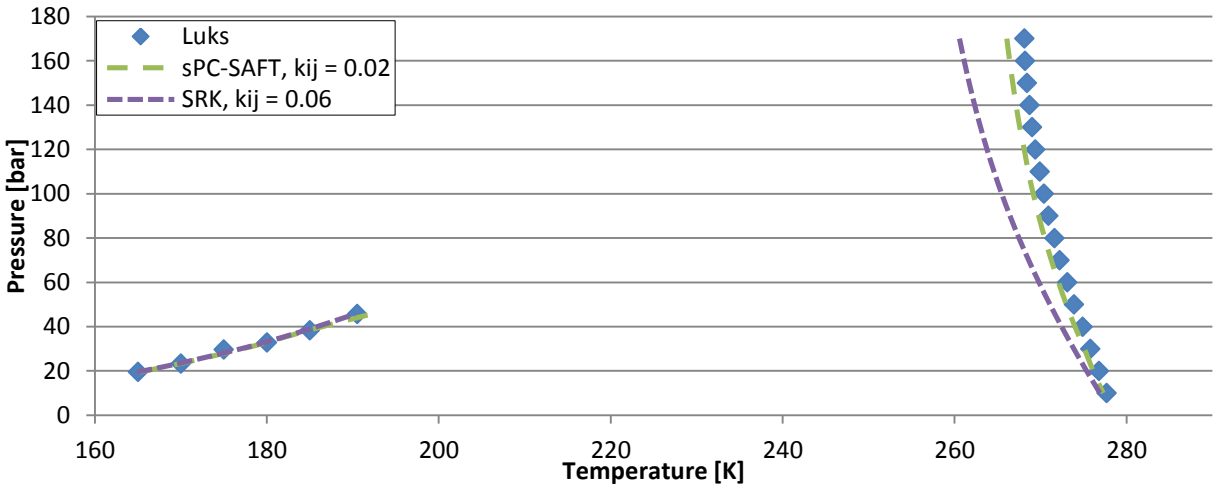


**Figure 48. Predictions of the methane-benzene SLV three phase loci with optimized interaction parameters**

### 5.3.3.3 Freeze out predictions by UMR-PRU, SRK EoS and sPC-SAFT for the $CH_4$- $C_2H_4$-benzene system

The experimental data from Tiffin, et al. [33] are based on three experimental runs. Figure 49 shows the freeze out predictions for the third run, where the ethane varies from 25 mole % to 10 mole %. The UMR-PRU model predicts a higher freeze out temperature than the other two models, with AAD 1.43 K. The AAD for SRK is 1.34 K and 1 K for sPC-SAFT.

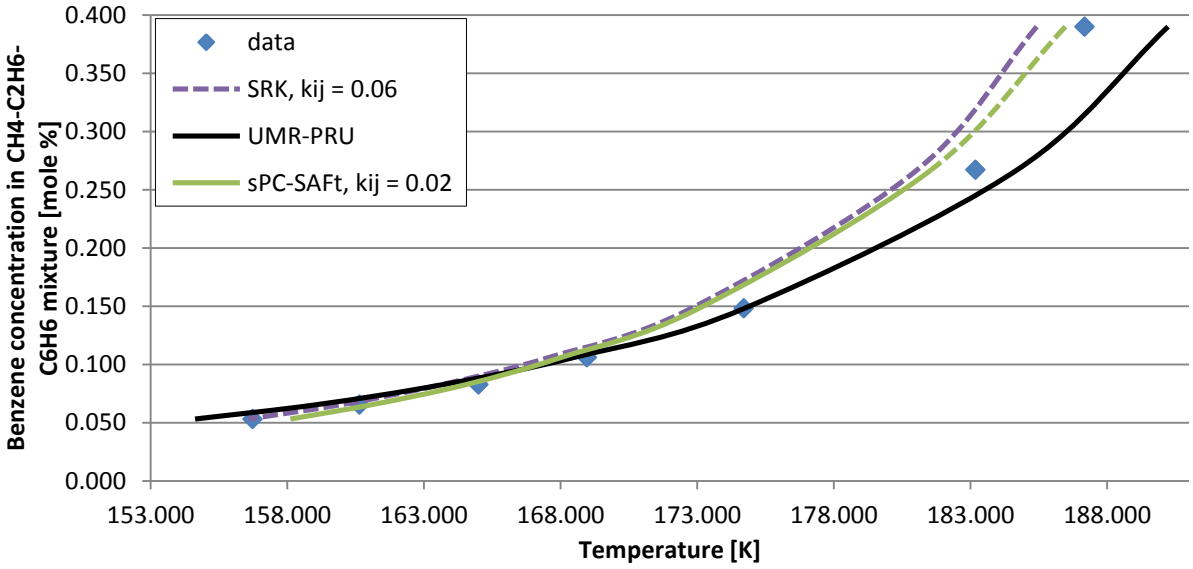


**Figure 49. Freeze out predictions for the $CH_4$-$C_2H_6$-$C_6H_6$ system**

### 5.3.4 SL and SLV data for the binary octane-methane system

The simulations with the octane-methane system prove to be a challenge for all three models. The UMR-PRU model was not able to give any results for low octane concentrations. For the lower SLV loci branch, the solubility of octane in the liquid mixture tended to be extremely pressure sensitive. As discussed in part 4.3.4, the K-point of the lower branch is very close to the critical point of pure methane. This can affect the density of the liquid, and thus the solubility will change when the pressure is increased. Another explanation for this behavior can be due to computational errors in the simulation file. This problem made it impossible to find the freeze out temperatures at low pressure levels. To avoid the problem all the simulations were done at pressures at 50 bar or higher, which is over this critical region. The pressures did not affect the solubility at this level.

#### 5.3.4.1 Prediction by SRK and sPC-SAFT without binary interaction parameter

Figure 50 shows the freeze out predictions of the solid octane in liquid methane for SRK and sPC-SAFT. SRK is not able to predict the freezing temperatures compared to the experimental data. sPC-SAFT predicts reasonable results, and compared to the experimental data from Kohn, et al. [57] the AAD is 8.4 K.

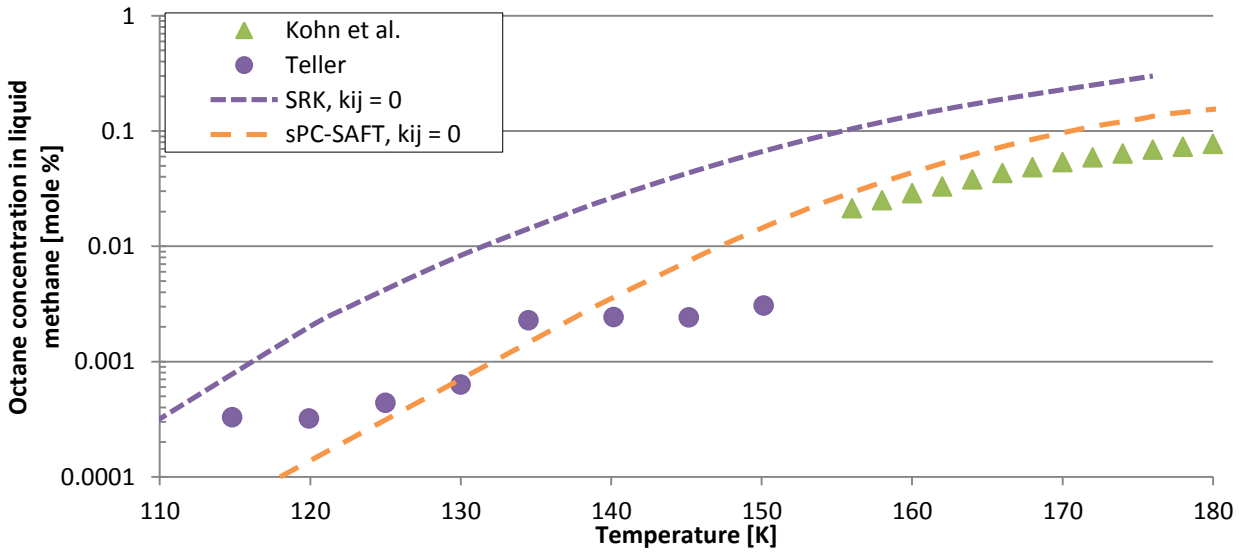


**Figure 50. Freeze out predictions for solid n-octane in liquid methane**

In Figure 51 the predictions of the three-phase equilibrium curve are shown. For the low temperature branch all of the models are able to give good SLV predictions. For the high temperature branch sPC-SAFT and UMR predicts good results compared to the data from Kohn, et al. [57], with AAD 0.653 K and 1.533 K. Both tends to give lower freezing points at higher pressures. SRK is unable to predict the high SLV temperature branch, giving AAD 4.26 K.

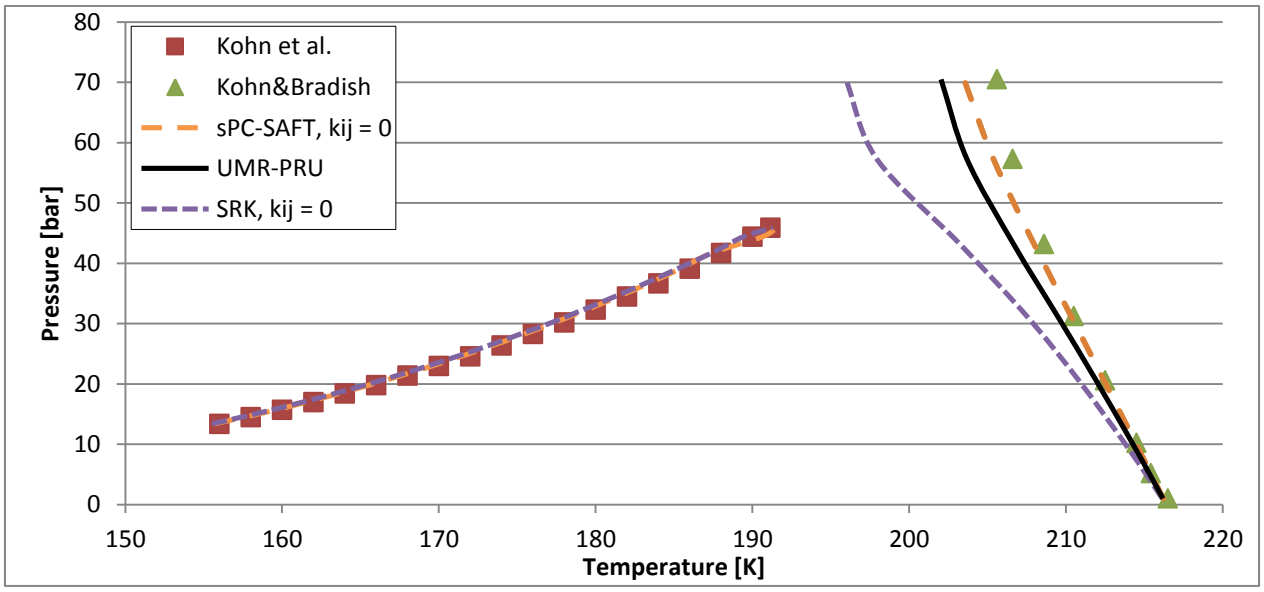


**Figure 51. Predictions of the methane-octane SLV three phase loci**

### 5.3.4.2 Freeze out predictions by SRK, sPC-SAFT and UMR-PRU at high octane concentration

Figure 52 shows the freeze out predictions for high octane concentrations. All of the models are able to give good predictions compared to the experimental data from Kohn and Bradish [5]. sPc-SAFT gives the best results with AAD 0.398 K, SRK second with 0.771 K and UMR with AAD 0.785 K. The SRK and UMR predictions are almost identical, and they both starts deviating from the experimental data at decreasing temperature.

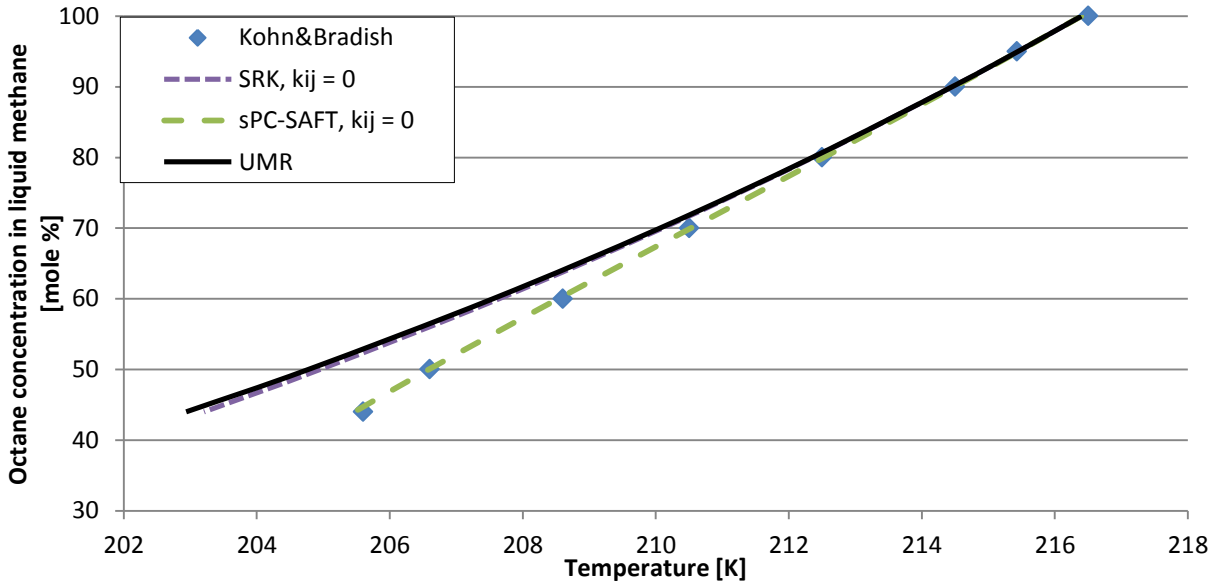


**Figure 52. Freeze out predictions of high concentrated octane in liquid methane**

### 5.3.4.3 Prediction by SRK EoS and sPC-SAFT EoS with binary interaction parameter

The optimal interaction parameter is found by minimizing the AAD compared to the experimental data from Kohn, et al. [57].

#### *Prediction by SRK EoS with binary interaction parameter*

The optimal interaction parameter is found to be $k_{ij} = 0.04$ at a pressure of 50 bar, which reduces the AAD to 2 K. At higher temperatures the effect of increased pressure increases the solubility of n-octane.

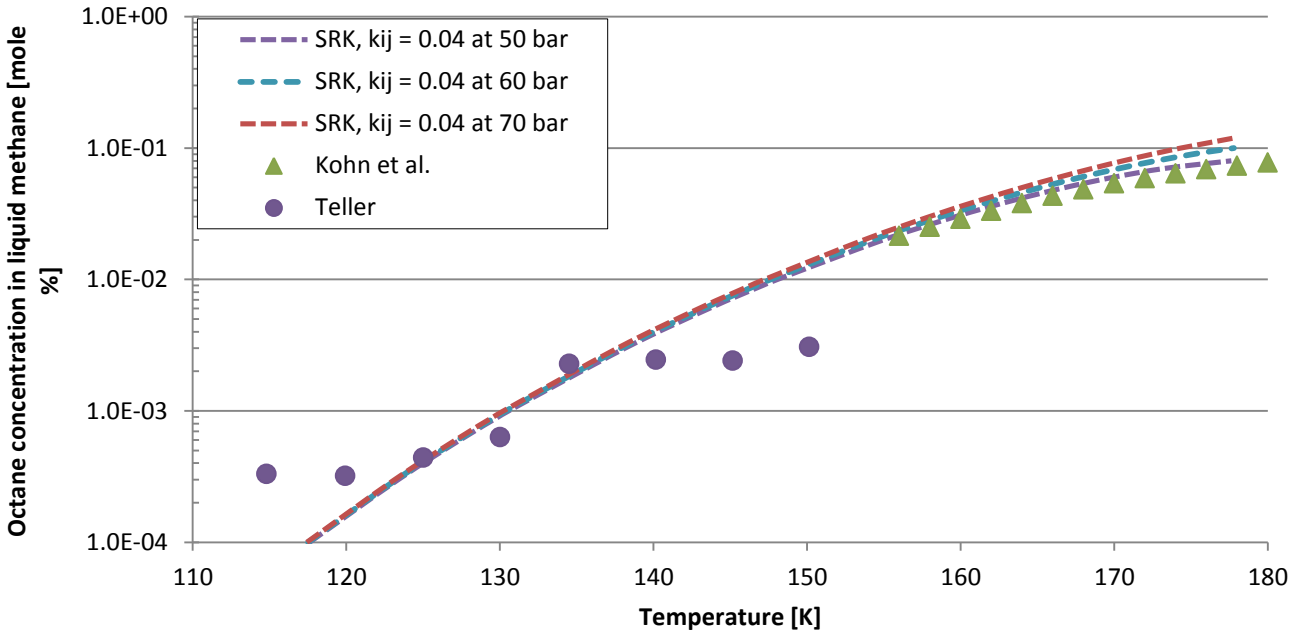


**Figure 53. Freeze out predictions of octane in liquid methane by SRK EoS with optimal interaction parameter**

#### *Prediction by sPC-SAFT EoS with binary interaction parameter*

The optimal interaction parameter for sPC-SAFT was found to be $k_{ij} = 0.01$, which minimized the AAD to 3.2 K. As it can be seen in Figure 54, with an increased interaction parameter the solubility has been lowered and the freeze out occurs earlier.

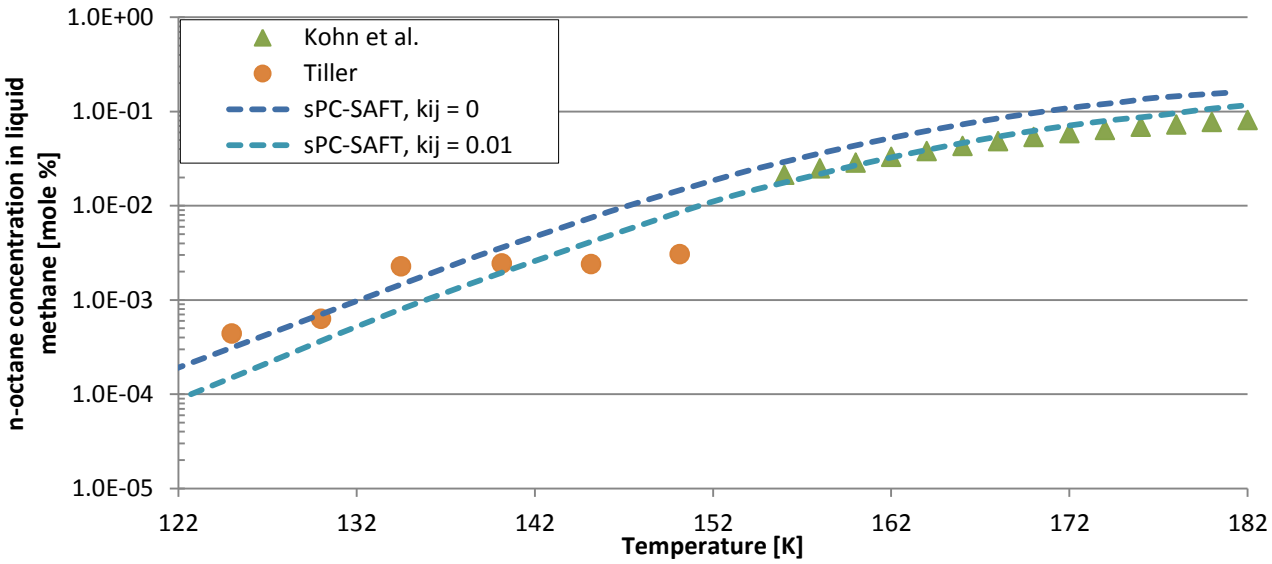


**Figure 54. Freeze out predictions of octane in liquid methane by sPC-SAFT with optimal interaction parameter**

### 5.3.4.3 Solid octane behavior in $CH_4$- $C_2H_4$-octane mixture

Data from two experimental runs from the work by Tiffin, et al. [33] have been compared to the simulation results. The ethane concentration varies from 39 % - 10 %. Figure 55 shows the freeze out predictions by the three EoS models compared with these data. The AAD for sPC-SAFT is 1.1 K and for SRK 3.38 K. The UMR-PRU model are not able to give any logical predictions.

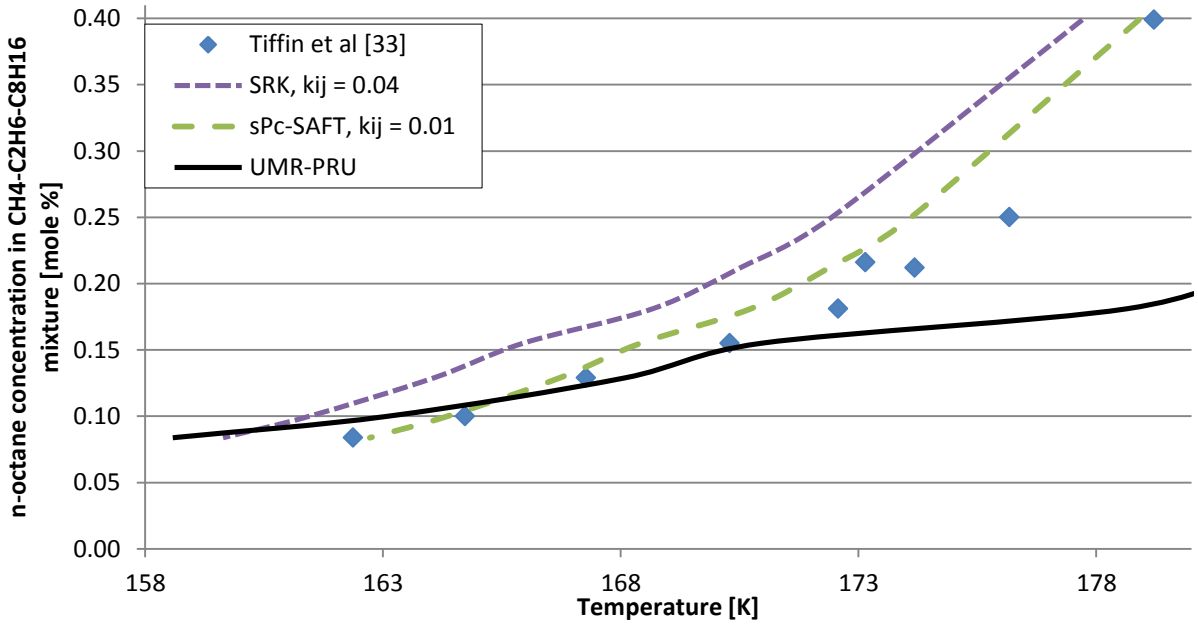


**Figure 55. Freeze out predictions for the CH4-C2H6-C8H16 system**

### 5.3.5 SL and SLV data for the binary cyclohexane-methane system

For low cyclohexane composition the simulations gave large deviations compared to the experimental data and in most cases the calculation failed. It was attempted to change the binary interaction parameters for SRK and sPC-SAFT to see if this could fix the problems. By changing the interaction parameters the calculations became very unstable, and gave illogical phase behavior compared to the experimental work and theory behind the cyclohexane –methane system. It was also tried to do simulations of a ternary system containing ethane, methane and cyclohexane, but the simulation results did not improve. Due to the simulation problems, this section only presents simulations of high octane concentration, and the prediction of the SLV three-phase loci**.**

#### 5.3.5.1 Prediction by UMR-PRU, SRK EoS and sPC-SAFT EoS without binary interaction parameter

Figure 56 shows the freeze out predictions at high cyclohexane concentrations compared to the data from Kohn and Bradish [56]. The models predicts higher freeze out temperatures than the experimental data. The simulation results with UMR-PRU represent a good linear correlation of the data, with absolute deviation 3.5 K. SRK and sPC-SAFT gives AAD 4.7 K and 7 K.

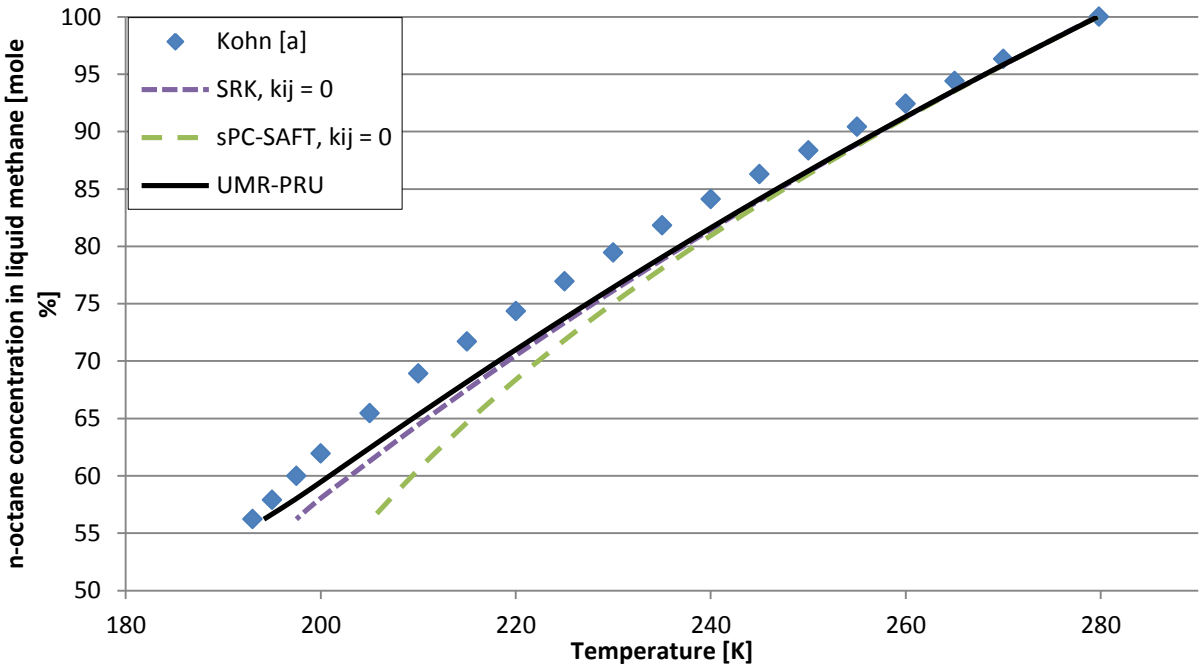


**Figure 56. Freeze out predictions at high octane concentrations in liquid methane**

Figure 57 shows the predicted behavior of the SLV three phase loci of the methane-cyclohexane system. The models are not able to predict the SLV phase behavior of this system. Instead they

predict a phase behavior that is similar to the n-hexane-methane system. The sPC-SAFT model gives the best predictions compared to the experimental data.

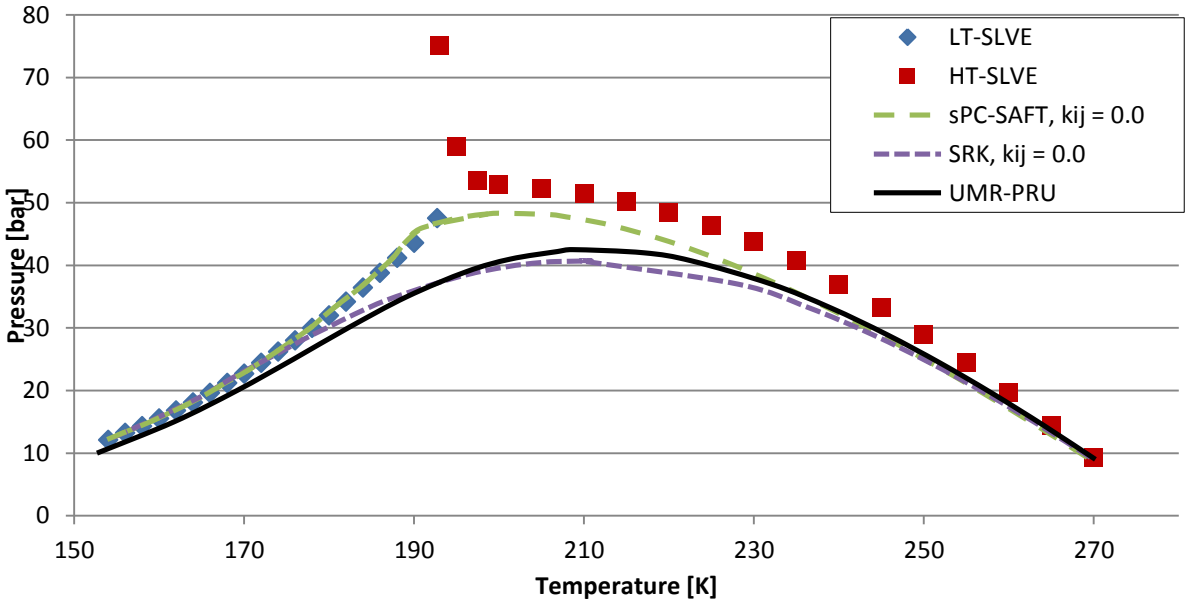


**Figure 57. Predictions of the methane-cyclohexane SLV three phase loci**

## 5.4 The freeze out risk in natural gas systems.

Figure 58 shows the prediction of the solubility of the investigated components in liquid methane. The data for cyclohexane is taken from the experimental work by Kohn and Bradish [56], since the simulation failed for this system.

According to the predictions, the solubility of n-hexane in liquid methane is higher than the other hydrocarbons. Carbon dioxide has also a higher solubility compared to the others. However, the amount of $CO_2$ in natural gas, is higher compared to the other components and the risk of $CO_2$ freeze out in natural gas is therefore more crucial.

Octane and benzene represents the components with lowest solubility in methane. An interesting observation here is the difference between benzene and cyclohexane. The molecular structure of these two components has much in common (triple points of benzene and c-hexane are 278 K and 279 K). However, as shown in Figure 58, the risk of benzene freeze out is much higher than of cyclohexane, when it is highly diluted in methane. As mentioned in section 4.3.5, the phase behavior of the binary cyclohexane-methane differ from the A phase behavior (2.2.1.1). While benzene-methane represents a typical A phase behavior, the c-hexane-methane system are more similar to the hexane – and heptane – methane systems.

In a natural gas, components such as ethane, propane, butane and nitrogen will be present. These components will have an effect on the solubility of the critical components. As it has been seen in the simulation results (5.2.3, 5.3.3.3 and 5.2.4.3), the addition of light hydrocarbons increases the solubility of these components in the mixture. This means that the freeze out risk will be less in natural gas compared to the freeze out risk in pure liquid methane.

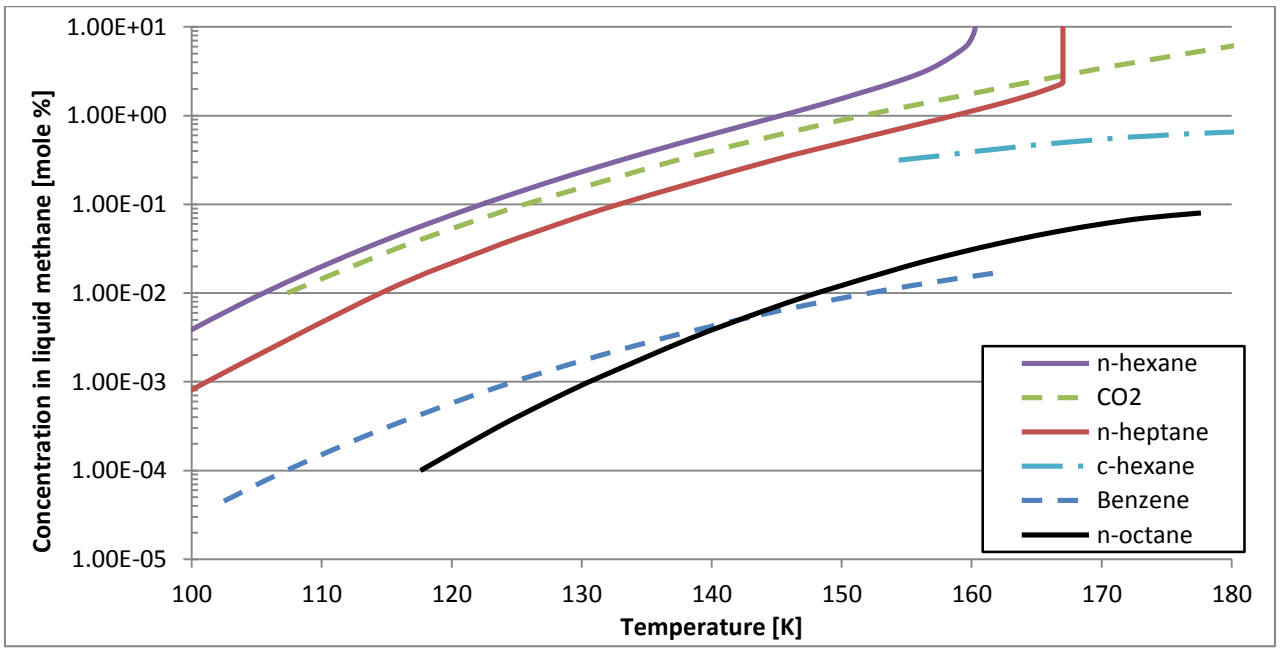


**Figure 58. Solubility of the investigated components in liquid methane**

# 6. Discussion

## 6.1 Evaluation of experimental data and simulation results

The understanding of the phase behavior of the different systems has been very important in order to evaluate the experimental data and the simulation results. In Table 14 all of the results have been summarized. The simulation results have been compared to different sources of experimental data. The quality and quantity of these experimental data vary a lot for the different systems. Carbon dioxide is the main component in natural gas, and therefore most of the solid-liquid experimental work has been done here. For systems involving heptane, benzene, octane and cyclohexane, the experimental data are scarce. This makes it difficult to evaluate the experimental data, which is crucial when evaluating the thermodynamic models. The quality of the results in this report regarding the systems, is therefore questionable. More quality experimental data are therefore required to be able to verify the models and correlate the model parameters ($k_{ij}$).

In this work, there has also been experienced a lot of simulation problems. Especially the sPC-SAFT model has been troubled with a lot of computational problems. It was attempted to do simulations with the sPC-SAFT model for the $CO_2$-methane system, but due a lot of errors during the simulation this was unfortunately not possible. For the benzene, octane and cyclohexane there were also experienced a lot of errors and especially the choice of pressure was crucial for the simulation to work. Based on this, the results with the sPC-SAFT model and the optimal $k_{ij}$ found, may be questionable. For the systems involving octane and cyclohexane, SRK, UMR-PRU and sPC-SAFT gave strange results and illogical phase behavior, especially at low pressures near the SLV loci. For the cyclohexane system, the models were unable to give any results at low cyclohexane concentrations. Both computational issues and a challenging phase behaviors can be the reason for this. The UMR-PRU model had a lot of challenges at low temperatures. In some cases, the simulation with the UMR-PRU model failed due to computational errors. The reason for this could be due to errors in the computational file, or that the UMR-PRU model is not fitted for low temperatures. This issue is investigated in the next chapter.

**Table 14. Summary Results**

| System | Type | Model | Compared to experimental data | | | | kij | Reliability of exp.data |
|---|---|---|---|---|---|---|---|---|
| | | | High temp. | AAD [K] | Low temp. | AAD [K] | | |
| $CO_2$-$CH_4$ | SLE | UMR-PRU | Good | 1.85 | Ok | 4.4 | - | Good |
| | SVE | UMR-PRU | Good | 0.69 | Ok | - | - | |
| | SLE | SRK | Good | 1.17 | Good | 0.86 | 0.0973 | |
| | SVE | SRK | Good | 0.69 | Good | - | 0.0973 | |
| $CO_2$-$N_2$-$CH_4$ | SLE | UMR-PRU | - | - | Ok | 3.44 | - | Good |
| | SLE | SRK | - | - | Good | 0.91 | 0.0956 | |
| $CO_2$-$C_2H_6$-$CH_4$ | SLE | UMR-PRU | - | - | Ok | 3.25 | - | Good |
| | SLE | SRK | - | - | Good | 0.66 | 0.0956 | |
| Hexane-$CH_4$ | SLE | UMR-PRU | Good | 1.64 | Poor (fails) | - | - | Good |
| | SLE | SRK | Good | - | Good | 1.42[a] | 0.03 | |
| | SLE | sPC-SAFT | Ok | - | Ok | 2.232[a] | 0 | |
| Heptane-$CH_4$ | SLE | UMR-PRU | Good | - | Poor (fails) | | - | Ok |
| | SLE | SRK | Good | - | Good | 1.76[a] | 0.037 | |
| | SLE | sPC-SAFT | Good | - | Ok | 3.12[a] | 0 | |
| Benzene - $CH_4$ | SLE | UMR-PRU | Good | 3.52 | Ok | 5.2 | | Ok |
| | SLE | SRK | Good | 3.18 | Good | 0.78 | 0.06 | |
| | SLE | sPC-SAFT | Fails[b] | | Ok | 2.62 | 0.02 | |
| Benzene-$C_2H_6$[d]-$CH_4$ | SLE | UMR-PRU | - | - | Good | 1.43 | | Poor[c] |
| | SLE | SRK | - | - | Good | 1.34 | 0.06 | |
| | SLE | sPC-SAFT | - | - | Good | 1 | 0.02 | |
| Octane - $CH_4$ | SLE | UMR-PRU | Good | 0.785 | Fails | - | - | Poor[c] |
| | SLE | SRK | Good | 0.771 | Ok | 2 | 0.04 | |
| | SLE | sPC-SAFT | Good | 0.398 | Ok | 3.2 | 0.01 | |
| Octane - $C_2H_6$[b]-$CH_4$ | SLE | UMR-PRU | - | - | Poor (Fails) | - | - | Poor[c] |
| | SLE | SRK | - | - | Ok | 3.38 | 0.04 | |
| | SLE | sPC-SAFT | - | - | Good | 1.1 | 0.01 | |
| Cyclohexane -$CH_4$ | SLE | UMR-PRU | Good | 3.5 | Fails | - | - | Poor[c] |
| | SLE | SRK | Ok | 4.7 | Poor | - | 0 | |
| | SLE | sPC-SAFT | Ok | 4.7 | Poor | - | 0 | |

**a:AAD over whole temperature range. b: Fails at high pressures. c: Exp data at low temp. needed. d: High ethane conc.**

## 6.2 Evaluation of the UMR-PRU model

The UMR-PRU model is able to give reasonable predictions of $CO_2$- natural gas component systems. At high $CO_2$ concentrations and temperatures, the UMR-PRU provides the same predictions as the SRK EoS. However, when the temperature is lowered the deviations between experimental data and the UMR-PRU are increased. This is reported for both freeze out in liquid methane and freeze out in vapor methane. By adding components such as nitrogen and ethane, the predictive ability of UMR-PRU is increased, see section 5.2.3. It seems like adding these components, which reduces the concentration of methane, makes the UMR-PRU model to give better predictions.

For methane mixtures containing heavier hydrocarbons, the UMR-PRU model can only give reasonable predictions at high temperatures and for high solute concentrations. At low solute concentrations the model predicts unrealistic freeze out temperatures. However, for the methane-benzene system, the UMR-PRU model is able to give reasonable results.

It was attempted to find a possible explanation for why UMR-PRU gives different results for the systems. Instead of binary interaction parameters, the UMR-PRU model utilizes UNIFAC group-interaction parameters (IPs), $A_{nm}$, $B_{nm}$, $C_{nm}$. The parameters used in the investigated systems are listed in Table 15, obtained from the NeqSim library. The heavy hydrocarbons, except benzene, belong to the same UNIFAC group, and therefore have the same parameters.

**Table 15. UNIFAC group-interaction parameters (IPs) $A_{nm}$, $B_{nm}$ and $C_{nm}$ for the UMR-PRU model**

| n | m | $A_{nm}$(K) | $B_{nm}$(K) | $C_{nm}$($K^{-1}$) |
|---|---|---|---|---|
| $CO_2$ | $CH_4$ | 272.73 | 0.9931 | 0 |
| $C_6H_{14}$ | $CH_4$ | -250.17 | -0.50672 | -0.004539 |
| $C_7H_{16}$ | $CH_4$ | -250.17 | -0.50672 | -0.004539 |
| $C_8H_{18}$ | $CH_4$ | -112.37 | -0.4585 | 0.000063 |
| $C_6H_{12}$ | $CH_4$ | -250.17 | -0.50672 | -0.004539 |
| $C_6H_6$ | $CH_4$ | -250.17 | -0.50672 | -0.004539 |

These parameters are utilized in the UNIFAC $\Psi$ function:

$$\Psi = \exp\left[-\frac{A_{nm} + B_{nm} \cdot (T - 298.15) + C_{nm} \cdot (T - 298.15)^2}{T}\right] \qquad (6.1)$$

The two terms, $B_{nm} \cdot (T - 298.15)$ and $C_{nm} \cdot (T - 298.15)^2$, have been plotted against low temperatures in Figure 59. The $C_{nm}$term seems only to affect the UNIFAC group 1 components: n-hexane, n-heptane, n-octane and cyclohexane. The term will have an exponential effect when the temperature is lowered under standard temperature 298 K. This might be the reason for why UMR-PRU fails for these components. For temperatures close to the standard state temperature 298 K the effect of this term is negligible.

The $B_{nm}$ term for the $CO_2$ – methane system (group 56) might be the explanation for why UMR-PRU almost linearly deviates from experimental data when the temperature is decreased, see section 5.2.1.3.

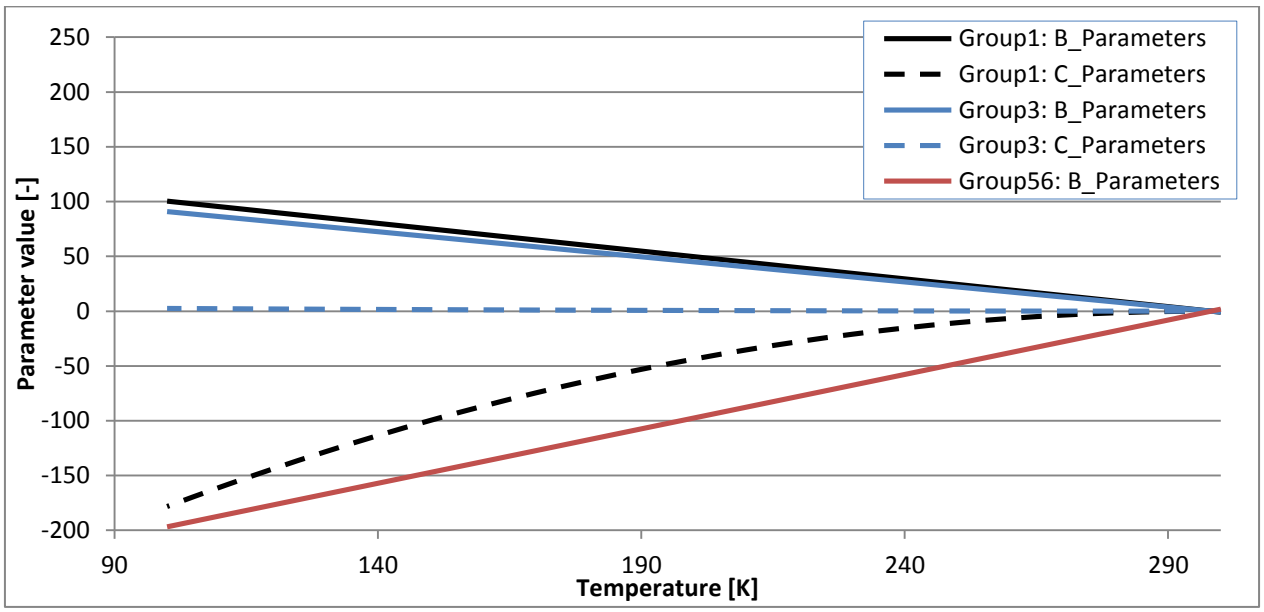


**Figure 59. The effect of UNIFAC parameter terms in the UMR-PRU model**

The result with UMR-PRU shows that the model has to be investigated more thoroughly and extended to be able to predict the solid-liquid behavior at low temperatures. New UNIFAC interaction parameters are probably necessary for the model to be more suitable at low temperatures.

## 6.3 Evaluation of SRK EoS and sPC-SAFT EoS

The SRK EoS is not able to predict the phase behavior of the systems investigated when the binary interaction parameter is set to zero. However, it shows good capability in correlating the experimental data with optimal $k_{ij}$ for all of the systems. For multicomponent systems this means that the model is highly dependable on fitting the $k_{ij}$ between the components. This will increase the complexity of the calculations, and therefore it is recommend that SRK is applied for systems for correlating experimental data

The sPC-SAFT EoS shows good ability to predict the phase behavior of the HHC-methane systems, when the $k_{ij}$ is zero. Compared to SRK, the sPC-SAFT EoS has problems correlating the experimental data with an interaction parameter. For most of the systems, changing the value of $k_{ij}$ did not improve the prediction results. However, it was a lot of computational problems with the sPC-SAFT model, and this may have affected the results. Still, on the basis on these results, the sPC-SAFT has proven to be very accurate to predict the solid-liquid equilibrium behavior.

## 6.4 Evaluation of the solid model

The model for calculating the fugacity in the solid phase is giving in section 3.4.2. The term involving heat of fusion is the dominant one, and the value of heat of fusion is therefore crucial for determine the solid fugacity. For the systems investigated the difference in heat capacity is set to the heat capacity of water. The effect of this is very small, since the two terms with $\Delta C_{Pi}$ will approximately cancel each other out. However, to get precisely results the correct $\Delta C_{Pi}$ should be implemented. The difference in molar volume between the components is set to zero, and the effect of this is very small. However, at higher pressure levels the effect might increase, and correct values should therefore be used.

# 7. Conclusion and recommendations

The literature review shows that the favored method for describing the solid-fluid phase equilibrium is based on equations of state for calculating the liquid phase, combined with an expression for the fugacity in the solid phase. In this work, the UMR-PRU model, SRK EoS and sPC-SAFT have been applied together with a solid model (eq.3.30) based on sub-cooled liquid.

The report covers that there is a limited amount of experimental data for the solid-liquid equilibrium systems, especially for binary methane rich systems in equilibrium with octane and cyclohexane. This makes it difficult to give a proper evaluation of the thermodynamic models, and to correlate the interaction parameters. More accurate experimental data for natural gas systems at low temperatures should therefore be acquired.

The SRK equation of state is able to predict the solid-liquid phase behavior when it is correlated to experimental data. However, it fails to give predictions without a binary interaction parameter. It is here that the sPC-SAFT shows its strength. The model gives reasonable predictions of the solid-liquid phase behavior for the HHC-methane rich systems. The model is less dependent on being correlated by experimental data.

The UMR-PRU model gives reasonable prediction results for $CO_2$-methane rich systems. However, when the temperature, drops the predictions starts deviating compared to the experimental data. For HHC-methane rich systems, the UMR-PRU model is only able to give predictions at high temperatures.

The UNIFAC interaction parameters utilized in the UMR-PRU model has been investigated. The components hexane, heptane, octane and cyclohexane belong to the same UNIFAC group. For these components the modelling with UMR-PRU fails. The components have the same parameter $C_{nm}$ , which gives an exponential effect in the UNIFAC equation (6.1). For the $CO_2$ –methane system this term is zero. This may have an effect on the UMR-PRU models ability to predict solid-liquid behavior at low temperatures. The UMR-PRU model should be investigated more extensively, and new UNIFAC parameters suited for low temperatures should probably be considered for the model.

# References


[1] BP. (2014, BP Energy Outlook 2035. Available: http://www.bp.com/

[2] BP. (2013, BP Statistical Review of World Energy. Available: http://www.bp.com/

[3] M. J. Moran and H. N. Shapiro, "Chemical and Phase Equilibrium," in *Fundamentals of Engineering Thermodynamics*, Wiley, Ed., Fifth edition ed, 2006.

[4] J. P. Kohn and K. D. Luks, "Solubility of Hydrocarbons in Cryogenic LNG and NGL Mixtures," Gas Processors Association, Gas Processors Association Research Report RR-221976.

[5] H. L. Chang, L. J. Hurt, and R. Kobayashi, "Vapor-liquid equilibria of light hydrocarbons at low temperatures and high pressures: The methane-n-heptane system," *AIChE Journal,* vol. 12, pp. 1212-1216, 1966.

[6] M. W. Hlavinka and V. N. Hernandez. (2006, PROPER INTERPRETATION OF FREEZING AND HYDRATE PREDICTION RESULTS FROM PROCESS SIMULATION Available: http://www.bre.com/portals/0/technicalarticles/Proper%20Interpretation%20of%20Freezing%20and%20Hydrate%20Prediction%20Results%20from%20Process%20Simulation%20Paper.pdf

[7] G. P. Kuebler and C. McKinley, "Solubility of Solid Benzene, Toluene, n-Hexane, and n-Heptane in Liquid Methane," in *Advances in Cryogenic Engineering*. vol. 19, K. D. Timmerhaus, Ed., ed: Springer US, 1995, pp. 320-326.

[8] J. C. de Hemptinne, "Benzene crystallization risks in the LIQUEFIN liquefied natural gas process," *Process Safety Progress,* vol. 24, pp. 203-212, 2005.

[9] A. L. Myers and J. M. Prausnitz, "Thermodynamics of Solid Carbon Dioxide Solubility in Liquid Solvents at Low Temperatures," *Industrial & Engineering Chemistry Fundamentals,* vol. 4, pp. 209-212, 1965/05/01 1965.

[10] T. Eggeman and S. Chafin, "Beware the pitfalls of CO2 freezing prediction," *Chem. Eng. Progress* vol. 101, pp. 39-44, 2005.

[11] J. G. Gmehling, T. F. Anderson, and J. M. Prausnitz, "Solid-Liquid Equilibria Using UNIFAC," *Industrial & Engineering Chemistry Fundamentals,* vol. 17, pp. 269-273, 1978/11/01 1978.

[12] Y. S. Wei and R. J. Sadus, "Equations of state for the calculation of fluid-phase equilibria," *AIChE Journal,* vol. 46, pp. 169-196, 2000.

[13] K. Carter and K. D. Luks, "Extending a classical EOS correlation to represent solid–fluid phase equilibria," *Fluid Phase Equilibria,* vol. 243, pp. 151-155, 2006.

[14] L. Zhang, R. Burgass, A. Chapoy, B. Tohidi, and E. Solbraa, "Measurement and modeling of CO 2 frost points in the CO 2-methane systems," *Journal of Chemical and Engineering Data,* vol. 56, pp. 2971-2975, 2011.

[15] L. Zhang and E. Solbraa, "Solid phase behavior in offshore natural gas liquefaction concepts," *Huagong Xuebao/CIESC Journal,* vol. 60, pp. 44-49, 2009.

[16] T. Shen, T. Gao, W. Lin, and A. Gu, "Determination of CO2 Solubility in Saturated Liquid CH4 + N2 and CH4 + C2H6 Mixtures above Atmospheric Pressure," *Journal of Chemical & Engineering Data,* vol. 57, pp. 2296-2303, 2012/08/09 2012.

[17] G. De Guido, S. Langè, S. Moioli, and L. A. Pellegrini, "Thermodynamic method for the prediction of solid CO2 formation from multicomponent mixtures," *Process Safety and Environmental Protection,* vol. 92, pp. 70-79, 2014.

[18] M. P. W. M. Rijkers, M. Malais, C. J. Peters, and J. de Swaan Arons, "Experimental determination of the phase behavior of binary mixtures of methane + benzene: Part I. Vapor + liquid, solid benzene + liquid, solid benzene + vapor and solid benzene + liquid + vapor equilibria," *Fluid Phase Equilibria,* vol. 77, pp. 327-342, 1992.

[19] L. Zhang and E. Solbraa, "Prediction of solubility of n-hexane and other heavy hydrocarbons in LNG processes," 2011, pp. 698-722.
[20] M. F. Gord, M. Roozbahani, H. R. Rahbari, and S. J. Haghighat Hosseini, "Modeling thermodynamic properties of natural gas mixtures using perturbed-chain statistical associating fluid theory," *Russian Journal of Applied Chemistry,* vol. 86, pp. 867-878, 2013.
[21] D. N. Justo-García, F. García-Sánchez, N. L. Díaz-Ramírez, and E. Díaz-Herrera, "Modeling of three-phase vapor–liquid–liquid equilibria for a natural-gas system rich in nitrogen with the SRK and PC-SAFT EoS," *Fluid Phase Equilibria,* vol. 298, pp. 92-96, 2010.
[22] V. Louli, G. Pappa, C. Boukouvalas, S. Skouras, E. Solbraa, K. O. Christensen, and E. Voutsas, "Measurement and prediction of dew point curves of natural gas mixtures," *Fluid Phase Equilibria,* vol. 334, pp. 1-9, 2012.
[23] E. Skouras, V. Louli, G. Pappa, C. Boukouvalas, E. Solbraa, and E. Voutsas, "Dew point prediction of synthetic and real natural gas mixtures with the UMR-PRU model," 2010.
[24] V. Louli, C. Boukouvalas, E. Voutsas, K. Magoulas, and D. Tassios, "Application of the UMR-PRU model to multicomponent systems: Prediction of the phase behavior of synthetic natural gas and oil systems," *Fluid Phase Equilibria,* vol. 261, pp. 351-358, 2007.
[25] G. Soave, "Equilibrium constants from a modified Redlich-Kwong equation of state," *Chemical Engineering Science,* vol. 27, pp. 1197-1203, 1972.
[26] N. von Solms, M. L. Michelsen, and G. M. Kontogeorgis, "Computational and Physical Performance of a Modified PC-SAFT Equation of State for Highly Asymmetric and Associating Mixtures," *Industrial & Engineering Chemistry Research,* vol. 42, pp. 1098-1105, 2003/03/01 2003.
[27] W. G. Chapman, K. E. Gubbins, G. Jackson, and M. Radosz, "SAFT: Equation-of-state solution model for associating fluids," *Fluid Phase Equilibria,* vol. 52, pp. 31-38, 1989.
[28] W. G. Chapman, K. E. Gubbins, G. Jackson, and M. Radosz, "New reference equation of state for associating liquids," *Industrial & Engineering Chemistry Research,* vol. 29, pp. 1709-1721, 1990/08/01 1990.
[29] J. Gross and G. Sadowski, "Perturbed-Chain SAFT: An Equation of State Based on a Perturbation Theory for Chain Molecules," *Industrial & Engineering Chemistry Research,* vol. 40, pp. 1244-1260, 2001/02/01 2001.
[30] E. Voutsas, K. Magoulas, and D. Tassios, "Universal Mixing Rule for Cubic Equations of State Applicable to Symmetric and Asymmetric Systems: Results with the Peng−Robinson Equation of State," *Industrial & Engineering Chemistry Research,* vol. 43, pp. 6238-6246, 2004/09/01 2004.
[31] A. Fredenslund, R. L. Jones, and J. M. Prausnitz, "Group-contribution estimation of activity coefficients in nonideal liquid mixtures," *AIChE Journal,* vol. 21, pp. 1086-1099, 1975.
[32] B. ZareNezhad, "Prediction of CO2 freezing points for the mixtures of CO2-CH4 at cryogenic conditions of NGL extraction plants," *Korean Journal of Chemical Engineering,* vol. 23, pp. 827-831, 2006/09/01 2006.
[33] J. M. Prausnitz, R. N. Lichtenthaler, and E. G. de Azevedo, "Solubilites of Solid in Liquids," in *Molecular thermodynamics of fluid-phase equilibria*, Third edition ed: Prentice-Hall PTR, 1999, p. 860.
[34] K. S. Pedersen, P. L. Christensen, and S. J. Azeem, "Wax Formation," in *Phase Behavior of Petroleum Reservoir Fluids*, ed: CRC Press, 2006, pp. 229-258.
[35] L. F. Ayala and J. E. Fernandez, "Evaluating Crystallization Risks in Liquefied-Natural-Gas (LNG) Production," 2009/6/1/ 2009.
[36] H. G. Donnelly and D. L. Katz, "Phase Equilibria in the Carbon Dioxide–Methane System," *Industrial & Engineering Chemistry,* vol. 46, pp. 511-517, 1954/03/01 1954.

[37] G. J. Boyle, in *Solid-Liquid Equilibrium Data Collection*. vol. VIII, H. Knapp, M. Teller, and R. Langhorst, Eds., ed DECHEMA Chemistry Data Series: DECHEMA, p. 48.
[38] C. J. Sterner, "Phase Equilibria in the CO2-Methane Systems," in *Advances in Cryogenic Engineering*. vol. 6, K. D. Timmerhaus, Ed., ed: Springer US, 1961, pp. 467-474.
[39] M. Streich, "Hydrogen Process Voume 49 , (86-88)," in *Solid-Liquid Equilibrium Data Collection*. vol. VIII, H. Knapp, M. Teller, and R. Langhorst, Eds., ed DECHEMA Chemistry Data Series: DECHEMA, 1970, p. 55.
[40] G. Voss, "DISS, TU BERLIN," in *Solid-Liquid Equilibrium Data Collection*. vol. VIII, H. Knapp, M. Teller, and R. Langhorst, Eds., ed DECHEMA Chemistry Data Series: DECHEMA, 1975, p. 56.
[41] F. Kurata, "Solubility of Solid Carbon Dioxide in Pure Light Hydrocarbons and Mixturesof Light Hydrocarbons," Gas Processors Association1974.
[42] M. J. Pikaar, "A study of Phase Equilibrium in Hydricarbon-CO2 Systems. ," PhD thesis, Department of Chemical engineering, University of London, 1959.
[43] J. A. Davis, N. Rodewald, and F. Kurata, "Solid-liquid-vapor phase behavior of the methane-carbon dioxide system," *AIChE Journal,* vol. 8, pp. 537-539, 1962.
[44] G. M. Agrawal and R. J. Laverman, "Phase Behavior of the Methane-Carbon Dioxide System in the Solid-Vapor Region," in *Advances in Cryogenic Engineering*. vol. 19, K. D. Timmerhaus, Ed., ed: Springer US, 1995, pp. 327-338.
[45] T. T. Le and M. A. Trebble, "Measurement of Carbon Dioxide Freezing in Mixtures of Methane, Ethane, and Nitrogen in the Solid−Vapor Equilibrium Region," *Journal of Chemical & Engineering Data,* vol. 52, pp. 683-686, 2007/05/01 2007.
[46] L. Zhang, "Solid-Fluid Phase Equilibrium for Natural Gas Processing at Low Temperatures," Ph.D., Department of Energy and Process Engineering, Norwegian University of Science and Technology, 2012.
[47] J. Brewer and F. Kurata, "Freezing points of binary mixtures of methane," *AIChE Journal,* vol. 4, pp. 317-318, 1958.
[48] E. Dickinson, C. M. Knobler, and R. L. Scott, "Solid/liquid phase equilibria in the mixtures methane + n-hexane and methane + n-pentane," *Journal of the Chemical Society, Faraday Transactions 1: Physical Chemistry in Condensed Phases,* vol. 69, pp. 2179-2187, 1973.
[49] K. D. Luks, J. D. Hottovy, and J. P. Kohn, "Three-phase solid-liquid-vapor equilibriums in the binary hydrocarbon systems methane-n-hexane and methane-benzene," *Journal of Chemical & Engineering Data,* vol. 26, pp. 402-403, 1981/10/01 1981.
[50] G. P. Kuebler and G. McKinley, "Solubility of Solid n-Butane and n-Pentane in Liquid Methane," in *Advances in Cryogenic Engineering*. vol. 21, K. D. Timmerhaus and D. H. Weitzel, Eds., ed: Springer US, 1975, pp. 509-515.
[51] A. Neumann and R. Mann, "Kaltetechnik-Klimatisierung,," in *Solid-Liquid Equilibrium Data Collection*. vol. VIII, H. Knapp, M. Teller, R. Langhorst, and Eds., ed DECHEMA Chemistry Data Series.: DECHEMA, 1970, p. 201.
[52] J. Shim and J. P. Kohn, "Multiphase and Volumetric Equilibria of Methane-n-Hexane Binary System at Temperatures Between -110° and 150° C," *Journal of Chemical & Engineering Data,* vol. 7, pp. 3-8, 1962/01/01 1962.
[53] D. L. Tiffin, K. D. Luks, and J. P. Kohn, "Solubility Enhancement of Solid Hydrocarbons in Liquid Methane due to the Presence of Ethane," in *Advances in Cryogenic Engineering*. vol. 23, K. D. Timmerhaus, Ed., ed: Springer US, 1978, pp. 538-543.
[54] M. Teller and H. Knapp, "Unpublished data," in *Solid-Liquid Equilibrium Data Collection*. vol. VIII, H. Knapp, M. Teller, and R. Langhorst, Eds., ed DECHEMA Chemistry Data Series.: DECHEMA, 1985, pp. 219-220.

[55] M. Teller, "DISS. TU BERLIN," in *Solid-Liquid Equilibrium Data Collection*. vol. VIII, H. Knapp, M. Teller, and R. Langhorst, Eds., ed DECHEMA Chemistry Data Series.: DECHEMA, 1982, p. 347.
[56] J. P. Kohn and W. F. Bradish, "Multiphase and Volumetric Equilibria of the Methane-n-Octane System at Temperatures between -110o and 150o C," *Journal of Chemical & Engineering Data,* vol. 9, pp. 5-8, 1964/01/01 1964.
[57] J. P. Kohn, K. D. Luks, P. H. Liu, and D. L. Tiffin, "Three-phase solid-liquid-vapor equilibriums of the binary hydrocarbon systems methane-n-octane and methane-cyclohexane," *Journal of Chemical & Engineering Data,* vol. 22, pp. 419-421, 1977/10/01 1977.
[58] J. P. Kohn and K. D. Luks, "Solubility of Hydrocarbons in Cryogenic LNG and NGL Mixtures," Gas Processors Association Research Report RR-271977

[59] D. L. Tiffin, J. P. Kohn, and K. D. Luks, "Solid hydrocarbon solubility in liquid methane-ethane mixtures along three-phase solid-liquid-vapor loci," *Journal of Chemical & Engineering Data,* vol. 24, pp. 306-310, 1979/10/01 1979.
[60] M. Christov and R. Dohrn, "High-pressure fluid phase equilibria: Experimental methods and systems investigated (1994–1999)," *Fluid Phase Equilibria,* vol. 202, pp. 153-218, 2002.
[61] R. Dohrn, S. Peper, and J. M. S. Fonseca, "High-pressure fluid-phase equilibria: Experimental methods and systems investigated (2000–2004)," *Fluid Phase Equilibria,* vol. 288, pp. 1-54, 2010.
[62] J. M. S. Fonseca, R. Dohrn, and S. Peper, "High-pressure fluid-phase equilibria: Experimental methods and systems investigated (2005–2008)," *Fluid Phase Equilibria,* vol. 300, pp. 1-69, 2011.
[63] V. De Stefani, A. Baba-Ahmed, and D. Richon, "A review of experimental methods for solid solubility determination in cryogenic systems," *Cryogenics,* vol. 44, pp. 631-641, 2004.

# Appendix A: Fundamentals Phase Equilibrium

This appendix gives a general introduction for the calculation of thermodynamic equilibrium.

The first law of thermodynamics is the law of energy conservation and is given by:

$$dU = dQ - dW$$

The second law of thermodynamics concerns the change in total entropy of a system. The law states that the entropy of an isolated system never decreases. In general, it is given by:

$$dS \geq \frac{dQ}{T}$$

In phase equilibrium calculations, it is appropriate to work with the Gibbs free energy, which is defined by

$$G = H - TS = U + PV - TS$$

Combining equation 1, 2 and 3 we get:

$$dG \leq VdP - SdT$$

For processes at constant pressure and temperature the equation is given by:

$$dG)_{T,p} \leq 0$$

## Chemical Potential

The chemical potential is defined as the molar Gibbs free energy, and is very useful for describing the phase behavior of mixture. The function is given by:

$$\mu_i = \bar{G}_i = \frac{\partial G}{\partial n_i}\Big)_{T,p,n_i}$$

The Gibbs free energy for a total system equals the Gibbs free energies for each phase

$$dG)_{T,p} = dG^1)_{T,p} + dG^2)_{T,p} = 0$$

$$dG)_{T,p} = \sum_{i=1}^{N} \mu_i^1 dn_i^1 + \sum_{i=1}^{N} \mu_i^2 dn_i^2 = 0$$

The system is close, and mass balance must apply. The equation can thus be rewritten as:

$$\mu_i^1 = \mu_i^2$$

The equation states that the chemical potential of any component i, at a fixed pressure and temperature, must be the same when two phases are in equilibrium.

## Fugacity

It is advantageous for many types of thermodynamic analyses to use fugacity instead of the chemical potential. The fugacity $f$, and is introduced with the expression:

$$\mu = \bar{R}T \ \ln f + C(T)$$

The fugacity has the same units as pressure and for ideal gas behavior the fugacity plats the same role as pressure. Equation xx can be rearranged to:

$$\bar{R}T \left(\frac{\partial \ln f}{\partial p}\right)_T = \bar{v}$$

Ideal gas behavior is approached as pressure tends to zero, and the constant term can be determined by requiring the fugacity of a pure component is equal to the pressure in the limit of zero pressure, describes as:

$$\lim_{p \to 0} \frac{f}{p} = 1$$

By combining the expression of fugacity with equation xx, the following equilibrium relation is given:

$$f_i^1 = f_i^2$$

The fugacity coefficient of component $i$, is defined as:

$$\varphi_i = \frac{f_i}{p_i}$$

A general relation to calculate fugacity is given by, Prausnitz, et al. [33]

$$RT \ln \varphi_i = RT \ln \frac{f_i}{y_i P} = \int_0^P \left(\bar{v}_i - \frac{RT}{P}\right) dP$$

where $\bar{v}_i = (\partial V / \partial n_i)_{T,P,n_i}$ is the partial molar volume of component $i$ , $\varphi_i$ is the fugacity coefficient $i$, $f_i$ is the fugacity of $i$ and $y_i$ is the molar fraction of $i$.

## Appendix B: Experimental Methods

This section introduces the experimental methods that have been used by the different authors to obtain the experimental data. The experimental methods used for fluid phase equilibria and solid-fluid phase equilibria are quite similar. The classification of the experimental methods are therefore based on the review articles, “"High-pressure fluid-phase equilibria: Experimental methods and systems investigated”, by Christov and Dohrn [60], Dohrn, et al. [61] and Fonseca, et al. [62]. Only methods suitable for solid-liquid equilibrium are included in this review.

The classification of experimental methods for high-pressure phase equilibria is shown in Figure 60. There are two main categories, depending on how the compositions of the equilibrium phases are determined (analytically or not) and whether the mixture to be investigated has been prepared (synthesized) with known composition or not: analytical methods and synthetic methods.

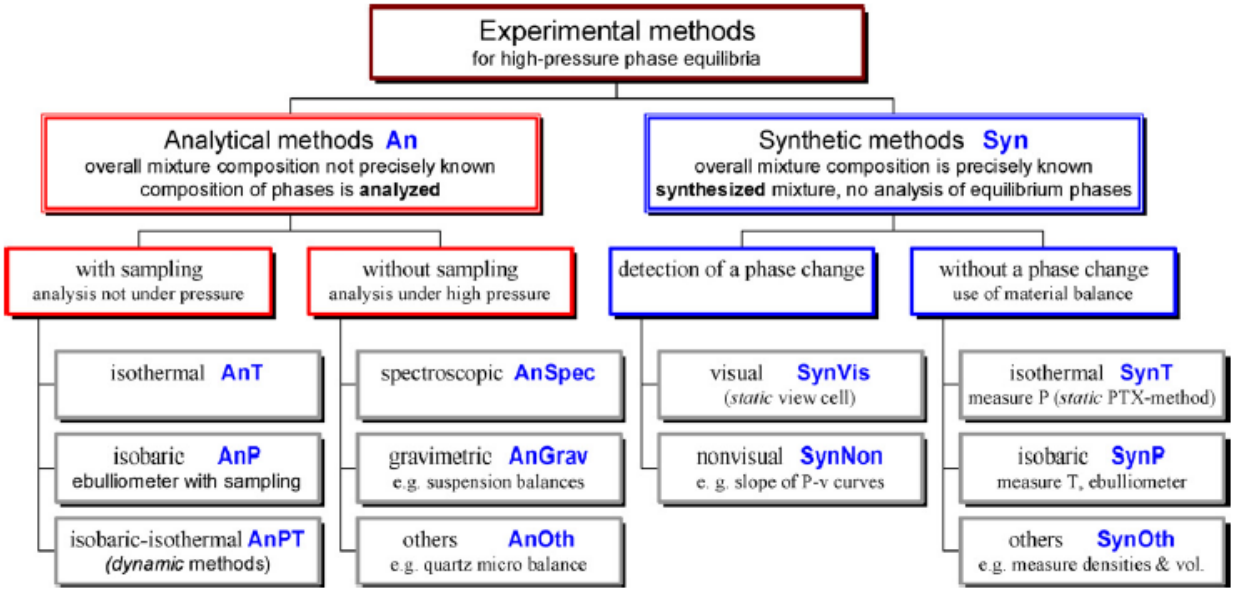


**Figure 60. Overview of Experimental methods for high-pressure phase equilibria**

### B.1 Analytical Method (An)

The analytical method (An) involves first a procedure of making the equilibrium solution and then an analytical determination of the compositions of the coexisting phases. This can be done with sampling or without sampling.

In analytical methods with samples, the samples are analyzed outside the equilibrium cell. The use of gas chromatography has been a common technique for analyzing the composition.

Analytical methods with sampling can be classified into: isothermal methods (AnT), isobaric-isothermal methods (AnPt) and isobaric methods (AnP).

Analytical methods without sampling use a physicochemical method of analysis inside the equilibrium cell under pressure, mainly spectroscopic methods (AnSpec). For cryogenic systems the infrared spectroscopy is most used among the available spectroscopic techniques, De Stefani, et al. [63].

### B.1.1 Analytical isobaric- isothermal methods (AnT)

The characterization of the isothermal method is that the temperature stays constant in the equilibrium cell. In the start of an experiment an equilibrium cell is charged with the mixture of interest, and is kept at the desired temperature. The pressure is adjusted above or below the desired equilibrium value. A technique of preparing the solution is to agitate the mixture in the presence of excess solute by mechanical stirring or recirculation of the vapor phase, Kuebler and McKinley [50].

### B.1.2 Analytical-isothermal methods (AnPT)

In isobaric-isothermal methods, often called dynamic models, one or more fluid flows continuously through another phase in the equilibrium cell. The cell is regulated at a desired temperature, and the pressure is kept constant during the experiment by controlling the vapor phase. For solid-fluid equilibrium experiments solutions can be formed using a single-pass mode either with solute precipitating from a feed mixture or a previously deposited solute dissolved into a pure solvent feed, Kuebler and McKinley [50]. Isobaric-isothermal methods have the advantage that sampling does not disturb the equilibrium, and large amounts of sample can be taken.

## B.2 Synthetic methods (Syn)

For syntactic methods sampling is not necessary. The idea is to prepare a mixture of a known composition, which is established by accurate weighing techniques. After the mixture is placed into the equilibrium cell, the temperature and pressure is adjusted so that the mixture is homogeneous, in a single phase. Depending on how the phase transition is detected, synthetic methods with a phase transitions can be divided into visual (SynVis) and non-visual synthetic methods (SynNon).

### B.2.1 Synthetic visual methods (SynVis)

In synthetic visual methods (often referred as cryoscopic methods) the new phase is detected by visual observation. When the mixture is homogenous, temperature or pressure is lowered or increased until the formation of a new phase is observed. For solid-liquid equilibrium detection, the frost points or freezing points are noted.

### B.2.2 Synthetic non-visual methods (SynNon)

Instead of visual observation, other physical properties can be detected to determine the phase transition. If the total volume of a variable-volume cell can be measured, the appearance of a new phase can be determined where there is a rapid change in the slope between pressure and volume.

Investigating Pressure-Temperature relationship: The temperature is reduced until the solid phase appears. The equilibrium cell is then slowly warmed, and pressures and temperatures are recorded until the solid melts. By investigating the p-T diagram, the transition will be where there is a sudden change in the p-T relationship.

# Appendix C: Simulation Results and Experimental Data

## C.1 Experimental data from literature and simulated data: Solid $CO_2$ formation in liquid methane

### C.1.1 Predictions and experimental data from Kurata [41]

| Number | Composition [mole %] | | Experimental data | | NeqSim (SRK), kij = 0.0 | | | NeqSim (UMR-PRU) | | | NeqSim (SRK), kij = 0.0973 | | |
|---|---|---|---|---|---|---|---|---|---|---|---|---|---|
| | $CH_4$ | $CO_2$ | Temperature [K] | Pressure [bar] | Temperature [K] | Pressure [bar] | AAD [K] | Temperature [K] | Pressure [bar] | AAD [K] | Temperature [K] | Pressure [bar] | AAD [K] |
| 1 | 10.000 | 90 | 214.3 | 20.79 | 212.490 | 50.000 | 1.810 | 212.940 | 50.000 | 1.360 | 212.820 | 50.000 | 1.480 |
| 2 | 13.500 | 86.5 | 213.7 | 24.31 | 211.150 | 50.000 | 2.550 | 212.065 | 50.000 | 1.635 | 211.758 | 50.000 | 1.942 |
| 3 | 20.000 | 80 | 212.6 | 30.14 | 208.800 | 50.000 | 3.800 | 210.390 | 50.000 | 2.210 | 210.100 | 50.000 | 2.500 |
| 4 | 23.200 | 76.8 | 211.2 | 36.39 | 207.696 | 50.000 | 3.504 | 209.762 | 50.000 | 1.438 | 209.434 | 50.000 | 1.766 |
| 5 | 30.000 | 70 | 210.4 | 39.37 | 205.450 | 50.000 | 4.950 | 208.639 | 50.000 | 1.761 | 208.278 | 50.000 | 2.122 |
| 6 | 40.000 | 60 | 209 | 43.57 | 202.318 | 50.000 | 6.682 | 207.400 | 50.000 | 1.600 | 207.119 | 50.000 | 1.881 |
| 7 | 45.700 | 54.3 | 207.6 | 46.47 | 200.567 | 50.000 | 7.033 | 206.845 | 50.000 | 0.755 | 206.652 | 50.000 | 0.948 |
| 8 | 50.000 | 50 | 207.3 | 46.93 | 199.230 | 50.000 | 8.070 | 206.445 | 50.000 | 0.855 | 206.334 | 50.000 | 0.966 |
| 9 | 57.400 | 42.6 | 206.2 | 48.18 | 196.800 | 50.000 | 9.400 | 205.712 | 50.000 | 0.488 | 205.790 | 50.000 | 0.410 |
| 10 | 79.500 | 20.5 | 201.3 | 48.18 | 185.942 | 50.000 | 15.358 | 200.270 | 50.000 | 1.030 | 200.678 | 50.000 | 0.622 |
| 11 | 84.610 | 15.39 | 196.9 | 45.18 | 181.150 | 50.000 | 15.750 | 197.800 | 50.000 | 0.900 | 197.150 | 50.000 | 0.250 |
| 12 | 89.920 | 10.08 | 189.3 | 39.54 | 173.604 | 50.000 | 15.696 | 189.350 | 50.000 | 0.050 | 189.200 | 50.000 | 0.100 |
| 13 | 94.150 | 5.85 | 182.2 | 32.91 | 163.739 | 50.000 | 18.461 | 180.234 | 50.000 | 1.966 | 179.300 | 50.000 | 2.900 |
| 14 | 97.060 | 2.94 | 169.9 | 22.35 | 151.960 | 50.000 | 17.940 | 169.515 | 50.000 | 0.385 | 167.600 | 50.000 | 2.300 |
| 15 | 98.170 | 1.83 | 162 | 16.7 | 144.547 | 50.000 | 17.453 | 162.750 | 50.000 | 0.750 | 160.225 | 50.000 | 1.775 |
| 16 | 99.070 | 0.93 | 150.4 | 10.53 | 135.000 | 50.000 | 15.400 | 153.900 | 50.000 | 3.500 | 150.627 | 50.000 | 0.227 |
| 17 | 99.420 | 0.58 | 144.5 | 8.08 | 129.000 | 50.000 | 15.500 | 148.237 | 50.000 | 3.737 | 144.546 | 50.000 | 0.046 |
| 18 | 99.630 | 0.37 | 139.4 | 6.29 | 123.786 | 50.000 | 15.614 | 143.190 | 50.000 | 3.790 | 139.183 | 50.000 | 0.217 |
| 19 | 99.750 | 0.25 | 135.2 | 5.07 | 119.557 | 50.000 | 15.643 | 139.000 | 50.000 | 3.800 | 134.817 | 50.000 | 0.383 |
| 20 | 99.840 | 0.16 | 129.6 | 3.57 | 115.084 | 50.000 | 65.084 | 134.630 | 50.000 | 5.030 | 130.172 | 50.000 | 0.572 |
| | | | | | **AAD** | | **13.785** | **AAD** | | **1.852** | **AAD** | | **1.170** |

## .1.2 Predictions and experimental data from Shen, et al. [16]

| Number | Composition [mole %] | | | Experimental data | | NeqSim (SRK), kij = 0.0973 | | | NeqSim (UMR-PRU) | | |
|---|---|---|---|---|---|---|---|---|---|---|---|
| | $CH_4$ | $C_2H_4$ | $CO_2$ | Temperature [K] | Pressure [bar] | Temperature [K] | Pressure [bar] | AAD [K] | Temperature [K] | Pressure [bar] | AAD [K] |
| 1 | 99.9787 | | 0.0213 | 112.00 | 0.93 | 112.58 | 5.93 | 0.585 | 117.80 | 5.93 | 5.804 |
| 2 | 99.9177 | | 0.0823 | 124.00 | 2.41 | 123.76 | 7.41 | 0.242 | 128.72 | 7.41 | 4.724 |
| 3 | 99.8587 | | 0.1413 | 129.70 | 3.65 | 128.90 | 8.65 | 0.802 | 133.68 | 8.65 | 3.978 |
| 4 | 99.7521 | | 0.2479 | 135.20 | 4.89 | 134.74 | 9.89 | 0.463 | 139.25 | 9.89 | 4.052 |
| 5 | 99.6322 | | 0.3678 | 139.40 | 6.17 | 139.17 | 11.17 | 0.233 | 143.45 | 11.17 | 4.046 |
| 6 | 99.4335 | | 0.5665 | 144.50 | 8 | 144.37 | 13.00 | 0.132 | 148.33 | 13.00 | 3.830 |
| 7 | 99.1775 | | 0.8225 | 150.40 | 10.55 | 149.17 | 15.55 | 1.229 | 152.81 | 15.55 | 2.406 |
| 8 | 98.236 | | 1.764 | 162.00 | 17.18 | 160.01 | 22.18 | 1.990 | 162.81 | 22.18 | 0.812 |
| 9 | 97.104 | | 2.896 | 169.90 | 23.15 | 167.81 | 28.15 | 2.087 | 169.97 | 28.15 | 0.067 |
| | | | | | | **AAD** | | 0.863 | AAD | | 3.302 |

## C.1.3 SLV predictions (pressure) and experimental data from Davis, et al. [43]

| Number | Experimental data | | NeqSim (SRK) | | | NeqSim (UMR-PRU) | | |
|---|---|---|---|---|---|---|---|---|
| | Temperature [K] | Pressure [bar] | Temperature [K] | Pressure [bar] | ABS [%] | Temperature [K] | Pressure [bar] | ABS [%] |
| 1 | 211.56 | 32.38 | 211.56 | 29.050 | 10.292 | 211.56 | 30.98 | 4.333 |
| 2 | 207.94 | 45.13 | 207.94 | 43.250 | 4.165 | 207.94 | 43.95 | 2.614 |
| 3 | 205.06 | 48.64 | 205.06 | 48.000 | 1.323 | 205.06 | 47.79 | 1.754 |
| 4 | 201.11 | 48.16 | 201.11 | 47.530 | 1.310 | 201.11 | 47.59 | 1.186 |
| 5 | 197.39 | 46.09 | 197.39 | 45.480 | 1.332 | 197.39 | 45.59 | 1.094 |
| 6 | 194.89 | 43.41 | 194.89 | 43.650 | 0.560 | 194.89 | 43.70 | 0.675 |
| 7 | 193.50 | 43.20 | 193.50 | 42.500 | 1.621 | 193.50 | 42.65 | 1.274 |
| 8 | 188.28 | 38.72 | 188.28 | 38.150 | 1.477 | 188.28 | 38.19 | 1.373 |
| 9 | 184.17 | 34.86 | 184.17 | 34.550 | 0.899 | 184.17 | 34.40 | 1.329 |
| 10 | 180.17 | 31.28 | 180.17 | 31.050 | 0.737 | 180.17 | 30.95 | 1.057 |
| 11 | 178.11 | 29.28 | 178.11 | 29.250 | 0.111 | 178.11 | 29.15 | 0.452 |
| 12 | 176.94 | 28.46 | 176.94 | 28.250 | 0.723 | 176.94 | 28.05 | 1.426 |
| 13 | 173.00 | 25.15 | 173.00 | 25.050 | 0.392 | 173.00 | 24.85 | 1.187 |
| 14 | 170.61 | 23.29 | 170.61 | 23.150 | 0.593 | 170.61 | 22.95 | 1.452 |
| 15 | 169.61 | 22.32 | 169.61 | 22.400 | 0.342 | 169.61 | 22.15 | 0.778 |
| 16 | 166.17 | 19.98 | 166.17 | 19.900 | 0.405 | 166.17 | 19.65 | 1.657 |
| 17 | 163.72 | 18.19 | 163.72 | 18.200 | 0.057 | 163.72 | 17.95 | 1.317 |
| 18 | 161.00 | 16.26 | 161.00 | 16.400 | 0.859 | 161.00 | 16.20 | 0.371 |
| 19 | 159.28 | 15.43 | 159.28 | 15.350 | 0.542 | 159.28 | 15.14 | 1.902 |
| 20 | 151.72 | 11.37 | 151.72 | 11.250 | 1.042 | 151.72 | 11.00 | 3.241 |
| 21 | 148.44 | 9.78 | 148.44 | 9.650 | 1.368 | 148.44 | 9.45 | 3.412 |
| 22 | 143.78 | 7.92 | 143.78 | 7.750 | 2.190 | 143.78 | 7.55 | 4.714 |
| 23 | 139.44 | 6.41 | 139.44 | 6.250 | 2.461 | 139.44 | 6.10 | 4.802 |
| 24 | 132.22 | 4.34 | 132.22 | 4.180 | 3.702 | 132.22 | 4.10 | 5.545 |
| 26 | 129.39 | 3.58 | 129.39 | 3.530 | 1.474 | 129.39 | 3.45 | 3.707 |
| 27 | 125.89 | 3.03 | 125.89 | 2.850 | 5.990 | 125.89 | 2.78 | 8.299 |
| 28 | 120.67 | 2.14 | 120.67 | 1.970 | 7.767 | 120.67 | 1.96 | 8.235 |
| 29 | 116.39 | 1.55 | 116.39 | 1.430 | 7.757 | 116.39 | 1.45 | 6.467 |
| 30 | 111.22 | 1.03 | 111.22 | 0.930 | 9.411 | 111.22 | 0.97 | 5.514 |
| 31 | 105.33 | 0.61 | 105.33 | 0.570 | 7.047 | 105.33 | 0.58 | 5.416 |
| 32 | 97.39 | 0.28 | 97.39 | 0.245 | 13.271 | 97.39 | 0.26 | 7.607 |
| | | | **AAD** | | **2.851** | **AAD** | | **2.943** |

# C.2 Experimental data from literature and simulated data: Solid $CO_2$ formation in vapor methane

## C.2.1 Predictions and experimental data from Agrawal and Laverman [44]

| Number | Composition [mole %] | | Experimental data | | NeqSim (SRK), kij = 0.0973 | | | NeqSim (UMR-PRU) | | | NeqSim (SRK), kij = 0.00 | | |
|---|---|---|---|---|---|---|---|---|---|---|---|---|---|
| | $CH_4$ | $CO_2$ | Temperature [K] | Pressure [bar] | Temperature [K] | Pressure [bar] | ABS | Temperature [K] | Pressure [bar] | AAD [K] | Temperature [K] | Pressure [bar] | AAD [K] |
| 1 | 99.88 | 0.12 | 137.54 | 1.79 | 142.53 | 1.79 | 4.990 | 145.10 | 1.79 | 7.561 | 142.47 | 1.79 | 4.930 |
| 2 | | | 143.21 | 3.45 | 146.26 | 3.45 | 3.053 | 148.57 | 3.45 | 5.362 | 146.14 | 3.45 | 2.933 |
| 3 | | | 144.32 | 5.17 | 148.54 | 5.17 | 4.220 | 150.70 | 5.17 | 6.380 | 148.36 | 5.17 | 4.037 |
| 4 | | | 147.82 | 6.83 | 150.05 | 6.83 | 2.230 | 152.12 | 6.83 | 4.304 | 149.81 | 6.83 | 1.989 |
| 5 | | | 149.76 | 8.55 | 151.22 | 8.55 | 1.460 | 153.22 | 8.55 | 3.460 | 150.90 | 8.55 | 1.140 |
| 6 | | | - | - | 151.99 | 10 | - | 153.94 | 10 | - | 151.60 | 10 | - |
| 7 | | | - | - | 152.50 | 11.25 | - | 154.55 | 11.7 | - | 152.08 | 11.7 | - |
| 8 | 99.03 | 0.97 | 155.15 | 1.79 | 156.46 | 1.79 | 1.310 | 158.11 | 1.79 | 2.962 | 156.40 | 1.79 | 1.252 |
| 9 | | | 158.21 | 3.79 | 161.84 | 3.79 | 3.629 | 163.19 | 3.79 | 4.981 | 161.71 | 3.79 | 3.504 |
| 10 | | | 161.26 | 5.24 | 164.19 | 5.24 | 2.930 | 165.42 | 5.24 | 4.160 | 164.02 | 5.24 | 2.755 |
| 11 | | | 163.98 | 6.96 | 166.23 | 6.96 | 2.250 | 167.36 | 6.96 | 3.382 | 166.00 | 6.96 | 2.016 |
| 12 | | | 166.48 | 10.82 | 169.29 | 10.82 | 2.810 | 170.28 | 10.82 | 3.796 | 168.90 | 10.82 | 2.420 |
| 13 | | | 168.37 | 13.79 | 170.84 | 13.79 | 2.470 | 171.76 | 13.79 | 3.387 | 170.32 | 13.79 | 1.946 |
| 14 | | | 170.59 | 17.86 | 172.29 | 17.86 | 1.700 | 173.15 | 17.86 | 2.557 | 171.55 | 17.86 | 0.961 |
| 15 | | | 172.04 | 20.68 | 172.95 | 20.68 | 0.910 | 173.79 | 20.68 | 1.752 | 172.04 | 20.68 | 0.002 |
| 16 | | | - | - | 173.51 | 25 | - | 174.61 | 26 | - | - | - | - |
| 17 | 98.2 | 1.8 | 158.21 | 1.72 | 160.88 | 1.72 | 2.670 | 162.29 | 1.72 | 4.076 | 160.83 | 1.72 | 2.620 |
| 18 | | | 159.32 | 1.86 | 161.47 | 1.86 | 2.150 | 162.84 | 1.86 | 3.525 | 161.42 | 1.86 | 2.096 |
| 19 | | | 163.98 | 3.45 | 166.24 | 3.45 | 2.258 | 167.36 | 3.45 | 3.383 | 166.13 | 3.45 | 2.147 |
| 20 | | | 164.54 | 3.52 | 166.39 | 3.52 | 1.850 | 167.51 | 3.52 | 2.973 | 166.28 | 3.52 | 1.742 |
| 21 | | | 168.37 | 5.24 | 169.52 | 5.24 | 1.150 | 170.49 | 5.24 | 2.122 | 169.35 | 5.24 | 0.982 |
| 22 | | | 170.32 | 6.96 | 171.75 | 6.96 | 1.430 | 172.62 | 6.96 | 2.299 | 171.52 | 6.96 | 1.199 |
| 23 | | | 174.15 | 8.62 | 173.40 | 8.62 | 0.750 | 174.20 | 8.62 | 0.053 | 173.11 | 8.62 | 1.036 |
| 24 | | | 174.26 | 12.13 | 175.95 | 12.13 | 1.690 | 176.65 | 12.13 | 2.388 | 175.53 | 12.13 | 1.266 |
| 25 | | | 176.04 | 15.72 | 177.75 | 15.72 | 1.709 | 178.37 | 15.72 | 2.325 | 177.16 | 15.72 | 1.116 |
| 26 | | | 176.76 | 22.61 | 179.81 | 22.61 | 3.050 | 180.35 | 22.61 | 3.594 | 178.84 | 22.61 | 2.077 |
| 27 | | | - | - | 180.44 | 27 | - | 180.97 | 27 | - | 179.11 | 27 | - |
| 28 | | | - | - | 180.52 | 31.3 | - | 181.06 | 31.5 | - | - | - | - |
| 29 | 96.93 | 3.07 | 159.59 | 1.72 | 165.21 | 1.72 | 5.620 | 166.39 | 1.72 | 6.796 | 165.16 | 1.72 | 5.568 |
| 30 | | | 160.43 | 1.79 | 165.53 | 1.79 | 5.100 | 166.69 | 1.79 | 6.260 | 165.48 | 1.79 | 5.046 |
| 31 | | | 166.21 | 3.52 | 171.00 | 3.52 | 4.790 | 171.99 | 3.52 | 5.780 | 170.98 | 3.52 | 4.772 |
| 32 | | | 166.43 | 3.55 | 171.16 | 3.55 | 4.730 | 172.06 | 3.55 | 5.628 | 171.05 | 3.55 | 4.622 |
| 33 | | | 170.82 | 5.24 | 174.44 | 5.24 | 3.620 | 175.20 | 5.24 | 4.382 | 174.28 | 5.24 | 3.463 |
| 34 | | | 174.98 | 6.96 | 176.85 | 6.96 | 1.870 | 177.51 | 6.96 | 2.528 | 176.63 | 6.96 | 1.649 |
| 35 | | | 179.37 | 14 | 182.56 | 14 | 3.190 | 183.00 | 14 | 3.632 | 182.08 | 14 | 2.706 |
| 36 | | | 181.59 | 20.62 | 185.30 | 20.62 | 3.710 | 185.64 | 20.62 | 4.047 | 184.50 | 20.62 | 2.913 |
| 37 | | | 183.21 | 20.82 | 185.36 | 20.82 | 2.150 | 185.69 | 20.82 | 2.484 | 184.55 | 20.82 | 1.343 |
| 38 | | | 182.15 | 21.44 | 185.54 | 21.44 | 3.390 | 185.87 | 21.44 | 3.717 | 184.70 | 21.44 | 2.548 |
| 39 | | | 184.04 | 27.85 | 186.85 | 27.85 | 2.808 | 187.12 | 27.85 | 3.082 | 185.58 | 27.85 | 1.535 |
| 40 | | | - | - | 187.18 | 32 | - | 187.45 | 32 | - | - | - | - |
| 41 | | | - | - | 186.88 | 36.8 | - | 187.15 | 37 | - | - | - | - |
| 42 | 89.33 | 10.67 | 177.71 | 1.72 | 176.40 | 1.72 | 1.308 | 177.08 | 1.72 | 0.627 | 176.36 | 1.72 | 1.352 |
| 43 | | | 184.32 | 3.52 | 183.30 | 3.52 | 1.017 | 183.74 | 3.52 | 0.582 | 183.21 | 3.52 | 1.107 |
| 44 | | | 187.65 | 5.24 | 187.30 | 5.24 | 0.355 | 187.60 | 5.24 | 0.046 | 187.16 | 5.24 | 0.493 |
| 45 | | | 191.21 | 7.1 | 190.39 | 7.1 | 0.822 | 190.61 | 7.1 | 0.603 | 190.20 | 7.1 | 1.011 |
| 46 | | | 193.98 | 8.69 | 192.45 | 8.69 | 1.528 | 192.61 | 8.69 | 1.367 | 192.22 | 8.69 | 1.764 |
| 47 | | | 196.65 | 10.34 | 194.22 | 10.34 | 2.430 | 194.33 | 10.34 | 2.317 | 193.93 | 10.34 | 2.716 |
| 48 | | | 197.71 | 12.07 | 195.78 | 12.07 | 1.934 | 195.85 | 12.07 | 1.863 | 195.44 | 12.07 | 2.274 |
| 49 | | | 198.09 | 14.13 | 197.34 | 14.13 | 0.755 | 197.36 | 14.13 | 0.726 | 196.93 | 14.13 | 1.162 |
| 50 | | | - | - | 202.47 | 25 | - | 202.34 | 25 | - | - | - | - |
| 51 | | | - | - | 204.59 | 35 | - | 204.36 | 35 | - | - | - | - |
| 52 | | | - | - | 204.22 | 48 | - | 203.92 | 48 | - | - | - | - |
| | | | | | **AAD** | | **2.471** | | | **3.268** | | | **2.243** |

## C.2.2 Predictions and experimental data from Zhang [46]

| Number | Composition [mole %] | | Experimental data | | NeqSim (SRK), kij = 0.0973 | | | NeqSim (UMR-PRU) | | | NeqSim (SRK), kij = 0.00 | | |
|---|---|---|---|---|---|---|---|---|---|---|---|---|---|
| | $CH_4$ | $CO_2$ | Temperature [K] | Pressure [bar] | Temperature [K] | Pressure [bar] | ABS | Temperature [K] | Pressure [bar] | AAD [K] | Temperature [K] | Pressure [bar] | AAD [K] |
| 1 | 89.2 | 10.8 | 205.3 | 44.46 | 205.06 | 44.46 | 0.242 | 204.76 | 44.46 | 0.540 | 200.27 | 20.31 | 5.034 |
| 2 | | | 200.5 | 20.31 | 200.89 | 20.31 | 0.390 | 200.83 | 20.31 | 0.326 | - | 44.46 | - |
| 3 | | | 197.5 | 13.42 | 196.98 | 13.42 | 0.520 | 197.00 | 13.42 | 0.500 | 196.60 | 13.42 | 0.900 |
| 4 | 82.2 | 17.8 | 210.3 | 29.43 | 211.27 | 29.43 | 0.966 | 211.00 | 29.43 | 0.700 | - | 29.43 | - |
| 5 | | | 205.1 | 15.81 | 205.35 | 15.81 | 0.248 | 205.24 | 15.81 | 0.139 | 204.95 | 15.81 | 0.150 |
| 6 | | | 197.4 | 8.69 | 198.80 | 8.69 | 1.400 | 198.83 | 8.69 | 1.433 | 198.60 | 8.69 | 1.200 |
| 7 | | | 191.1 | 4.97 | 192.64 | 4.97 | 1.535 | 192.80 | 4.97 | 1.700 | 192.52 | 4.97 | 1.420 |
| 8 | 66.6 | 33.4 | 209.5 | 11.44 | 210.68 | 11.44 | 1.180 | 210.55 | 11.44 | 1.050 | 210.50 | 11.44 | 1.000 |
| 9 | | | 203.8 | 7.27 | 205.09 | 7.27 | 1.290 | 205.04 | 7.27 | 1.240 | 204.98 | 7.27 | 1.180 |
| 10 | | | 202.6 | 5.72 | 202.16 | 5.72 | 0.438 | 202.16 | 5.72 | 0.440 | 202.08 | 5.72 | 0.523 |
| 11 | | | 199.5 | 4.48 | 199.22 | 4.48 | 0.280 | 199.27 | 4.48 | 0.230 | 199.16 | 4.48 | 0.345 |
| 12 | | | 194.2 | 3.07 | 194.78 | 3.07 | 0.580 | 194.92 | 3.07 | 0.720 | 194.73 | 3.07 | 0.530 |
| 13 | 57.6 | 42.4 | 210.3 | 8.54 | 210.50 | 8.54 | 0.200 | 210.40 | 8.54 | 0.100 | 210.40 | 8.54 | 0.100 |
| 14 | | | 202.5 | 4.78 | 203.14 | 4.78 | 0.640 | 203.13 | 4.78 | 0.630 | 203.09 | 4.78 | 0.588 |
| 15 | | | 196.5 | 2.93 | 197.17 | 2.93 | 0.670 | 197.27 | 2.93 | 0.770 | 197.14 | 2.93 | 0.643 |
| 16 | 45.8 | 54.2 | 209.1 | 5.69 | 208.78 | 5.69 | 0.323 | 208.70 | 5.69 | 0.400 | 208.74 | 5.69 | 0.363 |
| 17 | | | 202.7 | 3.29 | 201.74 | 3.29 | 0.960 | 201.76 | 3.29 | 0.935 | 201.72 | 3.29 | 0.980 |
| | | | | | **AAD** | | **0.698** | | | **0.697** | | | **0.997** |

## C.2.3 Predictions and experimental data from Davis, et al. [43]

| Number | Composition [mole %] | | | Experimental data | | NeqSim (SRK), kij = 0.0973 | | | NeqSim (UMR-PRU) | | |
|---|---|---|---|---|---|---|---|---|---|---|---|
| | $CH_4$ | $N_2$ | $CO_2$ | Temperature [K] | Pressure [bar] | Temperature [K] | Pressure [bar] | AAD [K] | Temperature [K] | Pressure [bar] | AAD[K] |
| 1 | 99.88 | - | 0.12 | 140.93 | 6.85 | 150.08 | 6.85 | 9.146 | 152.14 | 6.85 | 11.208 |
| 2 | 99.37 | - | 0.63 | 165.59 | 19.59 | 168.55 | 19.59 | 2.960 | 169.60 | 19.59 | 4.006 |
| 3 | 98.92 | - | 1.08 | 175.87 | 27.51 | 174.97 | 26.5 | 0.901 | 176.28 | 27.51 | 0.412 |
| 4 | 98.28 | - | 1.72 | 177.59 | 28.8 | 180.03 | 28.8 | 2.437 | 180.58 | 28.8 | 2.986 |
| 5 | 97.21 | - | 2.79 | 183.98 | 34.62 | 185.88 | 34.62 | 1.896 | 186.20 | 34.62 | 2.223 |
| 6 | 96.33 | - | 3.67 | 188.71 | 39.09 | 189.30 | 38.9 | 0.587 | 189.28 | 39.09 | 0.574 |
| 7 | 94.35 | - | 5.65 | 193.65 | 43.22 | 194.64 | 43.22 | 0.993 | 194.65 | 43.22 | 1.005 |
| 8 | 88.27 | - | 11.73 | 205.71 | 48.4 | 205.79 | 48.4 | 0.077 | 205.84 | 48.4 | 0.130 |
| | | | | | | AAD | | 2.37 | AAD | | 2.82 |

## C.3 Experimental data from literature and simulated data: Solid $CO_2$ formation in natural gas mixtures

### C.3.1 Predictions and experimental data from Shen, et al. [16] : Nitrogen

| Solvent | Number | Composition [mole %] | | | Experimental data | | NeqSim (SRK), kij = 0.0973 | | | NeqSim (UMR-PRU) | | | | |
|---|---|---|---|---|---|---|---|---|---|---|---|---|---|---|
| | | $CH_4$ | $N_2$ | $CO_2$ | Temperature [K] | Pressure [bar] | Temperature [K] | Pressure [bar] | AAD | Temperature [K] | Pressure [bar] | AAD | AAD - UMR | AAD - SRK |
| 98%CH4+2%N2 | 1 | 97.97795 | 1.99955 | 0.023 | 112.00 | 1.55 | 112.95 | 6.55 | 0.946 | 118.02 | 6.55 | 6.019 | | |
| | 2 | 97.91288 | 1.998222 | 0.089 | 124.00 | 3.26 | 124.44 | 8.26 | 0.444 | 129.25 | 8.26 | 5.250 | | |
| | 3 | 97.853 | 1.997 | 0.15 | 129.70 | 4.46 | 129.49 | 9.46 | 0.210 | 134.11 | 9.46 | 4.409 | | |
| | 4 | 97.755 | 1.995 | 0.25 | 135.20 | 5.96 | 134.84 | 10.96 | 0.357 | 139.22 | 10.96 | 4.019 | | |
| | 5 | 97.6374 | 1.9926 | 0.37 | 139.40 | 7.24 | 139.27 | 12.24 | 0.129 | 143.41 | 12.24 | 4.012 | | |
| | 6 | 97.461 | 1.989 | 0.55 | 144.50 | 9.29 | 144.05 | 14.29 | 0.446 | 147.91 | 14.29 | 3.408 | | |
| | 7 | 97.19542 | 1.98358 | 0.821 | 150.40 | 11.68 | 149.23 | 16.68 | 1.166 | 152.74 | 16.68 | 2.343 | | |
| | 8 | 96.285 | 1.965 | 1.75 | 162.00 | 18.45 | 160.05 | 23.45 | 1.948 | 162.75 | 23.45 | 0.745 | | |
| | 9 | 95.2854 | 1.9446 | 2.77 | 169.90 | 24.21 | 167.31 | 29.21 | 2.593 | 169.10 | 29.21 | 0.801 | **3.445** | **0.915617417** |
| 95%CH4+5%N2 | 10 | 94.97739 | 4.99881 | 0.024 | 112.00 | 2.68 | 113.31 | 7.68 | 1.307 | 118.17 | 7.68 | 6.175 | | |
| | 11 | 94.91365 | 4.995455 | 0.091 | 124.00 | 4.18 | 124.63 | 9.18 | 0.634 | 129.24 | 9.18 | 5.238 | | |
| | 12 | 94.8499 | 4.9921 | 0.158 | 129.70 | 5.45 | 130.03 | 10.45 | 0.328 | 134.43 | 10.45 | 4.732 | | |
| | 13 | 94.7568 | 4.9872 | 0.256 | 135.20 | 7.25 | 135.15 | 12.25 | 0.054 | 139.32 | 12.25 | 4.118 | | |
| | 14 | 94.64375 | 4.98125 | 0.375 | 139.40 | 8.80 | 139.50 | 13.80 | 0.100 | 143.44 | 13.80 | 4.043 | | |
| | 15 | 94.4851 | 4.9729 | 0.542 | 144.50 | 10.95 | 143.98 | 15.95 | 0.523 | 147.66 | 15.95 | 3.156 | | |
| | 16 | 94.221 | 4.959 | 0.82 | 150.40 | 13.85 | 149.37 | 18.85 | 1.034 | 152.69 | 18.85 | 2.293 | | |
| | 17 | 93.461 | 4.919 | 1.62 | 162.00 | 20.97 | 159.11 | 25.97 | 2.893 | 162.93 | 25.97 | 0.933 | | |
| | 18 | 92.454 | 4.866 | 2.68 | 169.90 | 26.85 | 167.10 | 31.85 | 2.796 | 169.09 | 31.85 | 0.806 | **3.499** | **1.074260802** |
| 90%CH4+10%N2 | 19 | 89.97714 | 9.99746 | 0.025 | 112.00 | 3.18 | 113.74 | 8.18 | 1.735 | 117.63 | 8.18 | 5.633 | | |
| | 20 | 89.91747 | 9.99083 | 0.092 | 124.00 | 5.8 | 124.73 | 10.80 | 0.727 | 128.21 | 10.80 | 4.209 | | |
| | 21 | 89.8569 | 9.9841 | 0.159 | 129.70 | 7.48 | 130.16 | 12.48 | 0.456 | 133.36 | 12.48 | 3.655 | | |
| | 22 | 89.7615 | 9.9735 | 0.265 | 135.20 | 9.68 | 135.65 | 14.68 | 0.454 | 138.52 | 14.68 | 3.316 | | |
| | 23 | 89.6607 | 9.9623 | 0.377 | 139.40 | 11.46 | 139.74 | 16.46 | 0.340 | 142.32 | 16.46 | 2.920 | | |
| | 24 | 89.5167 | 9.9463 | 0.537 | 144.50 | 13.97 | 144.10 | 18.97 | 0.403 | 147.49 | 18.97 | 2.993 | | |
| | 25 | 89.2656 | 9.9184 | 0.816 | 150.40 | 16.78 | 149.64 | 21.78 | 0.763 | 152.69 | 21.78 | 2.285 | | |
| | 26 | 88.569 | 9.841 | 1.59 | 162.00 | 24.48 | 159.35 | 29.48 | 2.653 | 160.24 | 29.48 | 1.760 | | |
| | 27 | 87.732 | 9.748 | 2.52 | 169.90 | 31.5 | 166.72 | 36.50 | 3.181 | 168.542 | 36.50 | 1.358 | **3.126** | **1.190217598** |

## C.3.2 Predictions and experimental data from Shen, et al. [16] : Ethane

| Solvent | Number | Composition [mole %] | | | Experimental data | | NeqSim (SRK), kij = 0.0956 and kij = 0.0312 | | | NeqSim (UMR-PRU) | | | | |
|---|---|---|---|---|---|---|---|---|---|---|---|---|---|---|
| | | $CH_4$ | C2H4 | $CO_2$ | Temperature [K] | Pressure [bar] | Temperature [K] | Pressure [bar] | AAD | Temperature [K] | Pressure [bar] | AAD | AAD - UMR | AAD-SRK |
| 98%CH4+2%C2H4 | 1 | 97.94345 | 1.998846 | 0.058 | 120.00 | 1.75 | 120.45 | 6.75 | 0.449 | 125.23 | 6.75 | 5.230 | | |
| | 2 | 97.91954 | 1.998358 | 0.082 | 124.00 | 2.33 | 123.56 | 7.33 | 0.435 | 128.27 | 7.33 | 4.274 | | |
| | 3 | 97.8481 | 1.9969 | 0.155 | 129.70 | 3.42 | 129.62 | 8.42 | 0.078 | 134.14 | 8.42 | 4.444 | | |
| | 4 | 97.74226 | 1.99474 | 0.263 | 135.20 | 4.73 | 135.15 | 9.73 | 0.055 | 139.44 | 9.73 | 4.241 | | |
| | 5 | 97.62368 | 1.99232 | 0.384 | 139.40 | 5.90 | 139.40 | 10.90 | 0.002 | 143.49 | 10.90 | 4.087 | | |
| | 6 | 97.43748 | 1.98852 | 0.574 | 144.50 | 7.70 | 144.22 | 12.70 | 0.276 | 148.04 | 12.70 | 3.535 | | |
| | 7 | 97.16308 | 1.98292 | 0.854 | 150.40 | 10.12 | 149.32 | 15.12 | 1.081 | 152.80 | 15.12 | 2.401 | | |
| | 8 | 96.1772 | 1.9628 | 1.86 | 162.00 | 16.32 | 160.34 | 21.32 | 1.657 | 163.00 | 21.32 | 1.004 | | |
| | 9 | 95.0306 | 1.9394 | 3.03 | 169.90 | 22.28 | 167.97 | 27.28 | 1.933 | 170.00 | 27.28 | 0.100 | 3.257387776 | 0.662881587 |
| 95%CH4+5%C2H4 | 10 | 94.94291 | 4.996995 | 0.06 | 120.00 | 1.71 | 120.59 | 6.71 | 0.594 | 124.96 | 6.71 | 4.961 | | |
| | 11 | 94.91023 | 4.995275 | 0.095 | 124.00 | 2.29 | 124.62 | 7.29 | 0.623 | 128.93 | 7.29 | 4.929 | | |
| | 12 | 94.85085 | 4.99215 | 0.157 | 129.70 | 3.31 | 129.48 | 8.31 | 0.218 | 133.67 | 8.31 | 3.975 | | |
| | 13 | 94.74635 | 4.98665 | 0.267 | 135.20 | 4.59 | 135.00 | 9.59 | 0.204 | 139.00 | 9.59 | 3.805 | | |
| | 14 | 94.63045 | 4.98055 | 0.389 | 139.40 | 5.78 | 139.20 | 10.78 | 0.201 | 143.03 | 10.78 | 3.629 | | |
| | 15 | 94.4262 | 4.9698 | 0.604 | 144.50 | 7.45 | 144.45 | 12.45 | 0.048 | 148.02 | 12.45 | 3.515 | | |
| | 16 | 94.17065 | 4.95635 | 0.873 | 150.40 | 9.82 | 149.15 | 14.82 | 1.254 | 152.43 | 14.82 | 2.032 | | |
| | 17 | 93.1665 | 4.9035 | 1.93 | 162.00 | 15.88 | 160.27 | 20.88 | 1.730 | 162.77 | 20.88 | 0.773 | | |
| | 18 | 91.9695 | 4.8405 | 3.19 | 169.90 | 21.55 | 168.04 | 26.55 | 1.864 | 169.92 | 26.55 | 0.017 | 3.07085122 | 0.748450525 |
| 90%CH4+10%C2H4 | 19 | 89.94384 | 9.99376 | 0.062 | 120.00 | 1.62 | 120.64 | 6.62 | 0.638 | 124.35 | 6.62 | 4.351 | | |
| | 20 | 89.91396 | 9.99044 | 0.096 | 124.00 | 2.18 | 124.42 | 7.18 | 0.416 | 128.12 | 7.18 | 4.122 | | |
| | 21 | 89.8569 | 9.9841 | 0.159 | 129.70 | 3.15 | 129.25 | 8.15 | 0.453 | 132.90 | 8.15 | 3.203 | | |
| | 22 | 89.7543 | 9.9727 | 0.273 | 135.20 | 4.37 | 134.81 | 9.37 | 0.385 | 138.35 | 9.37 | 3.153 | | |
| | 23 | 89.6445 | 9.9605 | 0.395 | 139.40 | 5.48 | 138.90 | 10.48 | 0.498 | 142.31 | 10.48 | 2.914 | | |
| | 24 | 89.4393 | 9.9377 | 0.623 | 144.50 | 7.08 | 144.29 | 12.08 | 0.212 | 147.48 | 12.08 | 2.983 | | |
| | 25 | 89.1693 | 9.9077 | 0.923 | 150.40 | 9.3 | 149.26 | 14.30 | 1.142 | 152.21 | 14.30 | 1.805 | | |
| | 26 | 88.218 | 9.802 | 1.98 | 162.00 | 14.88 | 159.83 | 19.88 | 2.167 | 162.11 | 19.88 | 0.115 | | |
| | 27 | 87.021 | 9.669 | 3.31 | 169.90 | 20.06 | 167.64 | 25.06 | 2.256 | 169.34 | 25.06 | 0.559 | 2.578187846 | 0.907386883 |

## C.3.3 Predictions and experimental data from Agrawal and Laverman [44] : Nitrogen

| Number | Composition [mole %] | | | Experimental data | | NeqSim (SRK), kij = 0.0973 | | | NeqSim (UMR-PRU) | | |
|---|---|---|---|---|---|---|---|---|---|---|---|
| | $CH_4$ | $N_2$ | $CO_2$ | Temperature [K] | Pressure [bar] | Temperature [K] | Pressure [bar] | AAD [K] | Temperature [K] | Pressure [bar] | AAD [K] |
| 1 | 98.36 | 0.68 | 0.96 | 154.93 | 1.76 | 156.215 | 1.76 | 1.287 | 157.881 | 1.76 | 2.953 |
| 2 | | | | 158.76 | 3.59 | 161.309 | 3.59 | 2.548 | 162.689 | 3.59 | 3.928 |
| 3 | | | | 161.48 | 5.24 | 164.049 | 5.24 | 2.565 | 165.284 | 5.24 | 3.801 |
| 4 | | | | 162.59 | 6.96 | 166.088 | 6.96 | 3.493 | 167.221 | 6.96 | 4.627 |
| 5 | | | | 165.87 | 10.41 | 168.881 | 10.41 | 3.009 | 169.882 | 10.41 | 4.009 |
| 6 | | | | 167.26 | 14.00 | 170.774 | 14.00 | 3.513 | 171.690 | 14.00 | 4.429 |
| 7 | | | | 169.21 | 17.24 | 171.947 | 17.24 | 2.741 | 172.814 | 17.24 | 3.608 |
| 8 | | | | 170.82 | 20.75 | 172.804 | 20.75 | 1.987 | 173.642 | 20.75 | 2.825 |
| 9 | | | | 171.65 | 22.41 | 173.080 | 22.41 | 1.430 | 173.912 | 22.41 | 2.262 |
| 10 | | | | 171.65 | 24.41 | 173.303 | 24.41 | 1.653 | 174.137 | 24.41 | 2.487 |
| 11 | 96.13 | 2.94 | 0.93 | 154.15 | 1.72 | 155.658 | 1.72 | 1.508 | 157.357 | 1.72 | 3.207 |
| 12 | | | | 158.48 | 3.45 | 160.595 | 3.45 | 2.112 | 162.012 | 3.45 | 3.529 |
| 13 | | | | 160.98 | 5.24 | 163.602 | 5.24 | 2.618 | 164.859 | 5.24 | 3.875 |
| 14 | | | | 163.15 | 6.96 | 165.625 | 6.96 | 2.475 | 166.780 | 6.96 | 3.630 |
| 15 | | | | 165.93 | 10.41 | 168.397 | 10.41 | 2.469 | 169.416 | 10.41 | 3.488 |
| 16 | | | | 168.09 | 13.93 | 170.243 | 13.93 | 2.148 | 171.177 | 13.93 | 3.082 |
| 17 | | | | 169.65 | 17.10 | 171.391 | 17.10 | 1.741 | 172.275 | 17.10 | 2.625 |
| 18 | | | | 171.93 | 20.75 | 172.280 | 20.75 | 0.352 | 173.131 | 20.75 | 1.204 |
| 19 | | | | 172.76 | 24.27 | 172.762 | 24.27 | 0.001 | 173.607 | 24.27 | 0.846 |
| | | | | | | **AAD** | | **1.714** | | | **3.641** |

## C.3.4 Predictions and experimental data from Le and Trebble [45] : Nitrogen

| Number | Composition [mole %] | | | Experimental data | | NeqSim (SRK), kij = 0.0973 | | | NeqSim (UMR-PRU) | | |
|---|---|---|---|---|---|---|---|---|---|---|---|
| | $CH_4$ | $CO_2$ | N2 | Temperature [K] | Pressure [bar] | Temperature [K] | Pressure [bar] | AAD [K] | Temperature [K] | Pressure [bar] | ADD [K] |
| 1 | 97.06 | 1.94 | 1 | 173.9 | 12.44 | 176.89 | 12.44 | 2.991 | 177.54 | 12.44 | 3.640 |
| 2 | | | | 174.4 | 13.04 | 177.23 | 13.04 | 2.831 | 177.87 | 13.04 | 3.466 |
| 3 | | | | 174.5 | 13.41 | 177.43 | 13.41 | 2.931 | 178.06 | 13.41 | 3.557 |
| 4 | | | | 176.6 | 15.91 | 178.61 | 15.91 | 2.006 | 179.18 | 15.91 | 2.585 |
| 5 | | | | 176.7 | 16.06 | 178.67 | 16.06 | 1.968 | 179.24 | 16.06 | 2.544 |
| 6 | | | | 177.2 | 16.49 | 178.84 | 16.49 | 1.640 | 179.41 | 16.49 | 2.210 |
| 7 | | | | 178 | 18.69 | 179.62 | 18.69 | 1.621 | 180.16 | 18.69 | 2.159 |
| 8 | | | | 178 | 18.61 | 179.60 | 18.61 | 1.595 | 180.13 | 18.61 | 2.135 |
| 9 | | | | 178.6 | 18.41 | 179.53 | 18.41 | 0.930 | 180.07 | 18.41 | 1.472 |
| 10 | | | | 182.4 | 22.11 | 180.54 | 22.11 | 1.861 | 181.04 | 22.11 | 1.358 |
| 11 | | | | 183 | 22.12 | 180.54 | 22.12 | 2.459 | 181.04 | 22.12 | 1.956 |
| 12 | | | | 183.1 | 22.39 | 180.60 | 22.39 | 2.500 | 181.10 | 22.39 | 1.999 |
| 13 | 96.11 | 1.94 | 1.95 | 174.4 | 13.21 | 177.32 | 13.21 | 2.925 | 177.95 | 13.21 | 3.553 |
| 14 | | | | 174.5 | 13.15 | 177.29 | 13.15 | 2.792 | 177.92 | 13.15 | 3.422 |
| 15 | | | | 175 | 13.31 | 177.38 | 13.31 | 2.378 | 178.00 | 13.31 | 3.004 |
| 16 | | | | 178.3 | 16.91 | 179.00 | 16.91 | 0.704 | 179.56 | 16.91 | 1.264 |
| 17 | | | | 178.4 | 16.67 | 178.91 | 16.67 | 0.512 | 179.48 | 16.67 | 1.076 |
| 18 | | | | 178.7 | 16.36 | 178.79 | 16.36 | 0.091 | 179.36 | 16.36 | 0.659 |
| 19 | | | | 179.6 | 18.38 | 179.52 | 18.38 | 0.077 | 180.06 | 18.38 | 0.462 |
| 20 | | | | 179.6 | 18.53 | 179.57 | 18.53 | 0.028 | 180.11 | 18.53 | 0.509 |
| 21 | | | | 179.7 | 18.74 | 179.64 | 18.74 | 0.061 | 180.17 | 18.74 | 0.474 |
| 22 | | | | 183.4 | 22.36 | 180.60 | 22.36 | 2.801 | 181.10 | 22.36 | 2.305 |
| 23 | | | | 183.5 | 22.62 | 180.65 | 22.62 | 2.846 | 181.15 | 22.62 | 2.352 |
| 24 | | | | 183.5 | 22.53 | 180.64 | 22.53 | 2.865 | 181.13 | 22.53 | 2.370 |
| | | | | | | **AAD** | | **1.809** | | | **2.105** |

## C.3.5 Predictions and experimental data from Le and Trebble [45] : Ethane

| Number | Composition [mole %] | | | Experimental data | | NeqSim (SRK), kij = 0.0973 | | | NeqSim (UMR-PRU) | | |
|---|---|---|---|---|---|---|---|---|---|---|---|
| | $CH_4$ | $CO_2$ | C2H6 | Temperature [K] | Pressure [bar] | Temperature [K] | Pressure [bar] | ABS | Temperature [K] | Pressure [bar] | ABS |
| 1 | 97.053 | 1.95 | 0.997 | 173.6 | 12.68 | 177.07 | 12.68 | 3.471 | 177.71 | 12.68 | 4.114 |
| 2 | | | | 173.9 | 12.93 | 177.21 | 12.93 | 3.310 | 177.85 | 12.93 | 3.948 |
| 3 | | | | 174.2 | 13.45 | 177.49 | 13.45 | 3.293 | 178.12 | 13.45 | 3.919 |
| 4 | | | | 176.3 | 15.67 | 178.54 | 15.67 | 2.243 | 179.13 | 15.67 | 2.827 |
| 5 | | | | 176.7 | 15.93 | 178.65 | 15.93 | 1.954 | 179.23 | 15.93 | 2.534 |
| 6 | | | | 176.7 | 16.03 | 178.69 | 16.03 | 1.995 | 179.27 | 16.03 | 2.573 |
| 7 | | | | 178.4 | 18.10 | 179.46 | 18.10 | 1.062 | 180.01 | 18.10 | 1.610 |
| 8 | | | | 178.9 | 17.79 | 179.36 | 17.79 | 0.457 | 179.91 | 17.79 | 1.009 |
| 9 | | | | 178.9 | 18.25 | 179.51 | 18.25 | 0.615 | 180.06 | 18.25 | 1.161 |
| 10 | | | | 182.4 | 22.30 | 180.60 | 22.30 | 1.796 | 181.11 | 22.30 | 1.290 |
| 11 | | | | 182.9 | 21.79 | 180.49 | 21.79 | 2.407 | 181.00 | 21.79 | 1.897 |
| 12 | | | | 183 | 22.37 | 180.62 | 22.37 | 2.380 | 181.13 | 22.37 | 1.875 |
| 13 | 96.05 | 1.96 | 1.99 | 174.8 | 13.15 | 177.38 | 13.15 | 2.575 | 178.01 | 13.15 | 3.206 |
| 14 | | | | 175.1 | 13.21 | 177.41 | 13.21 | 2.308 | 178.04 | 13.21 | 2.938 |
| 15 | | | | 175.3 | 13.07 | 177.34 | 13.07 | 2.035 | 177.97 | 13.07 | 2.668 |
| 16 | | | | 177 | 16.36 | 178.87 | 16.36 | 1.870 | 179.44 | 16.36 | 2.442 |
| 17 | | | | 177.4 | 16.52 | 178.93 | 16.52 | 1.532 | 179.50 | 16.52 | 2.100 |
| 18 | | | | 177.4 | 16.24 | 178.82 | 16.24 | 1.421 | 179.39 | 16.24 | 1.994 |
| 19 | | | | 179.6 | 18.39 | 179.60 | 18.39 | 0.004 | 180.14 | 18.39 | 0.539 |
| 20 | | | | 179.9 | 18.32 | 179.57 | 18.32 | 0.327 | 180.12 | 18.32 | 0.217 |
| 21 | | | | 180.2 | 18.48 | 179.63 | 18.48 | 0.573 | 180.17 | 18.48 | 0.031 |
| 22 | | | | 183.3 | 22.20 | 180.61 | 22.20 | 2.686 | 181.12 | 22.20 | 2.181 |
| 23 | | | | 183.6 | 22.23 | 180.62 | 22.23 | 2.981 | 181.12 | 22.23 | 2.475 |
| 24 | | | | 183.6 | 22.50 | 180.68 | 22.50 | 2.924 | 181.18 | 22.50 | 2.420 |
| | | | | | | **AAD** | | **1.926** | | | **2.165** |

## C.4 Experimental data from literature and simulated data: Solid hexane formation in liquid methane

### C.4.1 SLV predictions (pressure) and experimental data from Shim and Kohn [52] and Luks, et al. [49]

| Number | Composition [mole %] | | Experimental data | | NeqSim (SRK), kij = 0 | | | NeqSim (UMR-PRU) | | | NeqSim (sPC-SAFT), kij = 0 | | | NeqSim (SRK, kij= 0.038) | | |
|---|---|---|---|---|---|---|---|---|---|---|---|---|---|---|---|---|
| | $CH_4$ | $C_6H_{14}$ | Temperature [K] | Pressure [bar] | Temperature [K] | Pressure [bar] | ABS [%] | Temperature [K] | Pressure [bar] | ABS | Temperature [K] | Pressure [bar] | ABS [%] | Temperature [K] | Pressure [bar] | ABS [%] |
| 1 | 99.578 | 0.422 | 138.000 | 5.800 | 138.000 | 5.690 | 1.897 | 138.000 | 5.400 | 6.897 | 138.000 | 5.720 | 1.379 | 138.000 | 5.780 | 0.345 |
| 2 | 99.495 | 0.505 | 140.000 | 6.480 | 140.000 | 6.230 | 3.858 | 140.000 | 6.000 | 7.407 | 140.000 | 6.350 | 2.006 | 140.000 | 6.480 | 0.000 |
| 3 | 99.398 | 0.602 | 142.000 | 7.220 | 142.000 | 6.970 | 3.463 | 142.000 | 6.630 | 8.172 | 142.000 | 7.020 | 2.770 | 142.000 | 7.150 | 0.970 |
| 4 | 99.286 | 0.714 | 144.000 | 7.800 | 144.000 | 7.670 | 1.667 | 144.000 | 7.310 | 6.282 | 144.000 | 7.750 | 0.641 | 144.000 | 7.800 | 0.000 |
| 5 | 99.154 | 0.846 | 146.000 | 8.590 | 146.000 | 8.400 | 2.212 | 146.000 | 8.000 | 6.868 | 146.000 | 8.520 | 0.815 | 146.000 | 8.600 | 0.116 |
| 6 | 98.987 | 1.013 | 148.000 | 9.360 | 148.000 | 9.190 | 1.816 | 148.000 | 8.700 | 7.051 | 148.000 | 9.340 | 0.214 | 148.000 | 9.400 | 0.427 |
| 7 | 98.778 | 1.222 | 150.000 | 10.250 | 150.000 | 9.990 | 2.537 | 150.000 | 9.400 | 8.293 | 150.000 | 10.210 | 0.390 | 150.000 | 10.300 | 0.488 |
| 8 | 98.513 | 1.487 | 152.000 | 11.180 | 152.000 | 10.740 | 3.936 | 152.000 | 10.100 | 9.660 | 152.000 | 11.130 | 0.447 | 152.000 | 11.300 | 1.073 |
| 9 | 98.174 | 1.826 | 154.000 | 12.150 | 154.000 | 11.520 | 5.185 | 154.000 | 10.820 | 10.947 | 154.000 | 12.090 | 0.494 | 154.000 | 12.250 | 0.823 |
| 10 | 97.734 | 2.266 | 156.000 | 13.200 | 156.000 | 12.190 | 7.652 | 156.000 | 11.420 | 13.485 | 156.000 | 13.100 | 0.758 | 156.000 | 13.300 | 0.758 |
| 11 | 97.221 | 2.779 | 158.000 | 14.330 | 158.000 | 12.560 | 12.352 | 158.000 | 11.800 | 17.655 | 158.000 | 14.130 | 1.396 | 158.000 | 14.500 | 1.186 |
| 12 | 95.794 | 4.206 | 160.000 | 15.500 | 160.000 | 12.940 | 16.516 | 160.000 | 12.200 | 21.290 | 160.000 | 15.160 | 2.194 | 160.000 | 15.700 | 1.290 |
| 13 | 92.248 | 7.752 | 162.000 | 16.540 | 162.000 | 12.940 | 21.765 | 162.000 | 12.280 | 25.756 | 162.000 | 16.180 | 2.177 | 162.000 | 16.700 | 0.967 |
| 14 | 66.050 | 33.950 | 164.000 | 17.010 | 164.000 | 12.680 | 25.456 | 164.000 | 12.110 | 28.807 | 164.000 | 17.010 | 0.000 | 164.000 | 17.350 | 1.999 |
| 15 | 80.5 | 19.5 | 162.88 | 18 | 162.88 | 12.840 | 28.667 | 162.88 | 12.285 | 31.750 | 162.88 | 16.500 | 8.333 | 162.88 | 17.200 | 4.444 |
| 16 | 60 | 40 | 165.15 | 19.2 | 165.15 | 12.390 | 35.469 | 165.15 | 11.870 | 38.177 | 165.15 | 17.230 | 10.260 | 165.15 | 17.050 | 11.198 |
| 17 | 46.5 | 53.5 | 167.48 | 17.5 | 167.48 | 11.300 | 35.429 | 167.48 | 11.000 | 37.143 | 167.48 | 16.750 | 4.286 | 167.48 | 15.850 | 9.429 |
| 18 | 37.3 | 62.7 | 169.47 | 15 | 169.47 | 10.020 | 33.200 | 169.47 | 9.820 | 34.533 | 169.47 | 15.200 | 1.333 | 169.47 | 14.000 | 6.667 |
| 19 | 30 | 70 | 171.12 | 12.5 | 171.12 | 8.660 | 30.720 | 171.12 | 8.530 | 31.760 | 171.12 | 13.325 | 6.600 | 171.12 | 12.050 | 3.600 |
| 20 | 23.6 | 76.4 | 172.51 | 10 | 172.51 | 7.220 | 27.800 | 172.51 | 7.200 | 28.000 | 172.51 | 11.230 | 12.300 | 172.51 | 10.050 | 0.500 |
| 21 | 17.4 | 82.6 | 173.88 | 7.5 | 173.88 | 5.640 | 24.800 | 173.88 | 5.670 | 24.400 | 173.88 | 8.800 | 17.333 | 173.88 | 7.800 | 4.000 |
| 22 | 11.4 | 88.6 | 175.25 | 5 | 175.25 | 3.890 | 22.200 | 175.25 | 3.900 | 22.000 | 175.25 | 6.020 | 20.400 | 175.25 | 5.300 | 6.000 |
| 23 | 5.6 | 94.4 | 176.55 | 2.5 | 176.55 | 2.020 | 19.200 | 176.55 | 2.030 | 18.800 | 176.55 | 3.100 | 24.000 | 176.55 | 2.700 | 8.000 |
| | | | | | **AAD** | | **15.991** | **AAD** | | **19.354** | **AAD** | | **5.240** | **AAD** | | **2.795** |

## C.4.2 Predictions and experimental data from Shim and Kohn [52]

| Number | Composition [mole %] | | Experimental data | | NeqSim (SRK) | | | NeqSim (UMR-PRU) | | | NeqSim (sPC-SAFT) | | |
|---|---|---|---|---|---|---|---|---|---|---|---|---|---|
| | $CH_4$ | $C_6H_{14}$ | Temperature [K] | Pressure [bar] | Temperature [K] | Pressure [bar] | ABS | Temperature [K] | Pressure [bar] | ABS | Temperature [K] | Pressure [bar] | ABS |
| 1 | 80.5 | 19.5 | 162.88 | 18 | 156.038 | 12.840 | 6.842 | 151.560 | 12.285 | 6.950 | 163.630 | 16.500 | 0.750 |
| 2 | 60 | 40 | 165.15 | 19.2 | 162.920 | 12.390 | 2.230 | 162.000 | 11.870 | 1.91 | 166.933 | 17.230 | 1.783 |
| 3 | 46.5 | 53.5 | 167.48 | 17.5 | 166.870 | 11.300 | 0.610 | 166.514 | 11.000 | 0.577 | 169.000 | 16.750 | 1.520 |
| 4 | 37.3 | 62.7 | 169.47 | 15 | 169.340 | 10.020 | 0.130 | 169.570 | 9.820 | 0.059 | 170.590 | 15.200 | 1.120 |
| 5 | 30 | 70 | 171.12 | 12.5 | 171.170 | 8.660 | 0.050 | 171.079 | 8.530 | 0.024 | 171.930 | 13.325 | 0.810 |
| 6 | 23.6 | 76.4 | 172.51 | 10 | 172.710 | 7.220 | 0.200 | 172.658 | 7.200 | 0.086 | 173.140 | 11.230 | 0.630 |
| 7 | 17.4 | 82.6 | 173.88 | 7.5 | 174.130 | 5.640 | 0.250 | 174.100 | 5.670 | 0.127 | 174.350 | 8.800 | 0.470 |
| 8 | 11.4 | 88.6 | 175.25 | 5 | 175.450 | 3.890 | 0.200 | 175.440 | 3.900 | 0.108 | 175.530 | 6.020 | 0.280 |
| 9 | 5.6 | 94.4 | 176.55 | 2.5 | 176.680 | 2.020 | 0.130 | 176.680 | 2.030 | 0.074 | 176.700 | 3.100 | 0.150 |
| 11 | 68.5 | 31.5 | 164.35 | 18.9 | 160.188 | 18.900 | 4.162 | 158.430 | 18.9 | 3.602 | 165.780 | 18.900 | 1.430 |
| 12 | 68.5 | 31.5 | 164.45 | 48.1 | 160.070 | 48.100 | 4.380 | 158.080 | 48.1 | 3.874 | - | - | - |
| 13 | 68.5 | 31.5 | 164.55 | 65.5 | 160.010 | 65.500 | 4.540 | 157.876 | 65.5 | 4.056 | - | - | - |
| | | | | | **AAD** | | **1.825** | | | **1.649** | | | **0.688** |

## C.4.2 Predictions and experimental data from Luks, et al. [49]

| Number | Composition [mole %] | | Experimental data | | NeqSim (SRK) | | | NeqSim (UMR-PRU) | | | NeqSim (sPC-SAFT) | | |
|---|---|---|---|---|---|---|---|---|---|---|---|---|---|
| | $CH_4$ | $C_6H_{14}$ | Temperature [K] | Pressure [bar] | Temperature [K] | Pressure [bar] | ABS | Temperature [K] | Pressure [bar] | ABS | Temperature [K] | Pressure [bar] | ABS |
| 1 | 99.578 | 0.422 | 138.000 | 5.800 | 122.500 | 5.690 | 15.500 | - | 5.400 | - | 136.560 | 5.720 | 1.440 |
| 2 | 99.495 | 0.505 | 140.000 | 6.480 | 124.369 | 6.230 | 15.631 | - | 6.000 | - | 138.250 | 6.350 | 1.750 |
| 3 | 99.398 | 0.602 | 142.000 | 7.220 | 126.227 | 6.970 | 15.773 | - | 6.630 | - | 139.942 | 7.020 | 2.058 |
| 4 | 99.286 | 0.714 | 144.000 | 7.800 | 128.072 | 7.670 | 15.928 | - | 7.310 | - | 141.612 | 7.750 | 2.388 |
| 5 | 99.154 | 0.846 | 146.000 | 8.590 | 129.928 | 8.400 | 16.072 | - | 8.000 | - | 143.290 | 8.520 | 2.710 |
| 6 | 98.987 | 1.013 | 148.000 | 9.360 | 131.922 | 9.190 | 16.078 | - | 8.700 | - | 145.080 | 9.340 | 2.920 |
| 7 | 98.778 | 1.222 | 150.000 | 10.250 | 134.000 | 9.990 | 16.000 | - | 9.400 | - | 146.960 | 10.210 | 3.040 |
| 8 | 98.513 | 1.487 | 152.000 | 11.180 | 136.174 | 10.740 | 15.826 | - | 10.100 | - | 148.900 | 11.130 | 3.100 |
| 9 | 98.174 | 1.826 | 154.000 | 12.150 | 138.400 | 11.520 | 15.600 | - | 10.820 | - | 150.890 | 12.090 | 3.110 |
| 10 | 97.734 | 2.266 | 156.000 | 13.200 | 140.620 | 12.190 | 15.380 | - | 11.420 | - | 152.897 | 13.100 | 3.103 |
| 11 | 97.221 | 2.779 | 158.000 | 14.330 | 142.680 | 12.560 | 15.320 | - | 11.800 | - | 154.670 | 14.130 | 3.330 |
| 12 | 95.794 | 4.206 | 160.000 | 15.500 | 146.390 | 12.940 | 13.610 | - | 12.200 | - | 157.843 | 15.160 | 2.157 |
| 13 | 92.248 | 7.752 | 162.000 | 16.540 | 150.550 | 12.940 | 11.450 | 128.389 | 12.280 | 33.611 | 161.200 | 16.180 | 0.800 |
| 14 | 66.050 | 33.950 | 164.000 | 17.010 | 160.300 | 12.680 | 3.700 | 159.577 | 12.110 | 4.423 | 165.700 | 17.010 | 1.700 |
| | | | | | **AAD** | | **14.419** | | | **19.017** | | | **2.400** |

## C.4.3 Different binary interaction parameters (SRK), SLE: Predictions and experimental data from Shim and Kohn [43], Luks, et al. [49] and Kuebler and McKinley [7]

| Number | Composition [mole %] | | Experimental data | | NeqSim (SRK), kij = 0.0 | | | NeqSim (SRK, kij = 0.05) | | | NeqSim (SRK, kij = 0.025) | | | NeqSim (SRK, kij = 0.03) | | | NeqSim (SRK, kij = 0.035) | | | NeqSim (SRK, kij = 0.0325) | | | NeqSim (SRK, kij = 0.0325) | | | NeqSim (SRK, kij = 0.0325) | | |
|---|---|---|---|---|---|---|---|---|---|---|---|---|---|---|---|---|---|---|---|---|---|---|---|---|---|---|
| | $CH_4$ | $C_6H_{14}$ | Temperature [K] | Pressure [bar] | Temperature [K] | Pressure [bar] | ABS [%] | Temperature [K] | Pressure [bar] | ABS | Temperature [K] | Pressure [bar] | ABS | Temperature [K] | Pressure [bar] | ABS | Temperature [K] | Pressure [bar] | ABS | Temperature [K] | Pressure [bar] | ABS | Temperature [K] | Pressure [bar] | ABS | Temperature [K] | Pressure [bar] | ABS |
| 1 | 80.5 | 94.4 | 176.55 | 2.5 | 155.70 | 50 | 20.848 | 164.23 | 50 | 12.319 | 176.69 | 50 | 0.139 | 176.69 | 50 | 0.139 | 176.69 | 50 | 0.140 | 176.69 | 50 | 0.140 | 176.69 | 70 | 0.140 | 176.69 | 90 | 0.140 |
| 2 | 60 | 88.6 | 175.25 | 5 | 176.68 | 50 | 1.435 | 176.69 | 50 | 1.443 | 175.47 | 50 | 0.223 | 175.48 | 50 | 0.227 | 175.48 | 50 | 0.230 | 175.48 | 50 | 0.228 | 175.48 | 70 | 0.228 | 175.48 | 90 | 0.227 |
| 3 | 46.5 | 82.6 | 173.88 | 7.5 | 175.46 | 50 | 1.575 | 175.49 | 50 | 1.611 | 174.18 | 50 | 0.299 | 174.19 | 50 | 0.308 | 174.20 | 50 | 0.317 | 174.19 | 50 | 0.313 | 174.19 | 70 | 0.311 | 174.19 | 90 | 0.310 |
| 4 | 37.3 | 76.4 | 172.51 | 10 | 174.13 | 50 | 1.623 | 174.22 | 50 | 1.715 | 172.80 | 50 | 0.292 | 172.82 | 50 | 0.311 | 172.84 | 50 | 0.330 | 172.83 | 50 | 0.320 | 172.83 | 70 | 0.317 | 172.82 | 90 | 0.314 |
| 5 | 30 | 70 | 171.12 | 12.5 | 172.71 | 50 | 1.589 | 172.90 | 50 | 1.776 | 171.34 | 50 | 0.220 | 171.37 | 50 | 0.253 | 171.41 | 50 | 0.287 | 171.39 | 50 | 0.270 | 171.38 | 70 | 0.265 | 171.38 | 90 | 0.260 |
| 6 | 23.6 | 62.7 | 169.47 | 15 | 171.17 | 50 | 1.701 | 171.51 | 50 | 2.038 | 169.62 | 50 | 0.154 | 169.68 | 50 | 0.213 | 169.74 | 50 | 0.273 | 169.71 | 50 | 0.243 | 169.70 | 70 | 0.233 | 169.69 | 90 | 0.224 |
| 7 | 17.4 | 53.5 | 167.48 | 17.5 | 169.33 | 50 | 1.846 | 169.92 | 50 | 2.441 | 167.40 | 50 | 0.079 | 167.51 | 50 | 0.032 | 167.62 | 50 | 0.143 | 167.57 | 50 | 0.087 | 167.55 | 70 | 0.069 | 167.53 | 90 | 0.052 |
| 8 | 11.4 | 40 | 165.15 | 19.2 | 166.85 | 50 | 1.696 | 167.96 | 50 | 2.806 | 164.10 | 50 | 1.052 | 164.35 | 50 | 0.802 | 164.60 | 50 | 0.552 | 164.47 | 50 | 0.677 | 164.43 | 70 | 0.721 | 164.39 | 90 | 0.763 |
| 9 | 5.6 | 19.5 | 162.88 | 18 | 162.85 | 50 | 0.032 | 165.35 | 50 | 2.466 | 159.73 | 50 | 3.151 | 160.53 | 50 | 2.353 | 161.32 | 50 | 1.558 | 160.92 | 50 | 1.955 | 160.74 | 70 | 2.143 | 160.56 | 90 | 2.317 |
| 10 | 85.000 | 15.000 | 163.7 | 17 | 153.81 | 50 | 9.891 | 164.23 | 50 | 0.531 | 159.06 | 50 | 4.638 | 160.10 | 50 | 3.602 | 161.13 | 50 | 2.570 | 160.51 | 50 | 3.188 | 160.33 | 70 | 3.366 | 160.08 | 90 | 3.620 |
| 11 | 85.200 | 14.800 | 163.1 | 17 | 153.72 | 50 | 9.382 | 164.23 | 50 | 1.131 | 159.03 | 50 | 4.066 | 160.08 | 50 | 3.017 | 161.13 | 50 | 1.972 | 160.50 | 50 | 2.598 | 160.32 | 70 | 2.780 | 160.06 | 90 | 3.039 |
| 12 | 88.900 | 11.100 | 162.6 | 17 | 151.86 | 50 | 10.742 | 164.23 | 50 | 1.631 | 158.52 | 50 | 4.078 | 159.83 | 50 | 2.768 | 161.13 | 50 | 1.472 | 160.35 | 50 | 2.246 | 160.07 | 70 | 2.532 | 159.70 | 90 | 2.901 |
| 13 | 92.170 | 7.830 | 162 | 17 | 149.63 | 50 | 12.371 | 164.23 | 50 | 2.231 | 157.82 | 50 | 4.179 | 159.43 | 50 | 2.574 | 161.02 | 50 | 0.979 | 160.07 | 50 | 1.935 | 159.62 | 70 | 2.378 | 159.10 | 90 | 2.900 |
| 14 | 94.240 | 5.760 | 160.9 | 16 | 147.49 | 50 | 13.414 | 164.23 | 50 | 3.331 | 156.84 | 50 | 4.057 | 158.67 | 50 | 2.227 | 160.49 | 50 | 0.409 | 159.40 | 50 | 1.498 | 158.81 | 70 | 2.089 | 158.16 | 90 | 2.741 |
| 15 | 96.520 | 3.480 | 158.1 | 15 | 143.31 | 50 | 14.786 | 164.23 | 50 | 6.131 | 154.08 | 50 | 4.022 | 156.18 | 50 | 1.921 | 158.27 | 50 | 0.166 | 157.02 | 50 | 1.085 | 156.25 | 70 | 1.848 | 155.46 | 90 | 2.643 |
| 16 | 97.570 | 2.430 | 155.3 | 13 | 139.84 | 50 | 15.455 | 162.12 | 50 | 6.823 | 151.20 | 50 | 4.099 | 153.41 | 50 | 1.890 | 155.60 | 50 | 0.304 | 154.29 | 50 | 1.011 | 153.51 | 70 | 1.795 | 152.69 | 90 | 2.611 |
| 17 | 98.650 | 1.350 | 149.7 | 12 | 133.64 | 50 | 16.059 | 156.51 | 50 | 6.815 | 145.38 | 50 | 4.318 | 147.65 | 50 | 2.052 | 149.89 | 50 | 0.191 | 148.55 | 50 | 1.152 | 147.88 | 70 | 1.818 | 147.15 | 90 | 2.552 |
| 18 | 99.184 | 0.816 | 144.2 | 10 | 128.23 | 50 | 15.972 | 150.93 | 50 | 6.732 | 139.95 | 50 | 4.249 | 142.20 | 50 | 2.000 | 144.42 | 50 | 0.220 | 143.09 | 50 | 1.109 | 142.58 | 70 | 1.619 | 141.97 | 90 | 2.234 |
| 19 | 99.502 | 0.498 | 138.6 | 8 | 123.10 | 50 | 15.495 | 145.41 | 50 | 6.808 | 134.67 | 50 | 3.931 | 136.88 | 50 | 1.723 | 139.05 | 50 | 0.453 | 137.75 | 50 | 0.849 | 137.38 | 70 | 1.218 | 136.88 | 90 | 1.722 |
| 20 | 99.704 | 0.296 | 133 | 6 | 118.03 | 50 | 14.967 | 139.84 | 50 | 6.835 | 129.37 | 50 | 3.633 | 131.52 | 50 | 1.475 | 133.65 | 50 | 0.649 | 132.38 | 50 | 0.622 | 132.13 | 70 | 0.872 | 131.72 | 90 | 1.278 |
| 21 | 99.822 | 0.178 | 127.6 | 5 | 113.43 | 50 | 14.165 | 134.73 | 50 | 7.135 | 124.52 | 50 | 3.077 | 126.63 | 50 | 0.970 | 128.70 | 50 | 1.104 | 127.46 | 50 | 0.136 | 127.30 | 70 | 0.300 | 126.97 | 90 | 0.630 |
| 22 | 99.894 | 0.106 | 121.8 | 5 | 109.10 | 50 | 12.696 | 129.91 | 50 | 8.108 | 119.94 | 50 | 1.860 | 122.00 | 50 | 0.198 | 124.02 | 50 | 2.223 | 122.81 | 50 | 1.012 | 122.71 | 70 | 0.915 | 122.44 | 90 | 0.645 |
| 23 | 99.896 | 0.104 | 121.8 | 5 | 108.95 | 50 | 12.848 | 129.74 | 50 | 7.937 | 119.78 | 50 | 2.022 | 121.83 | 50 | 0.035 | 123.86 | 50 | 2.058 | 122.65 | 50 | 0.848 | 122.55 | 70 | 0.752 | 122.28 | 90 | 0.484 |
| 24 | 99.896 | 0.1043 | 121.8 | 5 | 108.97 | 50 | 12.825 | 129.76 | 50 | 7.963 | 119.80 | 50 | 1.997 | 121.86 | 50 | 0.059 | 123.88 | 50 | 2.083 | 122.67 | 50 | 0.873 | 122.58 | 70 | 0.777 | 122.31 | 90 | 0.509 |
| 25 | 99.897 | 0.1031 | 121.8 | 5 | 108.88 | 50 | 12.918 | 129.66 | 50 | 7.860 | 119.70 | 50 | 2.095 | 121.76 | 50 | 0.040 | 123.78 | 50 | 1.983 | 122.57 | 50 | 0.773 | 122.48 | 70 | 0.678 | 122.21 | 90 | 0.411 |
| 26 | 99.897 | 0.1027 | 121.8 | 5 | 108.85 | 50 | 12.949 | 129.63 | 50 | 7.825 | 119.67 | 50 | 2.128 | 121.73 | 50 | 0.073 | 123.75 | 50 | 1.949 | 122.54 | 50 | 0.740 | 122.45 | 70 | 0.645 | 122.18 | 90 | 0.379 |
| 27 | 99.941 | 0.0586 | 116.2 | 5 | 104.56 | 50 | 11.642 | 124.82 | 50 | 8.623 | 115.11 | 50 | 1.086 | 117.12 | 50 | 0.920 | 119.09 | 50 | 2.892 | 117.91 | 50 | 1.712 | 117.87 | 70 | 1.670 | 117.65 | 90 | 1.452 |
| 28 | 99.968 | 0.0317 | 110.6 | 5 | 100.25 | 50 | 10.347 | 119.99 | 50 | 9.394 | 110.53 | 50 | 0.066 | 112.49 | 50 | 1.888 | 114.41 | 50 | 3.809 | 113.26 | 50 | 2.660 | 113.26 | 70 | 2.659 | 113.08 | 90 | 2.481 |
| 29 | 99.984 | 0.0158 | 105 | 5 | 95.81 | 50 | 9.188 | 115.00 | 50 | 10.000 | 105.80 | 50 | 0.799 | 107.70 | 50 | 2.699 | 109.57 | 50 | 4.567 | 108.45 | 50 | 3.450 | 108.48 | 70 | 3.482 | 108.34 | 90 | 3.339 |
| 30 | 99.992 | 0.0077 | 99.4 | 5 | 91.65 | 50 | 7.753 | 110.31 | 50 | 10.906 | 101.35 | 50 | 1.953 | 103.20 | 50 | 3.800 | 105.02 | 50 | 5.618 | 103.93 | 50 | 4.530 | 103.99 | 70 | 4.587 | 103.87 | 90 | 4.470 |
| 31 | 99.997 | 0.00349 | 93.8 | 5 | 87.48 | 50 | 6.315 | 105.60 | 50 | 11.803 | 96.90 | 50 | 3.102 | 98.70 | 50 | 4.896 | 100.46 | 50 | 6.662 | 99.41 | 50 | 5.606 | 99.48 | 70 | 5.681 | 99.39 | 90 | 5.587 |
| | | | | | AAD | | 9.823 | AAD | | 5.651 | AAD | | 2.111 | AAD | | 1.467 | AAD | | 1.554 | AAD | | 1.415 | AAD | | 1.577 | AAD | | 1.717 |

## C.4.4 Different binary interaction parameters (sPC-SAFT), SLE: Predictions and experimental data from Shim and Kohn [43], Luks, et al. [49] and Kuebler and McKinley [7]

| Number | Composition [mole %] | | Experimental data | | NeqSim (sPC-SAFT), kij = 0.0 | | | NeqSim (sPC-SAFT), kij = 0.01 | | | NeqSim (sPC-SAFT), kij = 0.005 | | |
|---|---|---|---|---|---|---|---|---|---|---|---|---|---|
| | $CH_4$ | $C_6H_{14}$ | Temperature [K] | Pressure [bar] | Temperature [K] | Pressure [bar] | ABS [%] | Temperature [K] | Pressure [bar] | ABS | Temperature [K] | Pressure [bar] | ABS |
| 1 | 80.5 | 94.4 | 176.55 | 2.5 | 176.71 | 18 | 0.155 | 176.71 | 20 | 0.159 | 176.71 | 20 | 0.157 |
| 2 | 60 | 88.6 | 175.25 | 5 | 175.55 | 18 | 0.296 | 175.56 | 20 | 0.311 | 175.55 | 20 | 0.304 |
| 3 | 46.5 | 82.6 | 173.88 | 7.5 | 174.36 | 18 | 0.479 | 174.40 | 20 | 0.515 | 174.38 | 20 | 0.497 |
| 4 | 37.3 | 76.4 | 172.51 | 10 | 173.15 | 18 | 0.641 | 173.22 | 20 | 0.714 | 173.19 | 20 | 0.677 |
| 5 | 30 | 70 | 171.12 | 12.5 | 171.93 | 18 | 0.814 | 172.06 | 20 | 0.941 | 172.00 | 20 | 0.878 |
| 6 | 23.6 | 62.7 | 169.47 | 15 | 170.60 | 18 | 1.127 | 170.81 | 20 | 1.342 | 170.70 | 20 | 1.234 |
| 7 | 17.4 | 53.5 | 167.48 | 17.5 | 169.01 | 18 | 1.530 | 169.39 | 20 | 1.911 | 169.20 | 20 | 1.720 |
| 8 | 11.4 | 40 | 165.15 | 19.2 | 166.94 | 18 | 1.786 | 167.72 | 20 | 2.571 | 167.33 | 20 | 2.178 |
| 9 | 5.6 | 19.5 | 162.88 | 18 | 164.22 | 18 | 1.337 | 166.40 | 20 | 3.520 | 165.25 | 20 | 2.374 |
| 10 | 85.000 | 15.000 | 163.7 | 17 | 163.47 | 18 | 0.228 | 166.12 | 20 | 2.418 | 164.79 | 20 | 1.087 |
| 11 | 85.200 | 14.800 | 163.1 | 17 | 163.43 | 18 | 0.333 | 166.11 | 20 | 3.006 | 164.76 | 20 | 1.662 |
| 12 | 88.900 | 11.100 | 162.6 | 17 | 162.54 | 18 | 0.058 | 165.77 | 20 | 3.170 | 164.14 | 20 | 1.543 |
| 13 | 92.170 | 7.830 | 162 | 17 | 161.19 | 19 | 0.806 | 164.97 | 25 | 2.966 | 163.11 | 20 | 1.114 |
| 14 | 94.240 | 5.760 | 160.9 | 16 | 159.71 | 18 | 1.192 | 164.02 | 25 | 3.119 | 161.83 | 20 | 0.931 |
| 15 | 96.520 | 3.480 | 158.1 | 15 | 156.37 | 18 | 1.731 | 161.31 | 18 | 3.214 | 158.75 | 20 | 0.649 |
| 16 | 97.570 | 2.430 | 155.3 | 13 | 153.35 | 17 | 1.946 | 158.49 | 18 | 3.188 | 155.91 | 18 | 0.606 |
| 17 | 98.650 | 1.350 | 149.7 | 12 | 147.77 | 16 | 1.926 | 152.84 | 18 | 3.136 | 150.26 | 18 | 0.564 |
| 18 | 99.184 | 0.816 | 144.2 | 10 | 142.73 | 14 | 1.471 | 147.65 | 18 | 3.450 | 145.16 | 18 | 0.961 |
| 19 | 99.502 | 0.498 | 138.6 | 8 | 137.96 | 10 | 0.636 | 142.68 | 16 | 4.077 | 140.33 | 16 | 1.726 |
| 20 | 99.704 | 0.296 | 133 | 6 | 133.24 | 10 | 0.243 | 137.73 | 15 | 4.731 | 135.46 | 16 | 2.463 |
| 21 | 99.822 | 0.178 | 127.6 | 5 | 128.88 | 10 | 1.277 | 133.34 | 10 | 5.736 | 131.07 | 13 | 3.474 |
| 22 | 99.894 | 0.106 | 121.8 | 5 | 124.75 | 10 | 2.950 | 129.05 | 10 | 7.253 | 126.91 | 10 | 5.107 |
| 23 | 99.896 | 0.104 | 121.8 | 5 | 124.60 | 10 | 2.804 | 128.90 | 10 | 7.102 | 126.76 | 10 | 4.959 |
| 24 | 99.896 | 0.1043 | 121.8 | 5 | 124.63 | 10 | 2.826 | 128.92 | 10 | 7.124 | 126.78 | 10 | 4.981 |
| 25 | 99.897 | 0.1031 | 121.8 | 5 | 124.54 | 10 | 2.737 | 128.83 | 10 | 7.033 | 126.69 | 10 | 4.891 |
| 26 | 99.897 | 0.1027 | 121.8 | 5 | 124.51 | 10 | 2.708 | 128.80 | 10 | 7.002 | 126.66 | 10 | 4.861 |
| 27 | 99.941 | 0.0586 | 116.2 | 5 | 120.39 | 10 | 4.194 | 124.54 | 10 | 8.338 | 122.47 | 10 | 6.273 |
| 28 | 99.968 | 0.0317 | 110.6 | 5 | 116.25 | 8 | 5.652 | 120.24 | 10 | 9.639 | 118.25 | 10 | 7.647 |
| 29 | 99.984 | 0.0158 | 105 | 5 | 111.93 | 8 | 6.934 | 115.77 | 10 | 10.773 | 113.86 | 8 | 8.863 |
| 30 | 99.992 | 0.0077 | 99.4 | 5 | 107.85 | 7 | 8.451 | 111.56 | 50 | 12.157 | 109.71 | 8 | 10.310 |
| 31 | 99.997 | 0.00349 | 93.8 | 5 | 103.74 | 6 | 9.937 | 107.30 | 50 | 13.504 | 105.53 | 6 | 11.726 |
| | | | | | **AAD** | | **2.232** | **AAD** | | **4.649** | **AAD** | | **2.787** |

# C.5 Experimental data from literature and simulated data: Solid heptane formation in liquid methane

## C5.1 SLV predictions (pressure) and experimental data from Tiffin, et al. [53]

| Number | Composition [mole %] | | Experimental data | | NeqSim (SRK) | | | NeqSim (UMR-PRU) | | | NeqSim (sPC-SAFT) | | | NeqSim (SRK), kij = 0.037 ("optimal") | | |
|---|---|---|---|---|---|---|---|---|---|---|---|---|---|---|---|---|
| | $CH_4$ | $C_7H_{16}$ | Temperature [K] | Pressure [bar] | Temperature [K] | Pressure [bar] | ABS [%] | Temperature [K] | Pressure [bar] | ABS [%] | Temperature [K] | Pressure [bar] | ABS [%] | Temperature [K] | Pressure [bar] | ABS [%] |
| 1 | 99.9228 | 0.0772 | 131 | 3.7 | 131 | 3.860 | 4.324 | 131 | 3.690 | 0.270 | 131.0 | 3.88 | 4.86 | 131 | 3.85 | 4.05 |
| 2 | 99.899 | 0.101 | 134 | 4.5 | 134 | 4.600 | 2.222 | 134 | 4.440 | 1.333 | 134.0 | 4.61 | 2.44 | 134 | 4.62 | 2.67 |
| 3 | 99.868 | 0.132 | 137 | 5.3 | 137 | 5.440 | 2.642 | 137 | 5.270 | 0.566 | 137.0 | 5.45 | 2.83 | 137 | 5.45 | 2.83 |
| 4 | 99.83 | 0.17 | 140 | 6.2 | 140 | 6.370 | 2.742 | 140 | 6.220 | 0.323 | 140.0 | 6.38 | 2.90 | 140 | 6.40 | 3.23 |
| 5 | 99.781 | 0.219 | 143 | 7.3 | 143 | 7.380 | 1.096 | 143 | 7.280 | 0.274 | 143.0 | 7.43 | 1.78 | 143 | 7.40 | 1.37 |
| 6 | 99.721 | 0.279 | 146 | 8.4 | 146 | 8.570 | 2.024 | 146 | 8.450 | 0.595 | 146.0 | 8.59 | 2.26 | 146 | 8.60 | 2.38 |
| 7 | 99.647 | 0.353 | 149 | 9.6 | 149 | 9.820 | 2.292 | 149 | 9.710 | 1.146 | 149.0 | 9.88 | 2.92 | 149 | 9.90 | 3.13 |
| 8 | 99.556 | 0.444 | 152 | 11.1 | 152 | 11.200 | 0.901 | 152 | 11.050 | 0.450 | 152.0 | 11.29 | 1.71 | 152 | 11.40 | 2.70 |
| 9 | 99.447 | 0.553 | 155 | 12.6 | 155 | 12.650 | 0.397 | 155 | 12.400 | 1.587 | 155.0 | 12.84 | 1.90 | 155 | 13.00 | 3.17 |
| 10 | 99.31 | 0.69 | 158 | 14.2 | 158 | 14.090 | 0.775 | 158 | 13.730 | 3.310 | 158.0 | 14.52 | 2.25 | 158 | 14.70 | 3.52 |
| 11 | 99.119 | 0.881 | 161 | 15.9 | 161 | 15.220 | 4.277 | 161 | 14.820 | 6.792 | 161.0 | 16.33 | 2.70 | 161 | 16.60 | 4.40 |
| 12 | 98.84 | 1.16 | 164 | 18 | 164 | 15.850 | 11.944 | 164 | 15.530 | 13.722 | 164.0 | 18.28 | 1.56 | 164 | 18.60 | 3.33 |
| 13 | 98.32 | 1.68 | 167 | 20.1 | 167 | 15.760 | 21.592 | 167 | 15.600 | 22.388 | 167.0 | 20.33 | 1.14 | 167 | 20.80 | 3.48 |
| 14 | 97.64 | 2.36 | 169.35 | 21.87 | 169.35 | 15.080 | 31.047 | 169.35 | 15.110 | 30.910 | 169.4 | 21.95 | 0.37 | 169.35 | 20.78 | 4.98 |
| 15 | 68 | 32 | 169.35 | 21.87 | 169.35 | 15.080 | 31.047 | 169.35 | 15.110 | 30.910 | 169.4 | 21.95 | 0.37 | 169.35 | 20.78 | 4.98 |
| 16 | 61.9 | 38.1 | 170 | 21.7 | 170 | 14.810 | 31.751 | 170 | 14.870 | 31.475 | 170.0 | 22.00 | 1.38 | 170 | 20.50 | 5.53 |
| 17 | 55.9 | 44.1 | 171 | 21.1 | 171 | 14.270 | 32.370 | 171 | 14.400 | 31.754 | 171.0 | 22.57 | 6.97 | 171 | 19.80 | 6.16 |
| 18 | 50.7 | 49.3 | 172 | 20.3 | 172 | 13.640 | 32.808 | 172 | 13.820 | 31.921 | 172.0 | 22.19 | 9.31 | 172 | 18.90 | 6.90 |
| 19 | 45.8 | 54.2 | 173 | 19.4 | 173 | 12.900 | 33.505 | 173 | 13.120 | 32.371 | 173.0 | 21.36 | 10.10 | 173 | 17.80 | 8.25 |
| 20 | 41.2 | 58.8 | 174 | 18.2 | 174 | 12.030 | 33.901 | 174 | 12.330 | 32.253 | 174.0 | 20.16 | 10.77 | 174 | 16.50 | 9.34 |
| 21 | 36.5 | 63.5 | 175 | 16.9 | 175 | 11.060 | 34.556 | 175 | 11.350 | 32.840 | 175.0 | 18.65 | 10.36 | 175 | 15.20 | 10.06 |
| 22 | 32 | 68 | 176 | 15.2 | 176 | 9.970 | 34.408 | 176 | 10.280 | 32.368 | 176.0 | 16.84 | 10.79 | 176 | 13.70 | 9.87 |
| 23 | 27.6 | 72.4 | 177 | 13.3 | 177 | 8.770 | 34.060 | 177 | 9.100 | 31.579 | 177.0 | 14.80 | 11.28 | 177 | 12.00 | 9.77 |
| 24 | 23.1 | 76.9 | 178 | 11.4 | 178 | 7.450 | 34.649 | 178 | 7.750 | 32.018 | 178.0 | 12.52 | 9.82 | 178 | 10.10 | 11.40 |
| 25 | 18.7 | 81.3 | 179 | 9.4 | 179 | 6.020 | 35.957 | 179 | 6.290 | 33.085 | 179.0 | 10.07 | 7.13 | 179 | 8.20 | 12.77 |
| 26 | 14.3 | 85.7 | 180 | 7.4 | 180 | 4.470 | 39.595 | 180 | 4.700 | 36.486 | 180.0 | 7.44 | 0.54 | 180 | 6.00 | 18.92 |
| 27 | 9.7 | 90.3 | 181 | 5.4 | 181 | 2.82 | 47.778 | 181 | 2.95 | 45.370 | 181.0 | 4.65 | 13.89 | 181 | 3.80 | 29.63 |
| | | | | | **AAD** | | **20.173** | **AAD** | | **19.189** | **AAD** | | **4.976** | **AAD** | | **6.994** |

## C5.2 Predictions and experimental SL data from Tiffin, et al. [53]

| Number | Composition [mole %] | | Experimental data | | NeqSim (SRK), kij=0 | | | NeqSim (UMR-PRU) | | | NeqSim (sPC-SAFT), kij=0 | | | NeqSim (SRK), kij = 0.037 ("optimal") | | |
|---|---|---|---|---|---|---|---|---|---|---|---|---|---|---|---|---|
| | $CH_4$ | $C_7H_{16}$ | Temperature [K] | Pressure [bar] | Temperature [K] | Pressure [bar] | ABS | Temperature [K] | Pressure [bar] | ABS | Temperature [K] | Pressure [bar] | ABS | Temperature [K] | Pressure [bar] | ABS |
| 1 | 99.9228 | 0.0772 | 131 | 3.7 | 113.28 | 3.70 | 17.72 | - | 3.7 | 0.000 | 131.0 | 3.88 | 0.00 | 130.00 | 50.00 | 1.00 |
| 2 | 99.899 | 0.101 | 134 | 4.5 | 115.60 | 4.50 | 18.40 | - | 4.5 | 0.000 | 134.0 | 4.61 | 0.00 | 132.48 | 50.00 | 1.52 |
| 3 | 99.868 | 0.132 | 137 | 5.3 | 118.01 | 5.30 | 18.99 | - | 5.3 | 0.000 | 136.6 | 5.45 | 0.38 | 135.06 | 50.00 | 1.94 |
| 4 | 99.83 | 0.17 | 140 | 6.2 | 120.39 | 6.20 | 19.61 | - | 6.2 | 0.000 | 138.9 | 6.38 | 1.14 | 137.61 | 50.00 | 2.39 |
| 5 | 99.781 | 0.219 | 143 | 7.3 | 122.87 | 7.30 | 20.13 | - | 7.3 | 0.000 | 141.2 | 7.43 | 1.81 | 140.27 | 50.00 | 2.73 |
| 6 | 99.721 | 0.279 | 146 | 8.4 | 125.34 | 8.40 | 20.66 | - | 8.4 | 0.000 | 143.5 | 8.59 | 2.50 | 142.91 | 50.00 | 3.09 |
| 7 | 99.647 | 0.353 | 149 | 9.6 | 127.83 | 9.60 | 21.17 | - | 9.6 | 0.000 | 145.8 | 9.88 | 3.16 | 145.58 | 50.00 | 3.42 |
| 8 | 99.556 | 0.444 | 152 | 11.1 | 130.33 | 11.10 | 21.67 | - | 11.1 | 0.000 | 148.2 | 11.29 | 3.82 | 148.25 | 50.00 | 3.75 |
| 9 | 99.447 | 0.553 | 155 | 12.6 | 132.78 | 12.60 | 22.22 | - | 12.6 | 0.000 | 150.5 | 12.84 | 4.53 | 150.88 | 50.00 | 4.12 |
| 10 | 99.31 | 0.69 | 158 | 14.2 | 135.31 | 14.20 | 22.69 | - | 14.2 | 0.000 | 152.8 | 14.52 | 5.18 | 153.57 | 50.00 | 4.43 |
| 11 | 99.119 | 0.881 | 161 | 15.9 | 138.13 | 15.90 | 22.87 | - | 15.9 | 0.000 | 155.4 | 16.33 | 5.56 | 156.55 | 50.00 | 4.45 |
| 12 | 98.84 | 1.16 | 164 | 18 | 141.28 | 18.00 | 22.73 | - | 18 | 0.000 | 158.3 | 18.28 | 5.67 | 159.82 | 50.00 | 4.18 |
| 13 | 98.32 | 1.68 | 167 | 20.1 | 145.37 | 20.10 | 21.63 | - | 20.1 | 0.000 | 162.0 | 20.33 | 5.01 | 163.79 | 50.00 | 3.21 |
| *14 | 97.64 | 2.36 | 169.35 | 21.87 | 148.73 | 21.87 | 20.62 | - | 21.87 | 0.000 | 164.5 | 21.95 | 4.88 | 166.58 | 50.00 | 2.77 |
| *15 | 68 | 32 | 169.35 | 21.87 | 165.13 | 21.87 | 4.22 | 163.88 | 21.87 | 5.471 | 171.3 | 21.95 | 1.93 | 167.65 | 50.00 | 1.70 |
| 16 | 61.9 | 38.1 | 170 | 21.7 | 167.12 | 21.70 | 2.88 | 166.31 | 21.7 | 3.694 | 171.9 | 22.00 | 1.89 | 168.88 | 50.00 | 1.12 |
| 17 | 55.9 | 44.1 | 171 | 21.1 | 168.99 | 21.10 | 2.01 | 168.44 | 21.1 | 2.565 | 172.6 | 22.57 | 1.61 | 170.21 | 50.00 | 0.79 |
| 18 | 50.7 | 49.3 | 172 | 20.3 | 170.53 | 20.30 | 1.47 | 170.14 | 20.3 | 1.860 | 173.3 | 22.19 | 1.33 | 171.41 | 50.00 | 0.59 |
| 19 | 45.8 | 54.2 | 173 | 19.4 | 171.91 | 19.40 | 1.09 | 171.64 | 19.4 | 1.363 | 174.1 | 21.36 | 1.07 | 172.56 | 50.00 | 0.44 |
| 20 | 41.2 | 58.8 | 174 | 18.2 | 173.17 | 18.20 | 0.83 | 172.97 | 18.2 | 1.035 | 174.8 | 20.16 | 0.81 | 173.64 | 50.00 | 0.36 |
| 21 | 36.5 | 63.5 | 175 | 16.9 | 174.40 | 16.90 | 0.60 | 174.25 | 16.9 | 0.746 | 175.6 | 18.65 | 0.61 | 174.73 | 50.00 | 0.27 |
| 22 | 32 | 68 | 176 | 15.2 | 175.53 | 15.20 | 0.47 | 175.43 | 15.2 | 0.569 | 176.4 | 16.84 | 0.41 | 175.76 | 50.00 | 0.24 |
| 23 | 27.6 | 72.4 | 177 | 13.3 | 176.60 | 13.30 | 0.40 | 176.53 | 13.3 | 0.466 | 177.3 | 14.80 | 0.27 | 176.76 | 50.00 | 0.24 |
| 24 | 23.1 | 76.9 | 178 | 11.4 | 177.66 | 11.40 | 0.34 | 177.61 | 11.4 | 0.386 | 178.1 | 12.52 | 0.10 | 177.76 | 50.00 | 0.24 |
| 25 | 18.7 | 81.3 | 179 | 9.4 | 178.65 | 9.40 | 0.35 | 178.63 | 9.4 | 0.369 | 179.0 | 10.07 | 0.00 | 178.72 | 50.00 | 0.28 |
| 26 | 14.3 | 85.7 | 180 | 7.4 | 179.62 | 7.40 | 0.38 | 179.61 | 7.4 | 0.391 | 179.8 | 7.44 | 0.22 | 179.66 | 50.00 | 0.34 |
| 27 | 9.7 | 90.3 | 181 | 5.4 | 180.60 | 5.40 | 0.40 | 180.60 | 5.4 | 0.404 | 180.7 | 4.65 | 0.34 | 180.62 | 50.00 | 0.38 |
| | | | | | **AAD** | | **11.354** | **AAD** | | **-** | **AAD** | | **2.008** | **AAD** | | **0.276** |

## C.5.4 Different binary interaction parameters (SRK) : Predictions and experimental SL data from Tiffin, et al. [46]

| Number | Composition [mole %] | | Experimental data | | NeqSim (SRK), kij = 0 | | | NeqSim (SRK), kij = 0.03 | | | NeqSim (SRK), kij = 0.035 | | | NeqSim (SRK), kij = 0.036 | | | NeqSim (SRK), kij = 0.037 | | | NeqSim (SRK), kij = 0.038 | | |
|---|---|---|---|---|---|---|---|---|---|---|---|---|---|---|---|---|---|---|---|---|---|---|
| | $CH_4$ | $C_7H_{16}$ | Temperature [K] | Pressure [bar] | Temperature [K] | Pressure [bar] | ABS | Temperature [K] | Pressure [bar] | ABS | Temperature [K] | Pressure [bar] | ABS | Temperature [K] | Pressure [bar] | ABS | Temperature [K] | Pressure [bar] | ABS | Temperature [K] | Pressure [bar] | ABS |
| 1.0 | 97.6 | 2.4 | 166.5 | - | 147.0 | 50.0 | 19.5 | 162.9 | 50.0 | 3.6 | 165.5 | 50.0 | 1.0 | 166.1 | 50.0 | 0.4 | 166.6 | 50.0 | 0.1 | 167.0 | 50.0 | 0.5 |
| 2.0 | 98.5 | 1.5 | 163.7 | - | 142.5 | 50.0 | 21.2 | 158.9 | 50.0 | 4.8 | 161.7 | 50.0 | 2.0 | 162.2 | 50.0 | 1.5 | 162.8 | 50.0 | 0.9 | 163.4 | 50.0 | 0.3 |
| 3.0 | 98.7 | 1.3 | 160.9 | - | 140.4 | 50.0 | 20.5 | 156.9 | 50.0 | 4.0 | 159.7 | 50.0 | 1.2 | 160.2 | 50.0 | 0.7 | 160.8 | 50.0 | 0.1 | 161.3 | 50.0 | 0.4 |
| 4.0 | 98.9 | 1.1 | 160.9 | - | 139.1 | 50.0 | 21.8 | 155.6 | 50.0 | 5.3 | 158.3 | 50.0 | 2.6 | 158.9 | 50.0 | 2.0 | 159.4 | 50.0 | 1.5 | 160.0 | 50.0 | 0.9 |
| 5.0 | 99.2 | 0.8 | 155.6 | - | 134.9 | 50.0 | 20.7 | 151.2 | 50.0 | 4.4 | 153.9 | 50.0 | 1.7 | 154.4 | 50.0 | 1.2 | 155.0 | 50.0 | 0.6 | 155.5 | 50.0 | 0.1 |
| 6.0 | 99.3 | 0.7 | 155.6 | - | 133.8 | 50.0 | 21.8 | 150.1 | 50.0 | 5.5 | 152.7 | 50.0 | 2.9 | 153.2 | 50.0 | 2.4 | 153.8 | 50.0 | 1.8 | 154.3 | 50.0 | 1.3 |
| 7.0 | 99.5 | 0.5 | 150.1 | - | 129.7 | 50.0 | 20.4 | 145.7 | 50.0 | 4.4 | 148.2 | 50.0 | 1.9 | 148.7 | 50.0 | 1.4 | 149.2 | 50.0 | 0.9 | 149.7 | 50.0 | 0.4 |
| 8.0 | 99.7 | 0.3 | 144.4 | - | 124.7 | 50.0 | 19.7 | 140.2 | 50.0 | 4.2 | 142.6 | 50.0 | 1.8 | 143.1 | 50.0 | 1.3 | 143.6 | 50.0 | 0.8 | 144.1 | 50.0 | 0.3 |
| 9.0 | 99.8 | 0.2 | 138.7 | - | 119.8 | 50.0 | 18.9 | 134.9 | 50.0 | 3.8 | 137.3 | 50.0 | 1.4 | 137.7 | 50.0 | 1.0 | 138.2 | 50.0 | 0.5 | 138.7 | 50.0 | 0.0 |
| 10.0 | 99.8 | 0.2 | 138.7 | - | 119.6 | 50.0 | 19.1 | 134.6 | 50.0 | 4.1 | 137.0 | 50.0 | 1.7 | 137.4 | 50.0 | 1.3 | 137.9 | 50.0 | 0.8 | 138.4 | 50.0 | 0.3 |
| 11.0 | 99.9 | 0.1 | 133.1 | - | 115.3 | 50.0 | 17.8 | 129.9 | 50.0 | 3.2 | 132.2 | 50.0 | 0.9 | 132.7 | 40.0 | 0.4 | 133.1 | 40.0 | 0.0 | 133.6 | 40.0 | 0.5 |
| 12.0 | 99.9 | 0.1 | 127.6 | - | 110.7 | 50.0 | 16.9 | 125.0 | 50.0 | 2.6 | 127.2 | 50.0 | 0.4 | 127.6 | 30.0 | 0.0 | 128.1 | 30.0 | 0.5 | 128.5 | 30.0 | 0.9 |
| 13.0 | 100.0 | 0.0 | 122.0 | - | 106.5 | 50.0 | 15.5 | 120.3 | 50.0 | 1.7 | 122.5 | 50.0 | 0.5 | 122.9 | 50.0 | 0.9 | 123.4 | 50.0 | 1.4 | 123.8 | 50.0 | 1.8 |
| 14.0 | 100.0 | 0.0 | 122.0 | - | 106.4 | 50.0 | 15.6 | 120.2 | 50.0 | 1.8 | 122.4 | 50.0 | 0.4 | 122.8 | 50.0 | 0.8 | 123.2 | 50.0 | 1.2 | 123.6 | 50.0 | 1.6 |
| 15.0 | 100.0 | 0.0 | 118.6 | - | 103.6 | 50.0 | 15.0 | 117.1 | 50.0 | 1.5 | 119.3 | 50.0 | 0.7 | 119.7 | 50.0 | 1.1 | 120.1 | 50.0 | 1.5 | 120.5 | 50.0 | 1.9 |
| 16.0 | 100.0 | 0.0 | 116.4 | - | 102.1 | 50.0 | 14.3 | 115.6 | 50.0 | 0.8 | 117.7 | 50.0 | 1.3 | 118.1 | 50.0 | 1.7 | 118.5 | 50.0 | 2.1 | 118.9 | 50.0 | 2.5 |
| 17.0 | 100.0 | 0.0 | 110.9 | - | 98.0 | 50.0 | 12.9 | 111.1 | 50.0 | 0.2 | 113.1 | 50.0 | 2.2 | 113.5 | 50.0 | 2.6 | 113.9 | 50.0 | 3.0 | 114.3 | 50.0 | 3.4 |
| 18.0 | 100.0 | 0.0 | 110.9 | - | 97.9 | 50.0 | 13.0 | 111.0 | 50.0 | 0.1 | 113.0 | 50.0 | 2.1 | 113.4 | 50.0 | 2.5 | 113.8 | 50.0 | 2.9 | 114.2 | 50.0 | 3.3 |
| 19.0 | 100.0 | 0.0 | 110.9 | - | 97.9 | 50.0 | 13.0 | 110.9 | 50.0 | 0.0 | 113.0 | 50.0 | 2.1 | 113.4 | 50.0 | 2.5 | 113.8 | 50.0 | 2.9 | 114.2 | 50.0 | 3.3 |
| 20.0 | 100.0 | 0.0 | 105.3 | - | 93.9 | 50.0 | 11.4 | 106.6 | 50.0 | 1.3 | 108.6 | 50.0 | 3.3 | 109.0 | 50.0 | 3.7 | 109.4 | 50.0 | 4.1 | 109.7 | 50.0 | 4.4 |
| 21.0 | 100.0 | 0.0 | 99.8 | - | 89.8 | 50.0 | 10.0 | 102.1 | 50.0 | 2.3 | 104.1 | 50.0 | 4.3 | 104.5 | 50.0 | 4.7 | 104.8 | 50.0 | 5.0 | 105.2 | 50.0 | 5.4 |
| 22.0 | 100.0 | 0.0 | 94.2 | - | 85.7 | 50.0 | 8.5 | 97.7 | 50.0 | 3.5 | 99.6 | 50.0 | 5.4 | 99.9 | 50.0 | 5.7 | 100.3 | 50.0 | 6.1 | 100.7 | 50.0 | 6.5 |
| | | | | | **AAD** | | **16.699** | **AAD** | | **2.870** | AAD | | **1.893** | **AAD** | | **1.804** | **AAD** | | **1.763** | **AAD** | | **1.833** |

## C.5.5Different binary interaction parameters (sPC-SAFT): Predictions and experimental SL data from Tiffin, et al. [46]

| Number | Composition [mole %] | | Experimental data | | NeqSim (sPC-SAFT), kij = 0 | | | NeqSim (sPC-SAFT), kij = 0.005 | | |
|---|---|---|---|---|---|---|---|---|---|---|
| | $CH_4$ | $C_7H_{16}$ | Temperature [K] | Pressure [bar] | Temperature [K] | Pressure [bar] | ABS | Temperature [K] | Pressure [bar] | ABS |
| 1 | 97.63 | 2.37 | 166.50 | - | 163.06 | 50.00 | 3.44 | 165.90 | 50.00 | 0.60 |
| 2 | 98.48 | 1.52 | 163.70 | - | 159.14 | 50.00 | 4.56 | 162.03 | 50.00 | 1.67 |
| 3 | 98.74 | 1.26 | 160.90 | - | 157.31 | 50.00 | 3.59 | 160.19 | 50.00 | 0.71 |
| 4 | 98.88 | 1.12 | 160.90 | - | 156.13 | 50.00 | 4.77 | 158.99 | 50.00 | 1.91 |
| 5 | 99.23 | 0.77 | 155.60 | - | 152.37 | 50.00 | 3.23 | 155.15 | 50.00 | 0.45 |
| 6 | 99.30 | 0.70 | 155.60 | - | 151.36 | 50.00 | 4.24 | 154.12 | 50.00 | 1.48 |
| 7 | 99.52 | 0.48 | 150.10 | - | 147.62 | 50.00 | 2.48 | 150.29 | 50.00 | 0.19 |
| 8 | 99.70 | 0.30 | 144.40 | - | 142.97 | 50.00 | 1.43 | 145.53 | 50.00 | 1.13 |
| 9 | 99.82 | 0.18 | 138.70 | - | 138.47 | 50.00 | 0.23 | 140.93 | 50.00 | 2.23 |
| 10 | 99.83 | 0.18 | 138.70 | - | 138.53 | 50.00 | 0.17 | 140.68 | 50.00 | 1.98 |
| 11 | 99.89 | 0.11 | 133.10 | - | 134.31 | 50.00 | 1.21 | 136.76 | 50.00 | 3.66 |
| 12 | 99.94 | 0.06 | 127.60 | - | 130.00 | 50.00 | 2.40 | 132.00 | 50.00 | 4.40 |
| 13 | 99.96 | 0.04 | 122.00 | - | 125.93 | 50.00 | 3.93 | 127.98 | 50.00 | 5.98 |
| 14 | 99.97 | 0.03 | 122.00 | - | 125.79 | 50.00 | 3.79 | 127.98 | 50.00 | 5.98 |
| 15 | 99.98 | 0.02 | 118.60 | - | 123.11 | 50.00 | 4.51 | 125.25 | 50.00 | 6.65 |
| 16 | 99.98 | 0.02 | 116.40 | - | 121.73 | 50.00 | 5.33 | 123.84 | 50.00 | 7.44 |
| 17 | 99.99 | 0.01 | 110.90 | - | 117.73 | 50.00 | 6.83 | 119.77 | 50.00 | 8.87 |
| 18 | 99.99 | 0.01 | 110.90 | - | 117.66 | 50.00 | 6.76 | 119.70 | 50.00 | 8.80 |
| 19 | 99.99 | 0.01 | 110.90 | - | 117.61 | 50.00 | 6.71 | 119.65 | 50.00 | 8.75 |
| 20 | 100.00 | 0.00 | 105.30 | - | 112.69 | 50.00 | 7.39 | 115.68 | 50.00 | 10.38 |
| 21 | 100.00 | 0.00 | 99.80 | - | - | - | - | - | - | - |
| 22 | 100.00 | 0.00 | 94.20 | - | - | - | - | - | - | - |
| | | | | | **AAD** | | **3.849** | **AAD** | | **4.163** |

## C.6 Experimental data from literature and simulated data: Solid benzene formation in liquid methane

### C.6.1 SLV predictions (temperature) and experimental data from Kuebler and McKinley [7]

| Number | Composition [mole %] | | Experimental data | | NeqSim (SRK, kij = 0.00) | | | NeqSim (SRK, kij = 0.06) | | | NeqSim (sPC-SAFT, kij = 0) | | | NeqSim (sPC-SAFT, kij = 0.02) | | | NeqSim (sPC-SAFT, kij = 0.025) | | | NeqSim (UMR-PRU) | | |
|---|---|---|---|---|---|---|---|---|---|---|---|---|---|---|---|---|---|---|---|---|---|---|
| | $CH_4$ | $C_6H_6$ | Temperature [K] | Pressure [bar] | Temperature [K] | Pressure [bar] | ABS | Temperature [K] | Pressure [bar] | ABS | Temperature [K] | Pressure [bar] | ABS | Temperature [K] | Pressure [bar] | ABS | Temperature [K] | Pressure [bar] | ABS | Temperature [K] | Pressure [bar] | ABS |
| 1 | 27.54 | 72.46 | 268.1 | 170 | 251.6 | 170.0 | 16.5 | 260.6 | 170.0 | 7.5 | 254.0 | 170.0 | 14.1 | 266.1 | 170.0 | 2.0 | 260.5 | 170.0 | 7.6 | 256.0 | 170.0 | 12.1 |
| 2 | 26.92 | 73.08 | 268.2 | 160 | 252.5 | 160.0 | 15.7 | 261.1 | 160.0 | 7.1 | 255.0 | 160.0 | 13.2 | 266.4 | 160.0 | 1.8 | 261.0 | 160.0 | 7.2 | 256.8 | 160.0 | 11.4 |
| 3 | 25.91 | 74.09 | 268.4 | 150 | 253.4 | 150.0 | 15.0 | 261.7 | 150.0 | 6.7 | 256.0 | 150.0 | 12.4 | 266.8 | 150.0 | 1.6 | 261.6 | 150.0 | 6.8 | 257.6 | 150.0 | 10.8 |
| 4 | 24.63 | 75.37 | 268.7 | 140 | 254.5 | 140.0 | 14.2 | 262.3 | 140.0 | 6.4 | 256.9 | 140.0 | 11.8 | 267.2 | 140.0 | 1.5 | 262.2 | 140.0 | 6.5 | 258.5 | 140.0 | 10.2 |
| 5 | 23.58 | 76.42 | 269 | 130 | 255.6 | 130.0 | 13.4 | 263.0 | 130.0 | 6.0 | 257.8 | 130.0 | 11.2 | 267.6 | 130.0 | 1.4 | 262.8 | 130.0 | 6.2 | 259.4 | 130.0 | 9.6 |
| 6 | 22.25 | 77.75 | 269.4 | 120 | 256.8 | 120.0 | 12.6 | 263.8 | 120.0 | 5.6 | 258.8 | 120.0 | 10.6 | 268.1 | 120.0 | 1.3 | 263.5 | 120.0 | 5.9 | 260.4 | 120.0 | 9.0 |
| 7 | 20.69 | 79.31 | 269.9 | 110 | 258.1 | 110.0 | 11.8 | 264.6 | 110.0 | 5.3 | 259.9 | 110.0 | 10.0 | 268.6 | 110.0 | 1.3 | 264.3 | 110.0 | 5.6 | 261.5 | 110.0 | 8.4 |
| 8 | 19.08 | 80.92 | 270.4 | 100 | 259.5 | 100.0 | 10.9 | 265.5 | 100.0 | 4.9 | 261.1 | 100.0 | 9.3 | 269.1 | 100.0 | 1.3 | 265.2 | 100.0 | 5.2 | 262.7 | 100.0 | 7.7 |
| 9 | 17.51 | 82.49 | 270.9 | 90 | 261.1 | 90.0 | 9.8 | 266.4 | 90.0 | 4.5 | 262.4 | 90.0 | 8.5 | 269.8 | 90.0 | 1.1 | 266.1 | 90.0 | 4.8 | 263.9 | 90.0 | 7.0 |
| 10 | 15.56 | 84.44 | 271.6 | 80 | 262.7 | 80.0 | 8.9 | 267.5 | 80.0 | 4.1 | 263.8 | 80.0 | 7.8 | 270.5 | 80.0 | 1.1 | 267.2 | 80.0 | 4.4 | 265.2 | 80.0 | 6.4 |
| 11 | 14.02 | 85.98 | 272.2 | 70 | 264.4 | 70.0 | 7.8 | 268.6 | 70.0 | 3.6 | 265.4 | 70.0 | 6.8 | 271.3 | 70.0 | 0.9 | 268.3 | 70.0 | 3.9 | 266.7 | 70.0 | 5.5 |
| 12 | 11.76 | 88.24 | 273.1 | 60 | 266.3 | 60.0 | 6.8 | 269.8 | 60.0 | 3.3 | 267.0 | 60.0 | 6.1 | 272.1 | 60.0 | 1.0 | 269.5 | 60.0 | 3.6 | 268.2 | 60.0 | 4.9 |
| 13 | 9.81 | 90.19 | 273.9 | 50 | 268.2 | 50.0 | 5.7 | 271.1 | 50.0 | 2.8 | 268.8 | 50.0 | 5.1 | 273.0 | 50.0 | 0.9 | 270.8 | 50.0 | 3.1 | 269.7 | 50.0 | 4.2 |
| 14 | 7.53 | 92.47 | 274.9 | 40 | 270.1 | 40.0 | 4.8 | 272.4 | 40.0 | 2.5 | 270.6 | 40.0 | 4.3 | 274.0 | 40.0 | 0.9 | 272.2 | 40.0 | 2.7 | 271.4 | 40.0 | 3.5 |
| 15 | 5.67 | 94.33 | 275.8 | 30 | 272.2 | 30.0 | 3.6 | 273.9 | 30.0 | 1.9 | 272.5 | 30.0 | 3.3 | 275.1 | 30.0 | 0.7 | 273.7 | 30.0 | 2.1 | 273.1 | 30.0 | 2.7 |
| 16 | 3.65 | 96.35 | 276.8 | 20 | 274.2 | 20.0 | 2.6 | 275.4 | 20.0 | 1.4 | 274.4 | 20.0 | 2.4 | 276.1 | 20.0 | 0.7 | 275.2 | 20.0 | 1.6 | 274.8 | 20.0 | 2.0 |
| 17 | 1.85 | 98.15 | 277.7 | 10 | 276.4 | 10.0 | 1.3 | 276.9 | 10.0 | 0.8 | 276.4 | 10.0 | 1.3 | 277.3 | 10.0 | 0.4 | 276.8 | 10.0 | 0.9 | 276.6 | 10.0 | 1.1 |
| 18 | | | | | | | | | | | | | | | | | | | | | | |
| 19 | | | | | | | | | | | | | | | | | | | | | | |
| 20 | | | | | | | | | | | | | | | | | | | | | | |
| 21 | | | | | | | | | | | | | | | | | | | | | | |
| 22 | 99.989 | 0.011 | 165 | 19.5 | 164.9 | 19.5 | 0.2 | 164.9 | 19.5 | 0.1 | 165.2 | 19.5 | 0.2 | 165.2 | 19.5 | 0.2 | 165.2 | 19.5 | 0.2 | 165.7 | 19.5 | 0.7 |
| 23 | 99.9865 | 0.0135 | 170 | 23.3 | 169.7 | 23.3 | 0.3 | 169.7 | 23.3 | 0.3 | 170.0 | 23.3 | 0.0 | 169.9 | 23.3 | 0.1 | 169.9 | 23.3 | 0.1 | 170.1 | 23.3 | 0.1 |
| 24 | 99.985 | 0.015 | 175 | 29.7 | 176.5 | 29.7 | 1.4 | 176.7 | 29.7 | 1.7 | 176.9 | 29.7 | 1.9 | 176.9 | 29.7 | 1.8 | 176.8 | 29.7 | 1.8 | 176.9 | 29.7 | 1.9 |
| 25 | 99.9835 | 0.0165 | 180 | 32.8 | 179.7 | 32.8 | 0.3 | 179.7 | 32.8 | 0.3 | 179.9 | 32.8 | 0.1 | 179.9 | 32.8 | 0.1 | 179.9 | 32.8 | 0.1 | 179.9 | 32.8 | 0.1 |
| 26 | 99.983 | 0.017 | 185 | 38.4 | 184.6 | 38.4 | 0.4 | 184.6 | 38.4 | 0.4 | 184.9 | 38.4 | 0.1 | 184.9 | 38.4 | 0.1 | 184.9 | 38.4 | 0.1 | 184.8 | 38.4 | 0.3 |
| 27 | 99.985 | 0.015 | 190.5 | 45.66 | 190.4 | 45.7 | 0.2 | 190.3 | 45.7 | 0.3 | 190.4 | 45.7 | 0.2 | 192.2 | 45.7 | 1.7 | 192.2 | 45.7 | 1.7 | 189.9 | 45.7 | 0.6 |
| | | | | | **AAD** | | **7.14593** | **AAD** | | **3.370** | **AAD** | | **6.120** | **AAD** | | **1.045** | **AAD** | | **3.552** | **AAD** | | **5.218** |

## C.6.2 Predictions and experimental SL data from Kuebler and McKinley [7]

| Number | Composition [mole %] | | Experimental data | | NeqSim (SRK,kij = 0.0) | | | NeqSim (UMR-PRU) | | | NeqSim (sPC-SAFT, kij = 0) | | | NeqSim (SRK,kij = 0.06_"optimal") | | | NeqSim (SRK,kij = 0.06_"optimal") | | | NeqSim (SRK,kij = 0.06_"optimal") | | |
|---|---|---|---|---|---|---|---|---|---|---|---|---|---|---|---|---|---|---|---|---|---|---|
| | $CH_4$ | $C_6H_6$ | Temperature [K] | Pressure [bar] | Temperature [K] | Pressure [bar] | ABS | Temperature [K] | Pressure [bar] | ABS | Temperature [K] | Pressure [bar] | ABS | Temperature [K] | Pressure [bar] | ABS | Temperature [K] | Pressure [bar] | ABS | Temperature [K] | Pressure [bar] | ABS |
| 1 | 99.86000 | 0.140000 | 199.8 | 136.8 | - | - | - | - | - | - | - | - | - | - | - | - | - | - | - | - | - | - |
| 2 | 99.87100 | 0.129000 | 199.8 | 126.1 | - | - | - | - | - | - | - | - | - | - | - | - | - | - | - | - | - | - |
| 3 | 99.89200 | 0.108000 | 199.8 | 105.4 | - | - | - | - | - | - | - | - | - | - | - | - | - | - | - | - | - | - |
| 4 | 99.90840 | 0.091600 | 188.7 | 136.1 | - | - | - | - | - | - | - | - | - | - | - | - | - | - | - | - | - | - |
| 5 | 99.91320 | 0.086800 | 188.7 | 125.4 | - | - | - | - | - | - | - | - | - | - | - | - | - | - | - | - | - | - |
| 6 | 99.92210 | 0.077900 | 188.7 | 105.4 | - | - | - | - | - | - | - | - | - | - | - | - | - | - | - | - | - | - |
| 7 | 99.92890 | 0.071100 | 183.1 | 136.1 | - | - | - | - | - | - | - | - | - | - | - | - | - | - | - | - | - | - |
| 8 | 99.93860 | 0.061400 | 183.1 | 105.4 | - | - | - | - | - | - | - | - | - | - | - | - | - | - | - | - | - | - |
| 9 | 99.94630 | 0.053700 | 183.1 | 86.1 | - | - | - | - | - | - | - | - | - | - | - | - | - | - | - | - | - | - |
| 10 | 99.95600 | 0.044000 | 183.1 | 61.3 | - | - | - | - | - | - | - | - | - | - | - | - | - | - | - | - | - | - |
| 11 | 99.95810 | 0.041900 | 183.1 | 54.1 | - | - | - | - | - | - | - | - | - | - | - | - | - | - | - | - | - | - |
| 12 | 99.96370 | 0.036300 | 177.6 | 54.1 | - | - | - | - | - | - | - | - | - | - | - | - | - | - | - | - | - | - |
| 13 | 99.97070 | 0.029300 | 172 | 54.1 | - | - | - | - | - | - | - | - | - | - | - | - | - | - | - | - | - | - |
| 14 | 99.97050 | 0.029500 | 166.4 | 135.8 | - | - | - | - | - | - | - | - | - | - | - | - | - | - | - | - | - | - |
| 15 | 99.97300 | 0.027000 | 166.4 | 105.4 | - | - | - | - | - | - | - | - | - | - | - | - | - | - | - | - | - | - |
| 16 | 99.97480 | 0.025200 | 166.4 | 86.1 | - | - | - | - | - | - | - | - | - | - | - | - | - | - | - | - | - | - |
| 17 | 99.97740 | 0.022600 | 166.4 | 54.1 | - | - | - | - | - | - | - | - | - | - | - | - | - | - | - | - | - | - |
| 18 | 99.98330 | 0.016700 | 160.9 | 54.1 | 132.23 | 50.00 | 28.67 | 168.44 | 50.00 | 7.54 | 145.15 | 50.00 | 21.25 | 161.63 | 50.00 | 0.73 | 157.29 | 70.00 | 3.61 | 159.05 | 90.00 | 1.85 |
| 19 | 99.98780 | 0.012200 | 155.3 | 54.1 | 127.78 | 50.00 | 27.52 | 161.90 | 50.00 | 6.60 | 141.18 | 50.00 | 19.72 | 155.47 | 50.00 | 0.17 | 152.33 | 70.00 | 2.97 | 153.67 | 90.00 | 1.63 |
| 20 | 99.99181 | 0.008190 | 149.8 | 54.1 | 122.69 | 50.00 | 27.11 | 155.39 | 50.00 | 5.59 | 136.87 | 40.00 | 18.43 | 148.95 | 50.00 | 0.85 | 146.66 | 70.00 | 3.14 | 147.68 | 90.00 | 2.12 |
| 21 | 99.99379 | 0.006210 | 144.2 | 135.8 | 119.45 | 50.00 | 24.75 | 151.50 | 50.00 | 7.30 | 133.89 | 40.00 | 15.91 | 144.96 | 50.00 | 0.76 | 143.06 | 70.00 | 1.14 | 143.92 | 90.00 | 0.28 |
| 22 | 99.99386 | 0.006140 | 144.2 | 126.1 | 119.32 | 50.00 | 24.88 | 151.34 | 50.00 | 7.14 | 133.77 | 40.00 | 10.43 | 144.81 | 50.00 | 0.61 | 142.92 | 70.00 | 1.28 | 143.78 | 90.00 | 0.42 |
| 23 | 99.99411 | 0.005890 | 144.2 | 105.4 | 118.85 | 50.00 | 25.35 | 150.79 | 50.00 | 6.59 | 133.34 | 40.00 | 10.86 | 144.24 | 50.00 | 0.04 | 142.40 | 70.00 | 1.80 | 143.24 | 90.00 | 0.96 |
| 24 | 99.99435 | 0.005650 | 144.2 | 83.7 | 118.39 | 50.00 | 25.81 | 150.25 | 50.00 | 6.05 | 132.91 | 40.00 | 11.29 | 143.68 | 50.00 | 0.52 | 141.89 | 70.00 | 2.31 | 142.70 | 90.00 | 1.50 |
| 25 | 99.99455 | 0.005450 | 144.2 | 69.9 | 117.99 | 50.00 | 26.21 | 149.78 | 50.00 | 5.58 | 132.55 | 40.00 | 11.65 | 143.20 | 50.00 | 1.00 | 141.45 | 70.00 | 2.75 | 142.25 | 90.00 | 1.95 |
| 26 | 99.99450 | 0.005500 | 144.2 | 60.6 | 118.09 | 50.00 | 26.11 | 149.90 | 50.00 | 5.70 | 132.64 | 40.00 | 11.56 | 143.32 | 50.00 | 0.88 | 141.56 | 70.00 | 2.64 | 142.36 | 90.00 | 1.84 |
| 27 | 99.99453 | 0.005470 | 144.2 | 54.1 | 118.03 | 50.00 | 26.17 | 149.83 | 50.00 | 5.63 | 132.59 | 40.00 | 11.61 | 143.25 | 50.00 | 0.95 | 141.49 | 70.00 | 2.71 | 142.29 | 90.00 | 1.91 |
| 28 | 99.99651 | 0.003490 | 138.6 | 54.1 | 113.33 | 50.00 | 25.27 | 144.41 | 50.00 | 5.81 | 128.23 | 40.00 | 15.97 | 137.65 | 50.00 | 0.95 | 136.28 | 70.00 | 2.32 | 136.91 | 90.00 | 1.69 |
| 29 | 99.99794 | 0.002060 | 133 | 54.1 | 108.36 | 50.00 | 24.64 | 138.77 | 50.00 | 5.77 | 123.88 | 20.00 | 14.72 | 131.81 | 50.00 | 1.19 | 130.74 | 70.00 | 2.26 | 131.24 | 90.00 | 1.76 |
| 30 | 99.99875 | 0.001250 | 127.4 | 54.1 | 104.09 | 50.00 | 23.31 | 133.97 | 50.00 | 6.57 | 119.78 | 20.00 | 13.22 | 126.84 | 50.00 | 0.56 | 125.97 | 70.00 | 1.43 | 126.38 | 90.00 | 1.02 |
| 31 | 99.99903 | 0.000970 | 125.1 | 54.1 | 102.07 | 50.00 | 23.03 | 131.70 | 50.00 | 6.60 | 117.83 | 20.00 | 9.57 | 124.49 | 50.00 | 0.61 | 123.70 | 70.00 | 1.40 | 124.08 | 90.00 | 1.02 |
| 32 | 99.99924 | 0.000760 | 121.8 | 136.1 | 100.20 | 50.00 | 21.60 | 129.61 | 50.00 | 7.81 | 116.02 | 20.00 | 9.08 | 122.33 | 50.00 | 0.53 | 121.61 | 70.00 | 0.19 | 121.95 | 90.00 | 0.15 |
| 33 | 99.99929 | 0.000710 | 121.8 | 54.1 | 99.69 | 50.00 | 22.11 | 129.04 | 50.00 | 7.24 | 115.53 | 20.00 | 6.27 | 121.75 | 50.00 | 0.05 | 121.04 | 70.00 | 0.76 | 121.38 | 90.00 | 0.42 |
| 34 | 99.99964 | 0.000360 | 116.2 | 54.1 | 94.93 | 50.00 | 21.27 | 123.69 | 50.00 | 7.49 | 111.01 | 20.00 | 10.79 | 116.24 | 50.00 | 0.04 | 115.68 | 70.00 | 0.52 | 115.95 | 90.00 | 0.25 |
| 35 | 99.99980 | 0.000200 | 110.6 | 54.1 | 91.18 | 50.00 | 19.42 | 119.48 | 50.00 | 8.88 | 107.30 | 5.00 | 8.90 | 111.93 | 50.00 | 1.33 | 111.45 | 70.00 | 0.85 | 111.68 | 90.00 | 1.08 |
| 36 | 99.99991 | 0.000090 | 105 | 54.1 | 86.58 | 50.00 | 18.42 | 114.26 | 50.00 | 9.26 | 102.70 | 5.00 | 7.90 | 106.61 | 50.00 | 1.61 | 106.23 | 70.00 | 1.23 | 106.41 | 90.00 | 1.41 |
| 37 | 99.99996 | 0.000039 | 99.4 | 54.1 | 82.26 | 50.00 | 17.14 | 109.32 | 50.00 | 9.92 | 98.33 | 5.00 | 6.67 | 101.61 | 50.00 | 2.21 | 101.30 | 70.00 | 1.90 | 101.45 | 90.00 | 2.05 |
| | | | | | **AAD** | | **17.100** | **AAD** | | **6.954** | **AAD** | | **8.779** | **AAD** | | **0.557** | **AAD** | | **1.329** | **AAD** | | **0.905** |

## C.6.3 Different binary interaction parameters (SRK), SLE: Predictions and experimental SL data from Kuebler and McKinley [7]

| Number | Composition [mole %] | | Experimental data | | NeqSim (SRK), kij=0.0209 | | | NeqSim (SRK), kij=0.05 | | | NeqSim (SRK), kij=0.058 | | | NeqSim (SRK), kij=0.06 | | | NeqSim (SRK), kij=0.062 | | | NeqSim (SRK), kij=0.00 | | |
|---|---|---|---|---|---|---|---|---|---|---|---|---|---|---|---|---|---|---|---|---|---|---|
| | $CH_4$ | $C_6H_6$ | Temperature [K] | Pressure [bar] | Temperature [K] | Pressure [bar] | ABS | Temperature [K] | Pressure [bar] | ABS | Temperature [K] | Pressure [bar] | ABS | Temperature [K] | Pressure [bar] | ABS | Temperature [K] | Pressure [bar] | ABS | Temperature [K] | Pressure [bar] | ABS |
| 1 | 99.98330 | 0.016700 | 160.9 | - | 142.66 | 50.00 | 18.24 | 156.74 | 50.00 | 4.16 | 160.64 | 50.00 | 0.26 | 161.63 | 50.00 | 0.73 | 162.63 | 50.00 | 1.73 | 132.23 | 50.00 | 28.67 |
| 2 | 99.98780 | 0.012200 | 155.3 | - | 137.78 | 50.00 | 17.52 | 151.02 | 50.00 | 4.28 | 154.58 | 50.00 | 0.72 | 155.47 | 50.00 | 0.17 | 156.35 | 50.00 | 1.05 | 127.78 | 50.00 | 27.52 |
| 3 | 99.99181 | 0.008190 | 149.8 | - | 132.27 | 50.00 | 17.53 | 144.81 | 50.00 | 4.99 | 148.12 | 50.00 | 1.68 | 148.95 | 50.00 | 0.85 | 149.76 | 50.00 | 0.04 | 122.69 | 50.00 | 27.11 |
| 4 | 99.99379 | 0.006210 | 144.2 | - | 128.79 | 50.00 | 15.41 | 140.97 | 50.00 | 3.23 | 144.17 | 50.00 | 0.03 | 144.96 | 50.00 | 0.76 | 145.75 | 50.00 | 1.55 | 119.45 | 50.00 | 24.75 |
| 5 | 99.99386 | 0.006140 | 144.2 | - | 128.66 | 50.00 | 15.54 | 140.82 | 50.00 | 3.38 | 144.01 | 50.00 | 0.19 | 144.81 | 50.00 | 0.61 | 145.59 | 50.00 | 1.39 | 119.32 | 50.00 | 24.88 |
| 6 | 99.99411 | 0.005890 | 144.2 | - | 128.16 | 50.00 | 16.04 | 140.27 | 50.00 | 3.93 | 143.45 | 50.00 | 0.75 | 144.24 | 50.00 | 0.04 | 145.02 | 50.00 | 0.82 | 118.85 | 50.00 | 25.35 |
| 7 | 99.99435 | 0.005650 | 144.2 | - | 127.66 | 50.00 | 16.54 | 139.73 | 50.00 | 4.47 | 142.90 | 50.00 | 1.30 | 143.68 | 50.00 | 0.52 | 144.46 | 50.00 | 0.26 | 118.39 | 50.00 | 25.81 |
| 8 | 99.99455 | 0.005450 | 144.2 | - | 127.24 | 50.00 | 16.96 | 139.26 | 50.00 | 4.94 | 142.42 | 50.00 | 1.78 | 143.20 | 50.00 | 1.00 | 143.98 | 50.00 | 0.22 | 117.99 | 50.00 | 26.21 |
| 9 | 99.99450 | 0.005500 | 144.2 | - | 127.35 | 50.00 | 16.85 | 139.38 | 50.00 | 4.82 | 142.54 | 50.00 | 1.66 | 143.32 | 50.00 | 0.88 | 144.10 | 50.00 | 0.10 | 118.09 | 50.00 | 26.11 |
| 10 | 99.99453 | 0.005470 | 144.2 | - | 127.28 | 50.00 | 16.92 | 139.31 | 50.00 | 4.89 | 142.47 | 50.00 | 1.73 | 143.25 | 50.00 | 0.95 | 144.03 | 50.00 | 0.17 | 118.03 | 50.00 | 26.17 |
| 11 | 99.99651 | 0.003490 | 138.6 | - | 122.27 | 50.00 | 16.33 | 133.86 | 50.00 | 4.74 | 136.90 | 50.00 | 1.70 | 137.65 | 50.00 | 0.95 | 138.39 | 50.00 | 0.21 | 113.33 | 50.00 | 25.27 |
| 12 | 99.99794 | 0.002060 | 133 | - | 116.99 | 50.00 | 16.01 | 128.17 | 50.00 | 4.84 | 131.08 | 50.00 | 1.92 | 131.81 | 50.00 | 1.19 | 132.52 | 50.00 | 0.48 | 108.36 | 50.00 | 24.64 |
| 13 | 99.99875 | 0.001250 | 127.4 | - | 112.47 | 50.00 | 14.93 | 123.31 | 50.00 | 4.09 | 126.14 | 50.00 | 1.26 | 126.84 | 50.00 | 0.56 | 127.53 | 50.00 | 0.13 | 104.09 | 50.00 | 23.31 |
| 14 | 99.99903 | 0.000970 | 125.1 | - | 110.32 | 50.00 | 14.78 | 121.01 | 50.00 | 4.09 | 123.80 | 50.00 | 1.30 | 124.49 | 50.00 | 0.61 | 125.17 | 50.00 | 0.07 | 102.07 | 50.00 | 23.03 |
| 15 | 99.99924 | 0.000760 | 121.8 | - | 108.35 | 50.00 | 13.45 | 118.90 | 50.00 | 2.90 | 121.65 | 50.00 | 0.15 | 122.33 | 50.00 | 0.53 | 123.01 | 50.00 | 1.21 | 100.20 | 50.00 | 21.60 |
| 16 | 99.99929 | 0.000710 | 121.8 | - | 107.81 | 50.00 | 13.99 | 118.32 | 50.00 | 3.48 | 121.07 | 50.00 | 0.73 | 121.75 | 50.00 | 0.05 | 122.42 | 50.00 | 0.62 | 99.69 | 50.00 | 22.11 |
| 17 | 99.99964 | 0.000360 | 116.2 | - | 102.77 | 50.00 | 13.43 | 112.93 | 50.00 | 3.27 | 115.59 | 50.00 | 0.61 | 116.24 | 50.00 | 0.04 | 116.89 | 50.00 | 0.69 | 94.93 | 50.00 | 21.27 |
| 18 | 99.99980 | 0.000200 | 110.6 | - | 98.81 | 50.00 | 11.79 | 108.70 | 50.00 | 1.90 | 111.29 | 50.00 | 0.69 | 111.93 | 50.00 | 1.33 | 112.56 | 50.00 | 1.96 | 91.18 | 50.00 | 19.42 |
| 19 | 99.99991 | 0.000090 | 105 | - | 93.94 | 50.00 | 11.06 | 103.49 | 50.00 | 1.51 | 105.99 | 50.00 | 0.99 | 106.61 | 50.00 | 1.61 | 107.22 | 50.00 | 2.22 | 86.58 | 50.00 | 18.42 |
| 20 | 99.99996 | 0.000039 | 99.4 | - | 89.37 | 50.00 | 10.03 | 98.60 | 50.00 | 0.80 | 101.03 | 50.00 | 1.63 | 101.61 | 50.00 | 2.21 | 102.22 | 50.00 | 2.82 | 82.26 | 50.00 | 17.14 |
| | | | | | **AAD** | | **15.168** | **AAD** | | **3.736** | **AAD** | | **1.054** | **AAD** | | **"Optimal"** | **AAD** | | **0.888** | **AAD** | | **23.940** |

## C.6.4 Different binary interaction parameters (sPC-SAFT), SLE: Predictions and experimental SL data from Kuebler and McKinley [7]

| Composition [mole %] | | Experimental data | | NeqSim (sPC-SAFT), kij=0.0 | | | NeqSim (sPC-SAFT), kij=0.020 | | | NeqSim (sPC-SAFT), kij=0.0209 | | | NeqSim (sPC-SAFT), kij=0.025 | | | NeqSim (sPC-SAFT), kij=0.03 | | |
|---|---|---|---|---|---|---|---|---|---|---|---|---|---|---|---|---|---|---|
| $CH_4$ | $C_6H_6$ | Temperature [K] | Pressure [bar] | Temperature [K] | Pressure [bar] | ABS | Temperature [K] | Pressure [bar] | ABS | Temperature [K] | Pressure [bar] | ABS | Temperature [K] | Pressure [bar] | ABS | Temperature [K] | Pressure [bar] | ABS |
| 99.98330 | 0.016700 | 160.9 | - | 145.15 | 50.00 | 15.75 | 155.23 | 50.00 | 5.67 | 155.68 | 50.00 | 5.22 | 157.80 | 50.00 | 3.10 | 160.40 | 50.00 | 0.50 |
| 99.98780 | 0.012200 | 155.3 | - | 141.18 | 50.00 | 14.12 | 150.73 | 50.00 | 4.57 | 151.16 | 50.00 | 4.14 | 153.12 | 50.00 | 2.18 | 155.53 | 50.00 | 0.23 |
| 99.99181 | 0.008190 | 149.8 | - | 136.87 | 40.00 | 12.93 | 145.65 | 50.00 | 4.15 | 146.05 | 50.00 | 3.75 | 147.90 | 50.00 | 1.90 | 150.15 | 50.00 | 0.35 |
| 99.99379 | 0.006210 | 144.2 | - | 133.89 | 40.00 | 10.31 | 142.74 | 40.00 | 1.46 | 143.13 | 40.00 | 1.07 | 144.61 | 50.00 | 0.41 | 146.77 | 50.00 | 2.57 |
| 99.99386 | 0.006140 | 144.2 | - | 133.77 | 40.00 | 10.43 | 142.61 | 40.00 | 1.59 | 143.01 | 40.00 | 1.19 | 144.48 | 50.00 | 0.28 | 146.64 | 50.00 | 2.44 |
| 99.99411 | 0.005890 | 144.2 | - | 133.34 | 40.00 | 10.86 | 142.14 | 40.00 | 2.06 | 142.53 | 40.00 | 1.67 | 144.00 | 50.00 | 0.20 | 146.16 | 50.00 | 1.96 |
| 99.99435 | 0.005650 | 144.2 | - | 132.91 | 40.00 | 11.29 | 141.67 | 40.00 | 2.53 | 142.06 | 40.00 | 2.14 | 143.53 | 50.00 | 0.67 | 145.68 | 50.00 | 1.48 |
| 99.99455 | 0.005450 | 144.2 | - | 132.55 | 40.00 | 11.65 | 141.27 | 40.00 | 2.93 | 141.66 | 40.00 | 2.54 | 143.13 | 50.00 | 1.07 | 145.27 | 50.00 | 1.07 |
| 99.99450 | 0.005500 | 144.2 | - | 132.64 | 40.00 | 11.56 | 141.47 | 40.00 | 2.73 | 141.76 | 40.00 | 2.44 | 143.33 | 50.00 | 0.87 | 145.37 | 50.00 | 1.17 |
| 99.99453 | 0.005470 | 144.2 | - | 132.59 | 40.00 | 11.61 | 141.31 | 40.00 | 2.89 | 141.70 | 40.00 | 2.50 | 143.18 | 50.00 | 1.02 | 145.31 | 50.00 | 1.11 |
| 99.99651 | 0.003490 | 138.6 | - | 128.23 | 40.00 | 10.37 | 136.59 | 40.00 | 2.01 | 137.19 | 30.00 | 1.41 | 138.42 | 50.00 | 0.18 | 140.46 | 50.00 | 1.86 |
| 99.99794 | 0.002060 | 133 | - | 123.88 | 20.00 | 9.12 | 131.57 | 40.00 | 1.43 | 132.11 | 30.00 | 0.89 | 134.00 | 20.00 | 1.00 | 135.32 | 50.00 | 2.32 |
| 99.99875 | 0.001250 | 127.4 | - | 119.78 | 20.00 | 7.62 | 127.25 | 40.00 | 0.15 | 127.89 | 20.00 | 0.49 | 129.46 | 20.00 | 2.06 | 131.19 | 30.00 | 3.79 |
| 99.99903 | 0.000970 | 125.1 | - | 117.83 | 20.00 | 7.27 | 125.45 | 20.00 | 0.35 | 125.79 | 20.00 | 0.69 | 127.33 | 20.00 | 2.23 | 129.05 | 30.00 | 3.95 |
| 99.99924 | 0.000760 | 121.8 | - | 116.02 | 20.00 | 5.78 | 123.52 | 20.00 | 1.72 | 123.85 | 20.00 | 2.05 | 125.37 | 20.00 | 3.57 | 127.07 | 30.00 | 5.27 |
| 99.99929 | 0.000710 | 121.8 | - | 115.53 | 20.00 | 6.27 | 123.00 | 20.00 | 1.20 | 123.33 | 20.00 | 1.53 | 124.83 | 20.00 | 3.03 | 126.66 | 20.00 | 4.86 |
| 99.99964 | 0.000360 | 116.2 | - | 111.01 | 20.00 | 5.19 | 118.04 | 20.00 | 1.84 | 118.36 | 20.00 | 2.16 | 119.80 | 20.00 | 3.60 | 121.55 | 20.00 | 5.35 |
| 99.99980 | 0.000200 | 110.6 | - | 107.30 | 5.00 | 3.30 | 114.12 | 20.00 | 3.52 | 114.43 | 20.00 | 3.83 | 115.82 | 10.00 | 5.22 | 117.52 | 10.00 | 6.92 |
| 99.99991 | 0.000090 | 105 | - | 102.70 | 5.00 | 2.30 | 109.32 | 10.00 | 4.32 | 109.61 | 10.00 | 4.61 | 110.95 | 10.00 | 5.95 | 112.58 | 10.00 | 7.58 |
| 99.99996 | 0.000039 | 99.4 | - | 98.33 | 5.00 | 1.07 | 104.69 | 10.00 | 5.29 | 104.97 | 10.00 | 5.57 | 106.29 | 5.00 | 6.89 | 107.86 | 5.00 | 8.46 |
| | | | | **AAD** | | **8.941** | **AAD** | | **2.621** | **AAD** | | **2.494** | **AAD** | | **2.271** | **AAD** | | **3.162** |

## C.6.5 Solid benzene behavior in CH4-C2H6 –benzene mixture. Experimental data from Tiffin, et al. [59]

| Run | | Number | Composition [mole %] | | | Experimental data | | NeqSim (SRK), kij = 0.038_"optimal" | | | NeqSim (UMR), kij = 0.0 | | | NeqSim (sPC-SAFT), kij = 00 | | |
|---|---|---|---|---|---|---|---|---|---|---|---|---|---|---|---|---|
| | | | CH4 | C2H6 | C6H6 | Temperature [K] | Pressure [bar] | Temperature [K] | Pressure [bar] | ABS | Temperature [K] | Pressure [bar] | ABS | Temperature [K] | Pressure [bar] | ABS |
| 1 | | 1.000 | 88.200 | 11.690 | 0.113 | 190.170 | 38.960 | - | 50.0 | | - | 50.0 | - | | | |
| | | 2.000 | 88.700 | 11.220 | 0.085 | 184.650 | 31.680 | 179.55 | 50.0 | 5.10 | - | 50.0 | - | | | |
| | | 3.000 | 88.980 | 10.950 | 0.077 | 180.870 | 28.340 | 177.13 | 50.0 | 3.74 | - | 50.0 | - | | | |
| | | 4.000 | 84.910 | 14.980 | 0.113 | 181.900 | 27.530 | 179.54 | 50.0 | 2.36 | - | 50.0 | - | | | |
| | | 5.000 | 81.580 | 18.270 | 0.148 | 182.540 | 26.710 | 180.80 | 50.0 | 1.74 | 184.02 | 50.0 | 1.48 | | | |
| | | 6.000 | 75.770 | 24.030 | 0.205 | 182.350 | 24.400 | 180.15 | 50.0 | 2.20 | 183.32 | 50.0 | 0.97 | | | |
| | | 7.000 | 64.260 | 35.420 | 0.315 | 181.490 | 20.110 | 177.21 | 50.0 | 4.28 | 181.22 | 50.0 | 0.27 | | | |
| | | 8.000 | 73.770 | 26.040 | 0.193 | 179.940 | 22.360 | 176.17 | 50.0 | 3.77 | 178.83 | 50.0 | 1.11 | | | |
| | | 9.000 | 79.740 | 20.140 | 0.121 | 177.000 | 22.220 | 172.99 | 50.0 | 4.01 | 174.96 | 50.0 | 2.04 | | | |
| | | 10.000 | 82.400 | 17.510 | 0.090 | 174.170 | 21.130 | 169.95 | 50.0 | 4.22 | 171.61 | 50.0 | 2.56 | | | |
| | | 11.000 | 84.080 | 15.850 | 0.070 | 171.000 | 19.430 | 166.84 | 50.0 | 4.16 | 168.25 | 50.0 | 2.75 | | | |
| 2 | | 12.000 | 86.180 | 13.680 | 0.145 | 187.660 | 33.240 | - | 50.0 | | - | 50.0 | - | | | |
| | | 13.000 | 87.780 | 12.130 | 0.097 | 182.670 | 29.360 | - | 50.0 | | - | 50.0 | - | | | |
| | | 14.000 | 88.320 | 11.600 | 0.079 | 178.450 | 25.960 | 176.41 | 50.0 | 2.04 | 179.85 | 50.0 | 1.40 | | | |
| | | 15.000 | 88.800 | 11.140 | 0.061 | 172.820 | 21.810 | 170.63 | 50.0 | 2.19 | 173.38 | 50.0 | 0.56 | | | |
| | | 16.000 | 89.100 | 10.850 | 0.047 | 168.050 | 18.680 | 165.37 | 50.0 | 2.68 | 167.64 | 50.0 | 0.41 | | | |
| | | 17.000 | 87.290 | 12.650 | 0.058 | 168.360 | 18.270 | 167.19 | 50.0 | 1.17 | 169.23 | 50.0 | 0.87 | | | |
| | | 18.000 | 85.960 | 13.980 | 0.064 | 169.440 | 18.680 | 167.42 | 50.0 | 2.02 | 169.22 | 50.0 | 0.22 | | | |
| | | 19.000 | 82.290 | 17.240 | 0.084 | 170.550 | 18.480 | 168.84 | 50.0 | 1.71 | 170.36 | 50.0 | 0.19 | | | |
| | | 20.000 | 66.000 | 33.850 | 0.149 | 169.980 | 16.640 | 163.92 | 50.0 | 6.06 | 163.94 | 50.0 | 6.04 | | | |
| | | 21.000 | 45.070 | 54.650 | 0.292 | 169.800 | 13.440 | 162.90 | 50.0 | 6.90 | 166.76 | 50.0 | 3.04 | | | |
| | | 22.000 | 65.240 | 34.600 | 0.158 | 168.850 | 15.140 | 164.40 | 50.0 | 4.45 | 164.70 | 50.0 | 4.15 | | | |
| | | 23.000 | 77.180 | 22.730 | 0.081 | 165.470 | 14.870 | 162.28 | 50.0 | 3.19 | 161.87 | 50.0 | 3.60 | | | |
| | | 24.000 | 81.050 | 18.900 | 0.056 | 162.050 | 13.710 | 159.42 | 50.0 | 2.63 | 158.86 | 50.0 | 3.19 | | | |
| | | 25.000 | 82.170 | 17.780 | 0.049 | 160.380 | 13.100 | 158.22 | 50.0 | 2.16 | 157.62 | 50.0 | 2.76 | | | |
| 3 | | 26.000 | 67.310 | 32.300 | 0.390 | 187.180 | 25.010 | 185.43 | 50.0 | 1.75 | 190.23 | 50.0 | 3.05 | 186.48 | 30.00 | 0.70 |
| | | 27.000 | 71.460 | 28.270 | 0.267 | 183.180 | 23.790 | 181.05 | 50.0 | 2.13 | 184.71 | 50.0 | 1.53 | 181.56 | 30.00 | 1.62 |
| | | 28.000 | 75.910 | 23.940 | 0.148 | 174.700 | 19.570 | 172.77 | 50.0 | 1.93 | 174.72 | 50.0 | 0.02 | 173.05 | 30.00 | 1.65 |
| | | 29.000 | 77.460 | 22.440 | 0.106 | 168.970 | 16.570 | 167.58 | 50.0 | 1.39 | 168.50 | 50.0 | 0.47 | 168.03 | 30.00 | 0.94 |
| | | 30.000 | 78.140 | 21.770 | 0.083 | 165.000 | 14.400 | 163.63 | 50.0 | 1.37 | 163.68 | 50.0 | 1.32 | 164.53 | 25.00 | 0.47 |
| | | 31.000 | 78.610 | 21.330 | 0.066 | 160.640 | 12.350 | 159.99 | 50.0 | 0.65 | 159.10 | 50.0 | 1.54 | 161.12 | 25.00 | 0.48 |
| | | 32.000 | 78.880 | 21.060 | 0.053 | 156.730 | 10.590 | 156.57 | 50.0 | 0.16 | 154.62 | 50.0 | 2.11 | 158.11 | 20.00 | 1.38 |
| | | | | | | | | **AAD RUN 3** | | **1.341** | **AAD RUN 3** | | **1.435** | **AAD RUN** | | **1.036** |

## C.7 Experimental data from literature and simulated data: Solid octane formation in liquid methane

### C.7.1 Solid octane behavior in CH4-octane mixture: Experimental data from kohn et al [57]

| Number | Composition [mole %] | | Experimental data | | NeqSim (SRK), kij = 0.00 | | | NeqSim (sPC-SAFT),kij = 0.00 | | |
|---|---|---|---|---|---|---|---|---|---|---|
| | $CH_4$ | C8H18 | Temperature [K] | Pressure [bar] | Temperature [K] | Pressure [bar] | ABS | Temperature [K] | Pressure [bar] | ABS |
| 1 | 99.98 | 0.0214 | 156 | 13.4 | 137.32 | 13.52 | 18.680 | 153.1619355 | 50.000 | 2.838 |
| 2 | 99.98 | 0.025 | 158 | 14.5 | 138.73 | 14.71 | 19.272 | 154.5511266 | 50.000 | 3.449 |
| 3 | 99.97 | 0.0288 | 160 | 15.7 | 140.05 | 15.95 | 19.955 | 155.8594772 | 50.000 | 4.141 |
| 4 | 99.97 | 0.0331 | 162 | 17 | 141.38 | 17.28 | 20.625 | 157.1916724 | 50.000 | 4.808 |
| 5 | 99.96 | 0.038 | 164 | 18.4 | 142.73 | 18.66 | 21.269 | 158.5630665 | 50.000 | 5.437 |
| 6 | 99.96 | 0.0431 | 166 | 19.8 | 144.00 | 20.15 | 22.000 | 159.8627338 | 50.000 | 6.137 |
| 7 | 99.95 | 0.0483 | 168 | 21.4 | 145.18 | 21.70 | 22.823 | 161.0834352 | 50.000 | 6.917 |
| 8 | 99.95 | 0.0538 | 170 | 23 | 146.32 | 23.35 | 23.682 | 162.2839756 | 50.000 | 7.716 |
| 9 | 99.94 | 0.0589 | 172 | 24.6 | 147.30 | 25.00 | 24.702 | 163.3304618 | 50.000 | 8.670 |
| 10 | 99.94 | 0.0638 | 174 | 26.4 | 148.18 | 26.80 | 25.821 | 164.2867038 | 50.000 | 9.713 |
| 11 | 99.93 | 0.0689 | 176 | 28.3 | 149.04 | 28.80 | 26.958 | 165.2398585 | 50.000 | 10.760 |
| 12 | 99.93 | 0.073 | 178 | 30.2 | 149.70 | 30.80 | 28.299 | 165.9802537 | 50.000 | 12.020 |
| 13 | 99.92 | 0.0772 | 180 | 32.3 | 150.35 | 32.93 | 29.652 | 166.7187964 | 50.000 | 13.281 |
| 14 | 99.92 | 0.0809 | 182 | 34.5 | 150.90 | 35.05 | 31.104 | 167.3554032 | 50.000 | 14.645 |
| 15 | 99.92 | 0.0837 | 184 | 36.7 | 151.30 | 37.35 | 32.702 | 167.8298135 | 50.000 | 16.170 |
| 16 | 99.92 | 0.0836 | 186 | 39.1 | | | | | | |
| 17 | 99.92 | 0.0766 | 188 | 41.7 | | | | | | |
| 18 | 99.93 | 0.0653 | 190 | 44.4 | | | | | | |
| 19 | 99.94 | 0.0592 | 191.15 | 45.9 | | | | | | |
| | | | | | AAD | | 19.34444263 | | | 6.66848876 |

## C.7.2 Solid octane behavior in CH4-octane mixture at temperature: Experimental data from Kohn&Bradish [5]

| Number | Composition [mole %] | | Experimental data | | NeqSim (SRK, kij = 0.00) | | | NeqSim (sPC-SAFT, kij = 0.00) | | | NeqSim (UMR-PRU) | | |
|---|---|---|---|---|---|---|---|---|---|---|---|---|---|
| | $CH_4$ | C8H18 | Temperature [K] | Pressure [bar] | Temperature [K] | Pressure [bar] | ABS | Temperature [K] | Pressure [bar] | ABS | Temperature [K] | Pressure [bar] | ABS |
| 1 | 0.000 | 100 | 216.5 | 1 | 216.3981226 | 1 | 0.102 | 216.3981226 | 1 | 0.102 | 216.3981226 | 1 | 0.102 |
| 2 | 5.000 | 95 | 215.43 | 5.2 | 215.44502 | 5.2 | 0.015 | 215.4529297 | 5.2 | 0.023 | 215.4449413 | 5.2 | 0.015 |
| 3 | 10.000 | 90 | 214.5 | 10.25 | 214.455826 | 10.25 | 0.044 | 214.490087 | 10.25 | 0.010 | 214.4546067 | 10.25 | 0.045 |
| 4 | 20.000 | 80 | 212.5 | 20.6 | 212.3643854 | 20.6 | 0.136 | 212.5252411 | 20.6 | 0.025 | 212.3527336 | 20.6 | 0.147 |
| 5 | 30.000 | 70 | 210.5 | 31.25 | 210.1024596 | 31.25 | 0.398 | 210.5277257 | 31.25 | 0.028 | 210.0630234 | 31.25 | 0.437 |
| 6 | 40.000 | 60 | 208.6 | 43.2 | 207.6424783 | 43.2 | 0.958 | 208.5317616 | 43.2 | 0.068 | 207.5503391 | 43.2 | 1.050 |
| 7 | 50.000 | 50 | 206.6 | 57.3 | 204.9526283 | 57.3 | 1.647 | 206.5871537 | 57.3 | 0.013 | 204.7761547 | 57.3 | 1.824 |
| 8 | 56.000 | 44 | 205.6 | 70.5 | 203.2078945 | 70.5 | 2.392 | 205.4705379 | 70.5 | 0.129 | 202.9392073 | 70.5 | 2.661 |
| | | | | | | | 0.711 | | | 0.398 | | | 0.785 |

## C.7.4 Different binary interaction parameters (SRK), SLE: Predictions and experimental SL data from Kohn et al [57]

| Number | Composition [mole %] | | Experimental data | | NeqSim (SRK), kij = 0.00 | | | NeqSim (SRK,kij = 0.01) | | | NeqSim (SRK), kij = 0.035 | | | NeqSim (SRK), kij = 0.038 | | | NeqSim (SRK), kij = 0.04 | | | NeqSim (SRK), kij = 0.04 | | | NeqSim (SRK), kij = 0.04 | | |
|---|---|---|---|---|---|---|---|---|---|---|---|---|---|---|---|---|---|---|---|---|---|---|---|---|---|
| | $CH_4$ | C8H18 | Temperature [K] | Pressure [bar] | Temperature [K] | Pressure [bar] | ABS | Temperature [K] | Pressure [bar] | ABS | Temperature [K] | Pressure [bar] | ABS | emperature [K | Pressure [bar] | ABS | emperature [K | Pressure [bar] | ABS | Temperature [K] | Pressure [bar] | ABS | Temperature [K] | Pressure [bar] | ABS |
| 1 | 99.98 | 0.0214 | 156 | 13.4 | 137.3195261 | 13.52 | 0.120 | 157.8513 | 50.000 | 1.851 | 153.5595084 | 50.000 | 2.440 | 154.8472507 | 50.000 | 1.153 | 155.704021 | 50.000 | 0.296 | 154.9895113 | 60.000 | 1.010 | 154.3808795 | 70.000 | 1.619 |
| 2 | 99.98 | 0.025 | 158 | 14.5 | 138.7280698 | 14.705 | 0.205 | 159.2985 | 50.000 | 1.298 | 155.270296 | 50.000 | 2.730 | 156.5869397 | 50.000 | 1.413 | 157.4642066 | 50.000 | 0.536 | 156.6616885 | 60.000 | 1.338 | 155.9880812 | 70.000 | 2.012 |
| 3 | 99.97 | 0.0288 | 160 | 15.7 | 140.0451415 | 15.95 | 0.250 | 160.712 | 50.000 | 0.712 | 156.8981832 | 50.000 | 3.102 | 158.2462653 | 50.000 | 1.754 | 159.1459837 | 50.000 | 0.854 | 158.2460001 | 60.000 | 1.754 | 157.502646 | 70.000 | 2.497 |
| 4 | 99.97 | 0.0331 | 162 | 17 | 141.3751027 | 17.281 | 0.281 | 162.165459 | 50.000 | 0.165 | 158.5754893 | 50.000 | 3.425 | 159.9608552 | 50.000 | 2.039 | 160.8875916 | 50.000 | 1.112 | 159.8698012 | 60.000 | 2.130 | 159.0454185 | 70.000 | 2.955 |
| 5 | 99.96 | 0.038 | 164 | 18.4 | 142.7305382 | 18.66 | 0.260 | 163.67674 | 50.000 | 0.323 | 160.3272109 | 50.000 | 3.673 | 161.7584226 | 50.000 | 2.242 | 162.7189469 | 50.000 | 1.281 | 161.5544011 | 60.000 | 2.446 | 160.6337507 | 70.000 | 3.366 |
| 6 | 99.96 | 0.0431 | 166 | 19.8 | 144.0001424 | 20.15 | 0.350 | 165.12792 | 50.000 | 0.872 | 162.0164788 | 50.000 | 3.984 | 163.500586 | 50.000 | 2.499 | 164.5008568 | 50.000 | 1.499 | 163.1652434 | 60.000 | 2.835 | 162.1387352 | 70.000 | 3.861 |
| 7 | 99.95 | 0.0483 | 168 | 21.4 | 145.1773203 | 21.7 | 0.300 | 166.5122 | 50.000 | 1.488 | 163.6356044 | 50.000 | 4.364 | 165.1811857 | 50.000 | 2.819 | 166.2288875 | 50.000 | 1.771 | 164.6934596 | 60.000 | 3.307 | 163.5514995 | 70.000 | 4.449 |
| 8 | 99.95 | 0.0538 | 170 | 23 | 146.3184459 | 23.35 | 0.350 | 167.8998 | 50.000 | 2.100 | 165.2674434 | 50.000 | 4.733 | 166.8896894 | 50.000 | 3.110 | 167.9983542 | 50.000 | 2.002 | 166.2137316 | 60.000 | 3.786 | 164.9396507 | 70.000 | 5.060 |
| 9 | 99.94 | 0.0589 | 172 | 24.6 | 147.2978412 | 25 | 0.400 | 169.13674 | 50.000 | 2.863 | 166.7315934 | 50.000 | 5.268 | 168.4400309 | 50.000 | 3.560 | 169.6204383 | 50.000 | 2.380 | 167.5560467 | 60.000 | 4.444 | 166.1480868 | 70.000 | 5.852 |
| 10 | 99.94 | 0.0638 | 174 | 26.4 | 148.178734 | 26.8 | 0.400 | 170.296174 | 50.000 | 3.704 | 168.1143754 | 50.000 | 5.886 | 169.9261418 | 50.000 | 4.074 | 171.1973468 | 50.000 | 2.803 | 168.799615 | 60.000 | 5.200 | 167.250517 | 70.000 | 6.749 |
| 11 | 99.93 | 0.0689 | 176 | 28.3 | 149.0419112 | 28.8 | 0.500 | 171.4887 | 50.000 | 4.511 | 169.5505055 | 50.000 | 6.449 | 171.5030957 | 50.000 | 4.497 | 172.9088954 | 50.000 | 3.091 | 170.0591485 | 60.000 | 5.941 | 168.3471719 | 70.000 | 7.653 |
| 12 | 99.93 | 0.073 | 178 | 30.2 | 149.7010769 | 30.8 | 0.600 | 172.4488 | 50.000 | 5.551 | 170.7205667 | 50.000 | 7.279 | 172.8269916 | 50.000 | 5.173 | 174.3983774 | 50.000 | 3.602 | 171.0544037 | 60.000 | 6.946 | 169.1970929 | 70.000 | 8.803 |
| 13 | 99.92 | 0.0772 | 180 | 32.3 | 150.347783 | 32.93 | 0.630 | 173.446189 | 50.000 | 6.554 | 171.9544883 | 50.000 | 8.046 | 174.2863747 | 50.000 | 5.714 | 176.1533765 | 50.000 | 3.847 | 172.0652745 | 60.000 | 7.935 | 170.042804 | 70.000 | 9.957 |
| 14 | 99.92 | 0.0809 | 182 | 34.5 | 150.895814 | 35.05 | 0.550 | 174.349049 | 50.000 | 7.651 | 173.0949572 | 50.000 | 8.905 | 175.7402984 | 50.000 | 6.260 | 178.2412327 | 50.000 | 3.759 | 172.9543332 | 60.000 | 9.046 | 170.7697917 | 70.000 | 11.230 |
| 15 | 99.92 | 0.0837 | 184 | 36.7 | 151.2981428 | 37.35 | 0.650 | 175.05721 | 50.000 | 8.943 | 174.012632 | 50.000 | 9.987 | 177.0649315 | 50.000 | 6.935 | - | - | | 173.6297896 | 60.000 | 10.370 | 171.310152 | 70.000 | 12.690 |
| 16 | 99.92 | 0.0836 | 186 | 39.1 | | | | | | | | | 5.351377799 | | | 3.549396062 | | | 2.059391754 | | | 4.151239 | | | 5.433134 |

## C.7.5 Different binary interaction parameters (sPC-SAFT), SLE: Predictions and experimental SL from Kohn et al [57]

| Number | Composition [mole %] | | Experimental data | | NeqSim (sPC-SAFT), kij = 0.0 | | | NeqSim (sPC-SAFT), kij = 0.01 | | | NeqSim (sPC-SAFT), kij = 0.005 | | |
|---|---|---|---|---|---|---|---|---|---|---|---|---|---|
| | $CH_4$ | C8H18 | Temperature [K] | Pressure [bar] | Temperature [K] | Pressure [bar] | ABS | Temperature [K] | Pressure [bar] | ABS | Temperature [K] | Pressure [bar] | ABS |
| 1 | 99.979 | 0.021 | 155 | 13.8 | 152.996 | 50.000 | 2.004 | 157.631 | 50.000 | 2.631 | 155.307 | 50.000 | 0.307 |
| 2 | 99.970 | 0.03 | 160 | 16.7 | 156.245 | 50.000 | 3.755 | 161.132 | 50.000 | 1.132 | 158.674 | 50.000 | 1.326 |
| 3 | 99.958 | 0.042 | 165 | 20.2 | 159.592 | 50.000 | 5.408 | 164.823 | 50.000 | 0.177 | 162.176 | 50.000 | 2.824 |
| 4 | 99.941 | 0.059 | 170 | 24 | 163.350 | 50.000 | 6.650 | 169.161 | 50.000 | 0.839 | 166.180 | 50.000 | 3.820 |
| 5 | 99.919 | 0.081 | 175 | 28.4 | 167.372 | 50.000 | 7.628 | 174.374 | 50.000 | 0.626 | 170.635 | 50.000 | 4.365 |
| 6 | 99.892 | 0.108 | 180 | 33.4 | 171.815 | 50.000 | 8.185 | 180.096 | 50.000 | 0.096 | 176.235 | 50.000 | 3.765 |
| 7 | 99.873 | 0.127 | 183 | 36.9 | 175.083 | 50.000 | 7.917 | 184.270 | 50.000 | 1.270 | 179.128 | 50.000 | 3.872 |
| | | | | | AAD | | 5.935235714 | | | 0.967351714 | | | 2.897074714 |

# Appendix D: Thermodynamic properties

| | | | |
|---|---|---|---|
| Chemical Abstracts Name:methane | | | $CH_4$ |
| IUPAC Name:methane | | | methane |
| Synonyms: | fire damp<br>marsh gas | methyl hydride<br>refrigerant 50 | |
| Chemical Abstracts Number*: 74-82-8 | | | Structural Formula: $CH_4$ |

| Property (click property name for references and data) | Units | Value | Note | Quality Code | | |
|---|---|---|---|---|---|---|
| | | | | Data type | Uncertainty | Source type |
| Molecular Weight | kg/kmol | 16.042 | | | | |
| Critical Temperature | K | 190.564 | | Smoothed | < 0.2% | Evaluated |
| Critical Pressure | Pa | 4.59900E+06 | | Smoothed | < 0.2% | Evaluated |
| Critical Volume | m^3/kmol | 9.86000E-02 | | Experimental | < 0.2% | Evaluated |
| Crit Compress Factor | unitless | 0.286 | | Defined | | Staff |
| Melting Point | K | 90.694 | 1 | Predicted | < 0.2% | Staff |
| Triple Pt Temperature | K | 90.694 | 2 | Experimental | < 0.2% | Evaluated |
| Triple Pt Pressure | Pa | 1.16960E+04 | | Experimental | < 1% | Evaluated |
| Normal Boiling Point | K | 111.66 | | Experimental | < 1% | Evaluated |
| Liq Molar Volume | m^3/kmol | 3.79694E-02 | 3 | Experimental | < 1% | Staff |
| IG Heat of Formation | J/kmol | -7.45200E+07 | | Experimental | < 1% | Evaluated |
| IG Gibbs of Formation | J/kmol | -5.04900E+07 | 4 | Defined | < 1% | Staff |
| IG Absolute Entropy | J/kmol*K | 1.86270E+05 | | Experimental | < 1% | Evaluated |
| Std Heat of Formation | J/kmol | -7.45200E+07 | | Experimental | < 1% | Evaluated |
| Std Gibbs of Formation | J/kmol | -5.04900E+07 | 5 | Defined | < 1% | Staff |
| Std Absolute Entropy | J/kmol*K | 1.86270E+05 | | Experimental | < 1% | Evaluated |
| Heat Fusion at Melt Pt | J/kmol | 9.41400E+05 | | Experimental | < 1% | Evaluated |
| Std Net Heat of Comb | J/kmol | -8.02620E+08 | | Experimental | < 0.2% | Evaluated |
| Acentric Factor | unitless | 1.15478E-02 | | Defined | | Staff |
| Radius of Gyration | m | 1.11800E-10 | | Defined | < 3% | Staff |
| Solubility Parameter | (J/m^3)^0.5 | 1.16000E+04 | 6 | Defined | | Staff |
| Dipole Moment | C*m | 0.0 | | | | |
| van der Waals Volume | m^3/kmol | 1.70500E-02 | | Defined | < 3% | Staff |
| van der Waals Area | m^2/kmol | 2.88000E+08 | 7 | Defined | < 3% | Staff |
| Refractive Index | unitless | 1.0004 | 8 | Experimental | < 0.2% | Evaluated |
| Flash Point | K | 87.12 | 9 | Predicted | < 3% | Staff |
| Lower Flammability Limit | vol% in air | 5 | | Experimental | < 1% | Unevaluated |
| Upper Flammability Limit | vol% in air | 15 | | Experimental | < 3% | Unevaluated |
| Lower Flamm Limit Temp | K | 86.15 | | Unknown | | Unevaluated |
| Upper Flamm Limit Temp | K | 92.3 | 10 | Predicted | | Staff |
| Auto Ignition Temp | K | 810 | | Experimental | Unknown | Unevaluated |
| Parachor | unitless | 72.2 | 11 | Experimental | < 1% | Unevaluated |
| Heat of Sublimation | J/kmol | 9.64000E+06 | 12 | Experimental | < 0.2% | Staff |
| Dielectric Constant | unitless | 1.6 | 13 | Experimental | < 5% | Evaluated |

Chemical Abstracts Name:carbon dioxide $CO_2$

IUPAC Name:carbon dioxide carbon dioxide

Synonyms: carbonic acid gas, carbonic anhydride, dry ice, refrigerant 744

Chemical Abstracts Number*: 124-38-9 Structural Formula: OCO

| Property (click property name for references and data) | Units | Value | Note | Quality Code | | |
|---|---|---|---|---|---|---|
| | | | | Data type | Uncertainty | Source type |
| Molecular Weight | kg/kmol | 44.0095 | 1 | | | |
| Critical Temperature | K | 304.21 | | Experimental | < 1% | Evaluated |
| Critical Pressure | Pa | 7.38300E+06 | | Experimental | < 3% | Evaluated |
| Critical Volume | m^3/kmol | 9.40000E-02 | | Experimental | < 5% | Evaluated |
| Crit Compress Factor | unitless | 0.274 | | Defined | | Staff |
| Melting Point | K | 216.58 | 2 | Experimental | < 1% | Evaluated |
| Triple Pt Temperature | K | 216.58 | | Experimental | < 1% | Evaluated |
| Triple Pt Pressure | Pa | 5.18000E+05 | 3 | Experimental | < 1% | Staff |
| Normal Boiling Point | K | | 1 | | | |
| Liq Molar Volume | m^3/kmol | 6.16782E-02 | 4 | Experimental | < 1% | Staff |
| IG Heat of Formation | J/kmol | -3.93510E+08 | | Experimental | < 0.2% | Evaluated |
| IG Gibbs of Formation | J/kmol | -3.94370E+08 | 5 | Defined | | Staff |
| IG Absolute Entropy | J/kmol*K | 2.13677E+05 | | Experimental | < 0.2% | Evaluated |
| Std Heat of Formation | J/kmol | -3.93510E+08 | | Experimental | < 0.2% | Evaluated |
| Std Gibbs of Formation | J/kmol | -3.94370E+08 | 6 | Defined | < 1% | Staff |
| Std Absolute Entropy | J/kmol*K | 2.13677E+05 | | Experimental | < 0.2% | Evaluated |
| Heat Fusion at Melt Pt | J/kmol | 9.01900E+06 | 7 | Experimental | < 5% | Evaluated |
| Std Net Heat of Comb | J/kmol | | 8 | | | |
| Acentric Factor | unitless | 0.223621 | | Defined | | Staff |
| Radius of Gyration | m | 1.04000E-10 | | Defined | < 3% | Staff |
| Solubility Parameter | (J/m^3)^0.5 | 1.45600E+04 | 9 | Defined | | Staff |
| Dipole Moment | C*m | 0.0 | | | | |
| van der Waals Volume | m^3/kmol | 1.97000E-02 | | Defined | < 3% | Staff |
| van der Waals Area | m^2/kmol | 3.23000E+08 | 10 | Defined | < 5% | Staff |
| Refractive Index | unitless | 1.00041 | 11 | Experimental | Unknown | Evaluated |
| Flash Point | K | | 8 | | | |
| Lower Flammability Limit | vol% in air | | 8 | | | |
| Upper Flammability Limit | vol% in air | | 8 | | | |
| Lower Flamm Limit Temp | K | | | | | |
| Upper Flamm Limit Temp | K | | | | | |
| Auto Ignition Temp | K | | 8 | | | |
| Parachor | unitless | | | | | |
| Heat of Sublimation | J/kmol | 2.38000E+07 | 12 | Experimental | < 1% | Staff |
| Dielectric Constant | unitless | 1.6 | 13 | Experimental | < 5% | Evaluated |

Chemical Abstracts Name:hexane $C_6H_{14}$

IUPAC Name:hexane n-hexane

Synonyms: hexyl hydride
skellysolve

Chemical Abstracts Number*: 110-54-3 Structural Formula: $CH_3(CH_2)_4CH_3$

| Property (click property name for references and data) | Units | Value | Note | Quality Code | | |
|---|---|---|---|---|---|---|
| | | | | Data type | Uncertainty | Source type |
| Molecular Weight | kg/kmol | 86.17536 | | | | |
| Critical Temperature | K | 507.6 | | Smoothed | < 0.2% | Evaluated |
| Critical Pressure | Pa | 3.02500E+06 | | Smoothed | < 1% | Evaluated |
| Critical Volume | m^3/kmol | 0.371 | | Experimental | < 3% | Evaluated |
| Crit Compress Factor | unitless | 0.266 | | Defined | | Staff |
| Melting Point | K | 177.83 | | Experimental | < 0.2% | Evaluated |
| Triple Pt Temperature | K | 177.83 | | Predicted | < 0.2% | Staff |
| Triple Pt Pressure | Pa | 0.901695 | | Predicted | < 5% | Staff |
| Normal Boiling Point | K | 341.88 | | Experimental | < 1% | Evaluated |
| Liq Molar Volume | m^3/kmol | 0.131362 | | Experimental | < 1% | Staff |
| IG Heat of Formation | J/kmol | -1.66940E+08 | | Experimental | < 1% | Evaluated |
| IG Gibbs of Formation | J/kmol | -6.63400E+04 | 1 | Defined | < 1% | Staff |
| IG Absolute Entropy | J/kmol*K | 3.88740E+05 | | Experimental | < 1% | Evaluated |
| Std Heat of Formation | J/kmol | -1.98660E+08 | | Experimental | < 1% | Unevaluated |
| Std Gibbs of Formation | J/kmol | -4.15400E+06 | 2 | Defined | < 1% | Staff |
| Std Absolute Entropy | J/kmol*K | 2.96060E+05 | | Experimental | < 1% | Unevaluated |
| Heat Fusion at Melt Pt | J/kmol | 1.30800E+07 | | Experimental | < 1% | Evaluated |
| Std Net Heat of Comb | J/kmol | -3.85510E+09 | | Experimental | < 0.2% | Evaluated |
| Acentric Factor | unitless | 0.301261 | | Defined | | Staff |
| Radius of Gyration | m | 3.76900E-10 | | Defined | < 3% | Staff |
| Solubility Parameter | (J/m^3)^0.5 | 1.48800E+04 | | Defined | < 3% | Staff |
| Dipole Moment | C*m | 0.0 | | | | |
| van der Waals Volume | m^3/kmol | 6.82600E-02 | | Defined | < 1% | Staff |
| van der Waals Area | m^2/kmol | 9.64000E+08 | | Defined | < 1% | Staff |
| Refractive Index | unitless | 1.37226 | | Experimental | < 0.2% | Evaluated |
| Flash Point | K | 250.15 | | Experimental | < 1% | Unevaluated |
| Lower Flammability Limit | vol% in air | 1.2 | | Experimental | < 5% | Unevaluated |
| Upper Flammability Limit | vol% in air | 7.2 | | Smoothed | < 5% | Staff |
| Lower Flamm Limit Temp | K | 247.15 | | Experimental | | Unevaluated |
| Upper Flamm Limit Temp | K | 277 | 3 | Experimental | | Unevaluated |
| Auto Ignition Temp | K | 498 | | Experimental | Unknown | Unevaluated |
| Parachor | unitless | 270.7 | 4 | Experimental | < 1% | Unevaluated |
| Heat of Sublimation | J/kmol | | | | | |
| Dielectric Constant | unitless | 1.8865 | 5 | Experimental | | Unevaluated |

Chemical Abstracts Name:heptane — $C_7H_{16}$

IUPAC Name:heptane — n-heptane

Synonyms: dipropylmethane; heptyl hydride

Chemical Abstracts Number*: 142-82-5 — Structural Formula: $CH_3(CH_2)_5CH_3$

| Property (click property name for references and data) | Units | Value | Note | Quality Code | | |
|---|---|---|---|---|---|---|
| | | | | Data type | Uncertainty | Source type |
| Molecular Weight | kg/kmol | 100.20194 | | | | |
| Critical Temperature | K | 540.2 | | Smoothed | < 0.2% | Evaluated |
| Critical Pressure | Pa | 2.74000E+06 | | Smoothed | < 3% | Evaluated |
| Critical Volume | m^3/kmol | 0.428 | | Experimental | < 5% | Evaluated |
| Crit Compress Factor | unitless | 0.261 | | Defined | | Staff |
| Melting Point | K | 182.57 | | Experimental | < 0.2% | Evaluated |
| Triple Pt Temperature | K | 182.57 | | Predicted | < 0.2% | Staff |
| Triple Pt Pressure | Pa | 0.182694 | | Predicted | < 5% | Staff |
| Normal Boiling Point | K | 371.58 | | Experimental | < 1% | Evaluated |
| Liq Molar Volume | m^3/kmol | 0.147024 | | Experimental | < 1% | Staff |
| IG Heat of Formation | J/kmol | -1.87650E+08 | | Experimental | < 1% | Evaluated |
| IG Gibbs of Formation | J/kmol | 8.16500E+06 | 1 | Defined | < 1% | Staff |
| IG Absolute Entropy | J/kmol*K | 4.27980E+05 | | Experimental | < 1% | Evaluated |
| Std Heat of Formation | J/kmol | -2.24050E+08 | | Experimental | < 1% | Unevaluated |
| Std Gibbs of Formation | J/kmol | 1.40400E+06 | 2 | Defined | < 1% | Staff |
| Std Absolute Entropy | J/kmol*K | 3.28570E+05 | | Experimental | < 1% | Unevaluated |
| Heat Fusion at Melt Pt | J/kmol | 1.40500E+07 | | Experimental | < 1% | Evaluated |
| Std Net Heat of Comb | J/kmol | -4.46473E+09 | | Experimental | < 0.2% | Evaluated |
| Acentric Factor | unitless | 0.349469 | | Defined | | Staff |
| Radius of Gyration | m | 4.17300E-10 | | Defined | < 3% | Staff |
| Solubility Parameter | (J/m^3)^0.5 | 1.52400E+04 | | Defined | < 3% | Staff |
| Dipole Moment | C*m | 0.0 | | | | |
| van der Waals Volume | m^3/kmol | 7.84900E-02 | | Defined | < 1% | Staff |
| van der Waals Area | m^2/kmol | 1.09900E+09 | | Defined | < 1% | Staff |
| Refractive Index | unitless | 1.38511 | | Experimental | < 0.2% | Evaluated |
| Flash Point | K | 269 | | Experimental | < 3% | Unevaluated |
| Lower Flammability Limit | vol% in air | 1.05 | 3 | Experimental | < 3% | Unevaluated |
| Upper Flammability Limit | vol% in air | 6.7 | | Experimental | < 5% | Unevaluated |
| Lower Flamm Limit Temp | K | 269.15 | | Experimental | | Unevaluated |
| Upper Flamm Limit Temp | K | 299 | 4 | Experimental | | Unevaluated |
| Auto Ignition Temp | K | 477 | | Experimental | Unknown | Unevaluated |
| Parachor | unitless | 309.7 | 5 | Smoothed | < 5% | Evaluated |
| Heat of Sublimation | J/kmol | 5.67000E+07 | 6 | Predicted | < 10% | Staff |
| Dielectric Constant | unitless | 1.9209 | 7 | Experimental | | Unevaluated |

Chemical Abstracts Name:benzene — $C_6H_6$

IUPAC Name:benzene — benzene

Synonyms: benzol, benzolene, bicarburet of hydrogen, carbon oil, coal naphtha, cyclohexatriene, mineral naphtha, motor benzol, phenyl hydride, pyrobenzole

Chemical Abstracts Number*: 71-43-2 — Structural Formula: -CHCHCHCHCH-

| Property (click property name for references and data) | Units | Value | Note | Quality Code | | |
|---|---|---|---|---|---|---|
| | | | | Data type | Uncertainty | Source type |
| Molecular Weight | kg/kmol | 78.11184 | | | | |
| Critical Temperature | K | 562.05 | | Smoothed | < 0.2% | Evaluated |
| Critical Pressure | Pa | 4.89500E+06 | | Smoothed | < 0.2% | Evaluated |
| Critical Volume | m^3/kmol | 0.256 | | Smoothed | < 3% | Evaluated |
| Crit Compress Factor | unitless | 0.268 | | Defined | | Staff |
| Melting Point | K | 278.68 | | Experimental | < 1% | Evaluated |
| Triple Pt Temperature | K | 278.68 | 1 | Predicted | < 1% | Staff |
| Triple Pt Pressure | Pa | 4.76422E+03 | | Predicted | < 3% | Staff |
| Normal Boiling Point | K | 353.24 | | Experimental | < 1% | Evaluated |
| Liq Molar Volume | m^3/kmol | 8.94764E-02 | | Experimental | < 1% | Staff |
| IG Heat of Formation | J/kmol | 8.28800E+07 | | Experimental | < 3% | Evaluated |
| IG Gibbs of Formation | J/kmol | 1.29600E+08 | 2 | Defined | < 3% | Staff |
| IG Absolute Entropy | J/kmol*K | 2.69300E+05 | | Experimental | < 3% | Evaluated |
| Std Heat of Formation | J/kmol | 4.89500E+07 | | Experimental | < 5% | Unevaluated |
| Std Gibbs of Formation | J/kmol | 1.24400E+08 | 3 | Defined | < 5% | Staff |
| Std Absolute Entropy | J/kmol*K | 1.73260E+05 | | Experimental | < 5% | Unevaluated |
| Heat Fusion at Melt Pt | J/kmol | 9.86600E+06 | | Experimental | < 1% | Evaluated |
| Std Net Heat of Comb | J/kmol | -3.13600E+09 | | Experimental | < 3% | Evaluated |
| Acentric Factor | unitless | 0.2103 | | Defined | | Staff |
| Radius of Gyration | m | 3.00400E-10 | | Defined | < 3% | Staff |
| Solubility Parameter | (J/m^3)^0.5 | 1.87300E+04 | | Defined | < 1% | Staff |
| Dipole Moment | C*m | 0.0 | | | | |
| van der Waals Volume | m^3/kmol | 4.84000E-02 | | Defined | < 1% | Staff |
| van der Waals Area | m^2/kmol | 6.00000E+08 | | Defined | < 1% | Staff |
| Refractive Index | unitless | 1.49792 | | Experimental | < 0.2% | Evaluated |
| Flash Point | K | 262 | | Experimental | < 3% | Unevaluated |
| Lower Flammability Limit | vol% in air | 1.2 | 4 | Experimental | < 10% | Unevaluated |
| Upper Flammability Limit | vol% in air | 8 | 4 | Experimental | < 10% | Unevaluated |
| Lower Flamm Limit Temp | K | 261 | 4 | Experimental | | Unevaluated |
| Upper Flamm Limit Temp | K | 288 | 4 | Experimental | | Unevaluated |
| Auto Ignition Temp | K | 833.15 | | Experimental | Unknown | Unevaluated |
| Parachor | unitless | 206.2 | 5 | Smoothed | < 5% | Evaluated |
| Heat of Sublimation | J/kmol | 4.53000E+07 | 6 | Experimental | < 1% | Staff |
| Dielectric Constant | unitless | 2.2825 | 7 | Experimental | | Unevaluated |

Chemical Abstracts Name:octane — $C_8H_{18}$

IUPAC Name:octane — n-octane

Synonym: octyl hydride

Chemical Abstracts Number*: 111-65-9 — Structural Formula: $CH_3(CH_2)_6CH_3$

| Property (click property name for references and data) | Units | Value | Note | Quality Code | | |
|---|---|---|---|---|---|---|
| | | | | Data type | Uncertainty | Source type |
| Molecular Weight | kg/kmol | 114.22852 | | | | |
| Critical Temperature | K | 568.7 | | Smoothed | < 0.2% | Evaluated |
| Critical Pressure | Pa | 2.49000E+06 | | Smoothed | < 3% | Evaluated |
| Critical Volume | m^3/kmol | 0.486 | 1 | Predicted | < 5% | Staff |
| Crit Compress Factor | unitless | 0.256 | | Defined | < 10% | Staff |
| Melting Point | K | 216.38 | | Experimental | < 0.2% | Evaluated |
| Triple Pt Temperature | K | 216.38 | 2 | Predicted | < 0.2% | Staff |
| Triple Pt Pressure | Pa | 2.1083 | | Predicted | < 5% | Staff |
| Normal Boiling Point | K | 398.83 | | Experimental | < 1% | Evaluated |
| Liq Molar Volume | m^3/kmol | 0.162561 | 3 | Experimental | < 1% | Staff |
| IG Heat of Formation | J/kmol | -2.08750E+08 | | Experimental | < 1% | Evaluated |
| IG Gibbs of Formation | J/kmol | 1.60000E+07 | 4 | Defined | < 1% | Staff |
| IG Absolute Entropy | J/kmol*K | 4.67230E+05 | | Experimental | < 1% | Evaluated |
| Std Heat of Formation | J/kmol | -2.49780E+08 | | Experimental | < 1% | Unevaluated |
| Std Gibbs of Formation | J/kmol | 6.58700E+06 | 5 | Defined | < 1% | Staff |
| Std Absolute Entropy | J/kmol*K | 3.61200E+05 | | Experimental | < 1% | Unevaluated |
| Heat Fusion at Melt Pt | J/kmol | 2.07400E+07 | | Experimental | < 1% | Evaluated |
| Std Net Heat of Comb | J/kmol | -5.07415E+09 | | Experimental | < 0.2% | Evaluated |
| Acentric Factor | unitless | 0.399552 | | Defined | | Staff |
| Radius of Gyration | m | 4.54600E-10 | | Defined | < 3% | Staff |
| Solubility Parameter | (J/m^3)^0.5 | 1.54900E+04 | | Defined | < 3% | Staff |
| Dipole Moment | C*m | 0.0 | | | | |
| van der Waals Volume | m^3/kmol | 8.87200E-02 | | Defined | < 1% | Staff |
| van der Waals Area | m^2/kmol | 1.23400E+09 | | Defined | < 1% | Staff |
| Refractive Index | unitless | 1.39505 | | Experimental | < 0.2% | Evaluated |
| Flash Point | K | 287.15 | | Experimental | < 1% | Unevaluated |
| Lower Flammability Limit | vol% in air | 0.96 | 6 | Experimental | < 3% | Unevaluated |
| Upper Flammability Limit | vol% in air | 6.5 | 7 | Experimental | < 5% | Unevaluated |
| Lower Flamm Limit Temp | K | 287 | 8 | Predicted | | Staff |
| Upper Flamm Limit Temp | K | 323 | 9 | Experimental | | Unevaluated |
| Auto Ignition Temp | K | 479 | 10 | Experimental | Unknown | Unevaluated |
| Parachor | unitless | 350.6 | 11 | Experimental | < 1% | Unevaluated |
| Heat of Sublimation | J/kmol | 6.34000E+07 | 12 | Predicted | < 10% | Staff |
| Dielectric Constant | unitless | 1.948 | 13 | Experimental | | Unevaluated |

Chemical Abstracts Name:cyclohexane $C_6H_{12}$

IUPAC Name:cyclohexane cyclohexane

Synonyms: hexahydrobenzene hexanaphthene
hexamethylene

Chemical Abstracts Number*: 110-82-7 Structural Formula: $-(CH_2)_6-$

| Property (click property name for references and data) | Units | Value | Note | Quality Code | | |
|---|---|---|---|---|---|---|
| | | | | Data type | Uncertainty | Source type |
| Molecular Weight | kg/kmol | 84.15948 | | | | |
| Critical Temperature | K | 553.8 | 1 | Smoothed | < 0.2% | Evaluated |
| Critical Pressure | Pa | 4.08000E+06 | | Experimental | < 1% | Evaluated |
| Critical Volume | m^3/kmol | 0.308 | | Experimental | < 1% | Evaluated |
| Crit Compress Factor | unitless | 0.273 | | Defined | | Staff |
| Melting Point | K | 279.69 | | Experimental | < 1% | Evaluated |
| Triple Pt Temperature | K | 279.69 | 2 | Predicted | < 1% | Staff |
| Triple Pt Pressure | Pa | 5.36251E+03 | | Predicted | < 3% | Staff |
| Normal Boiling Point | K | 353.87 | | Experimental | < 1% | Evaluated |
| Liq Molar Volume | m^3/kmol | 0.108856 | | Experimental | < 1% | Staff |
| IG Heat of Formation | J/kmol | -1.23300E+08 | | Experimental | < 3% | Evaluated |
| IG Gibbs of Formation | J/kmol | 3.19100E+07 | 3 | Defined | < 3% | Staff |
| IG Absolute Entropy | J/kmol*K | 2.97276E+05 | | Experimental | < 3% | Evaluated |
| Std Heat of Formation | J/kmol | -1.56150E+08 | | Experimental | < 1% | Unevaluated |
| Std Gibbs of Formation | J/kmol | 2.67700E+07 | 4 | Defined | < 1% | Staff |
| Std Absolute Entropy | J/kmol*K | 2.04350E+05 | | Experimental | < 1% | Unevaluated |
| Heat Fusion at Melt Pt | J/kmol | 2.74000E+06 | | Experimental | < 3% | Unevaluated |
| Std Net Heat of Comb | J/kmol | -3.65600E+09 | | Experimental | < 3% | Evaluated |
| Acentric Factor | unitless | 0.208054 | | Defined | | Staff |
| Radius of Gyration | m | 3.24200E-10 | | Defined | < 3% | Staff |
| Solubility Parameter | (J/m^3)^0.5 | 1.67300E+04 | | Defined | < 3% | Staff |
| Dipole Moment | C*m | 0.0 | 5 | Experimental | Unknown | Evaluated |
| van der Waals Volume | m^3/kmol | 6.14000E-02 | | Defined | < 1% | Staff |
| van der Waals Area | m^2/kmol | 8.10000E+08 | | Defined | < 1% | Staff |
| Refractive Index | unitless | 1.42354 | | Experimental | < 0.2% | Evaluated |
| Flash Point | K | 255.93 | | Unknown | < 3% | Unevaluated |
| Lower Flammability Limit | vol% in air | 1.3 | 6 | Experimental | < 5% | Unevaluated |
| Upper Flammability Limit | vol% in air | 7.8 | | Experimental | < 10% | Unevaluated |
| Lower Flamm Limit Temp | K | 257.2 | 7 | Predicted | | Staff |
| Upper Flamm Limit Temp | K | 288 | 8 | Experimental | | Unevaluated |
| Auto Ignition Temp | K | 518.15 | | Experimental | Unknown | Unevaluated |
| Parachor | unitless | 241.2 | 9 | Smoothed | < 5% | Evaluated |
| Heat of Sublimation | J/kmol | 3.63000E+07 | 10 | Experimental | < 3% | Staff |
| Dielectric Constant | unitless | 2.0243 | 11 | Experimental | | Unevaluated |